



**Advanced amperometric nanocomposite
sensors based on carbon nanotubes and
graphene: Characterization, Optimization,
Functionalization and Applications**

By

Jose María Muñoz Martín

Thesis to opt for the PhD in Chemistry

Directors: María del Mar Baeza and Francisco Céspedes

Departament de Química

Facultat de Ciències

September 2015

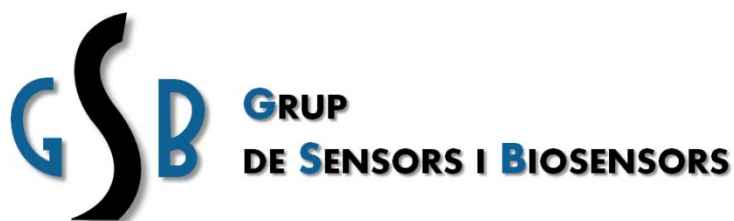
The presented Thesis titled “Advanced amperometric nanocomposite sensors based on carbon nanotubes and graphene: Characterization, Optimization, Functionalization and Applications” has been performed by Jose María Muñoz Martín at the laboratory of *Sensors i Biosensors del Departament de Química de l’Universitat Autònoma de Barcelona (UAB)* under the supervision of Dr. María del Mar Baeza Labat and Dr. Francisco Céspedes Mulero, both Titular Professors at UAB.

Bellaterra, 16 de Julio de 2015

Jose María Muñoz Martín

Dr. María del Mar Baeza Labat

Dr. Francisco Céspedes Mulero



The present PhD Thesis was carried out thanks to the financial support provided by *Universitat Autònoma de Barcelona* through a PIF pre-doctoral scholarship and to the support of the following projects:

- **Desarrollo de (bio)materials basados en nanoestructuras. Optimización y caracterización para su aplicación en (bio)sensores y energías renovables.** Grant by *Ministerio de Ciencia e Innovación*, Spain. Project: CTQ2009-13873.
 - **Minituarización, integración y paralelización de ensayos químicos y biológicos mediante nuevas plataformas de microfluídica.** Grant by *Ministerio de Ciencia e Innovación*, Spain. Project: CTQ2012-36165.
-

ACKNOWLEDGEMENTS

En primer lugar, quisiera agradecer esta Tesis Doctoral a los doctores María del Mar Baeza y Francisco Céspedes, por la dirección de la misma, así como por sus conocimientos científicos y por abrirme las puertas al *Grup de Sensors i Biosensors de l'Universitat Autònoma de Barcelona*. Gracias a vosotros he podido culminar el sueño por el que tanto me he esforzado: llegar a realizar el ansiado doctorado. Además, quiero destacar su trato tan humano y los consejos que me han transmitido durante estos cuatro largos años de trabajo. En especial, a María del Mar Baeza, por estar siempre al pie del cañón, sobre todo en este *sprint* final y, conseguir así, que hoy esté escribiendo estas líneas. ¡GRACIAS!

También agradecer al profesor Yurii Gun'ko por abrirme las puertas de su laboratorio en el *Trinity College of Dublin*, a sus doctores y doctorandos, y a todas las amistades que allí realicé por hacerme vivir una experiencia única e inolvidable. Sin duda, significó un cambio personal importantísimo en mi vida y todos vosotros sois partícipes de ello. Cómo olvidaros... También agradecerle a todas las personas que han colaborado en esta Tesis, fruto de múltiples colaboraciones. En especial a la Dra. Arántzazu González por sus consejos y, sobre todo, por su amistad. ¡Gracias *pequenia!*

Respecto a mis compañeros de laboratorio y de planta, quisiera hacer una especial mención a los ya doctores Cristina Ocaña, Julio Bastos y Oriol Baltrons, con los cuales he forjado una bonita y sincera amistad bajo el nombre del *Petit Comité*. Nunca podré olvidar estos años a vuestro lado... ¡ni tu boda, Cris! También quiero destacar a mis compañeros de *Cocktails Night*: Anna Artigues, Fran Blanco, Júlia Senyé y Elena Peralta. Me he sentido muy querido a vuestro lado, hemos compartido muchos momentos, muchos grandes momentos... *Us estimo!* Finalmente, subrayar el buen ambiente, dentro y fuera del laboratorio, con tod@s mis compañer@s de unidad: Adri, Alejandra, Andrea, Andreu, Anna H., Anna P., Bea, Berta, Delfina, Ferdia, Gina, Olga, Miky, Montse R., Núria, Raquel, Sandra, Sole, Susana, Tamara, Toni, Vanessa, Xavi y Yara. ¡Me lo habéis puesto muy fácil para venir siempre con una sonrisa al laboratorio! Sólo tengo palabras bonitas para todos vosotros, por ello quiero deciros que siempre

podréis contar conmigo y, sin duda, nos vemos en el camino que nos queda por recorrer. Y por qué no, a todos mis alumnos de grado que, entre todos vosotros, habéis conseguido la motivación y la ilusión por continuar algún día en el duro pero gratificante mundo de la docencia. ¡Lucharé por conseguirlo!

Realizar una Tesis es psicológicamente muy duro y, evidentemente, sólo se puede rendir al 100% cuando personalmente uno es feliz. Yo tengo la suerte de estar rodeado de grandísimas personas que me aportan la *chispa* y la ilusión por seguir adelante, además de esa felicidad personal que te hace estar en forma para afrontar lo desconocido... Y sí, aquí es dónde venís vosotros: mi familia. Esta Tesis es fruto de muchos años de educación, dedicación y donación de valores por parte de unos padres y hermano que se han volcado en mí. Gracias Juanma por todos tus consejos y apoyarme en todo lo que hago. Seguramente no os lo digo lo suficiente, pero aquí quedará grabado para siempre: sin vosotros, no soy nada y por ello os dedico esta Tesis. ¡OS QUIERO! No me quiero olvidar de una persona muy especial y que, sin duda, su pérdida marcó uno de los días más tristes de toda mi vida: mi abuelo Juan. Ni quiero, ni puedo olvidarte. También tiene un papel muy importante mi prima María Lourdes “Mari”, por ser como es, una persona ejemplar, admirable, todo corazón... Y una gran amiga. ¡Gracias *cosina*!

Y uno no llega solo a ninguna parte... Siempre me acompañan mis grandes amigos, mis confidentes: Aida, Clara, Gemma, Dani, Silvia G., Silvia T. y Yisel. No sabéis lo feliz que me siento a vuestro lado y la suerte que tengo de teneros. Grandes amigos pero, por encima de todo, ¡grandes personas! En especial a Gemma, mi *super compi*, por todo el apoyo ofrecido en estos últimos meses, llenos de cambios personales y emocionales. Has sabido aportarme la estabilidad, la serenidad y el poder ver el vaso medio lleno para afrontar el empujón final. También a todos mis otros amigos, incluyendo ex compañeros de universidad y de trabajo, que están ahí para risas, viajes, juergas, psicología... No os voy a poner a todos, pero seguro que os sentiréis identificados.

Y para finalizar, debo agradecerle también a todas aquellas personas que a lo largo de esta Tesis han estado en algún momento de mi vida y que con más o menos suerte me ha ayudado... A los que hoy no están, a los que acabáis de llegar y a los que llegaréis, ¡gracias! Estos agradecimientos van por toda una vida.

“Una ilusión eterna, o por lo menos que renace a menudo en el alma, está muy cerca de ser una realidad”

André Maurois

TABLE OF CONTENTS

Table of Contents	i
Acronyms & Symbols	vii
Summary	xi
Resum	xiii
Resumen	xv
CHAPTER I General Introduction	1
1.1 Carbon Nanotubes	4
1.2 Conducting nanocomposite electrodes based on CNTs	12
1.3 Electrochemical nanocomposite sensors based on CNTs.....	16
1.4 Characterization strategies of CNT–based nanocomposite electrodes... 21	
1.4.1 Electrochemical characterization: Electrochemical Impedance Spectroscopy and Cyclic Voltammetry	22
1.4.1.1 Electrochemical Impedance Spectroscopy	22
1.4.1.2 Cyclic Voltammetry	25
1.4.2 Electrical characterization through the Percolation Theory	27
1.4.3 Morphological characterization: Microscopic techniques.....	30
1.4.4 Electroanalytical evaluation: Hydrodynamic Amperometry	32
1.5. Tunability of CNT–based nanocomposite sensors with modifiers.....	34
1.5.1. Intermatrix Synthesis Technique for CNT–based nanocomposite electrodes modification with nanoparticles.....	38
1.6. Beyond CNTs: Trends in graphene–based electrochemical nanocomposite sensors	40
1.7. References	45
CHAPTER II Motivation and Aims	61
2.1 General Aim	62
2.2 Specific Aims	62

CHAPTER III	Materials and Methods.....	65
3.1	Chemicals and Reagents.....	65
3.2	Fabrication of nanocomposite electrodes.....	67
3.2.1	Synthesis of Nanoparticles for nanocomposite electrodes modification: Functionalization and Incorporation.....	68
3.2.1.1	Synthesis of FMNPs.....	70
3.2.1.2	Synthesis of CdS–QDs.....	71
3.2.1.3	Synthesis of CuO–NPs.....	72
3.2.2	Synthesis of graphene–based nanomaterials for nanocomposite electrode purposes: Functionalization and Incorporation.....	74
3.2.2.1	Synthesis of GO and rGO.....	74
3.2.2.2	Synthesis of Au–NPs@rGO and β –CD-SH/Au–NPs@rGO hybrid materials.....	75
3.3	Characterization Techniques and Instrumentation.....	76
3.3.1	Physical characterization of nanostructured carbon materials ..	77
3.3.1.1	Microscopy characterization.....	77
3.3.1.2	Thermogravimetric analysis.....	77
3.3.1.3	Spectroscopic techniques.....	78
3.3.2	Characterization and evaluation of the developed sensors based on nanocomposite materials.....	78
3.3.2.1	Electrical characterization.....	78
3.3.2.2	Electrochemical experiments.....	79
3.3.2.3	Electroanalytical performance.....	80
3.3.2.4	Morphological, Topographical and Current studies.....	82
3.4	References.....	82
CHAPTER IV	Influence of MWCNT nature on the electroanalytical performance of nanocomposite sensors.....	85
4.1	Results and Discussion.....	87
4.1.1	Influence of MWCNT diameter.....	88
4.1.1.1	Physical characterization of MWCNTs.....	88
4.1.1.2	Electrical characterization.....	90
4.1.1.3	Voltammetric experiments.....	92
4.1.1.4	Impedimetric experiments.....	95
4.1.1.5	Morphological studies.....	99
4.1.1.6	Electroanalytical performance.....	100

4.1.2 Influence of MWCNT purity.....	102
4.1.2.1 Physical characterization of MWCNTs.....	102
4.1.2.2 Electrical characterization.....	105
4.1.2.3 Voltammetric experiments.....	107
4.1.2.4 Impedimetric experiments.....	108
4.1.2.5 Morphological studies.....	111
4.1.2.6 Electroanalytical performance.....	112
4.2 Conclusions.....	114
4.3 References.....	116

CHAPTER V Tunability of MWCNT/epoxy nanocomposite electrodes with nanoparticles for sensing improvements121

5.1 Results and Discussion.....	123
5.1.1 Customized preparation of modified-electrodes with Functional Metal Nanoparticles.....	124
5.1.1.1 Physical characterization of FMNPs incorporated by Route A.....	124
5.1.1.2 Impedimetric experiments of modified-electrodes by Route A.....	126
5.1.1.3 Electroanalytical evaluation of Au-/Pd-NPs modified-sensors by Route A.....	129
5.1.1.4 Alternative routes for electrodes modification: A comparative electrochemical and electroanalytical study.....	130
5.1.2 CdS quantum dots as a scattering material in MWCNT-based nanocomposite sensors for microelectrode array behaviour.....	134
5.1.2.1 Physical characterization of CdS-QDs nanocrystals.....	134
5.1.2.2 Voltammetric experiments.....	136
5.1.2.3 Impedimetric experiments.....	138
5.1.2.4 Morphological studies.....	140
5.1.2.5 Polarization potential determination.....	143
5.1.2.6 Electroanalytical performance.....	143
5.1.3 Electrocatalytical activity of CuO nanoparticles for free chlorine amperometric detection.....	146
5.1.3.1 Physical characterization of CuO-NPs.....	146
5.1.3.2 Voltammetric experiments.....	148
5.1.3.3 Impedimetric experiments.....	150
5.1.3.4 Electroanalytical performance.....	152

5.1.3.5 Specificity, Stability and Reproducibility of modified-sensors by Route B	154	
5.2 Conclusions	156	
5.3 References	158	
CHAPTER VI	Towards to the electroanalytical enhancement of graphene– polymer nanocomposite (bio)sensors	161
6.1 Results and Discussion.....		163
6.1.1 Characterization protocol to achieve the optimum graphene– polymer ratio for electrochemical sensing applications		164
6.1.1.1 Physical characterization of GO and rGO.....		164
6.1.1.2 Electrical characterization.....		167
6.1.1.3 Voltammetric experiments.....		168
6.1.1.4 Impedimetric experiments.....		170
6.1.1.5 Morphological studies.....		173
6.1.1.6 Electroanalytical performance.....		176
6.1.2 Modified graphene–based nanocomposite sensor for the sensitive biorecognition of Thyroxine		178
6.1.2.1 Physical characterization of hybrid nanomaterials.....		178
6.1.2.2 Voltammetric experiments at the biorecognition electrode .		181
6.1.2.3 Electrochemical behaviour of the different graphene–based electrodes		183
6.1.2.4 Electroanalytical performance at the biorecognition sensor		185
6.1.2.5 Stability and Reproducibility		187
6.2 Conclusions		188
6.3 References		189
CHAPTER VII	General Conclusions and Future Perspectives.....	193
7.1 General Conclusions.....		193
7.2 Future Perspectives.....		197
ANNEX A	Accepted Publications	
A1 J. Muñoz , J. Bartrolí, F. Céspedes and M. Baeza. Influence of raw carbon nanotubes diameter for the optimization of the load composition ratio in epoxy amperometric composite sensors. <i>Journal of Materials Science</i> , 50 (2015) 652–661.		

A2. **J. Muñoz**, F. Céspedes and M. Baeza. Effect of carbon nanotubes purification on electroanalytical response of near-percolation amperometric nanocomposite sensors. *Journal of the Electrochemical Society*, 162 (2015) B217–B224.

A3. **J. Muñoz**, J. Bastos-Arrieta, M. Muñoz, D. Muraviev, F. Céspedes and M. Baeza. Simple green routes for the customized preparation of sensitive carbon nanotubes/epoxy nanocomposite electrodes with Functional Metal Nanoparticles. *RSC Advances*, 4 (2014) 44517–44524.

A4. **J. Muñoz**, F. Céspedes and M. Baeza. Modified multiwall carbon nanotubes/epoxy amperometric nanocomposite sensors with CuO nanoparticles for electrocatalytic detection of free chlorine. *Microchemical Journal*, 122 (2015) 189–196.

ANNEX B Submitted Publications

B1. **J. Muñoz**, J. Bastos-Arrieta, M. Muñoz, D. Muraviev, F. Céspedes and M. Baeza. CdS quantum dots as a scattering nanomaterial for microelectrode array behavior. *Journal of Materials Science*, (2015)

B2. **J. Muñoz**, L.J. Brennan, F. Céspedes, Y.K. Gun'ko and M. Baeza. Characterization protocol to improve the electroanalytical response of graphene-polymer nanocomposite sensors. *Composite Science and Technology*, (2015)

B3. **J. Muñoz**, M. Riba-Moliner, L.J. Brennan, Y.K. Gun'ko F. Céspedes, A. González-Campo and M. Baeza. Near-percolation nanocomposite sensor based on modified-graphene for the sensitive electrochemical biorecognition of Thyroxine. *Chemical Communications*, (2015)

ANNEX C Curriculum Vitae

ACRONYMS & SYMBOLS

General symbols:

§ Section

Materials & Reagents:

CD	Cyclodextrin
β-CD-SH	Per-6-thio-β-cyclodextrin
CNTs	Carbon Nanotubes
DWCNTs	Double Walled Carbon Nanotubes
FMNPs	Functional Metal Nanoparticles
FMNPs@MWCNTs	Multi Walled Carbon Nanotubes containing Functional Metal Nanoparticles
FMNPs@rGO	Reduced Graphene Oxide containing Functional Metal Nanoparticles
GO	Graphene Oxide
MO-NPs	Metal Oxide Nanoparticles
MWCNTs	Multi Walled Carbon Nanotubes
MWCNTs-COOH	Activated Multi Walled Carbon Nanotubes
NPs	Nanoparticles
QDs	Quantum Dots
rGO	Reduced Graphene Oxide
SWCNTs	Single Walled Carbon Nanotubes
T₄	Thyroxine

Physical Parameters of CNTs:

θ	Chiral Angle
C_h	Chiral Vector (Hamada vector)
a, b	Pair of Vector Directions of the Chiral Vector
n, m	Pair of Integers defining a real number of unit vectors

Percolation Theory:

HRC	High Resistance Composites
LRC	Low Resistance Composites
NPC	Near-Percolation Composites
PC	Percolation Composites

Electrochemical Impedance Spectroscopy (EIS):

j	Imaginary Unit
θ	Phase Angle
ω	Frequency
φ	Phase Shift
AC	Alternating Current
C	Capacitors
C_{dl}	Double-layer Capacitance
E(t)	Alternating Current Voltage
E°	Amplitude of Potential
I(t)	Alternating Current
I°	Amplitude of Current
R	Resistors
R_Ω	Solution Resistance
R_{ct}	Charge Transfer Resistance
t	Time
Z	Impedance
Z°	Amplitude Impedance
Z_{imag}	Imaginary Part of Impedance
Z_{real}	Real Part of Impedance
Z_w	Warburg Impedance

Cyclic Voltammetry (CV):

α	Symmetry Factor
ΔE	Peak Separation Potential
v	Scan Rate
A	Electroactive Area

A_{geom}	Geometric Area
C^*	Bulk Concentration of the Electroactive Species
d	Stagnant Layer
D	Diffusion Coefficient of the Redox Species
E_{eq}	Equilibrium Potential
E_{pa}	Anodic Peak Potential
E_{pc}	Cathodic Peak Potential
F	Faraday Constant
i_0	Exchange Current
I	Measure Current
I_p	Peak Current
I_{pa}	Anodic Peak Current
I_{pc}	Cathodic Peak Current
n	Number of Electrons Transferred
R	Universal Gas Constant
T	Absolute Temperature

Microscopic Tools:

AFM	Atomic Force Microscopy
CM3D	Confocal Microscopy 3 Dimensions
CSAFM	Current Sensing Atomic Force Microscopy
F	Applied Force
HR-(S)TEM	High Resolution Scanning Transmission Electron Microscopy
HR-TEM	High Resolution Transmission Electron Microscopy
k	Spring Constant
SEM	Scanning Electron Microscopy
TEM	Transmission Electron Microscopy
x	Displacement

Spectroscopic Tools:

D	Raman D band
EDS	Energy Dispersive X-Ray Spectroscopy

G	Raman G Band
I_D	Intensity of Raman D Band
I_G	Intensity of Raman G Band
FTIR	Fourier Transform Infrared Spectroscopy
UV-vis	Ultraviolet-Visible Absorption Spectroscopy
XPS	X-Ray Fluorescence Spectroscopy

Additional Techniques:

IMS	Intermatrix Synthesis Technique
LSV	Linear Sweep Voltammetry
RA	Route A for Nanoparticles Synthesis
RB	Route B for Nanoparticles Synthesis
RC	Route C for Nanoparticles Synthesis
TGA	Thermogravimetric Analysis

SUMMARY

Among the wide range of nanocomposites, the incorporation of conducting nanostructured carbon materials, such as carbon nanotubes (CNTs) and graphene, into an insulating polymeric matrix is a very attractive way to combine the unique mechanical and electrical properties of individual filler with the advantages of plastics. Concretely, carbon-based nanocomposite materials have played a leading role in the analytical electrochemistry field, particularly in (bio)sensor devices, due to their interesting advantages regarding to a pure conductive material, such as versatility, durability, easy surface regeneration and integration, facile incorporation of a variety of (bio)modifiers or low background current, among others.

Accordingly, this thesis tackles the development of advanced amperometric nanocomposite sensors that having been optimized regarding to carbon/polymer composition ratios, can be tunable with different types of nanoparticles (NPs) for improving their electroanalytical efficiency.

The electrical properties of these nanocomposites and, therefore, their analytical applicability, are directly influenced by the conducting particles nature and the amount and spatial distribution of them through the insulating polymeric matrix. One of the most important electrochemical properties of these materials is the similarity of their electrochemical behavior with a microelectrode array. Thus, an optimization of the carbon/polymer ratio with respect to the nature of the conducting material will allow to achieve a greater dispersion of the conducting areas through the non-conducting areas, presenting similar benefits to the microelectrode array. In addition, it is known that some parameters, such as composite resistivity, heterogeneous electron transfer rate, material robustness and background capacitance current are strongly influenced by the physical nature of the raw CNT sample, such as their diameter/length ratio and purity, fact that may strongly influences the final electroanalytical response of the transducer material.

Under this context, the first step of this thesis consisted of implementing a group of instrumental techniques that, systematically applied, have allowed the characterization and optimization of nanocomposite materials composition based on CNTs and epoxy resin (Epotek H77) in relation to the nature of the raw CNT sample for the fabrication of more efficient electrochemical sensors. The developed characterization protocol includes electrical, electrochemical, morphological, microscopic, spectroscopic and electroanalytical tools.

Having been optimized the MWCNT/epoxy composition ratios, the next step consisted of enhancing the analytical performance of these electrochemical nanocomposite sensors introducing some electrocatalytical effect by the incorporation of different NPs. For this goal, a simple methodology for synthesizing a wide range of different NPs has been developed. Intermatrix Synthesis (IMS) has been used as a green technique to design three different routes for CNT/epoxy nanocomposite electrodes modification, which offer a customized way for the preparation of sensitive amperometric sensors.

Finally, the characterization and functionalization studies applied for CNT-based electrochemical nanocomposite sensors have been extended for nanocomposite materials based on another allotropic form of carbon: the graphene, which is the last discovery in terms of nanostructured carbon material.

RESUM

Dins de l'amplia gama de nanocompòsits, la incorporació de materials conductors de carboni nanoestructurats, entre els quals s'hi troben els nanotubs de carboni (NTCs) i el grafè, a dins d'una matriu polimèrica aïllant, és una forma molt atractiva de combinar les propietats mecàniques i elèctriques úniques del material de farciment amb els atributs dels plàstics. Concretament, els materials nanocompòsits basats en carboni han jugat un gran lideratge en el camp de l'electroquímica analítica, sobre tot en el desenvolupament de dispositius (bio)sensors, degut a les seves interessants avantatges respecte a un material conductor pur. Aquestes avantatges els hi proporcionen un alt valor afegit, com versatilitat, durabilitat, una fàcil regeneració de la superfície i integració, simplicitat a l'hora d'incorporar diferents (bio)modificadors o una baixa corrent de fons, entre d'altres.

En aquest sentit, aquesta tesi aborda el desenvolupament de sensors nanocompòsits avançats de tipus amperomètrics que, havent sigut optimitzada la seva relació carboni/polímer, poden ser modificats amb un ampli ventall de nanopartícules (NPs) per millorar-ne la seva eficiència electroanalítica.

Les propietats elèctriques d'aquests nanocompòsits i, per tant, la seva aplicabilitat analítica, es troben directament influenciades tant per la naturalesa de les partícules conductores com per la quantitat i distribució espacial de les mateixes a través de la matriu polimèrica aïllant. Una de les propietats electroquímiques més importants que envolten a aquests materials, és la similitud del seu comportament electroquímic amb el d'un array de microelèctrodes. Per tant, una optimització de la seva relació carboni/polímer respecte a la naturalesa del material conductor de partida, permetrà assolir una major dispersió de les àrees conductores a través de les zones no conductores, presentant així beneficis similars als d'un array de microelèctrodes. A més, és conegut que alguns paràmetres, tals com la resistivitat del material compost, la transferència electrònica, la robustesa del material i la corrent capacitiva es troben fortament influenciades per la naturalesa física de la mostra de nanotubs de partida, com

és la seva relació longitud/diàmetre i la seva puresa, fet que poden influir fortament la resposta electroanalítica final del material transductor.

Sota aquest context, la primera etapa de la Tesi va consistir en la implementació d'un conjunt de tècniques instrumentals que, aplicades de manera sistemàtica, han permès la caracterització i la optimització de la composició dels materials nanocompòsits basats en nanotubs de carboni i resina epoxi (Epotek H77) en relació a la naturalesa dels NTCs de partida per a la fabricació de sensors electroquímics més eficients. El protocol de caracterització dut a terme inclou eines elèctriques, electroquímiques, morfològiques, microscòpiques, espectroscòpiques i electroanalítiques.

Un cop optimitzada les proporcions de CNT/epoxi, el següent pas va consistir en millorar el rendiment analític d'aquests sensors electroquímics nanocompòsits incorporant-ne diferents NPs per a la introducció d'algun tipus d'efecte electrocatalític. Per arribar a aquesta fita, es va desenvolupar una metodologia simple per a la síntesi d'una ampla gama de NPs. La Síntesi Intermatricial (IMS) va ser utilitzada com a tècnica verda per al disseny de tres rutes diferents que permetin una incorporació personalitzada d'aquestes NPs dintre del material transductor, obtenint així sensors amperomètrics més sensibles a diferents analits.

Finalment, els estudis de caracterització i funcionalització implementats en els sensors nanocompòsits basats en NTCs han estat estesos a materials nanocompòsits basats en una altra forma al·lotròpica del carboni: el grafè, el qual és l'últim descobriment en termes de material de carboni nanoestructurat.

RESUMEN

Entre la amplia gama de nanocompósitos, la incorporación de materiales conductores nanoestructurados de carbono, entre los que se encuentran los nanotubos de carbono (NTCs) y el grafeno, dentro de una matriz polimérica aislante, es una forma muy atractiva de combinar las propiedades mecánicas y eléctricas únicas del material de relleno con los atributos de los plásticos. Concretamente, los materiales nanocompósitos basados en carbono han jugado un gran liderazgo en el campo de la electroquímica analítica, sobre todo en el desarrollo de dispositivos (bio)sensores, debido a sus interesantes ventajas con respecto a un material conductor puro. Dichas ventajas les proporcionan un alto valor añadido, como versatilidad, durabilidad, fácil regeneración de la superficie e integración, simple incorporación de (bio)modificadores o baja corriente de fondo, entre otras.

En este sentido, esta tesis aborda el desarrollo de sensores nanocompósitos avanzados de tipo amperométrico que, habiendo sido optimizada su relación carbono/polímero, pueden ser modificados con un amplio abanico de nanopartículas (NPs) para mejorar su eficiencia electroanalítica.

Las propiedades eléctricas de estos nanocompósitos y, por lo tanto, su aplicabilidad analítica, están directamente influenciadas tanto por la naturaleza de las partículas conductoras como por la cantidad y distribución espacial de éstas a través de la matriz polimérica aislante. Una de las propiedades electroquímicas más importantes que envuelven a estos materiales es la similitud de su comportamiento electroquímico con respecto a un array de microelectrodos. Por lo tanto, una optimización de la relación carbono/polímero con respecto a la naturaleza del material conductor de partida permitirá lograr una mayor dispersión de las áreas conductoras a través de las zonas no conductoras, presentando beneficios similares a los de un array de microelectrodos. Además, es conocido que algunos parámetros, tales como la resistividad del material compuesto, la transferencia electrónica, la robustez del material y la corriente capacitiva están fuertemente influenciadas por la naturaleza física de la muestra de nanotubos de

partida, como son su relación longitud/diámetro o su pureza, hecho que pueden influir fuertemente en la respuesta electroanalítica final del material transductor.

Bajo este contexto, la primera etapa de esta tesis consistió en la implementación de un conjunto de técnicas instrumentales que, aplicadas de manera sistemática, han permitido, la caracterización y optimización de la composición de materiales nanocompuestos basados en nanotubos de carbono y resina epoxi (Epotek H77) con respecto a la naturaleza de los NTCs de partida para la fabricación de sensores electroquímicos más eficientes. El protocolo de caracterización llevado a cabo incluye herramientas eléctricas, electroquímicas, morfológicas, microscópicas, espectroscópicas y electroanalíticas.

Una vez optimizada las proporciones de NTC/epoxi, el siguiente paso consistió en mejorar el rendimiento analítico de estos sensores electroquímicos nanocompuestos incorporándoles diferentes NPs con la finalidad de introducir algún tipo de efecto electrocatalítico. Para alcanzar este objetivo, se desarrolló una metodología simple para la síntesis de una amplia gama de NPs. La Síntesis Intermatricular (IMS) fue utilizada como técnica verde para el diseño de tres rutas diferentes que permitan una incorporación personalizada de estas NPs en el material transductor, obteniendo así sensores amperométricos más sensibles a diferentes analitos.

Finalmente, los estudios de caracterización y funcionalización implementados en los sensores nanocompuestos basados en NTCs han sido extendidos para materiales nanocompuestos basados en otra forma alotrópica del carbono: el grafeno, el cual es el último descubrimiento en términos de material de carbono nanoestructurado.

CHAPTER I

General Introduction

CHAPTER I

General Introduction

Nowadays, nanotechnology is a topic attracting scientists, industrialists, journalists, governments and even a common people alike. Nanotechnology has become a new era, also named the fourth industrial revolution, in which everybody has acknowledged that our future is *nano*. The concept of nanotechnology was first introduced by Nobel laureate Richard Feynman in 1959.¹ Since then, the recent advances in nanoscience and nanotechnology have brought novel devices and materials at the nanometer scale, mainly triggered by the demand of miniaturizing electronic, optical, sensing and actuating systems and their components. In this way, carbon nanotubes (CNTs) and other carbon nanostructures are supposed to be a key component of nanotechnology. Having realized their tremendous application potential in nanotechnology, a huge amount of efforts and energy has been invested in CNT projects worldwide since they were discovered in 1991 by Iijima.² The potential for nanocomposites reinforced with CNTs, having extraordinary specific stiffness and strength, represent tremendous opportunity for application in the 21st century.³

In this new era, the concept of nanocomposite has been resurfaced since it has been present in nature and used from historical times.⁴ In general, a nanocomposite material can be defined as the result of combining two or more different materials in solid phase where, at least, one of the constituent parts has a nanometer scale dimension.⁵ In addition, these (nano)materials do not lose their individual identities but still impart their properties to the product resulting from their combination. Building blocks with dimensions in the nanosize range enable us the possibility to design and develop new materials with unprecedented versatility and improvement in their physical and chemical properties.⁶ In this sense, the use of carbon nanostructures for developing nanocomposite materials is currently one of the most explored areas in materials science and engineering, and is becoming increasingly topical in analytical chemistry.⁷

Among the wide range of nanocomposites, the development of nanocomposites based on conductive phases dispersed in polymeric matrices has led to important

advances in electronics and electrochemistry.^{8,9} In general, nanocomposite materials based on different forms of carbon nanostructures as conductive phase (such as graphite, carbon nanotubes and graphene) have played a leading role in the analytical electrochemistry field, particularly in sensor devices due to their interesting advantages as easy surface renewal or low background current, among others.^{10,11,12} Specifically, incorporation of CNTs into a polymeric matrix is a very attractive way to combine the mechanical and electrical properties of individual nanotubes with the advantages of plastics.¹³ CNTs arise as ideal conducting phase due to their unique mechanical, chemical, electrical, thermal and structural properties.^{14,15} From an analytical point of view, CNTs dispersed in an inert matrix, provide interesting electrochemical properties since the polymeric matrix, together with the CNTs, confers mechanical robustness and high electric conductivity to the final nanocomposite sensor.¹⁶ Furthermore, its high malleability before being hardened allows an easy incorporation of a variety of modifiers, among others, nanoparticles (NPs),¹⁷ enzymes¹⁸ and chemical (bio)recognition agents.¹⁹ Despite the benefits of using electrochemical nanocomposite sensors based on CNTs, it is known that some parameters, such as composite resistivity, heterogeneous electron transfer rate, material robustness and background capacitance current are strongly influenced by the raw CNT nature, which in turn also affects the CNT/polymer composition ratio.

The main drawback in CNT-based nanocomposite materials to achieve both high reproducibility and repeatability on the electrochemical response of the sensor resides in the lack of homogeneity of the different commercial CNT lots. This fact is due to different amount of impurities in the nanotubes, as well as dispersion in their diameter/length and state of aggregation. Since these variations are difficult to quantify, an accurate characterization protocol of these physical parameters before being used as a conductor material for sensing purposes is required. Another important point of consideration is the optimization of the CNT/polymer ratio as function of the raw CNT nature. It has been demonstrated that optimizing this parameter is possible to improve the electrochemical properties and analytical response of the CNT-based nanocomposite sensors.²⁰ Depending on the conductive load, nanocomposites can behave as microelectrode arrays which are known to provide efficient mass transport of the electroactive species due to radial diffusion on the spaced carbon particles.²¹ This improvement on the mass transport favours the sensitive electroanalysis of a variety of

analytes. Moreover, the carbon surface chemistry also influences significantly the electron transfer processes at these sensors. Thus, a previous electrochemical characterization of the nanocomposites before being used as chemical sensors makes also mandatory to obtain devices with a similar behaviour to a microelectrode array.

Seeking to deduce the optimum CNT/polymer nanocomposite composition depending on the nature of the raw CNT has been the first objective of this research. Consequently, a description of CNTs and the different techniques to be synthesized and characterized, including physical parameters such as length, diameter and purity, will be first introduced. Secondly, research on the electrical percolation performance of CNT-based nanocomposites as well as the fundamentals of CNT electrochemical behaviour and its applications towards the development of nanocomposite sensors based on CNT dispersed in a polymeric matrix (mainly looked at epoxy resin, Epotech H77) will be highlighted. Furthermore, different morphological strategies may be used to fully understand the electrochemical behaviour of the CNT-based nanocomposite materials and the dispersion of their conducting microzones in the polymeric matrix, and thus they will be also focus of discussion.

In addition, the functionalization of CNTs with different NPs is showing an upward trend up during the last few decades. NPs, and concretely metal nanoparticles (MNPs), have been used extensively in the fields of physical, chemical and material sciences due to their surface-volume ratio that gives them special properties, different from the analogous bulk material.^{22,23} Combining the unique properties of CNTs and MNPs, the resulting advanced nanomaterials have shown excellent electrocatalytic activity due to the fast electron transfer ability of these modified-CNTs, leading to an enhancement of the electron transfer between redox centres in the analyte and the sensor.^{17,24} Quantum Dots (QDs) are a relevant type of NPs, concretely semi-conducting NPs, which have generated considerable interest in optical and semi-conducting properties,^{25,26} and are already being employed for electrochemical sensing.²⁷ Due to these facts, the improvement of the electrochemical response of the optimized-nanocomposite sensors with different kinds of NPs, such as Pd-NPs, Au-NPs, CuO-NPs and CdS-QDs has been also focused of study in this research. Because of this, the synthesis of these NPs and their use as catalysts, molecular supports, and novelty as scattering materials have also been presented.

Finally, the characterization studies applied for CNT-based electrochemical nanocomposite sensors have been extended for nanocomposite materials based on another allotropic form of carbon: the graphene, which is the last discovery in terms of carbon nanostructure material.²⁸ Graphene oxide (GO), which is generated from graphite oxide, has attracted strong scientific and technological interest in recent years.²⁹ It has shown great promise in many applications, such as polymer composites, energy-related materials, sensors, ‘paper’-like materials and biomedical applications because of its unique physicochemical properties: high surface area, excellent thermal and electric conductivity, as well as strong mechanical strength.^{28,30} Furthermore, GO-based electrodes and its reduced form (reduced graphene oxide, rGO) have shown superior performance in terms of electrocatalytic activity and macroscopic scale conductivity than CNTs.^{31,32} These indicate that the opportunities in electrochemistry encountered by CNTs might be available for graphene. For its promising electrochemical features, GO has been synthesized, reduced, modified and used for electromechanical sensing purposes. Thus, a few descriptions about graphene and their nanocomposite materials will be also introduced.

1.1 Carbon Nanotubes

Carbon is considered a singular element which has led to molecules able to create new materials or even life through Mother Nature. Before the discovery of C₆₀ fullerene in 1985 by Kroto,³³ the classical allotropes of carbon (diamond and graphite) were the only known. Thanks to the enrichment provided by this third allotropic form of carbon, carbon-based nanostructures have become one of the hottest research topics in science. Afterwards, CNTs were rapidly discovered and, since then, they have constituted a significant milestone in modern analytical sciences.³⁴ The first observation of their formation in substantial quantities was described by Iijima in 1991,² although the first evidence for nano-sized carbon tubes is believed to have been published in 1952 by Radushkevich and Lukyanovich.³⁵ Even though the most usual forms of this nanomaterial are formed by one (single wall carbon nanotubes, SWCNTs), two (double wall carbon nanotubes, DWCNTs) or multiple cylindrical layers of graphene sheets (see Figure 1.1), the advances in generation of CNTs has led to new structures with fascinating geometries.³⁶ Delgado *et al.* have recently reviewed the general

characteristics of these new forms, which includes cup-stacked carbon nanotubes, carbon nanohorns, carbon nanotori or carbon nanobuds.³⁷

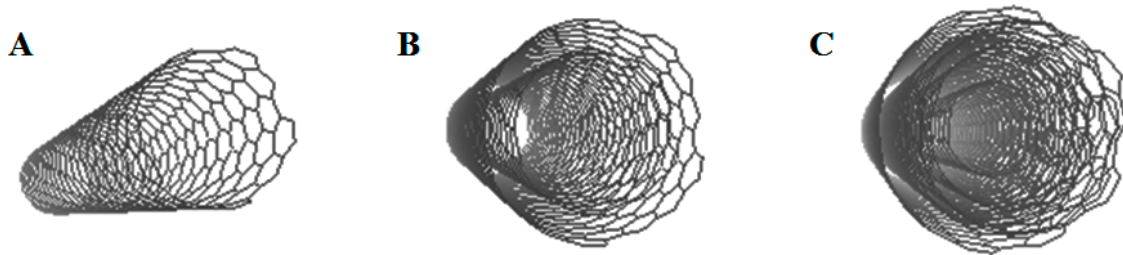


Figure 1.1 Different forms of CNTs, which are formed by A) one (SWCNTs), B) two (DWCNTs) or C) multiple cylindrical layers of graphene, respectively.

Regarding CNTs, they are built from sp^2 carbon units and present a seamless structure with hexagonal honeycomb lattices. CNTs have closed topology and tubular structure and are typically several nanometers in diameter and many microns in length.³⁸ While the circular curvature makes σ bonds which are slightly out plane, the π orbital is more delocalized outside the tube.³⁹ The diameter and helicity of a defect free CNT can be uniquely characterized by the chiral vector (C_h), also called the Hamada vector, which connects crystallographically equivalent sites on a two-dimensional graphene sheet. Although graphite is a semi-metal, CNTs can be either metallic or semiconducting due to the topological defects from the fullerene-like end caps in CNTs (pentagons in a hexagonal lattice), which can be predicted by Hamada vector.⁴⁰ Hamada vector is defined by a pair of integers (n, m) defining the number of unit vectors along the directions a_1 and a_2 , as is shown in Figure 1.2. The angle between the chiral vector and zigzag nanotube axis is the chiral angle θ . Chiral angle together with the integers n and m already introduced before reveal three types of CNTs with these values: when $n = m$, the nanotube is called “armchair” type ($\theta = 0^\circ$); when $m = 0$, then it is of the “zigzag” type ($\theta = 30^\circ$). Otherwise, when $n \neq m$, it is a “chiral” tube and θ takes a value between 0° and 30° . The value of (n, m) determines the chirality of the nanotube and affects the optical, mechanical and electronic properties. In the case of MWCNTs, there are a number of morphological variations possible depending on the conditions and chosen method of CNT formation. They can be formed as “hallow-tube”, “herringbone” or “bamboo-like”, as is also shown in Figure 1.2.

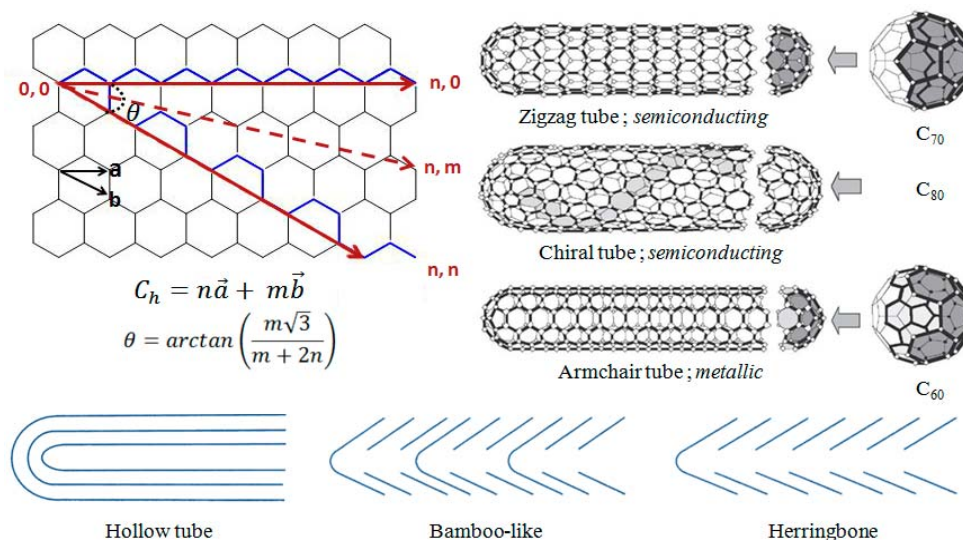


Figure 1.2 The different forms of CNTs can be defined as a chiral vector (C_h) formed by the components m and n . The C_h indicates how an infinite graphene sheet would be rolled up to make the tube. If $n \neq m$, the tube is metallic, otherwise it is a semiconductor. Appearance and names of the different types of nanotubes are defined by their rolling-up vector (adapted from Cooper, *et al.*⁴¹). Furthermore, an schematic cross-section through MWCNTs is also presented, showing various morphological variations (adapted from Banks, *et al.*⁴²).

Regarding those, herringbone and bamboo-like MWCNTs possess a proportionally higher number of edge-plane-like defect sites than hollow-tube MWCNTs because in the former two cases the plane of the graphite sheets is at an angle to the axis of the tube. This means that more graphite sheets must terminate at the surface of the tubes as an edge-plane-like site, where it is believed that these sites are responsible for much of the chemical and electrochemical activity of the CNTs. Thereby, the physico-mechanical properties of CNTs are dependent upon their dimensions, helicity or chirality.⁴³

At present, CNTs are manufactured by different methods in laboratories and industry. There are three basic methods to produce high quality CNTs: laser ablation (laser vaporization), electrical arc discharge and chemical vapour deposition (CVD), which are reported in Table 1.1.^{34,44}

The first two, employing solid state carbon precursors, lead to near perfect nanotubes structures, with large amounts of by-products being formed. Otherwise, CVD methods use hydrocarbon gases as sources of carbon atoms and catalyst particles that serve as seeds to nucleate the growth of CNTs. Recently, arc discharge in liquid media has been developed to synthesize several types of carbon nanostructures such as: carbon

onions, carbon nanohorns and CNTs.⁴⁵ The as-produced material is known to be inhomogeneous and contains a variety of impurities including carbon-coated metal clusters, amorphous carbon and other carbon compounds as fullerenes. The type and extent of these impurities change with the production method used. For this fact, different purification methods have been developed to remove the amorphous carbon and metal impurities, mainly based on acidic treatments.^{46,47} On the other hand, in spite of using the same methodology to grow CNTs, other physical properties of the raw material, such as length and diameter, tend to vary from sample to sample and can have a profound effect on the performance of the material for a given application. Accordingly, a primarily bulk measurements and characterization should be taken to distinguish among different types of CNTs.

Table 1.1 A summarized of the most common CNTs synthesis techniques and their advantages and disadvantages.

Method	Laser Ablation	Arc Discharge	CVD
Basics	Graphite target is vaporized by laser irradiation under flowing inert atmosphere and high temperature	Electric arc discharge generated between two graphite electrodes under an inert atmosphere	Decomposition of hydrocarbon gases in the presence of metal catalyst
SWCNTs	Long, 1 – 2 nm diameter	Short, 1.2 – 1.4 nm diameter	Long, 0.6 – 4 nm diameter
MWCNTs	Not applicable but possible	Short, 1 – 3 nm diameter	Long, 100 – 200 nm diameter
Yield	> 65%	> 90%	~ 100%
Advantages	High purity, defect free SWCNTs	Easy, defect-free CNTs, no catalyst	High purity, large scale production, simple
Disadvantages	Expensive, low scale production	Short, tangled nanotubes, random structures	Limited control over the structures, defects

Among the most common tools to characterize the morphologies and dimensions of raw CNTs (in powder form), Scanning Electron Microscopy (SEM) and Transmission Electron Microscopy (TEM) are by far the most popular.^{48,49,50} At the present, SEM and TEM imaging are used to characterize the overall morphology of MWCNT samples, and are also used to quantify the degree of purity within samples, as well as the dimensions of the nanotubes, as shown in Figure 1.3. The diameter of CNTs can be

roughly estimated from SEM/TEM images recorded at magnifications of greater than 20,000x for SEM and 100x for TEM. A representative average value and distribution of diameters is obtained from multiple and independent SEM/TEM images, compiling, at least, 250 tubes. Due to tube diameter is SEM dependent, it is recommended an accurate characterization with TEM and High Resolution Transmission Electron Microscopy (HR-TEM) analysis. Regarding the tube length, it can be estimated only if the tubes are straight and distinguishable. Thus, a great dispersion of the CNTs is necessary to estimate the average length. This problem can be resolved with an ultrasonic pre-treatment as well as optimizing the CNT concentration.⁵¹

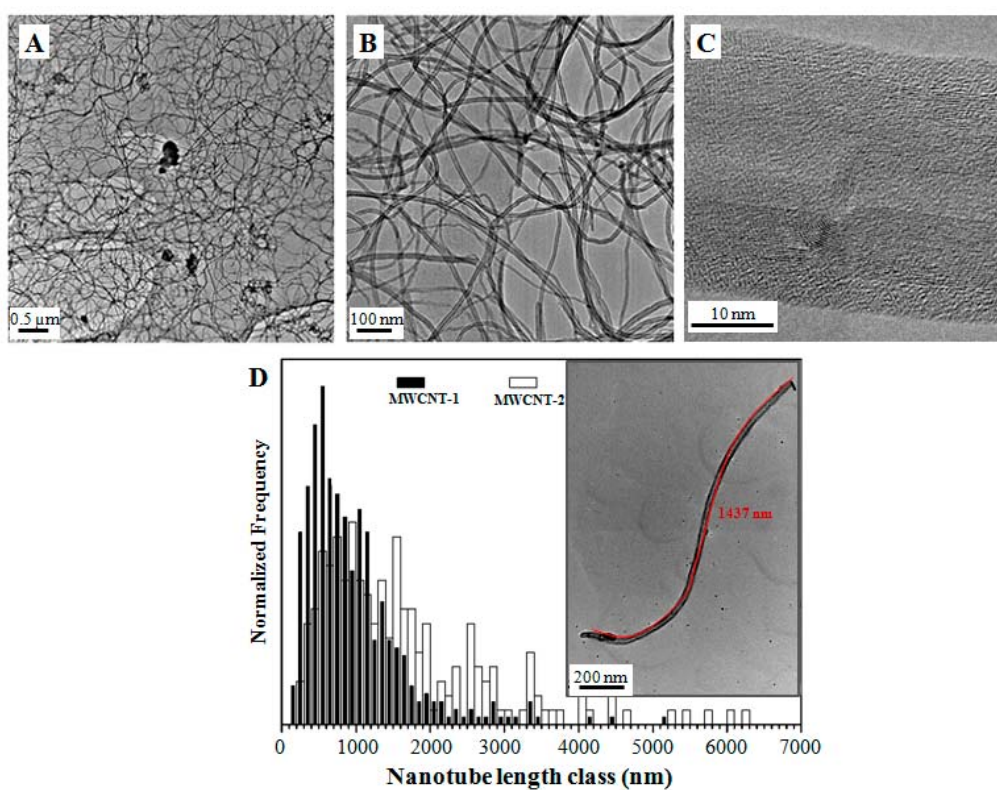


Figure 1.3 HR-TEM images of A) non-purified MWCNTs and B) purified MWCNTs; C) magnification of B). D) Length distribution of two different MWCNTs (adapted from Krause, *et al.*⁵¹), including an exemplary length measurement of one MWCNT.

For the characterization of CNT purity, an ensemble of measurements including Raman spectroscopy, thermogravimetric analysis (TGA) and X-ray microanalysis can be used to assess the quality of the sample, as shown in Figure 1.4. TGA is one of the most straightforward methods to characterize CNTs due to can be used to analyze the nanotubes powder directly, giving the percentage of amorphous carbon, catalytic metals

and graphitic structured carbons within the bulk sample.^{52,53} It is a destructive technique that measures carbon mass loss as a function of temperature, under assumption that upon heating to 1000 °C in air all carbon and metal are converted in the corresponding oxides.⁵⁴ The number of oxidation temperature peaks observed is also an indicator of material purity. The width of the peak can be used to indicate the amorphous carbon content on CNTs, with a narrow peak indicating a cleaner material.⁵⁵

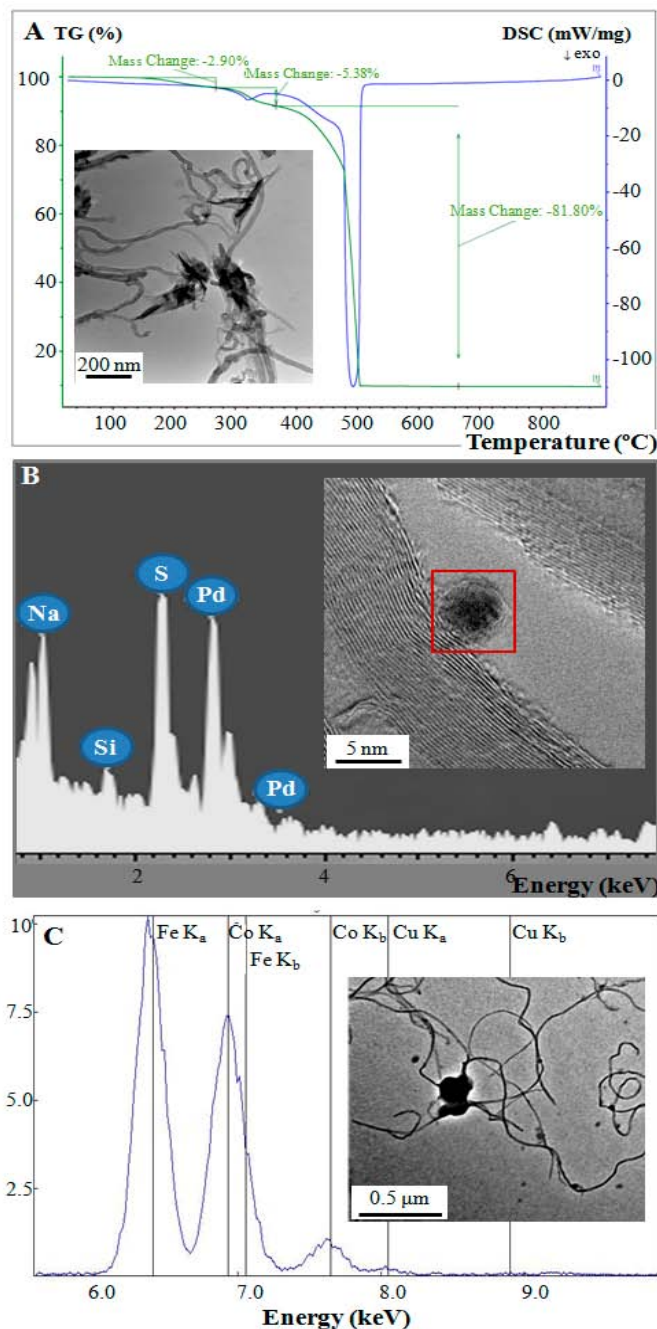


Figure 1.4 Different tools to characterize the purity of CNTs. Examples of A) TGA analysis corresponding to MWCNTs containing CuO-NPs; B) EDS spectrum corresponding to MWCNTs containing Pd-NPs and C) XPS spectrum corresponding to non-purified MWCNTs.

While TGA provides quantitative information about the percentage of catalytic metals in the CNTs, the percentages of different carbon forms are only semiquantitatively determined. Furthermore, TGA provides only quantitative data on the presence of total metal content in CNT material. For this reason, different techniques are needed to identify and quantify the metal content on raw CNT material. In this way, Energy Dispersive X-ray Spectroscopy (EDS) and X-ray Photoelectron Spectroscopy (XPS) are, respectively, the mainly tools used for identifying and quantifying the metal impurities present on the raw carbon material.^{56,57}

EDS spectra indicate the relative amounts of metals and other non-carbon elements in CNT materials. While EDS is a useful tool to identify metal content in CNTs, this tool tends to be reliable in determining carbon because of hydrocarbon contamination present in all SEMs and TEMs, and poor sensitivity of EDS detectors in the low-energy end of spectrum, where carbon peak is found. Therefore, XPS is usually used to determine the elemental composition of the samples. XPS is a simple and quick method to determine the average composition; practically no sample preparation is necessary. Its disadvantage is that it requires relatively large amounts of samples (50–100 mg). Finally, as it is shown in Figure 1.4, TGA, EDS and XPS can be also used to determine the metal content in CNTs when they are functionalized with different nanoparticles as well as their metal impurities content.¹⁷

Optical characterization reveals information regarding colour, purity defects and other properties. Fourier Transform Infrared Spectroscopy (FTIR) technique is commonly used to investigate the functional groups on the CNT surface.⁵⁸ CNT walls are not reactive, but their fullerene-like tips are known to be more reactive. Many applications utilizing CNTs require chemical modification on their walls to make them more amenable to rational and predictable manipulation. Different modification methods are used to generate functional groups (e.g. $-\text{COOH}$, $-\text{OH}$ or $-\text{C}=\text{O}$).⁴³ The extent of functionalization alters the wettability of the nanotubes in various surfactants and may thus also alter the toxicity. The main peaks that can be observed in a typical FTIR spectra of CNTs are: $\sim 1700\text{ cm}^{-1}$ ($-\text{COOH}$ groups), between 1580 and 1200 cm^{-1} (G-band and D-band, respectively), several peaks in the range of 3000 cm^{-1} (CH_x groups) and around 3400 cm^{-1} (associated with $-\text{OH}$), see Figure 1.5 A.^{58,59} On the other hand, for sp^2 carbon nanostructures such as graphene or CNTs, Raman spectroscopy

yields information about the purity, crystallite size, defects and tube alignment, and assists in the distinction the presence of MWCNTs relative to other carbon allotropes.⁶⁰ While this technique has been strikingly successful at describing the structural properties of SWCNTs, the interpretation of the spectra from a MWCNT is often very complicated.

For Raman scattering, MWCNTs can be said to be an ensemble of carbon nanotubes with diameters ranging from small ($< 0.5 \mu\text{m}$) to very large ($> 5 \mu\text{m}$). Despite this, a number of reports have indicated that Raman spectroscopy can have qualitative and even quantitative characterization power.⁶¹ Three aspects of Raman spectra are sensitive enough to provide unique information about the similarities and differences between the various carbon nanostructures, see Figure 1.5 B. These three aspects are: the G-band at $\sim 1582 \text{ cm}^{-1}$, which is common to all sp^2 carbon forms, the radial breathing mode (RBM) that makes the diameter and optical transition energy analysis of nanotubes possible and the D and G' bands that are significant in providing information about the electronic and geometrical structure through the double resonance process.⁶²

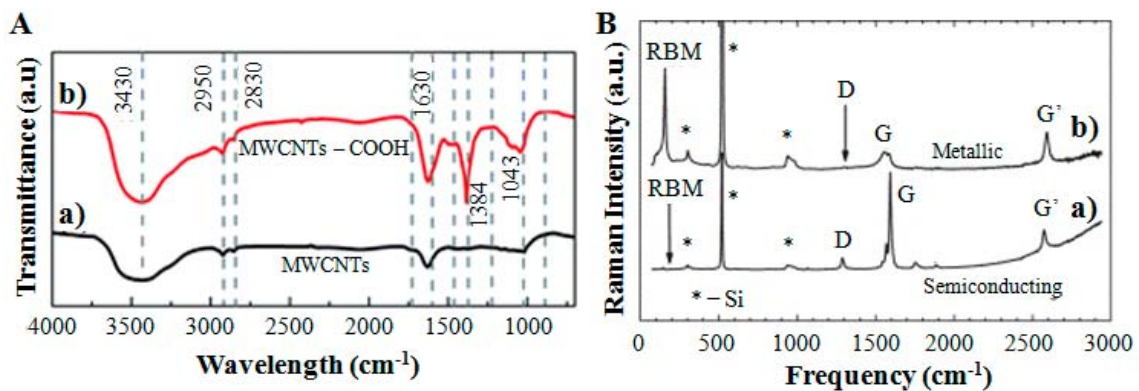


Figure 1.5 A) FTIR spectra corresponding to a) MWCNTs and b) acidic functionalized MWCNTs (MWCNTs-COOH). The strong peak around 3430 cm^{-1} (O-H stretching mode) and the peaks at 1384 cm^{-1} and 1043 cm^{-1} (C-OH and C-O stretching vibrations, respectively) verify the presence of carboxylic groups. B) Raman spectra as useful tool to identify (a) a metallic and (b) a semiconducting SWCNT at the single nanotube level. Both images have been adapted from Vinayan *et al.*⁶³ and Dresselhaus *et al.*,⁶⁰ respectively.

Finally, recent studies revealed that Near Infrared (NIR) absorption spectroscopy is a powerful technique to determine the purity indexes (NIR-PI) of SWCNTs.⁶⁴

1.2 Conducting nanocomposite electrodes based on CNTs for electrochemical purposes

Over the last 20 years, the number of publications detailing the unique mechanical, electrical, magnetic, optical and thermal properties of CNTs as well as potential areas of application has risen exponentially.⁶⁵ CNTs present unique atomic structure and properties, such as high aspect ratio, high strength-to-weight ratio, extraordinary mechanical properties (with an elastic modulus in the order of 1-2 TPa and tensile strength around 200 GPa),^{14,66} as well as high thermal conductivity (about twice as high as diamond)⁶⁷ and electrical conductivity (with an electric-current-carrying capacity 1000 times higher than copper wires).⁶⁸ These properties have led CNTs to their use as fillers in polymeric matrix nanocomposites.³

The effective utilization of CNTs in nanocomposite applications depends strongly on the ability to disperse them homogeneously throughout the matrix. This is a necessary condition for the improvement of the mechanical properties of such nanocomposites and better stability of the systems. There are different supporting materials for the incorporation of CNTs, including: amorphous, semicrystalline, thermoplastic, water-soluble, and conjugated polymers; resins; ceramics and metal matrices.^{69,70} Concretely, polymers play a very important role in numerous fields of everyday life due to their advantages over conventional materials (e.g. metals) such as lightness, resistance to corrosion, low-cost production, and ease of processing. Fillers are used in polymers for a variety of reasons: improved processing, density control, optical effects, thermal conductivity and control of thermal expansion. Moreover, improve electrical, magnetic and mechanical properties. The extraordinary properties of CNTs make them very promising and favourable as fillers for fabrication of a new class of polymeric heterostructures (polymer nanocomposite materials).¹³

Polymer nanocomposites are a class of materials in which nanometer scaled different nanomaterials are dispersed in an organic polymer matrix in order to improve the structures and properties of the polymers effectively. Advanced morphologies and improved properties are expected from the polymer nanocomposite materials due to the synergetic effect of the comprising components which could not be obtained from the individual materials. In this way, the incorporation of a small amount of nanomaterial (e.g. CNTs, graphite, graphene, nanodiamonds) into the polymeric matrix significantly

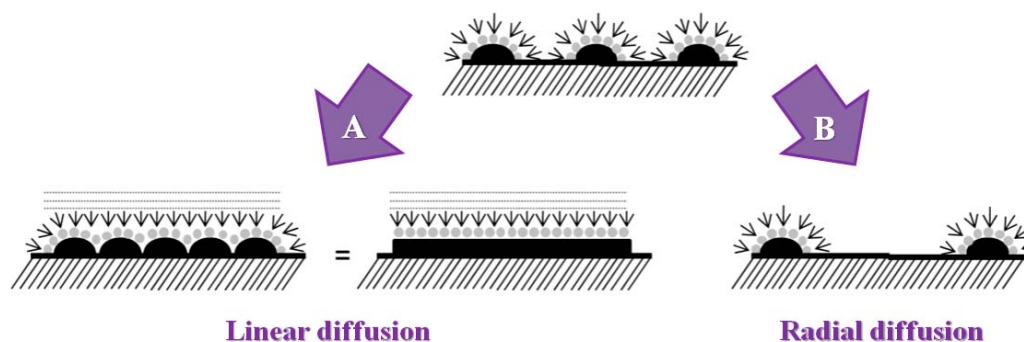
improves the performance of the polymer material. If any of its parts are conductor, the resultant nanocomposite material becomes conductor and such property confers it a suitable feature in order to be used as electrochemical sensors.

In this way, a key feature in any electrochemical sensor is a good detection limit that is associated with a high signal-to-noise ratio. The background current or noise in a macrosensor made of a pure conducting phase depends on the sensing area. This means that a contraction of the electroactive sensing surface implies a curtailment of the sensitivity as well. However, in accordance to the equation derived by Oldham,⁷¹ if the area is very small, as in microelectrodes, the perimeter of the surface has a more significant influence on the mass transport than the area itself. This is translated to a better sensing function, since a non-linear diffusion is established which generates a steady-state current that increases the signal-to-noise ratio. This is known as the Edge effect along with the reduced size of the electrode it has interesting and useful results. However, the generated currents are very low, calling for sophisticated and expensive voltammetric equipment. Hence, whenever small size is not required, the use of arrays or ensembles of microelectrode arrays is desirable. These ensembles can be seen, for example, as a macroelectrode formed by a great number of carbon filler microelectrodes. These microelectrodes are separated by an insulator and connected in parallel. The signal is the sum of the individual currents generated by each microelectrode. The end product is a sensor with a signal as strong as that of a macroelectrode but showing the signal-to-noise ratio of a microelectrode.

For a pre-design surface of a carbon microelectrodes array, Weber *et al.* showed that the layout of such an array has a maximum efficiency when the separation between the microelectrodes is around $0.1\ \mu\text{m}$.⁷² However, the implicit difficulty of constructing these electrodes is very high. On the other hand, electrodes based on carbon-based (nano)composites with a random distribution are easier to prepare. Indeed, in certain conditions, their electrochemical characteristics can resemble very well to a random ensemble microelectrode, all depends on the filler composition, its size, its layout, etc. One example is the study performed by O'Hare *et al.* for a random graphite/epoxy composite system.⁷³ Like the microelectrodes array, the composite electrodes present the possibility to generate higher current intensity. Such improvement is due, among

other things, to the way that the electroactive species diffuse on the electrode surface, which are radial or linear (see Scheme 1.1).

Accordingly, the carbon loading within polymeric matrix strongly influences the overall analytical performance of composite electrodes. It is due to that carbon loading influences directly not only on the electroactive surface but also on the inner structure (bulk resistance) of the composite material. Both parameters strongly affects on the overall analytical performance of such electrodes, as Zhao *et al.* shows in their studies.⁷⁴ The volume fraction of carbon has to be high enough in order for the carbon particles to be in contact for providing conducting pathways and sufficient low bulk resistivity.



Scheme 1.1 Scheme of the different diffusional modes in an array system. In the case A) the microelectrodes are too close, providing a linear diffusion due to the overlapping of each diffusion layer of each electrode in the array. In the case B) the microelectrodes are too far, providing a decrease of the sensitivity and higher bulk resistivity.

Under this context, the electrical properties of the conducting nanocomposite depend on the nature of each different (nano)component, their relative quantities and their distribution. Hence, a valid approximation to evaluate the conductivity behaviour of nanocomposite materials is by means of the percolation theory. This theory was developed by Broadbent and Hammersley in 1957.⁷⁵ However, it was not applied to describe the conductivity behaviour in a random conductive nanocomposite material until 1970.⁷⁶ The most important parameter that this theory contributes to is called percolation threshold. The percolation threshold is known as the lowest concentration of conductor material at which an interconnected network between polymeric matrix and conductor material can be formed.⁷⁷ In 1995, the percolation theory was applied for the first time to interpret analytically several aspects of the composite behaviour.⁷⁸ Recent examples of its application are the studies provided by Li *et al.* and Montes *et al.* In the

first work, the theory percolation is applied to compare different fabrication processes of composite materials based on carbon black.⁷⁹ The second one is based on the optimization of the optimum graphite load in epoxy biocomposites to improve the electrochemical and electroanalytical response of voltammetric biosensors.⁸⁰

Regarding CNTs, their dispersion in an orderly way in polymeric matrices can form an interconnected network at very low volume fractions due to their high aspect ratio. The low percolation thresholds attainable with CNTs can give them a competitive advantage over other more conventional conductive fillers such as carbon black⁸¹ or graphite¹⁰. Numerous studies have been performed on the evaluation of the electrical percolation threshold of CNT/polymer systems.^{82,83,84} Basically, such studies confirm, on the one hand, that the electrical properties depend on several parameters, such as nature, shape and size of the filler, the filler loading, matrix properties, fabrication process and dispersion of the filler in the matrix and electrode surface. On the other hand, it is also confirmed that the electrical properties affect directly on the electrochemical properties of the carbon-based nanocomposite materials as well as the electrode reproducibility due to the handmade electrode fabrication. Olivé-Monllau *et al.* presented the percolation curve of MWCT-based epoxy nanocomposite electrodes in which the construction of such curve represented the first step to optimize the nanocomposite composition for amperometric purposes.¹¹ Following the Figure 1.6, different zones can be distinguished regarding the electrical behavior of the nanocomposite material based on MWCNTs. The first zone (a) is the high resistance zone composites (HRC), and thus lowly conducting. The second one (b) is named percolation zone composites (PC), where the material starts to be conductor and possess high resistivity. The near-percolation zone (NPC) or second percolation zone (c) is where the material enhances its conductivity and decreases its resistivity to current flow. The last one (d) is the low resistivity zone composites (LRC), in which its conductivity is maximum.

To date, the conventional criteria used for the optimization of nanocomposite based on conductor materials dispersed in a non-conductive matrix only took account the electrical properties obtained from the percolation curve.^{85,86} Thus, the maximum load of conductor material was used as the optimum composition ratio, which allows the nanocomposite to be robust from a mechanical point of view. However, it has been

demonstrated that the dispersion of the conducting particles in the nanocomposite affects the electrochemical properties of the resultant nanocomposites, such as the rate of electron transfer and the background capacitance current, as well as the material stability. For this fact, a previous characterization of these materials, in terms of optimizing the CNT/polymer composition ratio, is essential to achieve electrochemical electrodes which provide the best electrochemical response for their subsequent application as analytical sensors.

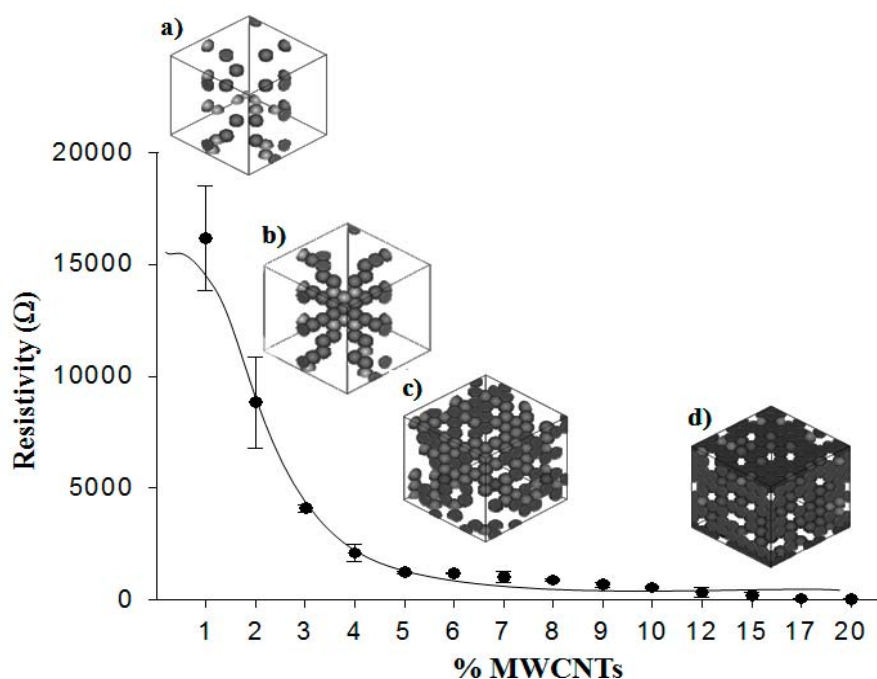


Figure 1.6 Theoretical dependence of nanocomposite resistivity on conductive filler content. a) HRC; b) PC; c) NPC and d) LRC.

1.3 Electrochemical nanocomposite sensors based on CNTs

A useful definition for a chemical sensor is “a small device that, as the result of a chemical interaction or process between the analyte and the sensor device, transforms (bio)chemical information of a quantitative or qualitative type into an analytically useful signal”. The definition is illustrated in Figure 1.7. All chemical sensors contain two basic components: a chemical recognition system (receptor) and a transducer, which transforms the stimulus measured at the receptor (primary signal) into a processable and measurable signal (secondary signal). There are a wide range of chemical sensors reported in the literature, which have been classified by IUPAC as optical, mechanical, electrical, electrochemical, thermal magnetic or piezoelectric sensors. Among these, the

electrochemical sensors have attracted a greater interest in the development of chemical sensors due to their remarkable sensitivity, experimental simplicity and low cost. Unlike other techniques, the electrochemical process takes place in the electrode–solution interface, without the necessity to interact with the whole volume of sample. The signal from an electrochemical sensor is electronic in nature, being a current, voltage or impedance/conductance changes caused by changing analyte composition or quality. As a result, three categories of electrochemical sensors can be described by conventional definition: amperometric, potentiometric or conductimetric sensors, respectively.⁸⁷

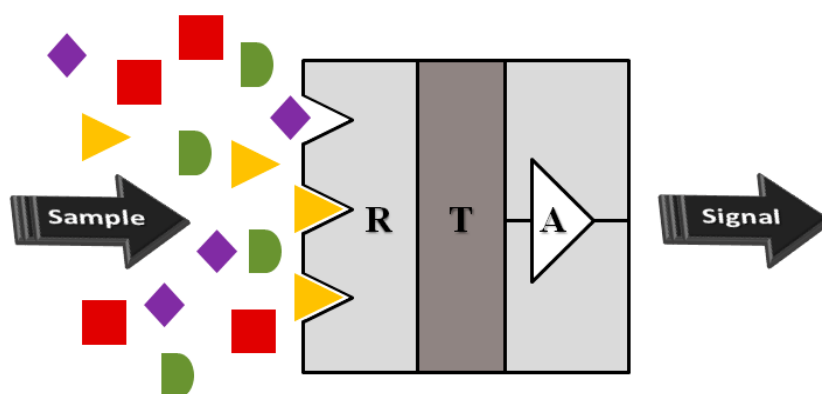


Figure 1.7 Schematic diagram how a chemical sensor operates. Only one component of the sample is recognized by the recognition system (R). The signal associated with this recognition process is converted into an electric signal by the transducer (T), which will be amplified (A), processed and subsequently expressed in data.

Carbon composites for electrochemical applications were introduced in 1958 by Adams, which consisted of a mixture a polycrystalline graphite powder with water-immiscible insulating organic liquid.⁸⁸ After that, other polymer alternatives have been used, such as epoxy, Nafion or conducting polymers, for a wide range of issues, including electroanalysis, pharmaceuticals, redox processes, biological and mechanistic electrochemistry.^{80,85,89} Concretely, CNTs offer exciting opportunities for the development of new nanocomposites in the electrochemical microelectrodes field because of their interesting electrochemical properties.⁹⁰ Electrochemical experiments with electrodes based on CNTs have shown an enhancement of their electron transfer reactivity, exhibiting strong electrocatalytic activity for a wide range of compounds, such as neurotransmitters,⁹¹ β -nicotinamide adenine dinucleotide,⁹² hydrogen peroxide,⁹³ ascorbic acid,⁹⁴ hydrogen sulphide,⁹⁵ glucose,⁹⁶ and cholesterol,⁹⁷ among others.⁹⁸ There are different studies where the origin of the electroactivity of CNTs has

been established, which is mainly attributed as much to presence of reactive groups on the surface as to the curvature of the tubes that originate changes in the energy bands close to the Fermi level.^{99,42}

In general, lower overpotentials and higher peak currents are observed in the voltammetric response of several molecules at CNT–modified electrodes compared to other electrode materials, which enables lower detection limits and enhanced sensitivity.¹⁰⁰ Comparing to conventional solid carbon electrodes such as the typical glassy carbon electrodes or other metal electrodes, CNT–based nanocomposite electrodes present a series of benefits, such as: (i) the host polymer provides big robustness to the final nanocomposite electrode; (ii) an easy surface renewal; (iii) randomly exposed edges on the electrode surface (usually quite electrochemically reactive); (iv) CNT–based nanocomposites retain the wide potential window of carbon materials compared with the conventional metals; (v) a considerable small background current, which is responsible of the noise in the electrochemical signal and (vi) under certain conditions, they can behave as an array of microelectrode with all the advantages that they comprise for electroanalytical applications.

Regarding the background current (v), it is responsible of the noise in the double layer charging capacitance of the electrode which is mainly determined by the electroactive area (A), that is the fractional area of conductor material (CNTs) exposed to the solution. For a composite electrode, the electroactive area is much smaller than the geometric area (A_{geom}) of the electrode since the remaining part is coated with the host polymer. On the other side, the Faradaic current related to the electrochemical electron transfer process is more proportional to the geometric area of the electrode if the electroactive areas are not so far away from each other. This makes the electrochemical signal to noise ratio be proportional to A_{geom}/A and hence, bigger than in the case of conventional metal electrodes of the same geometric area. Furthermore, the fact that the CNT–based nanocomposite electrodes can behave as an array of microelectrodes (vi), makes them the possibility to generate higher current intensity (Figure 1.8). Such improvement is due, among other factors, to the way that the electroactive substances diffuse on the electrode surface. Two different kinds of diffusion, radial and linear, are known.

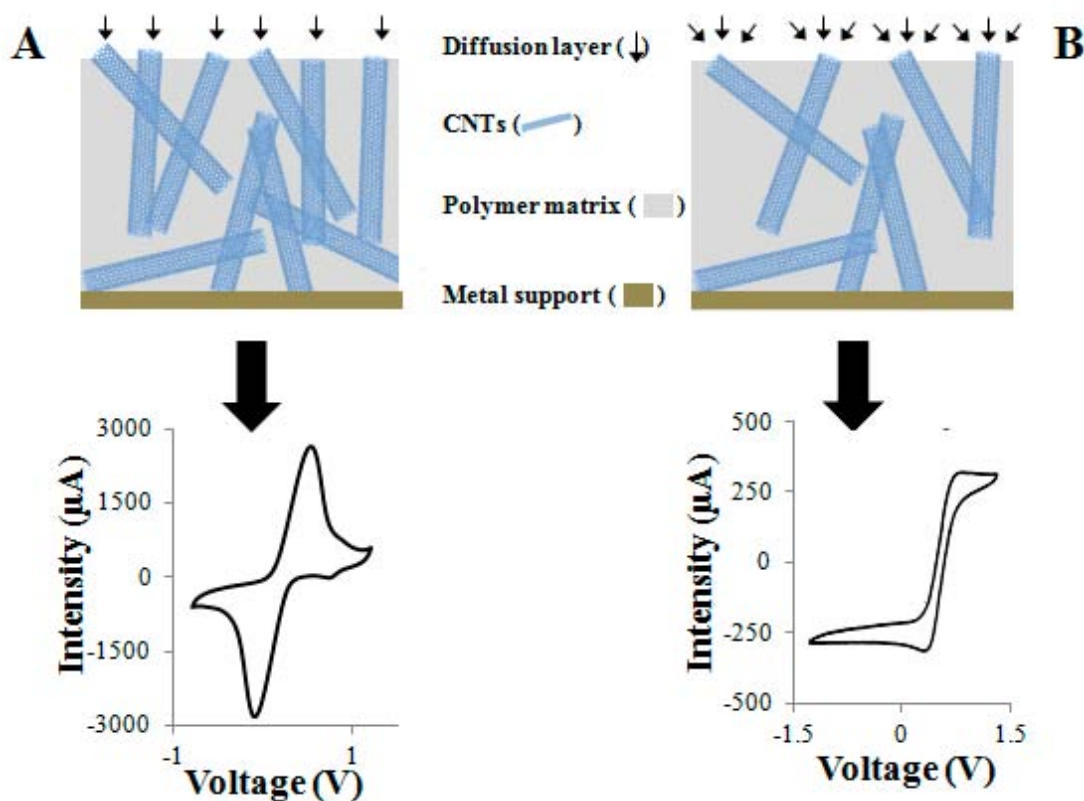


Figure 1.8 Schematics showing the diffusion profile of the electroactive species for nanocomposite electrodes containing A) 20% and B) 5% in MWCNT load. Where in A) the active exposed areas are closer, generating a linear diffusion of the electroactive species, in B) the conductive microzones are sufficiently far away that the diffusion profiles are hemispherical (microelectrode array behaviour). Adapted from Esplandiu *et al.*²¹

The linear one is usually given in solid electrode surfaces and the diffusion of the electroactive species is linear from bulk solution to electrode surface. On the other hand, the radial diffusion is usually given in array systems where alternating zones of conductive and non-conductive zones are present at certain interdistances. Such radial diffusion provides an increase of the mass transport to the interfacial reaction zone. From an electrochemical point of view, such increase in the mass transfer favours positively the electroanalytical signal, exhibiting low noise current which leads to lower limits of detection than macroelectrodes.¹⁰¹ Accordingly, both of these factors, the low background current and the enhanced mass transport lead to enhanced signal to noise ratios, high sensitivity, fast electrode response and low detection limits.

However, CNT-based nanocomposites present difficulties that can limit the desired electrochemical performance, such as difficulties in the dispersion and adhesion of CNTs with the polymer host and the lack of homogeneity of the different commercial

CNT lots, which includes different amounts of catalyst or amorphous carbon impurities in the nanotubes, as well as big dispersion in their diameter/length. These variations are difficult to quantify and make mandatory not only an electrical characterization but also an electrochemical characterization of the nanocomposite before being used as electrochemical sensor. Recently, this characterization has been performed by voltammetric techniques for the determination of electrochemical behaviour of conductive–non conductive phase composites as a function of different parameters, including thickness, proportion ratio and resistance of the composite electrode.⁷⁴ Under this context, another point of consideration is the optimization of the CNT loading in the nanocomposite materials for improving their electrochemical properties for analytical applications.

As mentioned before, the optimization of the carbon–based nanocomposite proportions of many research groups has been done under the criterion of maximizing the conductive material loading without losing its physical and mechanical stability. The goal of this criterion is to confer the lowest bulk resistivity value. However, working with nanocomposite electrodes based on the maximum attainable carbon loading has a series of limitations, including the low reproducibility of the nanocomposite electrochemical performance due to the heterogeneity of the different commercial lots of CNTs. At the same time, high carbon loadings can increase the background current and smear the Faradaic signal response, especially when the electroactive species are present in low concentration. Under this context, it is important to consider not only the conductivity of the nanocomposite material (which can be extracted from the electrical characterization through the percolation curves) but also the reproducibility regarding their electrochemical properties. In this way, and taking into account the main goal of this work, which is based on developing optimized CNT–based epoxy nanocomposite electrodes for their use in electroanalysis, different electrochemical, electrical, physical and microscopic techniques have been carried out to achieve the best electrode performance from an analytical point of view.

1.4 Characterization strategies of CNT-based nanocomposite electrodes

From an analytical point of view, the requirements to achieve a good electrochemical electrode performance are high sensitivity, rapid response time and low limit of detection, which are related with some physical parameters such as material resistivity, heterogeneous electron transfer rate and double-layer capacitance. Accordingly, optimizing those physical parameters, an enhanced analytical signal is ensured.

One of the main factors to be considered about nanocomposite electrodes based on carbon materials (such as graphite, graphene and CNTs) is their direct dependence between the electrochemical response and the carbon/polymer composition ratio. This composition must provide a low resistance value within the resulting nanocomposite in order to promote the electrode kinetics. Furthermore, this composition also drastically affects the electroactive area of the electrode surface. Additionally, it is important to highlight that both the conductive network within the nanocomposite and the distribution of the conductor material on the nanocomposite electrode surface are parameters which directly affect its electrochemical response. Nanocomposite electrodes containing a high carbon load show closer conductive microzones on their surfaces comparing to nanocomposite electrodes that contain a lower carbon load, where said microconductive zones are further separated. As mentioned above, the optimization of sensors based on microelectrode arrays mainly depends on the dimension and separation of these microzones. Due to the distribution of the conductive areas on the surface of CNT-based nanocomposite electrodes is completely random, an accurate characterization of the electrochemical, electrical and morphological parameters have allowed to determine the optimum carbon loading composite depending on the nature of the raw CNTs (concretely MWCNTs), and thus, the optimum separation between conductive microzones. This fact has enabled the development of effective amperometric (bio)sensors.

1.4.1 Electrochemical characterization: Electrochemical Impedance Spectroscopy and Cyclic Voltammetry

Different electrochemical techniques, such as Electrochemical Impedance Spectroscopy (EIS) and Cyclic Voltammetry (CV) have been used in order to develop an accurate characterization protocol which allows the improvement of the electroanalytical properties of nanocomposite sensors based on different kinds of MWCNTs by optimizing different physical parameters, such as ohmic resistance, charge transfer resistance and double-layer capacitance. These physical parameters, which will be described below, are directly related to the sensitivity, response time and signal to noise ratio, respectively, and also affect the reproducibility of the analytical signal.

1.4.1.1 Electrochemical Impedance Spectroscopy

The term impedance was coined in 1886 by the electrical engineer, mathematician and physicist Oliver Heaviside, who adapted complex numbers to the study of electrical circuits.¹⁰² The method of impedance measurements is widely used in many fields of electrochemistry, such as electrode kinetics, double layers studies, batteries, corrosion, solid-state electrochemistry and bioelectrochemistry. EIS is a characterization technique which provides electric information in the frequency domain. With this technique, a process occurring in an electrochemical cell can be modelled using combination of resistors (R) and capacitors (C), which means that a RC circuit can be built that gives the same current response that is produced by the electrochemical system. This is the principle of equivalent circuits. By using equivalent circuits, the experimental spectrum can be fitted with the theoretical curve corresponding to the selected circuit model, thus obtaining the values of electrical parameters.¹⁰³

EIS generally measures the resulting of applying a sinusoidal alternating current (AC) potential to an electrochemical cell and measuring the AC current that crosses through the cell. When an oscillating potential is applied to an electrode surface, the resulting current has the same frequency as the applied potential but may be shifted in phase. This phase-shift is dependent on the relative resistive and capacitive features of the electrochemical system. Consequently, the phase-shift can be used to monitor physical processes at the electrode surface. By definition, impedance is defined as the ability of a circuit element to resist the flow of current. Impedance is similar to

resistance (it is a ratio between voltage and current), but is also impacted by the ability of a circuit to store energy. In EIS, a sinusoidal AC voltage, $E(t)$, of a small magnitude, E° , is applied to an electrode over a range of frequencies (ω), and the resulting sinusoidal current is measured. The resulting AC current, $I(t)$, is of the same frequency as the applied potential, but shifted in phase, as is shown in Figure 1.9 A. The phase-shift is reported as the phase angle (θ) as it relates to the period of the sinusoidal waves.

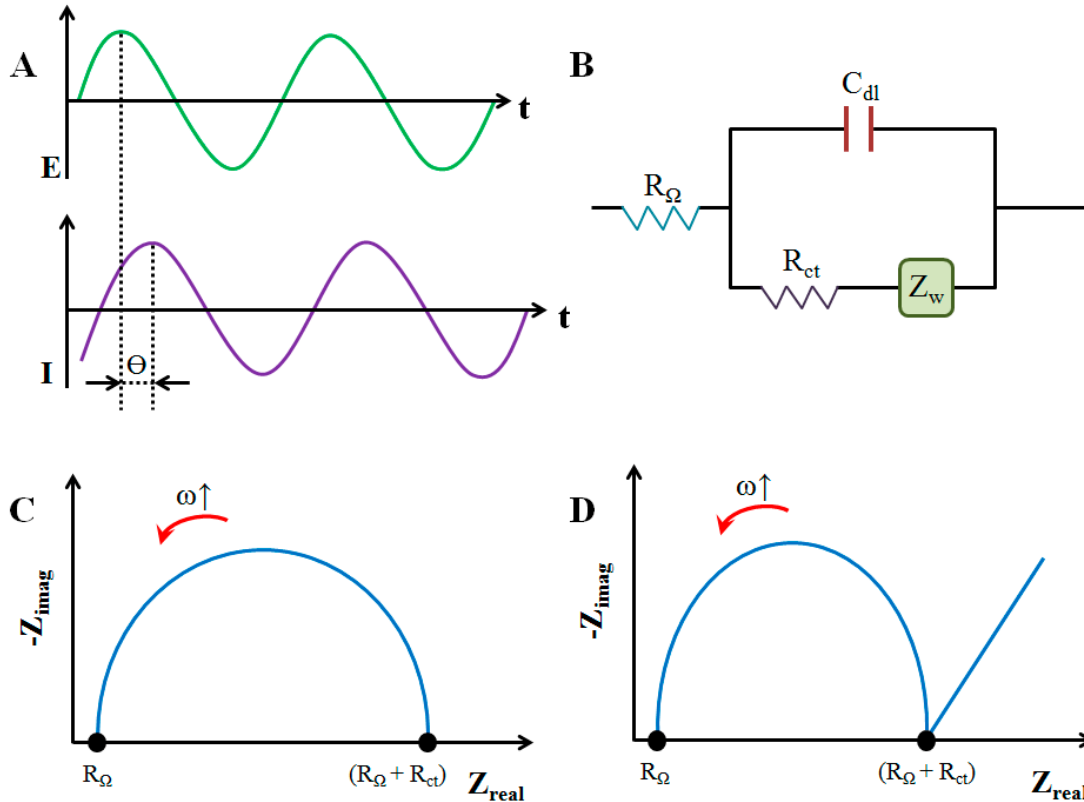


Figure 1.9 A) Excitation sinusoidal signal applied on the system and the sinusoidal current registered shifted in phase. B) Model equivalent circuit used for the impedance spectra fitting (Randles circuit). Nyquist plot for an electrochemical system with C) kinetic-control process and D) mixed kinetic and diffusion-control process.

This phase-shift (or phase angle) represents the relative capacitive, resistive and inductive character of the electrochemical system. Equations 1.1 and 1.2 describe the applied potential $E(t)$ and resulting current $I(t)$, respectively, where t is time and I° is the magnitude of the current oscillations.

$$E(t) = E^\circ \sin(\omega t) \quad \text{Equation 1.1}$$

$$I(t) = I^\circ \sin(\omega t - \theta) \quad \text{Equation 1.2}$$

The impedance of the system (Z) can be calculated by means of an expression analogous to Ohm's Law, Equation 1.3.

$$Z = \frac{E(t)}{I(t)} \quad \text{Equation 1.3}$$

Using the Euler's formula (Equation 1.4), and taking into account that the impedance has an amplitude $Z^\circ = E^\circ / I^\circ$ and a phase-shift Θ , it is possible to express Z in terms of complex numbers, following the Equation 1.5, where Z_{real} is the real part, $j = \sqrt{-1}$ and Z_{imag} is the imaginary part of the impedance.

$$e^{j\varphi} = \cos(\varphi) + j \sin(\varphi) \quad \text{Equation 1.4}$$

$$Z = Z^\circ [\cos(\varphi) + j \sin(\varphi)] = Z_{\text{real}} + j Z_{\text{imag}} \quad \text{Equation 1.5}$$

There are different ways to plot impedance. The most often used in the electrochemical literature when studying electron transfer kinetics is the Nyquist plots because they allow for an easy prediction of the circuits elements. Nyquist plots consist of plotting the Z_{imag} as a function of Z_{real} , usually showing a semicircle profile and provide visual insight into system dynamics at the electrochemical interface. Every experimental point in the plot corresponds to a different frequency. EIS data is commonly analyzed by fitting it to an equivalent electrical circuit model (see Figure 1.9 B). Most of the circuit elements in the model are common electrical elements such as resistors, capacitors, and inductors, which are combined to simulate the real impedance spectra. The utility of this technique resides on that each element in the model has a basis in the physical electrochemistry system, such as: solution resistance (R_Ω), which is dependent on the ionic concentration, the type of ions and also the electrode area; charge transfer resistance (R_{ct}), which is inversely proportional to the electron transfer rate; double-layer capacitance (C_{dl}), which is directly related to the charging or background current and Warburg impedance (Z_{w}), which arises from mass-transfer limitations and can be used to measure effective diffusion coefficients.¹⁰⁴

If the impedance spectrum is dominated by the semicircle feature, the electrochemical system is limited by the electron transfer rate and it is said that the electrochemical process is kinetically controlled. Figure 1.9 C shows the simplest

equivalent circuit to fit the impedance data obtained from an electrochemical system with kinetic-control process. However, normally such plot exhibits a kind of semicircle profile plus a linear region, demonstrating that the electron transfer is fast and the diffusion of the electroactive species is the limiting factor. In this case, it is said that the process is diffusion controlled. Figure 1.9 D represents the ideal impedance spectra from an electrochemical system with mixed kinetic and diffusion-control process.

Regarding the applicability of EIS technique for (bio)sensing purposes, it is important to highlight that EIS is becoming a popular electrochemical tool for numerous applications, such as immuno, genosensing and enzyme activities.¹⁰⁵ Recently, this technique has been applied as a tool to optimize the optimum filler/polymer nano(bio)composite composition.^{11,80} As previously mentioned, the carbon loading affects directly the rate of electron transfer, the material stability and the background capacitance current. Analytically, these parameters influence the levels of sensitivity, limit of detection and response time. Simultaneously, the nature of the raw CNT also influences these parameters. Accordingly, one way to optimize the CNT loading of the nanocomposite regarding to the nature of the raw carbon material will be by using the Electrochemical Impedance Spectroscopy (EIS).

1.4.1.2 Cyclic Voltammetry

Cyclic Voltammetry (CV) is the most widely used technique for acquiring qualitative information about electrochemical reactions because it offers a rapid location of redox potentials of the electroactive species. CV technique measures the current originated in an electrochemical cell under conditions where voltage is in excess of that predicted by the Nerst equation. In a typical cyclovoltammetric experiment, a stationary working electrode is dipped into an electrolyte solution. In order to minimize the ohmic resistance, a three-electrode arrangement is preferable. In this arrangement, the current passes between the working electrode (WE) and a counter electrode (CE). The potential of the working electrode is measured relative to a separate reference electrode (RE). The voltage is swept between two values at a fixed rate (V_1 and V_2). When the voltage turns from V_1 to V_2 , the scan is reversed and the voltage is swept back to V_1 , as is shown in Figure 1.10 A.

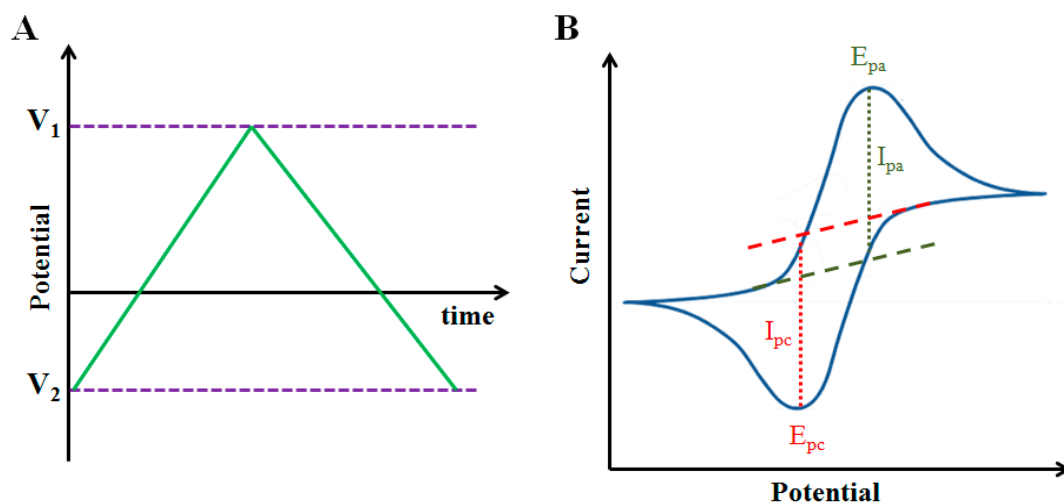


Figure 1.10 Schematic representation of a CV waveform (A) and the typical resulting current response (B). In a CV experiment, the voltage is swept linearly back and forth between two voltage limits (V_1 and V_2).

Figure 1.10 B shows a typical cyclic voltammogram recorded for a reversible redox couple. The most important parameters that can be extracted from a cyclic voltammogram are: cathodic current peak (I_{pc}) and anodic current peak (I_{pa}),⁴⁹ as well as their potential values in those points (cathodic peak potential, E_{pc} and anodic peak potential, E_{pa}). For a reversible electrochemical reaction, the cyclic voltammogram recorded has certain well defined characteristics:

- i) The voltage separation between the current peaks (ΔE) is $\Delta E = E_{pa} - E_{pc} = \frac{0.059}{n}$; where n corresponds to the number of electrons.
- ii) The positions of peak voltage do not alter as a function of voltage scan rate (v).
- iii) The ratio of the peak currents is equal to one ($|I_{pa}| = |I_{pc}|$).
- iv) The peak currents are proportional to the square root of the scan rate ($v^{1/2}$).

In order to carry out the previous feasibility studies of a electroanalytical device or to compare the behaviour of different electrochemical electrodes, a completely reversible redox system is generally used, such as $[\text{Fe}(\text{CN})_6]^{3-}/[\text{Fe}(\text{CN})_6]^{4-}$, $\text{Fe}^{2+}/\text{Fe}^{3+}$ or $[\text{Ru}(\text{NH}_3)_6]^{2+}/[\text{Ru}(\text{NH}_3)_6]^{3+}$. The kinetic processes of those species are strongly dependent on the state of the electrode surface. Thus, following the modified Randles–Sevcik equation (Equation 1.6) it is possible to calculate the electroactive area of the electrode in terms of peak current (I_p) and scan rate (v).¹⁰⁶

$$I_p = 3.01 \times 10^5 \cdot n^{3/2} (\alpha D \nu)^{1/2} A \cdot C^* \quad \text{Equation 1.6}$$

1.6

This equation is adequate for electron transfer-controlled processes,¹⁰⁷ where n is the number of electrons, C^* is the bulk concentration of the electroactive species, D corresponds to the diffusion coefficient of the oxidized/reduced species, α represents the symmetry factor and ν represents the scan rate. In addition, the exchange current (i_0) from Tafel plots (log current vs. potential) can also be extracted from a cyclic voltammogram (see Figure 1.11).

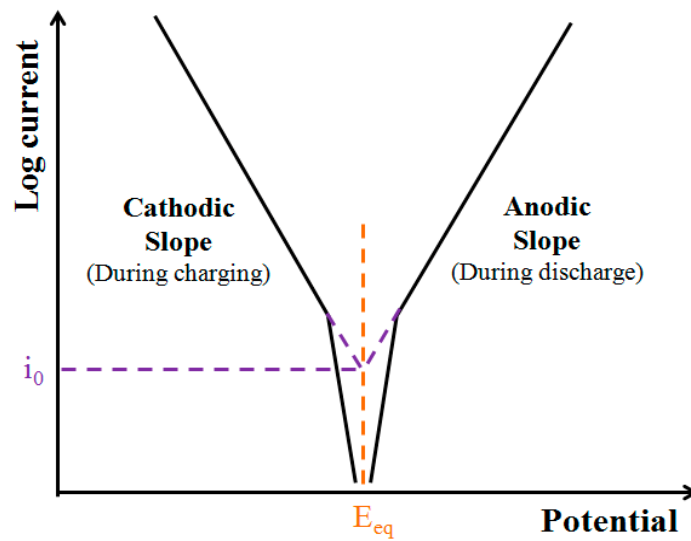


Figure 1.11 Typical Tafel plot for a reversible electrochemical system, where i_0 is the exchange current and E_{eq} is the equilibrium potential.

Since i_0 is a parameter which provides information about the reversibility of the process, from this value it is possible to evaluate the charge transfer resistance (R_{ct}) through the Equation 1.7.

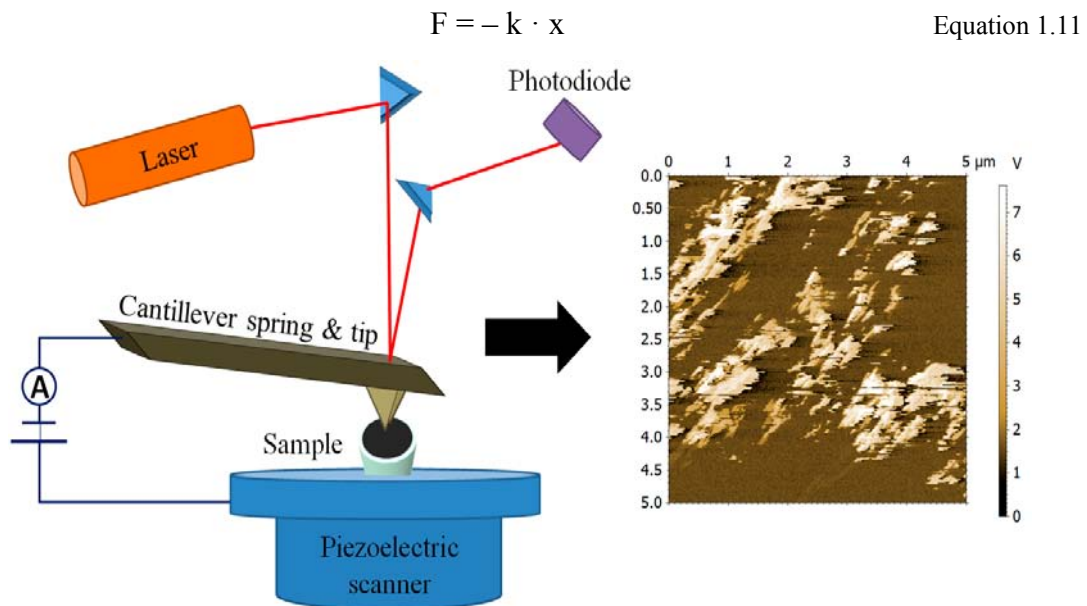
$$i_0 = \frac{RT}{nFR_{ct}} \quad \text{Equation 1.7}$$

1.4.2 Electrical characterization through the Percolation Theory

As mentioned before, under an electroanalytical context, the volume fraction of carbon in the nanocomposite has to be high enough to guarantee a conducting pathway. In turn, sufficiently low bulk resistivity produces a higher sensitivity due to a lower resistivity value.¹⁰⁸ In order to achieve an electrochemical behaviour of a microelectrode

array it is important to optimize the distance between microelectrodes (conductive microzones). However, due to the randomly structure of the nanocomposites, the distance between conductive microzones are not so easy to control. In this sense, advances in nanocomposites based on carbon materials have demonstrated that the distance between the conductive microzones can be slightly controlled by a decrease or an increase of the carbon loading.¹⁰⁹

Beyond percolation theory, another way to characterize the electrical properties of the carbon nanocomposites is by using Current Sensing Atomic Force Microscopy (CSAFM).^{92,108,110} The typical configuration is known as Atomic Force Microscopy (AFM) and it is classified a variant within the Spectroscopy Probe Microscopy, SPM, which was developed by Binnig & Rohrer in 1982.¹¹¹ This technique is a powerful tool for the fabrication and characterization of different nanomaterials mainly due to its high resolution, which allows operating in ambient conditions. Furthermore, it is able to characterize almost any type of sample, such as insulators, conductors, solid and liquids, among others. Different qualitative information can be obtained from CSAFM, such as size, shape and distribution of the conducting material in the nanocomposite structures and thus, an approximation of the filler distribution within the nanocomposite. This fact has led to significant progresses in the surface characterization of nanocomposites. CSAFM technique consists in the use of a conductive tip operating in standard contact mode with the sample (see Figure 1.12), providing a 3D profile of the surface on a nanoscale by measuring forces between a sharp probe (AFM tip), which is mounted on an oscillating cantilever spring. The amount of force between the probe and the sample is dependent on the spring constant of the cantilever. This force can be described using Hooke's Law (see Equation 1.11), where F is the applied force, k is the spring constant and x is the cantilever deflection. The relative position of the tip to the surface is controlled using a piezoelectronic scanner. The SCAFM tip gradually touches the surface and records the small force between the probe and the surface. When a voltage is applied between tip and sample, a current is generated, the intensity of which will depend on the sample nature. As the tip scan across a surface, the deflection of the cantilever is measured using a laser which is coupled to a photodiode. The photodiode measures the intensity of the frequency dependant laser as it reflects from the oscillating cantilever. Thus, a map of current distribution along the sample is measured simultaneously with the surface topography, also shown in Figure 1.12.



1.12 The operating principle of an SCAFM and an example of conductivity mapping of a MWCNT/epoxy nanocomposite electrode. The resulting map of current shows two regions: the conductive microzones (light regions) and the non-conductive insulating microzones (dark regions).

It is important to highlight that AFM can be operated in 3 modes: i) contact mode; ii) semi-contact mode or tapping mode and iii) non-contact mode. The type of AFM employed depends on the nature of the material under investigation as well as the resolution required. The first mode (contact mode) maintains a constant force between the probe and the sample in order to obtain images. It is generally used for generating images of rough surfaces with fast scanning speeds. The main disadvantage of using contact mode in AFM is the damage that can be caused to the tip and the sample during extended contact. On the other hand, tapping mode AFM is similar to the contact mode but in this mode the cantilever is oscillated over the sample at its resonant frequency. The tip gently taps the surface and probes the surface topography. Tapping mode AFM can be employed to produce high resolution images of samples that may be damaged in full contact mode. Finally, non-contact mode does not contact the sample surface during sample scanning. Changes in the cantilever amplitude are a result of attractive Van der Waals forces between the sample and the tip. This method of AFM can be used to image extremely delicate samples; however, images are generally of lower resolution than that obtained from contact or tapping AFM modes.

1.4.3 Morphological characterization: Microscopic techniques

Surface topography and, in particular, roughness and form, plays an important role in determining the functional performance of nanocomposite electrodes. Nanocomposite morphology is a microscale property, largely dictated by the insulating polymer or filler material portion exposed on the electrode surface. In this way, microscopic techniques are especially useful in determining these microscale properties, as the domains created by the nanocomposite morphology are large enough to be viewed using modern microscopy instruments. Some of the most commonly used microscopic techniques are Atomic Force Microscopy (AFM), Scanning Electron Microscopy (SEM) and Confocal Microscopy 3D (CM3D).

As previously mentioned, AFM is a powerful tool to determine not only the conductive microzones, which are exposed on the electrode surface, but also the roughness of the nanocomposite surface when it is used in tapping mode.¹¹²

On the other hand, another remarkable microscopic technique for its extensive use in characterization of materials is SEM. It uses a focused beam of high-energy electrons (between 100 eV and 50 KeV) to generate a variety of signals at the surface of solid specimens (e.g. nanocomposite materials). Accelerated electrons in an SEM carry significant amounts of kinetic energy, and this energy is dissipated as a variety of signals produced by electron-sample interactions when the incident electrons are decelerated in the solid sample. These signals include, among others, secondary electrons which are responsible of showing morphology and topography on samples, as is shown in Figure 1.13. In most applications, data are collected over a selected area of the surface of the sample, and a 2D image is generated that displays spatial variations in these properties.¹¹³ Areas ranging from approximately 1 cm to 5 μm in width can be imaged in a scanning mode using conventional SEM techniques (magnification ranging from 20x to approximately 30,000x spatial resolution of 50 to 100 nm). Furthermore, the SEM is also capable of performing analyses of selected point locations on the sample; this approach is especially useful in qualitatively or semi-quantitatively determining chemical compositions using EDS.

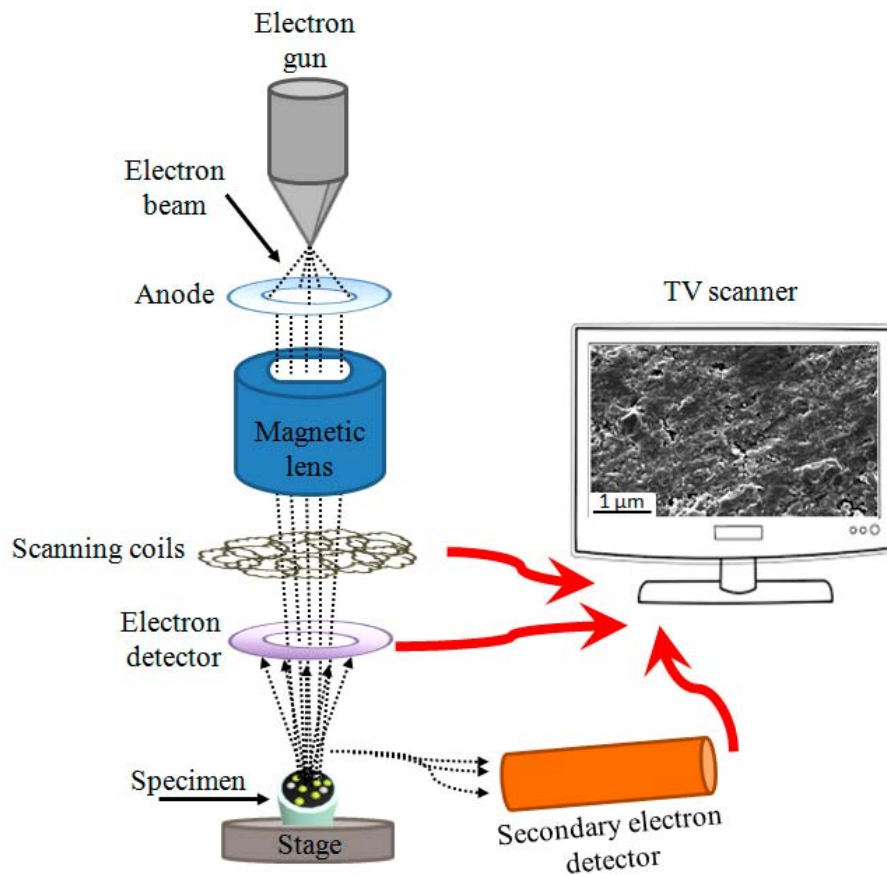


Figure 1.13 The operating principle of a SEM (insert an example of topography mapping of a MWCNT/epoxy nanocomposite electrode).

Finally, confocal microscopy has become a more and more powerful tool for surface characterization since it was described for first time by Minsky in 1957.¹¹⁴ The method of image formation in a confocal microscope is fundamentally different from that in a conventional wide-field microscope where the entire specimen is bathed in light from a mercury or xenon source, and the image can be viewed directly by eye. In contrast, the illumination in a confocal microscope is achieved by scanning one or more focused beams of light, usually from a laser, across the specimen.¹¹⁵ The basic principle of confocal microscopy is shown in Figure 1.14. Light emitted from a point light source (for example a laser beam focused onto an illumination pinhole) is imaged onto the object focal plane of a microscope objective (MO, the first focusing). A specimen location in focus leads to a maximum flux of light through the detector pinhole (the second focusing), whereas light from defocused object regions is partly suppressed.¹¹⁶ One of the basic properties of the confocal microscope is its ability to use a confocal aperture to reject out-of-focus signal. Therefore, confocal images are acquired from a narrow slice of the specimen.

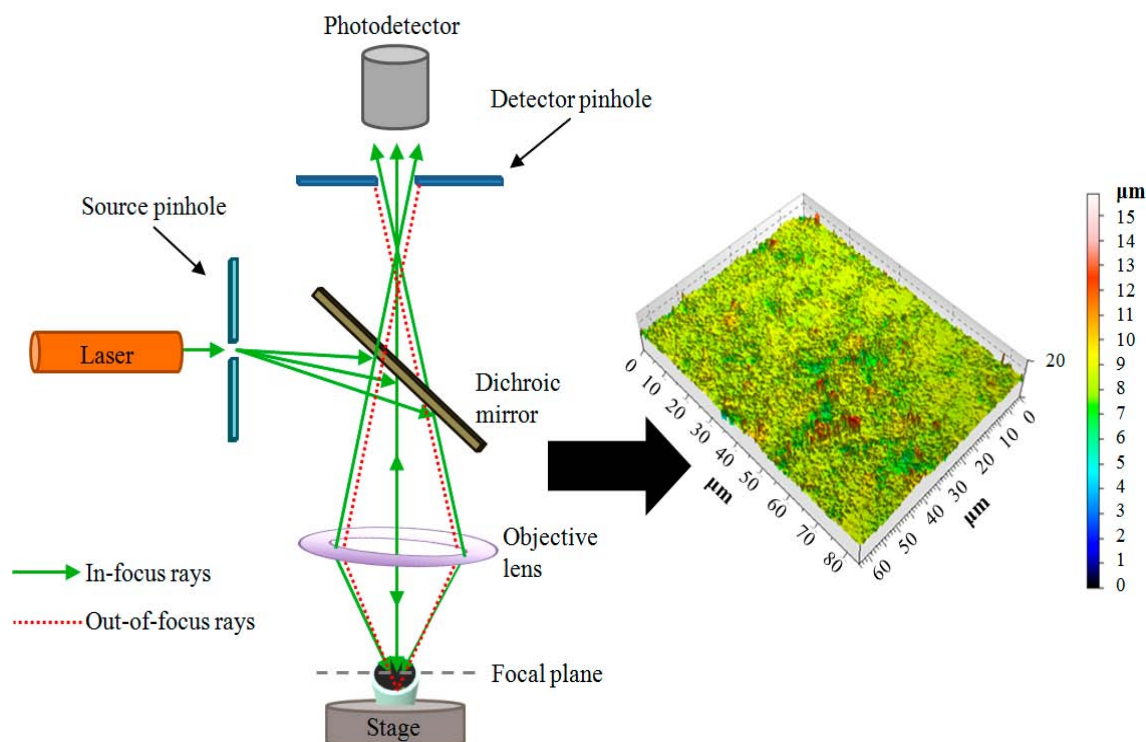


Figure 1.14 The operating principle of a confocal microscopy. Insert an example of topographic mapping for a nanocomposite electrode based on MWCNT/epoxy.

This optical sectioning capability gives the basic optical contrast mechanism of the confocal microscope and is commonly referred to as the z-contrast (axial contrast).¹¹⁷ Nowadays, CM3D combines the advantages of both confocal and interferometry, resulting in a very useful and flexible tool for super fast, precise and non destructive assessment of the micro and nano geometries of different material surfaces. Furthermore, it is possible to analyze with this technique rough (confocal) as well as smooth (Vertical Scanning Interferometry or VS) and super smooth (Phase Shift Interferometry or PSI) surfaces. This fact allows the CM3D to be used in a wide range of applications. As main remarkable novelty, CM3D has been also used as a complementary technique for the roughness study of nanocomposite electrodes based on MWCNT/epoxy.⁴⁸

1.4.4 Electroanalytical evaluation: Hydrodynamic Amperometry

As was mentioned above, an electrochemical sensor contains a transducer that transforms the response measured at the receptor into a detectable signal, which can be a current (amperometry), a voltage (potentiometry) or impedance/conductance changes

(conductimetry). Among these, amperometry presents a number of advantages over other electrochemical techniques, which will be described below. The first example of an amperometric sensor was reported by Clark in 1956 with advent of Clark oxygen electrode.¹¹⁸ Generally, the amperometry is based on measuring either value of density of current in an electrochemical cell at a constant applied potential value. The electrochemical cell is integrated for a working electrode, a reference electrode and a counter-electrode that are in connection through an electrolyte phase. The measured current (I) results from the presence in the solution of electrochemically active analytes, whose oxidation or reduction takes place on the working electrode surface. The fundamental process for sensing an analyte can be described in four steps: (i) the analyte diffuses to the sensing electrode; (ii) the analyte is adsorbed on the sensing electrode; (iii) the electrochemical reaction occurs and (iv) the reaction products desorb from the sensing electrode and diffuse away. During electrolysis the working electrode may serve as either anode or cathode depending on the nature of the substance measured and the voltage value applied.¹¹⁹ The produced current signal can be related to the concentration of the analytes by Faraday's Law (Equation 1.8) as well as the laws of mass transport.

$$I = nF \frac{\partial C}{\partial t} \quad \text{Equation 1.8}$$

Because of the heterogeneous nature of the process, the reaction rate depends on the rate of electron transfer at the surface of the electrode and on the mass transport ($\partial C/\partial t$). The rate of electron transfer can be accelerated by increasing the potential difference between the electrodes. When the reaction at the surface of the electrode is fast, due to the increased potential, a maximum overall rate of reaction is reached. This fast reaction, known as the reversible case, is limited by the maximum rate of mass transport, which occurs when the analyte concentration on the electrode is zero.¹²⁰ On the one hand, in a quiescent solution the resulting current (I) decreases with time (t) because of the slow spread of the diffusion layer out into the bulk solution combined with a decrease of the concentration gradient, as is described by the Cottrell equation (Equation 1.9). On the other hand, under forced convection (hydrodynamic amperometry) the mass transport to the electrode surface is controlled by diffusion through a stagnant layer formed on the electrode surface, being able to control the Faradaic current between the working electrode and counter-electrode. This fact assures

a linear dependence of the current on concentration of the analyte, as is described by the following equation (Equation 1.10), being d the thickness of the stagnant.

$$I = nFA \sqrt{D/\pi t} C^* \quad \text{Equation 1.9}$$

$$I = nFA \frac{D}{d} C^* \quad \text{Equation 1.10}$$

In general, amperometric sensors offer good sensitivity and wide linear range (around 3–4 orders).¹¹⁹ Concretely, amperometric nanocomposite sensors based on different carbon nanomaterials can be low-cost and can also be mass produced via microfabrication technology. This advantages allow them to be integrated as a detectors in a continuous flow analytical system, as a flow injection analysis (FIA) or a miniaturized device, to take advantage of all the benefits provided by these automatization techniques.^{20,108} They are simple to use and are widely used in different areas of chemical analysis such as environmental monitoring, surveillance, security, industrial safety, medical and health applications.

1.5 Tunability of CNT–based nanocomposites sensors with modifiers

As it has been discussed above, carbon–based composite sensors present different electrochemical improvements over conventional solid electrodes, such as robustness, renewable surface, small background current or the possibility to behave as microelectrode array, among others.¹⁰⁰ Additionally, the ease of modification is a further advantage of these composites. The surface modification of electrochemical sensors based on pure conductors is generally difficult and costly, needing complex surface treatments to bond the modifying species. In contrast, carbon–based composites permit the addition of a variety of reagents to the host material due to the plastic nature of the composite. Their modification can be carried out in a number of ways, depending on the type of filler material. For example, Creasy and Shaw studied the advantages and disadvantages of modification of carbon fiber ensemble electrodes either within the bulk (polymeric material) or on the carbon fiber surface.¹²¹ Comparing both modification ways, the modification on the carbon fiber produces stronger analytical signals because the redox modifier is in close contact with the conducting material. However, in bulk

modification, the modifiers are embedded or trapped in the polymer matrix and therefore a fraction of the redox modifier could be inactive because it is surrounded by the insulating polymer phase of the composite. In spite of that, bulk modification can be simpler and allow a great regeneration of a deteriorated surface by a simple polishing procedure. Additionally, with the advent of the CNT-based nanocomposites, another modification strategy became widely used. The viability of this carbon filler to be activate with functional groups (e.g. carboxylic groups) also allows them to be functionalized and hence, the modification of the nanocomposite material. In this way, three different methodologies to modify CNT-based nanocomposites with different modifier reagents exist, which offer a customized route for the preparation of sensitive nanocomposite sensors.¹⁷ These three routes are shown in Figure 1.15, and correspond to: a) covalently or non-covalently functionalization of CNTs with the modifiers and their subsequently mixed within the polymer; b) directly introduction of the modifiers in the CNT/epoxy matrix while it has been preparing, which remain embedded or trapped in the nanocomposite and c) immobilization of the (bio)species on the surface of the already prepared nanocomposite.

Such modifier reagents, which confer selectivity and sensitivity to the modified-nanocomposite sensor, include electrocatalysts, enzymes, different kind of nanoparticles such as functional metal nanoparticles (FMNPs) or quantum dots (QDs), proteins, ligands or chemical (bio)recognition agents that may perform several functions: (i) they may act on the analyte by pre-concentrating it on the nanocomposite electrode surface; (ii) they may be used as redox mediators, accelerating the oxidation or reduction of different analytes; (iii) they may alter the electrochemical and physical properties of the electrode surface; (iv) they can function as a catalysts or (v) as a template support to immobilize some of the (bio)molecules involve in the electrochemical reactions.¹²² Due to the easy regeneration of the surface by simple polishing, a homogeneous distribution of the modifier agents in the nanocomposite guarantees that a reproducible surface is obtained after each polishing. However, since the route of modifying is on the nanocomposite surface (Route C following the Figure 1.15), this surface cannot be renewable and must be regenerate after each polishing.

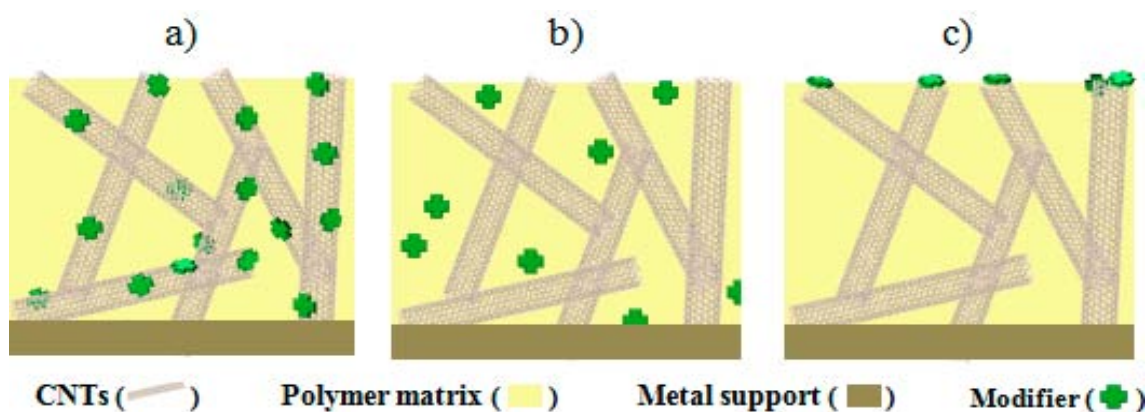


Figure 1.15 Three different routes for the customized preparation of modified-nanocomposites with (bio)chemical modifier agents.

Firstly, the pre-concentration of some analytes is achieved by ligands or chemical (bio)recognition agents and ion exchangers.¹²³ These species act selectively on the analyte, separating it from the initial sample and removing some interferents. The concentration of the analyte is determined by oxidation or reduction at the optimal potential. In this way, the incorporation of different chemical (bio)recognition agents into carbon-based nanocomposites (and concretely in CNT-based nanocomposites) has been widely exploited specially in the field of genosensors, immunosensors and enzymatic sensors.^{124,125}

Secondly, redox mediators represent another type of modifiers which consist of a metal atom whose oxidation states are stabilized by the π orbitals of aromatic structures.¹²¹ The integration of redox mediators and CNTs in polymeric matrixes for the development of electrochemical sensors may seem, at first, to be counterintuitive because both redox mediators and CNTs provide similar benefits to electrochemical sensing in terms of lowering the overpotentials of electrode processes.¹²⁶ Thus, the introduction of redox mediators within the CNT-based nanocomposite sensor could be perceived as a redundant and complicating factor in the sensor design. Regardless of these perception, however, Gorski *et al.* reported an electrochemical sensing platform based on the integration of redox mediators and CNTs in a polymeric matrix.¹²⁷ To demonstrate the concept, a redox mediator (Azure dye) and CNTs were co-immobilized in the matrix of a biopolymer chitosan, and tested as a sensing platform for the amperometric determination of β -nicotinamide adenine dinucleotide (NADH). The incorporation of CNT into chitosan-azure matrix facilitated the azure-mediated

electrooxidation of NADH. In particular, CNT decreased the overpotential for the mediated process by an extra 0.30 V and amplified the NADH current by ~35 times while reducing the response time from ~70 s for chitosan-azure to ~5 s for chitosan-azure/CNT films. It is important to highlight that an important drawback of these sensors is the poor stability of the mediator when one or both of its oxidation states is a soluble ionic species. Nonetheless, regeneration of the electrode is a simple manoeuvre, involving a simple polishing of the surface.

Thirdly, another class of modifiers comprises species that confer certain physical properties to the sensor. A problem encountered in composite-based electrodes is the high hydrophobicity provided by the polymer itself. For example, Wang and Liu have proposed the addition of fumed silica to the composite to make the material more hydrophilic, thus improving the sensitivity and the stability of the sensor.¹²⁸

Fourthly, some modifier agents have exhibited catalytic effect on a large number of chemical species, as is the case of some metals or oxides. Such metallic or oxide catalysts can be easily incorporated, providing a carbon based composite with a tailored sensing surface.^{129,130} In this way, one simple strategy for improving the electrochemical performance of CNT-based nanocomposites is incorporating different nanoparticles (NPs), including functional metal nanoparticles (FMNPs) or metal oxide nanoparticles (MO-NPs), such as Ag-, Pt-, CdS-QDs and CuO-NPs, as seen in the electrochemical detection of hydrogen peroxide and glucose.^{131,132,104,133} Accordingly, despite of the precursor reagent price, the great stability and oxidation resistance of these NPs make them more than a good alternative for the preparation of, for example, modified amperometric (bio)sensors. This fact is because of the fast electron transfer ability of CNT, which combined with these kind of nanoparticles, favours an enhancement of the electron transfer between analyte-electrode, decreasing the overpotentials of several analytically important electrochemical reactions.^{134,135}

Finally, different NPs, commonly gold and magnetic nanoparticles, can also be added to carbon composites as a support to attach different (bio)receptors for improving the strategies of (bio)receptor immobilization in the composite matrix, which may subsequently carry out an specific interaction or complexation with the analyte on the electrode surface, making possible a pre-concentration of the sample which results in a more sensitive device.^{136,137} For instance, it has been demonstrated that the integration

of magnetic beads to graphite/epoxy composites provides further advantages in terms of separation of the analyte from complex matrix and enhancement of the biological reactions, with promising application in food safety and environmental monitoring.¹³⁸

1.5.1 Intermatrix Synthesis Technique for CNT–based nanocomposite electrodes modification with nanoparticles

Recently, NPs have been used extensively in the fields of physical, chemical and material sciences because of their surface-volume ratio that provides them unique properties different from the analogous bulk material. As just discussed, CNTs are a feasible support for heterogeneous catalysts such as FMNPs.

Despite the benefits presented for the CNT–based modified-nanocomposites with a wide range of NPs,^{139,140} the surface modification of CNTs with NPs (e.g. FMNPs, QDs and MO–NPs) usually involves thermal evaporation,¹⁴¹ electroless deposition by galvanic replacement,¹⁴² NPs hydrosol absorption¹⁴³ or electrochemical deposition.¹⁴⁴ Moreover, the presence of stabilizers is sometimes required to prevent the agglomeration of nanoclusters. In this way, greener synthesis routes have also been used for the preparation of NPs on CNTs, such as seed-mediated growth in which metal salt solutions can be reduced by a strong reducing agent (e.g. NaBH₄) at room temperature and in an aqueous solution. Nonetheless, the possible aggregation of these nanoparticles limits their application in electrochemical systems.¹⁴⁵ Because of this fact, the preparation of FMNPs provides an extra level of stability and a favourable distribution in the final nanocomposite material. In this regard, the Intermatrix Synthesis technique (IMS) becomes a valid FMNPs preparation methodology.^{146,147} An scheme of this operation is shown in Figure 1.16. The first communication about IMS of FMNPs in ion exchange polymeric material dates back to 1949, in which Mills and Dickinson described the preparation of a weakly basic anion exchange resin containing Cu–NPs for its use to remove oxygen from water.¹⁴⁸

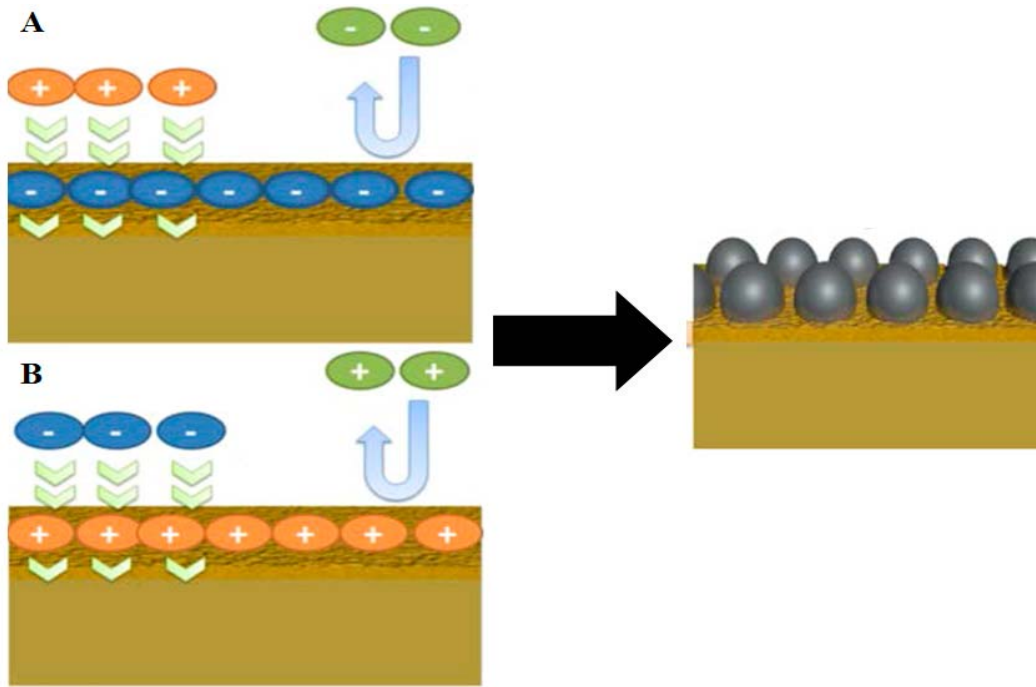
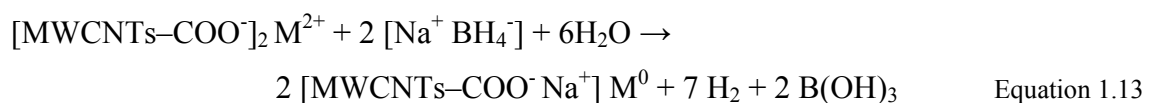
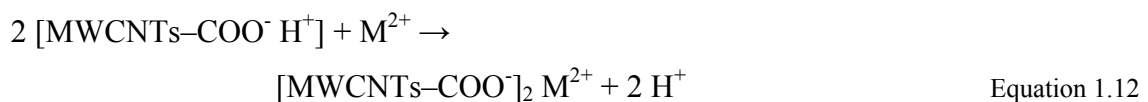


Figure 1.16 Scheme of ion exchange process for A) cationic exchanger and B) anionic exchanger. Afterwards, a favourable FMNPs distribution on the surface of the support is obtained.

IMS is based on the following two sequential steps:

- (i) Introduction of the FMNPs precursors into the support matrix by loading their functional groups with the desired metal ions or metal complex precursors of the nanoparticles. In the case of MWCNTs, they must be previously activated with carboxylic groups (MWCNTs–COOH).
- (ii) Their reduction to zero-valent state inside the support matrix is carried out by using an appropriate reducing agent such as NaBH₄ or ascorbic acid.

Equations 1.12 and 1.13 present the classical IMS upon cationic exchangers such as carboxylic groups (adapted for MWCNTs–COOH), being M²⁺ a divalent metal.



IMS takes advantage of the ion-exchange properties of the support matrix (e.g. sulfonic resins, MWCNTs–COOH...) for consecutive loading and reduction process

during the synthesis of FMNPs, as seen in Equation 1.13, increasing the amount of FMNPs content and their thickness. Furthermore, the fact that the FMNPs are synthesized *in situ*, allows them to exhibit long time stability against aggregation and oxidation. In addition, another advantage offered by IMS is the most favourable distribution of the FMNPs on the surface of the support. On the contrary, in *ex situ* synthesis approach, FMNPs are dispersed after their synthesis in a solid or liquid medium by using different methodologies. In those cases, the stabilization is limited by the re-aggregation of the nanoparticles along the time by the Oswald ripening mechanism. In addition, the final distribution of the FMNPs in the support is not entirely controlled and homogeneous.

Finally, it is important to highlight that IMS can be also adapted to introduce another kind of NPs beyond FMNPs, such as QDs and MO-NPs.

1.6 Beyond CNTs: Trends in graphene-based electrochemical nanocomposite sensors

Graphene is the most recent member of the multi-dimensional carbon-nanomaterial family, starting with fullerenes as a 0D, CNTs as 1D and ending with graphite as 3D nanomaterial. Graphene fills the gap for 2D carbon nanomaterials, as shown in Figure 1.17.¹⁴⁹

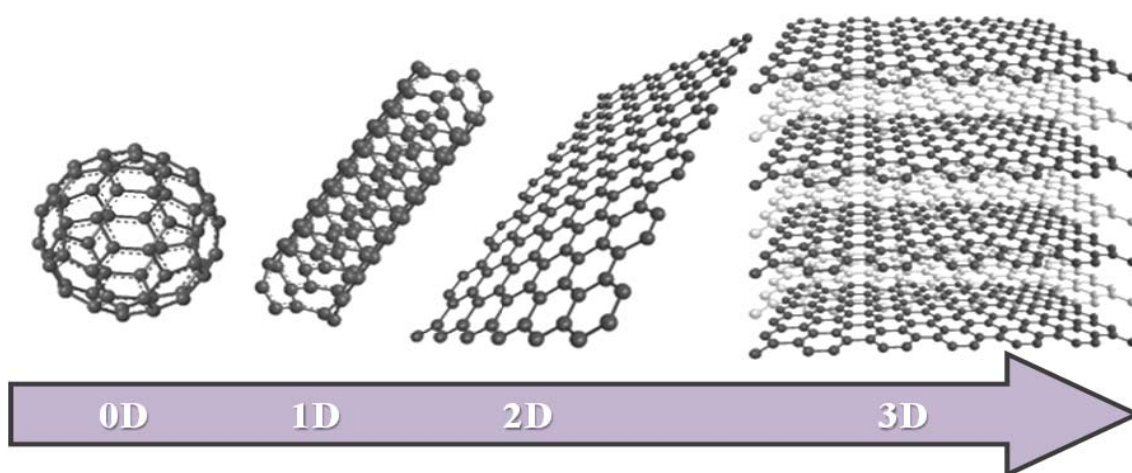


Figure 1.17 Forms of sp^2 -bonded carbon, starting with fullerenes as a 0D nanomaterial, SWCNTs as a 1D nanomaterial, graphene as a 2D nanomaterial and ending with graphite as a 3D material. Adapted from Pumera *et al.*¹⁴⁹

The direct observation and characterization of a mechanically exfoliated graphene monolayer by Novoselov *et al.* in 2004 has sparked the exponential growth of graphene research in both the scientific and engineering communities.¹⁵⁰ Graphene has demonstrated to have properties such as excellent thermal conductivity, superior electron mobility, the highest known electrical conductivity at room temperature, very large surface area and complete impermeability to any gases.¹⁵¹ Furthermore, it possesses Young's modulus of ~ 1 TPa and ultimate strength of 130 GPa, resulting the strongest material ever measured.¹⁵² These unique properties, in addition to its ease of mass production, make graphene an ideal candidate for a variety of applications, such as sensors, batteries, supercapacitors, fuel cells and nanocomposites, among others.^{153,154}

Graphene synthesis can be split into two different types of approach; top-down and bottom-up.¹⁵⁵ Top-down approaches involve breaking apart the stacked layers of graphite to yield single graphene sheets, whereas bottom-up methods involve synthesizing graphene from alternative carbon containing sources. On the one hand, for top-down methods separating the stacked sheets means that the Van der Waals forces that hold the layers together must be overcome, which is not a trivial task despite the relatively low interlayer bonding energy. This route of synthesis involves different exfoliation methods, being the exfoliation of graphene oxide (GO) and its subsequently reduction (rGO) the method which has received the most attention. The Hummers method remains the most widely used process.¹⁵⁶ The structure of GO has been described by a number of different models, as discussed by Dreyer *et al.*²⁹ One widely accepted model is the Lerf–Klinowski model, as is shown in Figure 1.18, which describes graphite oxide as having a layered structure with hydroxyl and epoxy groups on the basal planes and carboxylic and carbonyl groups at the sheet edges. These oxygen containing groups make graphite oxide hydrophilic, and the presence of functional groups between layers also results in graphite oxide having a larger interlayer spacing (6–12 Å, depending on the amount of intercalated water) than graphite (3–4 Å). On the other hand, for bottom-up methods, high levels of graphitization must be promoted to produce good quality material, so these methods generally require high temperatures. The processes involved are usually simple, although the material produced can contain higher levels of defects than observed for top-down methods. Finally, CNTs can be also used to generate another graphene form: Graphene nano-ribbons (GNR).¹⁵⁷ As known, CNTs have been described as rolled up graphene sheets,

and now GNR have been made from unravelling CNTs. They can be obtained by either suspending CNTs in concentrated sulphuric acid followed or being converted by controlled plasma-etching of CNTs that are partially embedded in a polymer film.^{158,159}

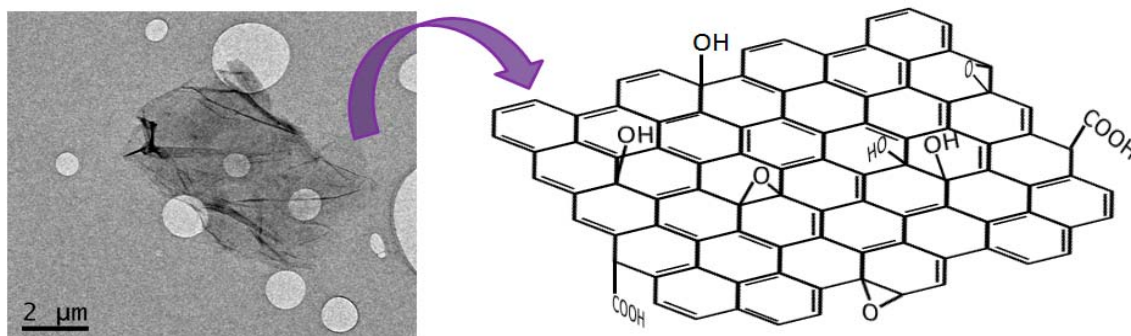


Figure 1.18 HR-TEM image of GO and one of its Lerf-Klinowski model, indicating the presence of functional groups on the periphery of the basal plane of the graphitic platelets of GO.

Recently large research interest has focused on graphene based on nanocomposite materials.^{149,160,161} Because of their good electrical properties, graphene and its derivatives are important filler materials for polymer nanocomposites in electrochemistry fields. From an electrochemical point of view, graphene-based nanocomposite materials possess important characteristics, such as large specific surface area, availability for surface functionalization and ultrafast charge mobility, which ensure high sensitivity and rapid response.^{93,162}

Moreover, the potential scope of graphene-based nanocomposite electrodes is enormous. They maintain the properties of other carbonaceous materials like potential windows, inert electrochemistry and good electrocatalytic activities for many redox reactions, while they provide new properties. In this way, many graphene-based nanocomposite electrochemical sensors have been reported to detect glucose,¹⁶³ ascorbic acid,¹⁶⁴ hydrogen peroxide¹⁶⁵ and dopamine,¹⁶⁶ among others. They present improvements in their electrochemical properties comparing to conventional carbon nanomaterials, such as graphite or CNTs, mainly attributed to the presence of more sp^2 -like planes and edge defects in graphene.¹⁶⁷ In comparison with CNTs, two advantages of graphene are apparent, as follows:

- (i) Graphene does not contain metallic impurities as CNTs do. In many cases, such impurities dominate the electrochemistry of CNT (even at impurities levels lower than 100 ppm), having a negative influence on different analytes, such as hydrazine, hydrogen peroxide and glucose, among others.
- (ii) The production of graphene uses graphite, which is cheap and accessible.

It is important to note that the term “graphene” used in the literature includes a wide range of graphene-like structures which differ in the preparation method and consequently in the chemical structure (usually the oxidation level), shape, size and number of layers. As another important member of graphene family, graphene oxide (GO) and reduced graphene oxide (rGO) are more electrochemically active as compared to pristine graphene owing to the oxygen-containing reactive sites at edges and in the basal plan.^{168,169} While the low intrinsic reactivity of graphene limits the interfacial interactions with the polymer affecting the load transfer across the interface and thus, the performance of the nanocomposites, GO is an alternative for use in polymer nanocomposites due to the presence of specific functionalities in the graphite sheets. Nevertheless, the main limitation of GO is that it disrupts the sp^2 network and dramatically worsen the electronic properties. The reduction of GO restores the conductivity albeit, as some defects or vacancies are irreversible, it remains lower than pristine graphene. In this sense, rGO brings together features of both graphene and GO and may lead to materials with reasonably good conductivity, as well as thermal stability and processability.^{170,171}

The properties and performances of graphene–polymer nanocomposites not only depend on the nature of the graphene filler and polymer matrix, but performance will also depend on the dispersity of the filler and the ratio of filler to the matrix.¹⁵¹ The electrical conductivity is one of the most important changes when graphene–based nanocomposites are prepared. There exist several methods employed to prepare graphene, each with specific characteristics of dimensions, shape, quantity and quality, which are strongly related to the final application to which graphene is directed.

Regarding the electrical conductivity of the graphene–based nanocomposite materials, in this system the bulk conductivity of the insulating polymers increases by several orders of magnitude when an appropriate amount of graphene is added,

following normally a percolation behaviour. Accordingly, to achieve electrical conductivity, the concentration of graphene must surpass the electrical percolation threshold, where a conductive network of filler material is formed.¹⁷² However, as already mentioned for CNT-based nanocomposites, and depending on the conductive load, nanocomposites can behave as microelectrode arrays which are known to provide efficient mass transport of the electroactive species due to radial diffusion on the spaced carbon particles,¹⁷³ favouring the sensitive electroanalysis of a variety of reagents. Under this context, another point of consideration is the optimization of the graphene loading in the nanocomposite materials for improving their electrochemical properties and analytical applications. The characterization methodology developed to optimize CNT-based electrochemical nanocomposite sensors has also been applied for graphene-based nanocomposite materials, concretely for rGO/epoxy electrochemical nanocomposite sensors.

Finally, the activated groups contained on GO (e.g. $-\text{COOH}$, $-\text{C}=\text{O}$ and $-\text{OH}$) may be used for its functionalization with different nanoparticles, such as Au-NPs and Pd-NPs.^{174,175} Modified electrodes have been developed to improve the electrode response in electroanalysis. Furthermore, as was discussed above, these nanoparticles can be also incorporated in the nanocomposite matrix to attach different (bio)receptors, which subsequently may carry out a specific interaction or complexation with the analyte on the electrode surface, making possible a pre-concentration of the analyte of interest (see § 1.5). An example of (bio)receptor is the well-known cyclodextrin.

Cyclodextrins are cyclic oligomers composed of 6, 7 or 8 d-glucopyranosidic units, for α , β and γ cyclodextrins, respectively (see Figure 1.19).¹⁷⁶

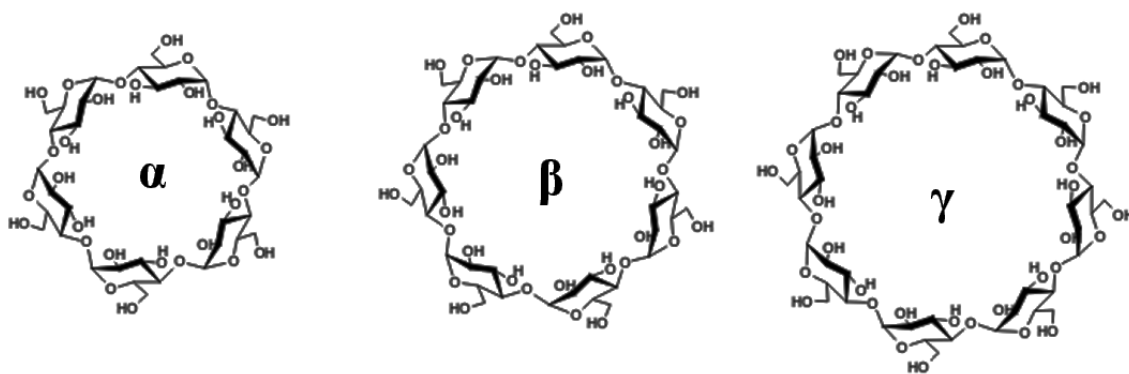


Figure 1.19 Molecular structures of the natural cyclodextrins.

They have been first described by Villiers in 1891. The cyclodextrins present a truncated cone shape (toroidal) structure where primary alcohols are exposed and readily accessible at the primary rim (narrow) and secondary alcohols at the secondary rim (wide).¹⁷⁷ Their three dimensional structures make them attractive because of the differential reactivity of their alcohol functions, which allow regioselectivity. Accordingly, the cyclodextrins have been widely used in supramolecular chemistry because of their shape and reactivity. The propensity of native cyclodextrins to form inclusion complexes with organic molecules have been extensively studied and explored, not only for academic purposes¹⁷⁸ but also for commercial applications.¹⁷⁹ Thus, a broad range of chemical or enzymatic modifications are now well established and broaden significantly the number of application fields of cyclodextrins. In this way, β -CD was chosen as a complexant agent for the sensitive biorecognition of Levo-Thyroxine (T₄).¹⁸⁰

1.7 References

1. Feynman, R. P., There's plenty of room at the bottom. *Engineering and Science* **1960**, *23* (5), 22-36.
2. Iijima, S., Helical microtubules of graphitic carbon. *Nature* **1991**, *354* (6348), 56-58.
3. Thostenson, E. T.; Ren, Z.; Chou, T.-W., Advances in the science and technology of carbon nanotubes and their composites: a review. *Composites Science and Technology* **2001**, *61* (13), 1899-1912.
4. José-Yacamán, M.; Rendón, L.; Arenas, J.; Puche, M. C. S., Maya blue paint: an ancient nanostructured material. *Science* **1996**, *273* (5272), 223-225.
5. Mamalis, A.; Vogtländer, L.; Markopoulos, A., Nanotechnology and nanostructured materials: trends in carbon nanotubes. *Precision Engineering* **2004**, *28* (1), 16-30.
6. Jordan, J.; Jacob, K. I.; Tannenbaum, R.; Sharaf, M. A.; Jasiuk, I., Experimental trends in polymer nanocomposites: A review. *Materials Science and Engineering: A* **2005**, *393* (1-2), 1-11.
7. Ajayan, P. M.; Schadler, L. S.; Braun, P. V., *Nanocomposite Science and Technology*. John Wiley & Sons: 2006.

8. Karttunen, M.; Ruuskanen, P.; Pitkänen, V.; Albers, W., Electrically Conductive Metal Polymer Nanocomposites for Electronics Applications. *Journal of Electronic Materials* **2008**, *37* (7), 951-954.
9. Candelaria, S. L.; Shao, Y.; Zhou, W.; Li, X.; Xiao, J.; Zhang, J.-G.; Wang, Y.; Liu, J.; Li, J.; Cao, G., Nanostructured carbon for energy storage and conversion. *Nano Energy* **2012**, *1* (2), 195-220.
10. Montes, R.; Bartrolí, J.; Céspedes, F.; Baeza, M., Towards to the improvement of the analytical response in voltammetric sensors based on rigid composites. *Journal of Electroanalytical Chemistry* **2014**, *733*, 69-76.
11. Olivé-Monllau, R.; Esplandiú, M. J.; Bartrolí, J.; Baeza, M.; Céspedes, F., Strategies for the optimization of carbon nanotube/polymer ratio in composite materials: applications as voltammetric sensors. *Sensors and Actuators B: Chemical* **2010**, *146* (1), 353-360.
12. Alwarappan, S.; Liu, C.; Kumar, A.; Li, C.-Z., Enzyme-doped graphene nanosheets for enhanced glucose biosensing. *The Journal of Physical Chemistry C* **2010**, *114* (30), 12920-12924.
13. Coleman, J. N.; Khan, U.; Blau, W. J.; Gun'ko, Y. K., Small but strong: A review of the mechanical properties of carbon nanotube–polymer composites. *Carbon* **2006**, *44* (9), 1624-1652.
14. Treacy, M.; Ebbesen, T.; Gibson, J., Exceptionally high Young's modulus observed for individual carbon nanotubes. *Nature* **1996**, 678-680.
15. Ebbesen, T.; Lezec, H.; Hiura, H.; Bennett, J.; Ghaemi, H.; Thio, T., Electrical conductivity of individual carbon nanotubes. *Nature* **1996**, 54-56.
16. Vashist, S. K.; Zheng, D.; Al-Rubeaan, K.; Luong, J. H.; Sheu, F.-S., Advances in carbon nanotube based electrochemical sensors for bioanalytical applications. *Biotechnology Advances* **2011**, *29* (2), 169-188.
17. Muñoz, J.; Bastos-Arrieta, J.; Muñoz, M.; Muraviev, D.; Céspedes, F.; Baeza, M., Simple green routes for the customized preparation of sensitive carbon nanotubes/epoxy nanocomposite electrodes with functional metal nanoparticles. *RSC Advances* **2014**, *4* (84), 44517-44524.
18. Joshi, P. P.; Merchant, S. A.; Wang, Y.; Schmidtke, D. W., Amperometric biosensors based on redox polymer-carbon nanotube-enzyme composites. *Analytical Chemistry* **2005**, *77* (10), 3183-3188.

19. Zelada-Guillén, G. A.; Tweed-Kent, A.; Niemann, M.; Göringer, H. U.; Riu, J.; Rius, F. X., Ultrasensitive and real-time detection of proteins in blood using a potentiometric carbon-nanotube aptasensor. *Biosensors and Bioelectronics* **2013**, *41*, 366-371.
20. Olivé-Monllau, R.; Pereira, A.; Bartrolí, J.; Baeza, M.; Céspedes, F., Highly sensitive CNT composite amperometric sensors integrated in an automated flow system for the determination of free chlorine in waters. *Talanta* **2010**, *81* (4–5), 1593-1598.
21. Esplandiu, M. J.; Baeza, M.; Olivé-Monllau, R.; Céspedes, F.; Bartrolí, J., Development of Tunable Nanocomposites Made from Carbon Nanotubes for Electrochemical Applications. *Advances in Composite Materials for Medicine and Nanotechnology*, Dr. Brahim Attaf (Ed.) **2011**.
22. Bao, L.; Mahurin, S.; Haire, R.; Dai, S., Silver-doped sol-gel film as a surface-enhanced Raman scattering substrate for detection of uranyl and neptunyl ions. *Analytical Chemistry* **2003**, *75* (23), 6614-6620.
23. Ma, R.; Sasaki, T.; Bando, Y., Layer-by-layer assembled multilayer films of titanate nanotubes, Ag-or Au-loaded nanotubes, and nanotubes/nanosheets with polycations. *Journal of the American Chemical Society* **2004**, *126* (33), 10382-10388.
24. Habibi, B.; Jahanbakhshi, M., Silver nanoparticles/multi walled carbon nanotubes nanocomposite modified electrode: Voltammetric determination of clonazepam. *Electrochimica Acta* **2014**, *118*, 10-17.
25. Michalet, X.; Pinaud, F. F.; Bentolila, L. A.; Tsay, J. M.; Doose, S.; Li, J. J.; Sundaresan, G.; Wu, A. M.; Gambhir, S. S.; Weiss, S., Quantum dots for live cells, in vivo imaging, and diagnostics. *Science* **2005**, *307* (5709), 538-544.
26. Biju, V.; Itoh, T.; Anas, A.; Sujith, A.; Ishikawa, M., Semiconductor quantum dots and metal nanoparticles: syntheses, optical properties, and biological applications. *Analytical and Bioanalytical Chemistry* **2008**, *391* (7), 2469-2495.
27. Hansen, J. A.; Wang, J.; Kawde, A.-N.; Xiang, Y.; Gothelf, K. V.; Collins, G., Quantum-dot/aptamer-based ultrasensitive multi-analyte electrochemical biosensor. *Journal of the American Chemical Society* **2006**, *128* (7), 2228-2229.
28. Geim, A. K.; Novoselov, K. S., The rise of graphene. *Nature Materials* **2007**, *6* (3), 183-191.
29. Dreyer, D. R.; Park, S.; Bielawski, C. W.; Ruoff, R. S., The chemistry of graphene oxide. *Chemical Society Reviews* **2010**, *39* (1), 228-240.

30. Park, S.; Ruoff, R. S., Chemical methods for the production of graphenes. *Nature Nanotechnology* **2009**, *4* (4), 217-224.
31. Wang, Y.; Li, Y.; Tang, L.; Lu, J.; Li, J., Application of graphene-modified electrode for selective detection of dopamine. *Electrochemistry Communications* **2009**, *11* (4), 889-892.
32. Alwarappan, S.; Erdem, A.; Liu, C.; Li, C.-Z., Probing the electrochemical properties of graphene nanosheets for biosensing applications. *The Journal of Physical Chemistry C* **2009**, *113* (20), 8853-8857.
33. Kroto, H. W.; Heath, J. R.; O'Brien, S. C.; Curl, R. F.; Smalley, R. E., C 60: buckminsterfullerene. *Nature* **1985**, *318* (6042), 162-163.
34. Jorio, A.; Dresselhaus, G.; Dresselhaus, M. S., *Carbon nanotubes: advanced topics in the synthesis, structure, properties and applications*. Springer: 2007; Vol. 111.
35. Radushkevich, L.; Lukyanovich, V., About the structure of carbon formed by thermal decomposition of carbon monoxide on iron substrate. *Journal of Physical Chemistry (Moscow)* **1952**, *26*, 88-95.
36. Pumera, M.; Escarpa, A., Nanomaterials as electrochemical detectors in microfluidics and CE: Fundamentals, designs, and applications. *Electrophoresis* **2009**, *30* (19), 3315-3323.
37. Delgado, J. L.; Herranz, M. a. A.; Martin, N., The nano-forms of carbon. *Journal of Materials Chemistry* **2008**, *18* (13), 1417-1426.
38. Zhao, Q.; Gan, Z.; Zhuang, Q., Electrochemical sensors based on carbon nanotubes. *Electroanalysis* **2002**, *14* (23), 1609-1613.
39. O'connell, M. J., *Carbon nanotubes: properties and applications*. CRC press: 2012.
40. Ouyang, M.; Huang, J.-L.; Lieber, C. M., Fundamental electronic properties and applications of single-walled carbon nanotubes. *Accounts of Chemical Research* **2002**, *35* (12), 1018-1025.
41. Balasubramanian, K.; Burghard, M., Chemically functionalized carbon nanotubes. *Small* **2005**, *1* (2), 180-192.
42. Cooper, D. R.; Nadeau, J. L., Nanotechnology for in vitro neuroscience. *Nanoscale* **2009**, *1* (2), 183-200.
43. Banks, C. E.; Davies, T. J.; Wildgoose, G. G.; Compton, R. G., Electrocatalysis at graphite and carbon nanotube modified electrodes: edge-plane sites and tube ends are the reactive sites. *Chemical Communications* **2005**, (7), 829-841.

44. Govindaraj, A.; Rao, C., Synthesis, growth mechanism and processing of carbon nanotubes. *Carbon nanotechnology. Amsterdam: Elsevier* **2006**, 15-51.
45. Jahanshahi, M.; Kiadehi, A. D., Fabrication, Purification and Characterization of Carbon Nanotubes: Arc-Discharge in Liquid Media (ADLM). **2013**.
46. Tohji, K.; Takahashi, H.; Shinoda, Y.; Shimizu, N.; Jeyadevan, B.; Matsuoka, I.; Saito, Y.; Kasuya, A.; Ito, S.; Nishina, Y., Purification procedure for single-walled nanotubes. *The Journal of Physical Chemistry B* **1997**, *101* (11), 1974-1978.
47. Li, Y.; Zhang, X.; Luo, J.; Huang, W.; Cheng, J.; Luo, Z.; Li, T.; Liu, F.; Xu, G.; Ke, X.; Li, L.; Geise, H. J., Purification of CVD synthesized single-wall carbon nanotubes by different acid oxidation treatments. *Nanotechnology* **2004**, *15* (11), 1645.
48. Muñoz, J.; Bartrolí, J.; Céspedes, F.; Baeza, M., Influence of raw carbon nanotubes diameter for the optimization of the load composition ratio in epoxy amperometric composite sensors. *Journal of Materials Science* **2015**, *50* (2), 652-661.
49. Castillo, F. Y.; Socher, R.; Krause, B.; Headrick, R.; Grady, B. P.; Prada-Silvy, R.; Pötschke, P., Electrical, mechanical, and glass transition behavior of polycarbonate-based nanocomposites with different multi-walled carbon nanotubes. *Polymer* **2011**, *52* (17), 3835-3845.
50. Benoit, J.; Buisson, J.; Chauvet, O.; Godon, C.; Lefrant, S., Low-frequency Raman studies of multiwalled carbon nanotubes: experiments and theory. *Physical Review B* **2002**, *66* (7), 073417.
51. Krause, B.; Boldt, R.; Pötschke, P., A method for determination of length distributions of multiwalled carbon nanotubes before and after melt processing. *Carbon* **2011**, *49* (4), 1243-1247.
52. Mansfield, E.; Kar, A.; Hooker, S. A., Applications of TGA in quality control of SWCNTs. *Analytical and Bioanalytical Chemistry* **2010**, *396* (3), 1071-1077.
53. Trigueiro, J. P. C.; Silva, G. G.; Lavall, R. L.; Furtado, C. A.; Oliveira, S.; Ferlauto, A. S.; Lacerda, R. G.; Ladeira, L. O.; Liu, J.-W.; Frost, R. L., Purity evaluation of carbon nanotube materials by thermogravimetric, TEM, and SEM methods. *Journal of Nanoscience and Nanotechnology* **2007**, *7* (10), 3477-3486.
54. McKee, G. S.; Vecchio, K. S., Thermogravimetric analysis of synthesis variation effects on CVD generated multiwalled carbon nanotubes. *The Journal of Physical Chemistry B* **2006**, *110* (3), 1179-1186.

55. Lima, A. M.; Musumeci, A. W.; Liu, H.-W.; Waclawik, E. R.; Silva, G. G., Purity evaluation and influence of carbon nanotube on carbon nanotube/graphite thermal stability. *Journal of Thermal Analysis and Calorimetry* **2009**, *97* (1), 257-263.

56. Arepalli, S.; Nikolaev, P.; Gorelik, O.; Hadjiev, V. G.; Holmes, W.; Files, B.; Yowell, L., Protocol for the characterization of single-wall carbon nanotube material quality. *Carbon* **2004**, *42* (8–9), 1783-1791.

57. Banks, C. E.; Crossley, A.; Salter, C.; Wilkins, S. J.; Compton, R. G., Carbon Nanotubes Contain Metal Impurities Which Are Responsible for the “Electrocatalysis” Seen at Some Nanotube-Modified Electrodes. *Angewandte Chemie International Edition* **2006**, *45* (16), 2533-2537.

58. Misra, A.; Tyagi, P. K.; Rai, P.; Misra, D., FTIR Spectroscopy of Multiwalled Carbon Nanotubes: A Simple Approach to Study the Nitrogen Doping. *Journal of Nanoscience and Nanotechnology* **2007**, *7* (6), 1820-1823.

59. Kouklin, N.; Tzolov, M.; Straus, D.; Yin, A.; Xu, J., Infrared absorption properties of carbon nanotubes synthesized by chemical vapor deposition. *Applied Physics Letters* **2004**, *85* (19), 4463-4465.

60. Dresselhaus, M. S.; Dresselhaus, G.; Saito, R.; Jorio, A., Raman spectroscopy of carbon nanotubes. *Physics Reports* **2005**, *409* (2), 47-99.

61. Vinayan, B.; Nagar, R.; Raman, V.; Rajalakshmi, N.; Dhathathreyan, K.; Ramaprabhu, S., Synthesis of graphene-multiwalled carbon nanotubes hybrid nanostructure by strengthened electrostatic interaction and its lithium ion battery application. *Journal of Materials Chemistry* **2012**, *22* (19), 9949-9956.

62. Dresselhaus, M. S.; Jorio, A.; Hofmann, M.; Dresselhaus, G.; Saito, R., Perspectives on Carbon Nanotubes and Graphene Raman Spectroscopy. *Nano Letters* **2010**, *10* (3), 751-758.

63. Saito, R.; Grüneis, A.; Samsonidze, G. G.; Brar, V.; Dresselhaus, G.; Dresselhaus, M.; Jorio, A.; Cançado, L.; Fantini, C.; Pimenta, M., Double resonance Raman spectroscopy of single-wall carbon nanotubes. *New Journal of Physics* **2003**, *5* (1), 157.

64. Vilela, D.; Ansón-Casaos, A.; Martínez, M. T.; González, M. C.; Escarpa, A., High NIR-purity index single-walled carbon nanotubes for electrochemical sensing in microfluidic chips. *Lab on a Chip* **2012**, *12* (11), 2006-2014.

65. Xie, X.-L.; Mai, Y.-W.; Zhou, X.-P., Dispersion and alignment of carbon nanotubes in polymer matrix: a review. *Materials Science and Engineering: R: Reports* **2005**, *49* (4), 89-112.
66. Wong, E. W.; Sheehan, P. E.; Lieber, C. M., Nanobeam mechanics: elasticity, strength, and toughness of nanorods and nanotubes. *Science* **1997**, *277* (5334), 1971-1975.
67. Kim, P.; Shi, L.; Majumdar, A.; McEuen, P., Thermal transport measurements of individual multiwalled nanotubes. *Physical Review Letters* **2001**, *87* (21), 215502.
68. Collins, P. G.; Avouris, P., Nanotubes for electronics. *Scientific American* **2000**, *283* (6), 62-69.
69. Mylvaganam, K.; Zhang, L., Chemical bonding in polyethylene-nanotube composites: A quantum mechanics prediction. *The Journal of Physical Chemistry B* **2004**, *108* (17), 5217-5220.
70. Shofner, M. L.; Khabashesku, V. N.; Barrera, E. V., Processing and mechanical properties of fluorinated single-wall carbon nanotube-polyethylene composites. *Chemistry of Materials* **2006**, *18* (4), 906-913.
71. Oldham, K. B., Edge effects in semiinfinite diffusion. *Journal of Electroanalytical Chemistry and Interfacial Electrochemistry* **1981**, *122*, 1-17.
72. Weber, S. G., Signal-to-noise ratio in microelectrode-array-based electrochemical detectors. *Analytical Chemistry* **1989**, *61* (4), 295-302.
73. O'Hare, D.; Macpherson, J. V.; Willows, A., On the microelectrode behaviour of graphite-epoxy composite electrodes. *Electrochemistry Communications* **2002**, *4* (3), 245-250.
74. Zhao, H.; O'Hare, D., Characterisation and modeling of conducting composite electrodes. *The Journal of Physical Chemistry C* **2008**, *112* (25), 9351-9357.
75. Hammersley, J. M., Percolation processes: Lower bounds for the critical probability. *The Annals of Mathematical Statistics* **1957**, 790-795.
76. Scher, H.; Zallen, R., Critical density in percolation processes. *The Journal of Chemical Physics* **1970**, *53* (9), 3759-3761.
77. Wilkinson, D.; Willemsen, J. F., Invasion percolation: a new form of percolation theory. *Journal of Physics A: Mathematical and General* **1983**, *16* (14), 3365.
78. Navarro-Laboulais, J.; Trijueque, J.; García-Jareño, J.; Vicente, F., Impedance analysis of graphite+ polyethylene and graphite+ epoxy composite electrodes. *Journal of Electroanalytical Chemistry* **1995**, *399* (1), 115-120.

79. Li, W.; Liu, Z. Y.; Yang, M. B., Preparation of carbon black/polypropylene nanocomposite with low percolation threshold using mild blending method. *Journal of Applied Polymer Science* **2010**, *115* (5), 2629-2634.

80. Montes, R.; Bartrolí, J.; Baeza, M.; Céspedes, F., Improvement of the detection limit for biosensors: Advances on the optimization of biocomposite composition. *Microchemical Journal* **2015**, *119*, 66-74.

81. Moniruzzaman, M.; Winey, K. I., Polymer nanocomposites containing carbon nanotubes. *Macromolecules* **2006**, *39* (16), 5194-5205.

82. Martin, C.; Sandler, J.; Shaffer, M.; Schwarz, M.-K.; Bauhofer, W.; Schulte, K.; Windle, A., Formation of percolating networks in multi-wall carbon-nanotube–epoxy composites. *Composites Science and Technology* **2004**, *64* (15), 2309-2316.

83. Faiella, G.; Piscitelli, F.; Lavorgna, M.; Antonucci, V.; Giordano, M., Tuning the insulator to conductor transition in a multiwalled carbon nanotubes/epoxy composite at substatistical percolation threshold. *Applied Physics Letters* **2009**, *95* (15), 153106.

84. Kara, S.; Arda, E.; Dolastir, F.; Pekcan, Ö., Electrical and optical percolations of polystyrene latex–multiwalled carbon nanotube composites. *Journal of Colloid and Interface Science* **2010**, *344* (2), 395-401.

85. Alegret, S.; Céspedes, F.; Martínez-Fàbregas, E.; Martorell, D.; Morales, A.; Centelles, E.; Muñoz, J., Carbon-polymer biocomposites for amperometric sensing. *Biosensors and Bioelectronics* **1996**, *11* (1), 35-44.

86. Pacios, M.; Del Valle, M.; Bartrolí, J.; Esplandiú, M., Electrochemical behavior of rigid carbon nanotube composite electrodes. *Journal of Electroanalytical Chemistry* **2008**, *619*, 117-124.

87. Stetter, J. R.; Penrose, W. R.; Yao, S., Sensors, chemical sensors, electrochemical sensors, and ECS. *Journal of The Electrochemical Society* **2003**, *150* (2), S11-S16.

88. Adams, R., Carbon paste electrodes. *Analytical Chemistry* **1958**, *30* (9), 1576-1576.

89. Ramanavičius, A.; Ramanavičienė, A.; Malinauskas, A., Electrochemical sensors based on conducting polymer—polypyrrole. *Electrochimica Acta* **2006**, *51* (27), 6025-6037.

90. Moulton, S. E.; Minett, A.; Wallace, G., Electrochemical properties of carbon nanotubes. *Northfields Avenue. Wollongong. NSW* **2006**, *2522*, 297-321.

91. Rubianes, M. D.; Rivas, G. A., Dispersion of multi-wall carbon nanotubes in polyethylenimine: A new alternative for preparing electrochemical sensors. *Electrochemistry Communications* **2007**, *9* (3), 480-484.
92. Balamurugan, A.; Ho, K.-C.; Chen, S.-M.; Huang, T.-Y., Electrochemical sensing of NADH based on Meldola Blue immobilized silver nanoparticle-conducting polymer electrode. *Colloids and Surfaces A: Physicochemical and Engineering Aspects* **2010**, *362* (1-3), 1-7.
93. Shao, Y.; Zhang, S.; Engelhard, M. H.; Li, G.; Shao, G.; Wang, Y.; Liu, J.; Aksay, I. A.; Lin, Y., Nitrogen-doped graphene and its electrochemical applications. *Journal of Materials Chemistry* **2010**, *20* (35), 7491-7496.
94. Ragupathy, D.; Gopalan, A. I.; Lee, K.-P., Electrocatalytic oxidation and determination of ascorbic acid in the presence of dopamine at multiwalled carbon nanotube-silica network-gold nanoparticles based nanohybrid modified electrode. *Sensors and Actuators B: Chemical* **2010**, *143* (2), 696-703.
95. Lawrence, N. S.; Deo, R. P.; Wang, J., Electrochemical determination of hydrogen sulfide at carbon nanotube modified electrodes. *Analytica Chimica Acta* **2004**, *517* (1), 131-137.
96. Wang, J.; Kawde, A.-N.; Musameh, M., Carbon-nanotube-modified glassy carbon electrodes for amplified label-free electrochemical detection of DNA hybridization. *Analyst* **2003**, *128* (7), 912-916.
97. Solanki, P. R.; Kaushik, A.; Ansari, A. A.; Tiwari, A.; Malhotra, B., Multi-walled carbon nanotubes/sol-gel-derived silica/chitosan nanobiocomposite for total cholesterol sensor. *Sensors and Actuators B: Chemical* **2009**, *137* (2), 727-735.
98. Crevillén, A. G.; Ávila, M.; Pumera, M.; González, M. C.; Escarpa, A., Food analysis on microfluidic devices using ultrasensitive carbon nanotubes detectors. *Analytical Chemistry* **2007**, *79* (19), 7408-7415.
99. Britto, P. J.; Santhanam, K. S.; Rubio, A.; Alonso, J. A.; Ajayan, P. M., Improved charge transfer at carbon nanotube electrodes. *Advanced Materials* **1999**, *11* (2), 154-157.
100. McCreery, R. L., Advanced carbon electrode materials for molecular electrochemistry. *Chemical Reviews* **2008**, *108* (7), 2646-2687.
101. Arrigan, D. W., Nanoelectrodes, nanoelectrode arrays and their applications. *Analyst* **2004**, *129* (12), 1157-1165.

102. Macdonald, D. D., Reflections on the history of electrochemical impedance spectroscopy. *Electrochimica Acta* **2006**, *51* (8–9), 1376-1388.

103. Pejcic, B.; De Marco, R., Impedance spectroscopy: Over 35 years of electrochemical sensor optimization. *Electrochimica Acta* **2006**, *51* (28), 6217-6229.

104. Zhang, J.; Tan, X.; Zhao, D.; Tan, S.; Huang, Z.; Mi, Y.; Huang, Z., Amperometric hydrogen peroxide biosensor based on multiwall carbon nanotubes and cadmium sulfide quantum dots. *Chemical Research in Chinese Universities* **2010**, *26*, 541-545.

105. Lisdat, F.; Schäfer, D., The use of electrochemical impedance spectroscopy for biosensing. *Analytical and Bioanalytical Chemistry* **2008**, *391* (5), 1555-1567.

106. Laoire, C. O.; Mukerjee, S.; Abraham, K.; Plichta, E. J.; Hendrickson, M. A., Elucidating the mechanism of oxygen reduction for lithium-air battery applications. *The Journal of Physical Chemistry C* **2009**, *113* (46), 20127-20134.

107. Banerjee, S.; Hemraj-Benny, T.; Wong, S. S., Covalent surface chemistry of single-walled carbon nanotubes. *Advanced Materials* **2005**, *17* (1), 17-29.

108. Olivé-Monllau, R.; Baeza, M.; Bartrolí, J.; Céspedes, F., Novel Amperometric Sensor Based on Rigid Near-Percolation Composite. *Electroanalysis* **2009**, *21* (8), 931-938.

109. Baeza, M.; Olivé-Monllau, R.; Esplandiú, M. J.; Céspedes, F.; Bartrolí, J., Advances on rigid conducting composites for electroanalytical applications. In *Resin Compos. Prop. Prod. Appl.*, Nova Science Publishers, Inc.: 2011; pp 153-211.

110. Santos, L. s. M.; Ghilane, J.; Fave, C.; Lacaze, P.-C.; Randriamahazaka, H.; Abrantes, L. M.; Lacroix, J.-C., Electrografting polyaniline on carbon through the electroreduction of diazonium salts and the electrochemical polymerization of aniline. *The Journal of Physical Chemistry C* **2008**, *112* (41), 16103-16109.

111. Binnig, G.; Rohrer, H.; Gerber, C.; Weibel, E., Surface studies by scanning tunneling microscopy. *Physical Review Letters* **1982**, *49* (1), 57.

112. Elazari, R.; Salitra, G.; Talyosef, Y.; Grinblat, J.; Scordilis-Kelley, C.; Xiao, A.; Affinito, J.; Aurbach, D., Morphological and structural studies of composite sulfur electrodes upon cycling by HRTEM, AFM and Raman spectroscopy. *Journal of the Electrochemical Society* **2010**, *157* (10), A1131-A1138.

113. Liu, H.; Slamovich, E. B.; Webster, T. J., Increased osteoblast functions among nanophase titania/poly(lactide-co-glycolide) composites of the highest nanometer surface roughness. *Journal of Biomedical Materials Research Part A* **2006**, 78A (4), 798-807.
114. Minsky, M., Microscopy apparatus. *U.S. Patent No. 3,013,467*. **1961**.
115. Paddock, S. W., Principles and practices of laser scanning confocal microscopy. *Molecular Biotechnology* **2000**, 16 (2), 127-149.
116. Jordan, H.-J.; Wegner, M.; Tiziani, H., Highly accurate non-contact characterization of engineering surfaces using confocal microscopy. *Measurement Science and Technology* **1998**, 9 (7), 1142.
117. Pawley, J., *Handbook of biological confocal microscopy*. Springer Science & Business Media: 2010.
118. Qlark Jr, L., Monitor and control of blood and tissue oxygen tensions. *ASAIO Journal* **1956**, 2 (1), 41-48.
119. Helm, I.; Jalukse, L.; Leito, I., Measurement uncertainty estimation in amperometric sensors: a tutorial review. *Sensors* **2010**, 10 (5), 4430-4455.
120. Alvarez-Icaza, M.; Bilitewski, U., Mass production of biosensors. *Analytical Chemistry* **1993**, 65 (11), 525A-533A.
121. Creasy, K. E.; Shaw, B. R., Polishable modified carbon fiber composite electrodes containing copolymers of (vinylferrocene) or (vinylpyridine) in a cross-linked polystyrene matrix. *Analytical Chemistry* **1989**, 61 (13), 1460-1465.
122. Alkire, R. C.; Kolb, D. M.; Lipkowski, J.; Ross, P. N., *Chemically modified electrodes*. John Wiley & Sons: 2009; Vol. 22.
123. Wildgoose, G. G.; Banks, C. E.; Leventis, H. C.; Compton, R. G., Chemically Modified Carbon Nanotubes for Use in Electroanalysis. *Microchimica Acta* **2006**, 152 (3-4), 187-214.
124. Esplandiu, M. J., Electrochemistry on Carbon-Nanotube-Modified Surfaces. In *Chemically Modified Electrodes*, Wiley-VCH Verlag GmbH & Co. KGaA **2009**, 117-168.
125. Merkoçi, A., Carbon Nanotubes in Analytical Sciences. *Microchimica Acta* **2006**, 152 (3-4), 157-174.
126. Antiochia, R.; Gorton, L., Development of a carbon nanotube paste electrode osmium polymer-mediated biosensor for determination of glucose in alcoholic beverages. *Biosensors and Bioelectronics* **2007**, 22 (11), 2611-2617.

127. Zhang, M.; Gorski, W., Electrochemical sensing based on redox mediation at carbon nanotubes. *Analytical Chemistry* **2005**, *77* (13), 3960-3965.

128. Wang, J.; Liu, J., Fumed-silica containing carbon-paste dehydrogenase biosensors. *Analytica Chimica Acta* **1993**, *284* (2), 385-391.

129. White, S. F.; Turner, A. P.; Schmid, R. D.; Bilitewski, U.; Bradley, J., Investigations of platinized and rhodinized carbon electrodes for use in glucose sensors. *Electroanalysis* **1994**, *6* (8), 625-632.

130. Wang, G.; He, X.; Wang, L.; Gu, A.; Huang, Y.; Fang, B.; Geng, B.; Zhang, X., Non-enzymatic electrochemical sensing of glucose. *Microchimica Acta* **2013**, *180* (3-4), 161-186.

131. Zhao, W.; Wang, H.; Qin, X.; Wang, X.; Zhao, Z.; Miao, Z.; Chen, L.; Shan, M.; Fang, Y.; Chen, Q., A novel nonenzymatic hydrogen peroxide sensor based on multi-wall carbon nanotube/silver nanoparticle nanohybrids modified gold electrode. *Talanta* **2009**, *80* (2), 1029-1033.

132. You, T.; Niwa, O.; Tomita, M.; Hirono, S., Characterization of platinum nanoparticle-embedded carbon film electrode and its detection of hydrogen peroxide. *Analytical Chemistry* **2003**, *75* (9), 2080-2085.

133. Yang, J.; Jiang, L.-C.; Zhang, W.-D.; Gunasekaran, S., A highly sensitive non-enzymatic glucose sensor based on a simple two-step electrodeposition of cupric oxide (CuO) nanoparticles onto multi-walled carbon nanotube arrays. *Talanta* **2010**, *82* (1), 25-33.

134. Wang, J.; Naser, N.; Angnes, L.; Wu, H.; Chen, L., Metal-dispersed carbon paste electrodes. *Analytical Chemistry* **1992**, *64* (11), 1285-1288.

135. Ward, K. R.; Gara, M.; Lawrence, N. S.; Hartshorne, R. S.; Compton, R. G., Nanoparticle modified electrodes can show an apparent increase in electrode kinetics due solely to altered surface geometry: The effective electrochemical rate constant for non-flat and non-uniform electrode surfaces. *Journal of Electroanalytical Chemistry* **2013**, *695*, 1-9.

136. Huang, K.-J.; Niu, D.-J.; Liu, X.; Wu, Z.-W.; Fan, Y.; Chang, Y.-F.; Wu, Y.-Y., Direct electrochemistry of catalase at amine-functionalized graphene/gold nanoparticles composite film for hydrogen peroxide sensor. *Electrochimica Acta* **2011**, *56* (7), 2947-2953.

137. Dong, X.-Y.; Mi, X.-N.; Zhang, L.; Liang, T.-M.; Xu, J.-J.; Chen, H.-Y., DNAzyme-functionalized Pt nanoparticles/carbon nanotubes for amplified sandwich electrochemical DNA analysis. *Biosensors and Bioelectronics* **2012**, *38* (1), 337-341.
138. Pividori, M. I.; Alegret, S., Micro and nanoparticles in biosensing systems for food safety and environmental monitoring. An example of converging technologies. *Microchimica Acta* **2010**, *170* (3-4), 227-242.
139. Shi, Y.; Yang, R.; Yuet, P. K., Easy decoration of carbon nanotubes with well dispersed gold nanoparticles and the use of the material as an electrocatalyst. *Carbon* **2009**, *47* (4), 1146-1151.
140. Lee, Y.; Song, H. J.; Shin, H. S.; Shin, H. J.; Choi, H. C., Spontaneous Formation of Transition-Metal Nanoparticles on Single-Walled Carbon Nanotubes Anchored with Conjugated Molecules. *Small* **2005**, *1* (10), 975-979.
141. Bittencourt, C.; Felten, A.; Ghijsen, J.; Pireaux, J.-J.; Drube, W.; Erni, R.; Van Tendeloo, G., Decorating carbon nanotubes with nickel nanoparticles. *Chemical Physics Letters* **2007**, *436* (4), 368-372.
142. Choi, H. C.; Shim, M.; Bangsaruntip, S.; Dai, H., Spontaneous reduction of metal ions on the sidewalls of carbon nanotubes. *Journal of the American Chemical Society* **2002**, *124* (31), 9058-9059.
143. Lee, K. Y.; Kim, M.; Hahn, J.; Suh, J. S.; Lee, I.; Kim, K.; Han, S. W., Assembly of metal nanoparticle-carbon nanotube composite materials at the liquid/liquid interface. *Langmuir* **2006**, *22* (4), 1817-1821.
144. Qu, L.; Dai, L.; Osawa, E., Shape/size-controlled syntheses of metal nanoparticles for site-selective modification of carbon nanotubes. *Journal of the American Chemical Society* **2006**, *128* (16), 5523-5532.
145. Murphy, C. J.; Jana, N. R., Controlling the aspect ratio of inorganic nanorods and nanowires. *Advanced Materials* **2002**, *14* (1), 80.
146. Ruiz, P.; Muñoz, M.; Macanás, J.; Muraviev, D. N., Intermatrix synthesis of polymer–copper nanocomposites with tunable parameters by using copper comproportionation reaction. *Chemistry of Materials* **2010**, *22* (24), 6616-6623.
147. Bastos-Arrieta, J.; Shafir, A.; Alonso, A.; Munoz, M.; Macanás, J.; Muraviev, D. N., Donnan exclusion driven intermatrix synthesis of reusable polymer stabilized palladium nanocatalysts. *Catalysis Today* **2012**, *193* (1), 207-212.

148. Xu, P.; Han, X.; Zhang, B.; Du, Y.; Wang, H.-L., Multifunctional polymer-metal nanocomposites via direct chemical reduction by conjugated polymers. *Chemical Society Reviews* **2014**, *43* (5), 1349-1360.

149. Pummera, M.; Ambrosi, A.; Bonanni, A.; Chng, E. L. K.; Poh, H. L., Graphene for electrochemical sensing and biosensing. *TrAC Trends in Analytical Chemistry* **2010**, *29* (9), 954-965.

150. Novoselov, K. S.; Geim, A. K.; Morozov, S.; Jiang, D.; Zhang, Y.; Dubonos, S.; Grigorieva, I.; Firsov, A., Electric field effect in atomically thin carbon films. *Science* **2004**, *306* (5696), 666-669.

151. Salavagione, H. J.; Díez-Pascual, A. M.; Lázaro, E.; Vera, S.; Gómez-Fatou, M. A., Chemical sensors based on polymer composites with carbon nanotubes and graphene: the role of the polymer. *Journal of Materials Chemistry A* **2014**, *2* (35), 14289-14328.

152. Lee, C.; Wei, X.; Kysar, J. W.; Hone, J., Measurement of the elastic properties and intrinsic strength of monolayer graphene. *Science* **2008**, *321* (5887), 385-388.

153. Huang, X.; Qi, X.; Boey, F.; Zhang, H., Graphene-based composites. *Chemical Society Reviews* **2012**, *41* (2), 666-686.

154. Warner, J. H.; Schaffel, F.; Rummeli, M.; Bachmatiuk, A., *Graphene: fundamentals and emergent applications*. Newnes: 2012.

155. Edwards, R. S.; Coleman, K. S., Graphene synthesis: relationship to applications. *Nanoscale* **2013**, *5* (1), 38-51.

156. Hummers Jr, W. S.; Offeman, R. E., Preparation of graphitic oxide. *Journal of the American Chemical Society* **1958**, *80* (6), 1339-1339.

157. Martín, A.; Hernández-Ferrer, J.; Vázquez, L.; Martínez, M.-T.; Escarpa, A., Controlled chemistry of tailored graphene nanoribbons for electrochemistry: a rational approach to optimizing molecule detection. *RSC Advances* **2014**, *4* (1), 132-139.

158. Kosynkin, D. V.; Higginbotham, A. L.; Sinitskii, A.; Lomeda, J. R.; Dimiev, A.; Price, B. K.; Tour, J. M., Longitudinal unzipping of carbon nanotubes to form graphene nanoribbons. *Nature* **2009**, *458* (7240), 872-876.

159. Jiao, L.; Zhang, L.; Wang, X.; Diankov, G.; Dai, H., Narrow graphene nanoribbons from carbon nanotubes. *Nature* **2009**, *458* (7240), 877-880.

160. Vashist, S. K.; Luong, J. H. T., Recent advances in electrochemical biosensing schemes using graphene and graphene-based nanocomposites. *Carbon* **2015**, *84* (0), 519-550.

161. Kim, H.; Abdala, A. A.; Macosko, C. W., Graphene/polymer nanocomposites. *Macromolecules* **2010**, *43* (16), 6515-6530.
162. Chen, D.; Tang, L.; Li, J., Graphene-based materials in electrochemistry. *Chemical Society Reviews* **2010**, *39* (8), 3157-3180.
163. Shan, C.; Yang, H.; Song, J.; Han, D.; Ivaska, A.; Niu, L., Direct electrochemistry of glucose oxidase and biosensing for glucose based on graphene. *Analytical Chemistry* **2009**, *81* (6), 2378-2382.
164. Keeley, G. P.; O'Neill, A.; McEvoy, N.; Peltekis, N.; Coleman, J. N.; Duesberg, G. S., Electrochemical ascorbic acid sensor based on DMF-exfoliated graphene. *Journal of Materials Chemistry* **2010**, *20* (36), 7864-7869.
165. Zhou, M.; Zhai, Y.; Dong, S., Electrochemical sensing and biosensing platform based on chemically reduced graphene oxide. *Analytical Chemistry* **2009**, *81* (14), 5603-5613.
166. Hou, S.; Kasner, M. L.; Su, S.; Patel, K.; Cuellari, R., Highly sensitive and selective dopamine biosensor fabricated with silanized graphene. *The Journal of Physical Chemistry C* **2010**, *114* (35), 14915-14921.
167. Shao, Y.; Wang, J.; Wu, H.; Liu, J.; Aksay, I. A.; Lin, Y., Graphene based electrochemical sensors and biosensors: a review. *Electroanalysis* **2010**, *22* (10), 1027-1036.
168. Martín, A.; Escarpa, A., Graphene: the cutting-edge interaction between chemistry and electrochemistry. *TrAC Trends in Analytical Chemistry* **2014**, *56*, 13-26.
169. Liu, Y.; Dong, X.; Chen, P., Biological and chemical sensors based on graphene materials. *Chemical Society Reviews* **2012**, *41* (6), 2283-2307.
170. Shin, H. J.; Kim, K. K.; Benayad, A.; Yoon, S. M.; Park, H. K.; Jung, I. S.; Jin, M. H.; Jeong, H. K.; Kim, J. M.; Choi, J. Y., Efficient reduction of graphite oxide by sodium borohydride and its effect on electrical conductance. *Advanced Functional Materials* **2009**, *19* (12), 1987-1992.
171. Fan, Y.; Liu, J.-H.; Yang, C.-P.; Yu, M.; Liu, P., Graphene-polyaniline composite film modified electrode for voltammetric determination of 4-aminophenol. *Sensors and Actuators B: Chemical* **2011**, *157* (2), 669-674.
172. Balogun, Y. A.; Buchanan, R. C., Enhanced percolative properties from partial solubility dispersion of filler phase in conducting polymer composites (CPCs). *Composites Science and Technology* **2010**, *70* (6), 892-900.

173. McCreery, R. L., Carbon electrodes: structural effects on electron transfer kinetics. *Electroanalytical Chemistry* **1991**, *17*, 221-374.

174. Muszynski, R.; Seger, B.; Kamat, P. V., Decorating graphene sheets with gold nanoparticles. *The Journal of Physical Chemistry C* **2008**, *112* (14), 5263-5266.

175. Scheuermann, G. M.; Rumi, L.; Steurer, P.; Bannwarth, W.; Mülhaupt, R., Palladium nanoparticles on graphite oxide and its functionalized graphene derivatives as highly active catalysts for the Suzuki–Miyaura coupling reaction. *Journal of the American Chemical Society* **2009**, *131* (23), 8262-8270.

176. Szejtli, J., Introduction and general overview of cyclodextrin chemistry. *Chemical Reviews* **1998**, *98* (5), 1743-1754.

177. Shahgaldian, P.; Pielec, U., Cyclodextrin derivatives as chiral supramolecular receptors for enantioselective sensing. *Sensors* **2006**, *6* (6), 593-615.

178. He, J.-L.; Yang, Y.; Yang, X.; Liu, Y.-L.; Liu, Z.-H.; Shen, G.-L.; Yu, R.-Q., β -Cyclodextrin incorporated carbon nanotube-modified electrode as an electrochemical sensor for rutin. *Sensors and Actuators B: Chemical* **2006**, *114* (1), 94-100.

179. Szejtli, J., Utilization of cyclodextrins in industrial products and processes. *Journal of Materials Chemistry* **1997**, *7* (4), 575-587.

180. Khafaji, M.; Shahrokhian, S.; Ghalkhani, M., Electrochemistry of Levo-Thyroxin on Edge-Plane Pyrolytic Graphite Electrode: Application to Sensitive Analytical Determinations. *Electroanalysis* **2011**, *23* (8), 1875-1880.

CHAPTER II

Motivation and Aims

CHAPTER II

Motivation and Aims

Being part of the *Sensors and Biosensors Group* has offered me the opportunity to be involved into the “Nano World” in an innovative and different way.

By the time I enrolled the group, its scientific background included the use of different carbon materials, such as graphite and carbon nanotubes (CNTs) for their use as filler materials in the development of electrochemical composites (bio)sensors based on epoxy resin as insulating polymer. The determination of the optimum composition ratio of the nanocomposite electrodes for the improvement of their electroanalytical performance has also been a goal of study. In this way, Electrochemical Impedance Spectroscopy (EIS) has become a powerful tool to characterize the composite electrodes and determine their optimum composition ratios. Working with those optimized composite electrodes, also named near-percolation composite electrodes (NPC electrodes), provides them some advantages, such as better limit of detection, wider lineal range, higher reproducibility in the electrodes production and increase of the stability as well as the repeatability of the analytical signal.

Consequently, new strategies were developed to improve the electroanalytical response of carbon-based composite (bio)sensors. Firstly, the determination of the optimum composite composition regarding the nature of carbon nanotubes has been one of the goal subjects of this thesis, due to the main drawback of CNT-based nanocomposite electrodes is their low reproducibility on the electrochemical response because of the lack of homogeneity of the different commercial CNT lots. Secondly, having achieved the optimum composition ratio, the next step consisted on incorporating different electrocatalytical nanoparticles, such as functional metal nanoparticles, quantum dots and metal oxide nanoparticles as well as (bio)recognition agents. Regarding this, new characterization techniques in addition to novel functionalization routes were included to the overall expertise of the group.

Finally, the fact of aiming to extend this characterization techniques to nanocomposite electrodes based on another nanostructured carbon materials, such as graphene, will allow us to venture for first time in our research group with this 2D nanomaterial, which is in full technological swing, for the development of enhanced graphene-based nanocomposite (bio)sensors.

2.1 General Aim

The general aim of this research work was focused on the characterization, optimization and functionalization of carbon-based epoxy amperometric nanocomposite sensors regarding to the nature of the raw filler nanomaterial with different electrocatalytic nanoparticles, which were chosen depending on the application of the final novel nanocomposite material, for the improvement of their electroanalytical performance.

2.2 Specific Aims

In order to accomplish the general aim presented above, some specific milestones and studies were carried out:

- i) Development of a characterization protocol to determine some physical parameters of the raw multiwalled carbon nanotubes (MWCNTs), such as purity, length and diameter, using the appropriated tools to indentify the differences between the obtained physical parameters and the ones given by the manufacturers.
- ii) Characterization and optimization of electrodes based on MWCNT/epoxy nanocomposites regarding to the nature of the raw MWCNT samples (previously evaluated) in order to determine whereas the nature of the raw MWCNTs affects their optimum composition ratio and thus their electroanalytical performance, using electrical, electrochemical, microscopic and morphological techniques.

- iii) Development of a synthesis method to tune the aforementioned nanocomposite electrodes with different types of nanoparticles through different routes: a) attachment of nanoparticles upon the MWCNT walls; b) incorporation of nanoparticles in bulk and c) modification of the electrode surface with nanoparticles.
- iv) Evaluation of the electrocatalytic effect of the modified-nanocomposite electrodes containing nanoparticles on their electroanalytical response, also depending on the route of electrode functionalization.
- v) Implement the established characterization protocol carried out for MWCNT-based nanocomposite electrodes to novel nanostructured carbon materials.
- vi) Preparation, characterization and functionalization of the optimum graphene/epoxy nanocomposite electrodes with nanoparticles for (bio)sensing approaches.

CHAPTER III

Materials and Methods

CHAPTER III

Materials and Methods

This chapter presents the different methodologies carried out during the development of the experimental part of this thesis. Firstly, a brief description of chemicals and reagents is described. Secondly, the fabrication procedure of the different sensors based on nanocomposite materials, modified or not, is also described. Thirdly, a consistent description of the experimental conditions used for each characterization technique, both nanostructured carbon materials as nanocomposite electrodes, is explained in detail. Finally, the basis of IMS technique for the electrode modification with a wide range of nanoparticles is also shown.

3.1 Chemicals and Reagents

Different commercial MWCNTs samples, which are summarized in Table 3.1, were used as conductor filler nanomaterial for their dispersion into an insulating polymer. Epotek H77A and its corresponding hardener Epotek H77B, from Epoxy Technology (Billerica, MA, USA), were used as the polymeric matrix. Graphene Oxide (GO) was synthesized from flaked graphite (Alfa Aesar, Karlsruhe, Germany) using the Hummers method. Reduced Graphene Oxide (rGO) was used as another filler nanomaterial and obtained through the reduction of GO, using ascorbic acid as a reducing agent.

All solutions were prepared using deionised water from a Milli-Q system (Millipore, Billerica, MA, USA). Potassium ferricyanide and potassium ferrocyanide ($K_3[Fe(CN)_6]/K_4[Fe(CN)_6]$, 99.8%), potassium nitrate (KNO_3 , 99.0%), potassium chloride (KCl, 99.5%), potassium phosphate dibasic anhydrous (KH_2PO_4 , >99.0%), potassium phosphate monobasic (K_2HPO_4 , >99.0%), potassium permanganate ($KMnO_4$, 99.99%), sodium nitrate ($NaNO_3$, >98%), sodium hydroxide (NaOH, >98%), sulphuric acid (H_2SO_4 , 95–98%), nitric acid (HNO_3 , 65%), hydrochloric acid (HCl, 30–35%) and ethanol C_2H_6O , >99.5%) were purchased from Sigma-Aldrich (St. Louis, MO, USA).

Table 3.1 Physical parameters of the different commercial MWCNTs samples given by the commercial supplier.

MWCNTs samples	Manufactured By	Diameter (nm)	Length (μm)	Purity (% in C)
MWCNT-1	HELIX Material Solutions (Richardson, TX, USA)	10–20	1–2	>95%
MWCNT-2	SES Research (Houston, TX, USA)	10–30	5–15	>95%
MWCNT-3	Sigma-Aldrich (St. Louis, MO, USA)	6–9	5	>95%
Raw MWCNTs	NC7000, Nanocyl S.A. (Sambreville, Belgium)	10	1.5	90%
Purified–MWCNTs	NC3100, Nanocyl S.A. (Sambreville, Belgium)	10	1.5	95%

Ascorbic acid ($\text{C}_6\text{H}_8\text{O}_6$, 99.5%), hydrogen peroxide (H_2O_2 , 30%), sodium hypochlorite (NaClO , 10-15% in free chlorine) and Levo-Thyroxine (T_4 or 3,5,3',5'-tetraiodothyroxin, >98%) have been used as analytes and were also procured from Sigma-Aldrich. Stock solutions were daily prepared except T_4 solution, which was stored in dark at 4 °C. Standard solutions were prepared by the dilution of the stock solutions. It is important to highlight that T_4 solution was prepared by dissolving it in a 0.1 M ethanolic NaOH solution.

Nanoparticles were synthesized using inorganic salts, which are summarized in Table 3.2. Sodium borohydride (NaBH_4 , 96%) was used as a reducing agent for Functional Metal Nanoparticles synthesis and provided by Panreac (Castellar del Vallès, Barcelona, Spain) and ion exchange resins were kindly supplied by Purolite® (Purolite Iberica S.I., Barcelona, Spain). Precipitating agents were sodium sulfide (Na_2S , >99%) and NaOH. Inorganic salts and precipitating agents were obtained from Sigma-Aldrich. The different salts used for the interfering experiments were also purchased from Sigma-Aldrich and were used as-received.

Finally, it is important to highlight that all reagents were of the highest grade available and used without further purification.

Table 3.2 Specifications of the different inorganic salts used to carry out the synthesis of NPs.

Type of NPs	Synthesis of NPs	Inorganic salt (% purity)	Reducing agent
FMNPs	Ag–NPs	AgNO ₃ (>99%)	NaBH ₄
	Au–NPs	[HAuCl ₄]·H ₂ O (>99.99%)	Cu ⁰ (by galvanic replacement)
	Cu–NPs	CuSO ₄ ·5H ₂ O (>98%)	NaBH ₄
	Pd–NPs	[Pd(NH ₃) ₄ Cl ₂]·H ₂ O (>99.99%)	NaBH ₄
	Pt–NPs	[Pt(NH ₃) ₄ (NO ₃) ₂] (99.995%)	NaBH ₄
QDs	CdS–QDs	Cd(NO ₃) ₂ ·4H ₂ O (>99%)	Na ₂ S
MO–NPs	CuO–NPs	Cu(NO ₃) ₂ ·3H ₂ O (99%)	NaOH

3.2 Fabrication of nanocomposite electrodes

Handmade working nanocomposite electrodes were prepared by mixing polymer Epotek H77A and its corresponding H77B hardener in a 20:3 (w/w) ratio and adding different amounts of conducting filler nanomaterial (MWCNTs or graphene). Then, the filler nanomaterials were dispersed in the resin and hardener agents by manually homogenization. The homogenization time depends on the filler nanomaterial used. Thus, MWCNT–based nanocomposite materials were homogenized for 1 h while graphene–based nanocomposite materials were 30 min. For the electrode construction, the nanocomposite was placed into a cylindrical PVC tube (6 mm of internal diameter and 20 mm of length) containing a copper disk (5 mm of diameter and 1 mm of thickness) soldered to an electrical connector end (2 mm of diameter), as is shown in Figure 3.1. Previously to soldering, the copper disk was attacked with a 5% HNO₃ solution (v/v) for 2 min in order to remove the oxide layer. The mixture was then incorporated in the hollow end of a PVC tube to form the body of the electrode.

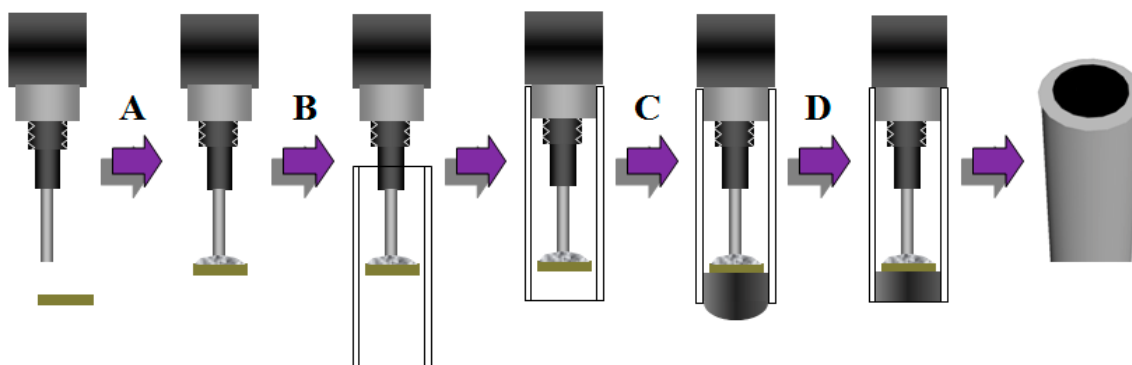


Figure 3.1 Stages for the construction of an electrode. A) A copper disk is soldered to a 2 mm female connector. B) Afterwards, it is introduced into a PVC tube. C) The filler/epoxy nanocomposite paste is incorporated in the hollow end of a PVC tube to form the body of the electrode. D) Finally, the nanocomposite paste is cured and polished, obtaining the working electrode.

The final paste-filled cavity was 3 mm long inside the PVC tube. Then, the nanocomposite paste electrodes were allowed to harden during 24 h at 80 °C.¹ Afterwards, in order to obtain a reproducible electrochemical surface, electrode surfaces were polished with different sandpapers of decreasing grain size (800 and 1200) and finally with alumina paper (polishing strips 948201, Orion). The resultant geometric area for the final electrodes was 28 mm².

While transducers based on MWCNT/epoxy the composition interval was defined between 1% and 20% (w/w) in MWCNTs, for graphene/epoxy transducers was between 8% and 20% (w/w) in graphene.

3.2.1 Synthesis of Nanoparticles for nanocomposite electrode modification: Functionalization and Incorporation

Intermatrix Synthesis (IMS) technique was used for MWCNT-based nanocomposite electrodes modification with a wide range of nanoparticles (NPs), including Functional Metal Nanoparticles (FMNPs), Quantum Dots (QDs) and Metal Oxide Nanoparticles (MO-NPs).

IMS technique offered three different methodologies for nanocomposite electrodes modification: (i) *in situ* functionalization of carbon nanotube surface, (ii) incorporation and dispersion within nanocomposite matrix (modification in bulk) and (iii) nanocomposite surface modification by drop-attachment.

(i) **Route A (RA):** The NPs were synthesized *in situ* upon activated-MWCNTs. Nanocomposites were made by dispersing the functionalized-MWCNTs in their optimum composition: 10% (w/w) for MWCNT-2 (see Table 3.1).

(ii) **Route B (RB):** The NPs (in powder form) were introduced in bulk, dispersing them within the nanocomposite matrix. Nanocomposites were prepared in their optimum composition ratio (10% (w/w) in MWCNT-2), adding an amount of powder NPs into the epoxy resin before hardening. The amount of NPs introduced in bulk was the same as those obtained by RA, which could be quantified by TGA.

For RB, the only difference for the preparation of the FMNPs respect the RA is the supporting matrix, a sulfonic gel-type exchange resin ($R-SO_3^- Na^+$) supplied by Purolite®. Finally, the resulting hybrid-material is calcined at 600°C for 4 h to obtain the FMNPs powder which keep their crystallographic properties.

(iii) **Route C (RC):** The NPs were synthesized by drop-attachment modifying the electrode surface. Nanocomposites were built in their optimum composition ratio (10% (w/w) in MWCNT-2). Before polishing, the electrode surface was activated with functional groups (carboxylic groups) by 2.5 M nitric acid treatment for 2 h. The NPs were directly synthesized on the electrode surface.

The metal loading was achieved by dropping of 0.01 M cationic metal (M^{n+}) aqueous solution (1.5 mL) followed by rinse with Milli-Q water and immersion under a 0.1 M $NaBH_4$ solution at room conditions. At last, the electrode rinsed once again with Milli Q water. This procedure was only used for the incorporation of Au- and Pd-NPs on the electrode surface in a 3:2 ratio. Thereby, the incorporation of Au-NPs was achieved by the galvanic replacement of previously prepared Cu-NPs as sacrifice nanotemplates. Later on, with the Au-NPs incorporation, the Pd-NPs were introduced.

Finally, it is important to highlight that in each case, after the redox stage, a rinse procedure was carried out with Milli-Q water.

3.2.1.1 Synthesis of FMNPs

Different FMNPs were prepared through IMS technique. This FMNPs are: Ag-, Au-, Cu-, Pd- and Pt-NPs. An scheme of the different methodologies for FMNPs incorporation is depicted in Figure 3.2 and are based on the following two sequential steps:²

- Introduction of the FMNPs precursors upon support matrix by loading their functional groups with the desired metal ions (e.g. a divalent cationic ion as M^{2+}) or metal complex precursors.
- Ion metal reduction to zero-valent state inside the support matrix through using a reducing agent ($NaBH_4$) for FMNPs incorporation.

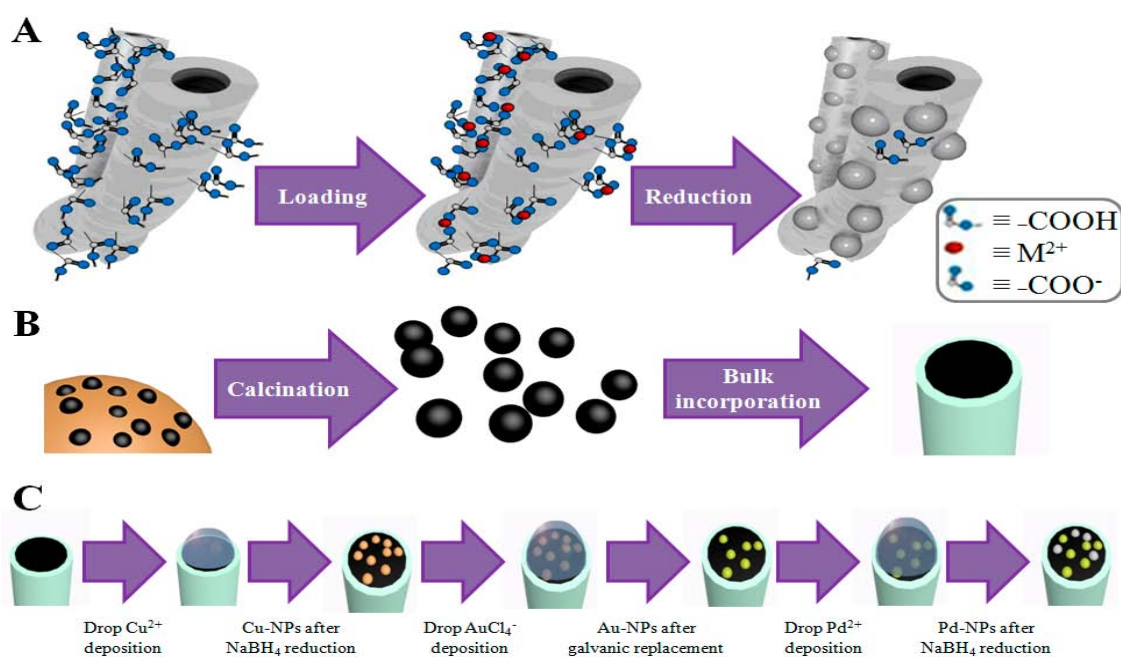
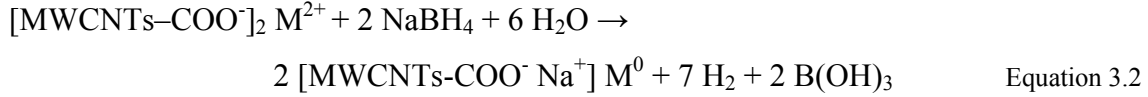
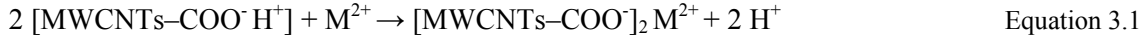


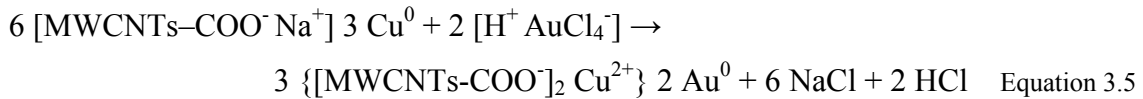
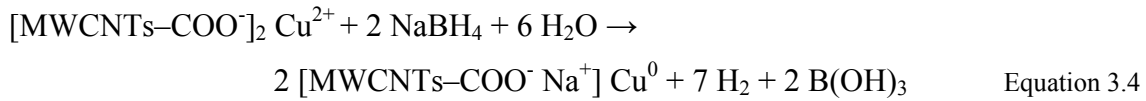
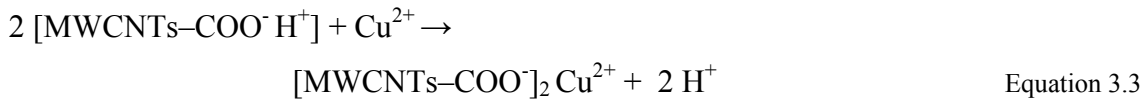
Figure 3.2 Routes of modification scheme: A) Example of *in situ* functionalization of MWCNTs surface for a M^{2+} by IMS technique, RA; B) After the calcination of the polymeric support, the remaining FMNPs are incorporated into the nanocomposite matrix (in bulk), RB and C) Au- and Pd-NPs are incorporated on the nanocomposite surface by drop-attachment, RC.

Regarding this, the general IMS procedure for FMNPs was carried out as shown in Equations 3.1 and 3.2. The functional groups of the carbon nanotubes were previously activated with 2.5 M HNO_3 for 90 min, obtaining the activated form of the MWCNTs (MWCNTs-COOH). Then the pH was adjusted to 6.0 by several washes with Milli-Q

water. Then, a 20 mL aqueous solution containing 260 mg of activated–MWCNTs were loading with a 20 mL 0.01 M cationic metal (M^{n+}) aqueous solution followed by reduction with 5 mL of 0.1 M NaBH_4 under magnetic stirring at room conditions.



As the precursor for Au–NPs is HAuCl_4 , a previous IMS of Cu–NPs was needed as sacrifice nanotemplates. Consequently, the hybrid-materials containing the Cu–NPs were immersed in a 0.01 M HAuCl_4 solution for a stoichiometry galvanic replacement reaction between Au^{3+} and Cu^0 as presented in Equations 3.3, 3.4 and 3.5.



Finally, as it is clearly seen from Equations 3.1 and 3.2, after carrying out the corresponding metal formation reaction on the MWCNT surface, the functional groups appear to be regenerated. This means that the metal formation cycle can be repeated again by using both equations without any additional pre-treatment of MWCNTs. This allows for accumulation of the desired amount of nanoparticles on the MWCNT surface.

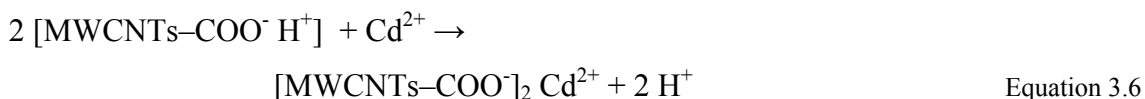
3.2.1.2 Synthesis of CdS–QDs

CdS–QDs were *in situ* synthesized on the MWCNTs walls by a modification of the aforementioned Route A.

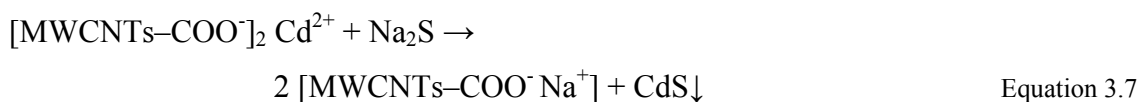
For this aim, the MWCNTs surface was previously activated with carboxylic groups by 2.5 M nitric acid treatment in ultrasound bath for 2 h. The pH was adjusted to

6 by several washes with Milli-Q water. Then, CdS-QDs were introduced on MWCNTs walls (CdS-QDs@MWCNTs), according with the following steps (Equations 3.6 and 3.7), which are summarized in Figure 3.3.

- Loading of Cd²⁺ ions (QDs precursors) onto the carboxylic groups of MWCNTs, Equation 3.6.



- Precipitation of CdS-QDs on the MWCNTs surface by adding Na₂S, Equation 3.7.



Thus, a 20 mL aqueous solution containing 260 mg of activated-MWCNTs were loading with a 20 mL 0.01 M Cd²⁺ aqueous solution followed by precipitation process with 5 mL of 0.1 M Na₂S under magnetic stirring at room conditions. Accordingly, the only changed regarding to FMNPs synthesis was the second step, where the reducing agent from Equation 3.2 is removed by a precipitating agent in Equation 3.7.

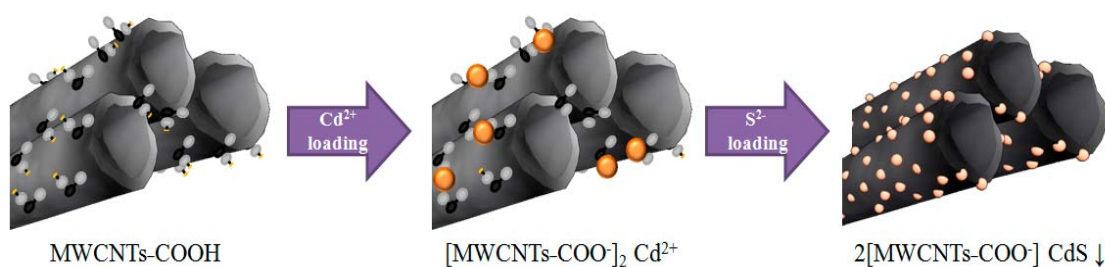
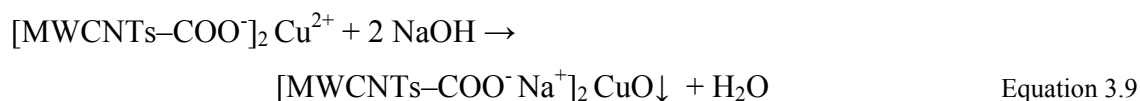
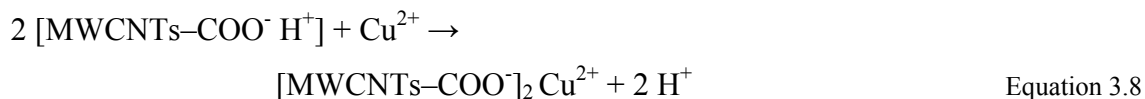


Figure 3.3 Scheme of *in situ* synthesis of CdS-QDs on the MWCNTs walls.

3.2.1.3 Synthesis of CuO-NPs

CuO-NPs were incorporated in MWCNT/epoxy nanocomposite electrodes by two different routes: Route A and Route B. Both routes are shown in Figure 3.4.

The methodology for CuO-NPs synthesis can be summarized in two Equations (Equations 3.8 and 3.9).



The first step consisted of the metal loading of 260 mg of MWCNTs by using 0.02 M Cu^{2+} aqueous solution in 300 mL of Milli-Q water. Then, a 1 mL of glacial acetic acid was added in order to avoid hydrolyzation of Cu^{2+} ions. The solution was rinsed during 20 min. Afterwards, 0.01 g of polyvinylpyrrolidone (PVP) as stabilizer and 1.0 M NaOH as reducing agent were added into the above mixture and then stirred with a Teflon-coated magnetic stirring bar (stirring rate: 800 rpm) for 10 min at 80 °C in a water bath.³ Then, the pH of this solution was adjusted to 12 using a NaOH solution. The resultant dark blue suspension was followed by high-intensity ultrasonication horn at 20 kHz in ambient air for 2 h. On completion of sonication, the suspension turned black. The product was centrifuged at 4000 rpm for 8 min and washed with Milli-Q water and ethanol for several times. The resultant product was dried at 80 °C for 24 h.

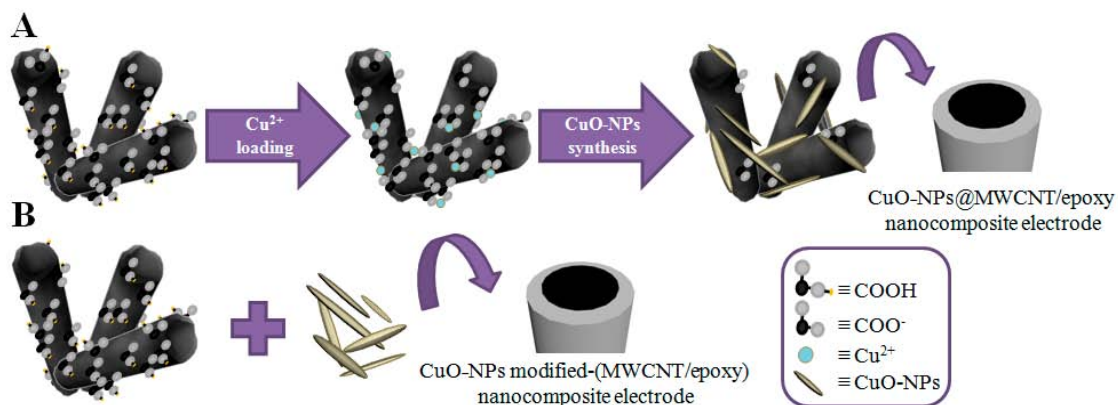


Figure 3.4 Scheme of the two different routes for MWCNT/epoxy nanocomposite electrodes modification with CuO-NPs. A) *In situ* synthesis of CuO-NPs on the MWCNTs surface, Route A; and B) Synthesis of CuO-NPs and their incorporation as powder form in bulk, Route B.

3.2.2 Synthesis of graphene-based nanomaterials for nanocomposite electrodes purposes: Functionalization and Incorporation

In this section it is detailed the synthesis routes to obtain the different graphene-based nanomaterials. Au-NPs were synthesized *in situ* upon GO surface, resulting the Au-NPs@rGO. The per-6-thio- β -cyclodextrin (β -CD-SH) was attached on Au-NPs@rGO nanomaterial, favoured for the strength of the gold-thiol interactions, which provides the basis to fabricate a robust hybrid material, the β -CD-SH/Au-NPs@rGO.

Finally, the modified-nanocomposite electrodes based on graphene resulted from the dispersion of the optimum loading of conducting filler nanomaterial (13% w/w) within epoxy resin.

3.2.2.1 Synthesis of GO and rGO

Graphene Oxide (GO) was synthesized from bulk graphite powder using the Hummers method.⁴ 1g of flaked graphite, 0.5 g of NaNO₃ and 23 mL of H₂SO₄ was added to a 500 mL round bottomed flask and stirred at 4 °C for 15 min. Then, 3 g of KMnO₄ was added slowly with vigorous stirring. Once all the KMnO₄ was added the ice bath was removed and the suspension heated to 35 °C for 30 min. This afforded a murky brownish grey solution. Following this, 46 mL of Milli-Q water was added and the suspension set to stir for 15 min more. The solution was then treated with a further 140 mL of water and 3.5 mL of H₂O₂ in order to reduce residual MnO₄⁻ and MnO₂ to the colourless, the soluble MnSO₄. The solution was washed several times though centrifugation (4000 rpm) with a 10% aqueous solution of HCl followed by copious amounts of water until the pH was 6. Finally, the product was dried overnight at 80°C. To prepare the suspensions of GO, the resulting GO was dispersed in Milli-Q water (1.0 mg·mL⁻¹) and ultra-sonicated with an ultra-sonic horn for 90 min in order to make a homogeneous brown dispersion. Then, the solution was centrifuged at 4000 rpm for 10 min to remove unexfoliated material; the supernatant was the final GO dispersion.

rGO was obtained from the reduction of GO with ascorbic acid.⁵ GO was dispersed in water at a concentration of 1.0 mg·mL⁻¹ and reacted with ascorbic acid (2.0 mM) at 95 °C for 15 min. The pH of the dispersion was previously adjusted to ~9–10 with 25% ammonia solution (~2 μ L per mL of dispersion) to promote the colloidal stability of the GO sheets through electrostatic repulsion. Afterwards, the product was centrifuged at

4000 rpm for 10 min and washed several times with Milli-Q water until the pH reached ~ 6 . The resultant product was dried overnight at 80°C . The suspensions of rGO were prepared in the same manner as that of the GO suspensions.

3.2.2.2 Synthesis of Au-NPs@rGO and β -CD-SH/Au-NPs@rGO hybrid-materials

350 mg of GO was dispersed in 250 mL of Milli-Q water and ultra-sonicated for 1 h. After ultra-sonication, the aqueous GO suspension was added to a 500 mL round bottomed flask and set to stir at room temperature for 30 min. Then, $2.5 \cdot 10^{-3}$ mol of HAuCl_3 (precursor for Au-NPs synthesis) was added to the suspension and left to stir for another 30 minutes. The solution was reduced with 250 mL of an aqueous 0.1 M NaBH_4 solution, which was added drop wise to the reaction vessel. The solution was left to stir for a further 1 h. Following this, the functionalized nanomaterial (Au-NPs@rGO) was washed several times with water through a high speed centrifugation at 4000 rpm for 10 min. After Au-NPs@rGO nanomaterial obtaining, the resultant product was dispersed in 250 mL of Milli-Q water and ultra-sonicated for 1 h. After ultra-sonication, the aqueous Au-NPs@rGO suspension was added to a 500 mL round bottomed flask and set to stir at room temperature for 30 min. Then, 250 mL of an aqueous (9:1 water/ethanol, v/v) 2.0 mM suspension of thiolated β -CD (β -CD-SH) was added. The solution was left to stir overnight. Afterwards, the product was centrifuged at 4000 rpm for 10 min and washed several times with Milli-Q water and ethanol, in order to remove the amount of β -CD not attached. The resultant product (β -CD-SH/Au-NPs@rGO) was dried overnight at 80°C . The presented synthesis procedure is summarized in Figure 3.5.

The per-6-thio- β -cyclodextrin (β -CD-SH) used in this thesis was synthesized by the Surfaces and Nanomaterials Group (Institut de Ciència de Materials de Barcelona, ICMAB-CSIC), following the established methodology.⁶ For this aim, 1 g of β -CD was dissolved in 10 mL of N,N-dimethylformamida (DMF). Then, 0.3 g of thiourea was added and the reaction mixture was heated to 70°C under a nitrogen atmosphere. After 20 h, the DMF was removed under reduced pressure to give a yellow oil, which was dissolved in 50 mL of Milli-Q water. After this, 0.3 g of KOH was added and the reaction mixture heated to a gentle reflux under a nitrogen atmosphere. After 1 h, the

resulting suspension was acidified with aqueous KHSO_4 and the precipitate filtered off, washed thoroughly with distilled water, and dried. To remove the last traces of DMF, the product was suspended in 50 mL of Milli-Q water and the minimum amount of KOH added to give a clear solution; the product was then reprecipitated by acidifying with aqueous KHSO_4 . The resulting fine precipitate was carefully filtered off and dried under vacuum to yield ~80% as an off-white powder, obtaining the β -CD-SH.

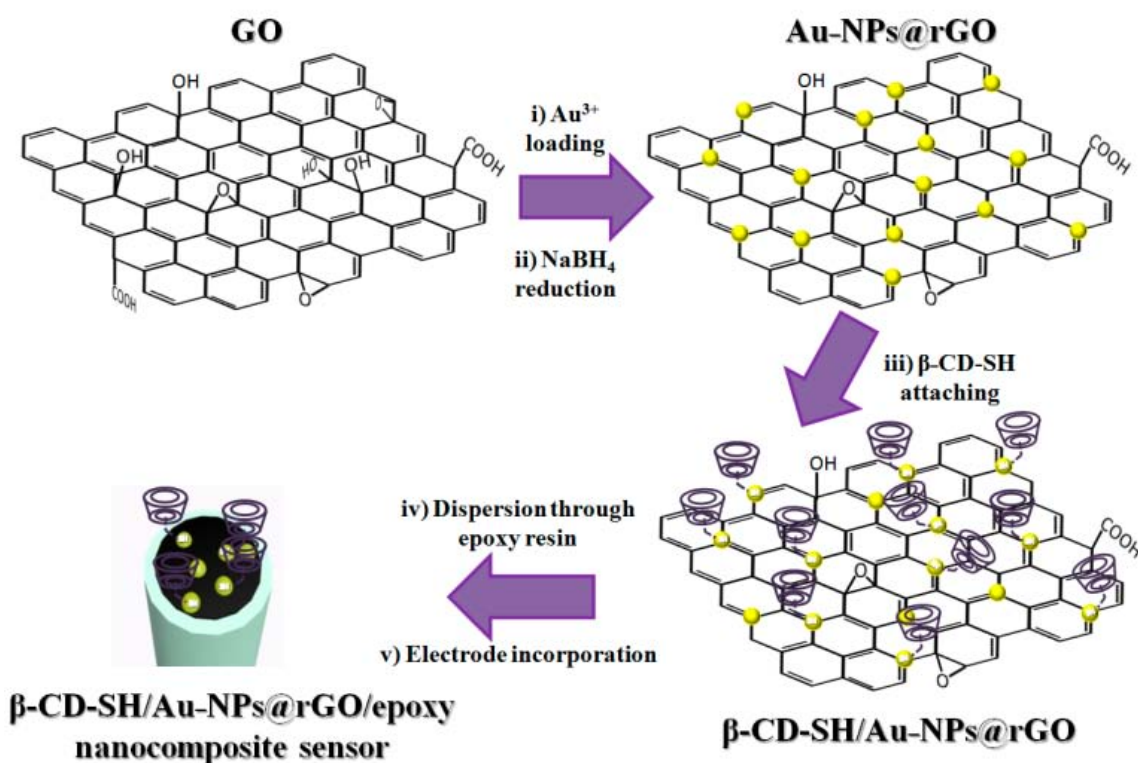


Figure 3.5 Synthetic route of Au-NPs@rGO and β -CD-SH/Au-NPs@rGO hybrid-materials and their subsequent dispersion in epoxy resin for nanocomposite sensor purposes.

3.3 Characterization Techniques and Instrumentation

Different electrical, electrochemical, analytical and morphological techniques have been systematically applied for characterization, optimization and evaluation of the different nanocomposite sensors developed during this thesis. However, previously to nanocomposite electrodes construction, different microscopy, thermogravimetric and spectroscopic techniques were used for characterizing different physical properties of the nanostructured carbon materials as well as to determine qualitatively and quantitatively the different NPs synthesized.

3.3.1 Physical characterization of nanostructured carbon materials

The following describes the different tools and the experimental conditions used to characterize the conducting filler nanomaterials (both modified with NPs or not).

3.3.1.1 Microscopy characterization

Microscopy images of MWCNTs, graphene and hybrid nanomaterials resulting from their functionalization with NPs were obtained using different microscopy tools.

High Resolution Transmission Electron Microscopy (HR-TEM) images and Energy Dispersive X-Ray Spectroscopy (EDS) analysis were obtained by JEM-1400 unit with an acceleration voltage of 120 kV. This tool was mainly used in order to characterized different physical parameters such as length and diameter of filler nanomaterials as well as average size of the different NPs. At the same time, EDS analysis was used for the qualitative determination of NPs contained in modified-nanomaterials. High Resolution Scanning Transmission Electron Microscopy (HR(S)TEM) experiments were carried out with a FEI Tecnai G2 F20 S-TWIN HR(S)TEM field emission of 200 kV with analytical EDS. This tool was only used for MWCNTs containing CdS-QDs sample.

For the characterization of the (modified-)MWCNTs, approximately 1 mg of sample was dispersed in 5 mL of acetone as organic solvent and then placed in ultrasound bath for 1 h. Then, a drop of the suspension was placed on a Holy Carbon grids and allowed to dry before analysis; however, for MWCNTs containing CuO-NPs, a gold grid was used. While physical parameters were compiled from at least 100 tubes, at least 200 NPs from different TEM images were evaluated for NPs distribution. For (modified)-graphene characterization, approximately 0.1 mg of sample was dispersed in 10 mL of Milli-Q water as solvent and then placed in ultrasound bath for 2 h. Then, a drop of the aqueous suspension was deposited onto Lacy Carbon grids and allowed to dry before analysis.

3.3.1.2 Thermogravimetric analysis

Thermogravimetric Analysis (TGA) technique was used to quantify the total metal content in the nanostructured carbon materials. The experiments were carried out using

a Netzsch instrument; model STA 449 F1 Jupiter®. Approximately 20 mg of sample was heated to 1000 °C at 10 °C/min, using flow of air. The mass of the sample was continuously measured as a function of temperature and the rate of weight loss (d.t.g.) was automatically recorded.

3.3.1.3 Spectroscopic techniques

On the one hand, Raman spectroscopy was employed as a means of monitoring the effect of graphene oxidation (GO) and subsequently reduction (rGO) on the characteristic Raman scattering peaks associated with graphene and graphene related materials. Raman spectra were recorded with a Renishaw 1000 micro – Raman system fitted with a Leica microscope and Grams Research™ analysis software. The excitation source used was a 633 nm HeNe laser (Renishaw RL633). The 50x objective lens was capable of focusing the beam to a spot size ~2-3 μm in diameter. The spectrometer was calibrated before use using a reference Si wafer centered at 520 cm⁻¹.

On the other hand, the optical characteristic of the graphene-based materials were monitored using UV-vis spectroscopy (Agilent Technologies, Cary 60 Uv-Vis scanning spectrometer) as the optical response of these materials is known to shift and modulate moving from an oxidized to a reduced material.

In addition, X-Ray Photoelectron Spectroscopy (XPS) technique was used in order to identify and quantify the metal impurities contented in non-purified MWCNTs.

3.3.2 Characterization and evaluation of the developed sensors based on nanocomposite materials

This section details the different electrical, electrochemical, analytical and morphological techniques used for the characterization of the different (modified-) nanocomposite sensors as well as their worked conditions.

3.3.2.1 Electrical characterization

The electrical properties of MWCNT/epoxy nanocomposite electrodes and rGO/epoxy nanocomposite electrodes were investigated applying the well-known percolation theory. The percolation curves were constructed by measuring the electrical resistance

of the different nanocomposite materials. The experiments were performed by means of a digital multimeter (Fluke, Everett, WA, USA). Different MWCNT/epoxy and rGO/epoxy compositions were prepared by varying the conducting filler nanomaterial loading in the epoxy matrix. The mainly compositions investigated were between 1% and 20% (w/w) in MWCNT loading and between 8% and 20% (w/w) in rGO loading. For each carbon composition, three equal electrodes were fabricated and evaluated.

3.3.2.2 Electrochemical experiments

Cyclic Voltammetry (CV) and Electrochemical Impedance Spectroscopy (EIS) measurements were performed using a computer controlled Autolab PGSTAT30 potentiostat/galvanostat (EcoChemie, Utrecht, The Netherlands) using GPES (v.4.9) software package provided by the manufacturer. A three electrode configuration cell was used for electrochemical measurements. An AgCl covered silver wire and a platinum-based electrode 52-671 (Crison Instruments, Alella, Barcelona, Spain) were used as reference and auxiliary respectively. The different nanocomposite electrodes based on nanostructured carbon materials, both modified with NPs or not, were used as working electrodes. For each carbon composition, three equal electrodes were fabricated and evaluated. To perform such electrochemical characterization, the $[\text{Fe}(\text{CN})_6]^{3-/4-}$ was used as a benchmark redox couple since it is very sensitive to the electrode surface characteristics. Accordingly, CV and EIS measurements were made in a 10.0 mL of 0.1 M KCl solution containing 0.01 M potassium $[\text{Fe}(\text{CN})_6]^{3-/4-}$, under quiescent conditions. The experiments were performed at room temperature (25 °C).

Cyclic voltammograms were mainly recorded from -1.0 to $+1.2$ V vs. Ag/AgCl. Different scan rates were selected depending on the working electrode used. Different parameters such as peak height (I_p), exchange current (i_0), cathodic and anodic peak potentials (E_{pc} and E_{pa} , respectively), equilibrium potential (E_{eq}), peak separation potential (ΔE) and electroactive area (A) have been extracted from the cyclic voltammograms.

Regarding to EIS experiments, the impedance spectra were recorded in the frequency range 0.1 Hz to 100 kHz (signal amplitude to perturb the system was 10 mV) at the redox equilibrium potential previously obtained by CV. This equilibrium potential was calculated following the Equation 3.10.

$$E_{\text{eq}} = E_{\text{pc}} + \left| \frac{E_{\text{pc}} - E_{\text{pa}}}{2} \right| \quad \text{Equation 3.10}$$

This tool uses a model circuit to describe individual circuit elements which are based on the physical electrochemistry system, such as solution resistance (R_{Ω}), charge transfer resistance (R_{ct}) and double-layer capacitance (C_{dl}). These physical parameters were obtained by fitting the spectra to a simple equivalent circuits: $R_{\Omega} \cdot (R_{\text{ct}} \cdot C_{\text{dl}})$ for CNT-based nanocomposite electrodes and $R_{\Omega} \cdot [C_{\text{dl}} \cdot (R_{\text{ct}} \cdot Z_w)]$ for graphene-based nanocomposite electrodes.

3.3.2.3 Electroanalytical performance

Linear Sweep Voltammetry (LSV) and hydrodynamic amperometry techniques were used for analytical evaluation and applications.

Firstly to amperometric experiments, LSV measurements were taken at the same experimental conditions of CV and carried out in order to determine the polarization potential (E_{app}) of each analyte for its subsequent used as working potential in electroanalytical application. Experiments were carried out using a the Autolab PGSTAT30 potential/galvanostat, using the GPES (v.4.9) software. A three-electrode configuration was used: a double junction reference electrode Ag/AgCl Orion 900200 (Thermo Electron Corporation, Beverly, MA, USA) and a platinum-based electrode 52-671 (Crison Instruments, Alella, Barcelona, Spain) were used as reference and auxiliary respectively; MWCNT/epoxy and rGO/epoxy nanocomposite electrodes (either modified or not with NPs) were used as different working electrodes. For E_{app} evaluation, different analytes concentrations were added in a 10.0 mL solution of their corresponding background electrolyte (see Table 3.3).

Afterwards, hydrodynamic amperometry measurements were made using an amperimeter LC-4C (Bio Analytical Systems INC., West Lafayette, IN, USA) for the application of the different developed nanocomposite sensors. The experiments were made using a three-electrode configuration. A double junction reference electrode Ag/AgCl Orion 900200 (Thermo Electron Corporation, Beverly, MA, USA) and a platinum-based electrode 52-671 (Crison Instruments, Alella, Barcelona, Spain) were used as reference and auxiliary respectively; MWCNT/epoxy and rGO/epoxy nanocomposite electrodes (modified or not) were used as different working electrodes.

Table 3.3 Specifications of the different experimental conditions to carry out both LSV and amperometric experiments.

MWCNT-based electrodes containing	Analytes	E_{app} (mV)	Background Electrolyte	Stock Solutions
MWCNT/epoxy	Ascorbic Acid	600	0.01 M HNO ₃ /KNO ₃	1.0·10 ⁻¹ M
	H ₂ O ₂	900	PBS at pH 7.0	1.0·10 ⁻² M
	Free Chlorine	-100	PBS at pH 5.5	1.0·10 ⁻² M
Au–Pd–NPs contained MWCNT/epoxy	H ₂ O ₂	700	PBS at pH 7.0	1.0·10 ⁻² M
CdS–QDs contained MWCNT/epoxy	Ascorbic Acid	600	0.01 M HNO ₃ /KNO ₃	1.0·10 ⁻¹ M
	H ₂ O ₂	900	PBS at pH 7.0	1.0·10 ⁻² M
CuO–NPs contained MWCNT/epoxy	Free Chlorine	-350	PBS at pH 5.5	1.0·10 ⁻² M
Graphene-based electrodes containing	Analytes	E_{app} (mV)	Background Electrolyte	Stock Solutions
rGO	Ascorbic Acid	600	0.01 M HNO ₃ /KNO ₃	1.0·10 ⁻¹ M
β–CD/Au–NPs contained rGO/epoxy	T ₄	850	0.1 M HCl	*5.0·10 ⁻⁶ M

*Prepared in a 0.1 M NaOH ethanolic solution.

Amperometric detection was made in a 10.0 mL solution of their respectively background electrolytes under force convection by stirring the solution with a magnetic stirrer (constant agitation). All the experiments were made at room temperature (25 °C). Table 3.3 summarized the experimental conditions applied for each system, including the working electrode with its corresponding working potential, background electrolyte and the studied analytes. Freshly prepared solutions of each analyte were used as stock solutions. Standard solutions were prepared by the dilution of the stock solutions. For free chlorine experiments, the NaClO solutions were previously analyzed using the standard N,N-diethyl-p-phenylenediamine (DPD) colorimetric method which consists in a Kit-commercial colorimeter (HACH, Düsseldorf, Germany) that provides measurements directly in mg·L⁻¹ of free chlorine.⁷ Limit of detection (LOD) was estimated three times by the S/N=3 criterion for each nanocomposite sensor.² The

reproducibility of the results was ascertained by carrying out triplicate experiments in each case with three different nanocomposite sensors. Limit of quantification (LOQ) was also determined three times (n=3) as the lowest concentration of the lineal response range.

3.3.2.4 Morphological, Topographical and Current studies

Morphological, topographical and current studies were made directly upon nanocomposite electrode surface. Measurements of nanocomposites topography were made by Confocal Microscopy 3D (CM3D). A Leica DCM 3D unit was used at 150x magnifications for measuring fifty-seven profiles in three different areas for each optimum composite electrode (ISO 4287). Topography and current measurements were obtained simultaneously by means of an Atomic Force Microscopy (AFM) (PicoSPM, Molecular Imaging, USA) equipment. Surface measurements were done using the current sensing mode: CSAFM and rectangular diamond coated tips (Nanoworld, Switzerland) with an estimated constant spring of $72 \text{ N}\cdot\text{m}^{-1}$.

Finally, Scanning Electron Microscopy (SEM) images were taken using Zeiss® MERLIN FE-SEM with an acceleration voltage of 15 kV. SEM technique was only used to characterize the electrode surface of the modified-MWCNT nanocomposite devices obtained by Route C (see § 3.2.1). For this aim, samples were prepared into a cylindrical plastic support (4 mm of diameter and 2 mm of length). Then, the nanocomposite was cured and polished in the same way as indicated in § 3.2. For effective resolution of the sample, a coating with a silver film around the walls of the support was necessary.

3.4 References

1. Pumera, M.; Merkoçi, A.; Alegret, S., Carbon nanotube-epoxy composites for electrochemical sensing. *Sensors and Actuators B: Chemical* **2006**, *113* (2), 617-622.
2. Muñoz, J.; Bastos-Arrieta, J.; Muñoz, M.; Muraviev, D.; Céspedes, F.; Baeza, M., Simple green routes for the customized preparation of sensitive carbon nanotubes/epoxy nanocomposite electrodes with functional metal nanoparticles. *RSC Advances* **2014**, *4* (84), 44517-44524.

3. Anandan, S.; Lee, G.-J.; Wu, J. J., Sonochemical synthesis of CuO nanostructures with different morphology. *Ultrasonics Sonochemistry* **2012**, *19* (3), 682-686.
4. Hummers Jr, W. S.; Offeman, R. E., Preparation of graphitic oxide. *Journal of the American Chemical Society* **1958**, *80* (6), 1339-1339.
5. Fernandez-Merino, M.; Guardia, L.; Paredes, J.; Villar-Rodil, S.; Solis-Fernandez, P.; Martinez-Alonso, A.; Tascon, J., Vitamin C is an ideal substitute for hydrazine in the reduction of graphene oxide suspensions. *The Journal of Physical Chemistry C* **2010**, *114* (14), 6426-6432.
6. Rojas, M. T.; Koeniger, R.; Stoddart, J. F.; Kaifer, A. E., Supported Monolayers Containing Preformed Binding Sites. Synthesis and Interfacial Binding Properties of a Thiolated. beta.-Cyclodextrin Derivative. *Journal of the American Chemical Society* **1995**, *117* (1), 336-343.
7. Apha, A., Wef. 2005. *Standard Methods for the Examination of Water and Wastewater. 21st ed. American Public Health Association. Washington, DC. Part 8000*, 94-100.

CHAPTER IV

**Influence of MWCNT nature on the electroanalytical
performance of nanocomposite sensors**

CHAPTER IV

Influence of MWCNT nature on the electroanalytical performance of nanocomposite sensors

Following the discovery of fullerene C₆₀ by Kroto¹ and the subsequent first observation of a real CNT by Iijima,² research into carbon based nanomaterials and their potential applications has expanded rapidly.³ CNTs may be fabricated using a variety of methods such as arc discharge methods, laser ablation and chemical vapour deposition. CNT synthesis inherently leads to the production of not only CNTs but also other carbonaceous bi-products such as amorphous carbon, fullerenes, nanocrystalline graphite and transition metals (Fe, Ni, Co, Cu) which were used as catalysts for growth.⁴ These non-nanotube materials frequently hinder the advantageous properties of CNTs and limit their optimal performance in applications as new functional devices with enhanced sensing characteristics. Purification methods attempt to remove any unwanted carbon and metal impurities without damaging the CNTs as it is generally believed that the accurate purification of the raw carbon materials results in a greater analytical response for amperometric detection.^{5,6}

Due to their remarkable electrical, thermal and mechanical properties, high interest is focused on nanocomposites based on CNTs in general, and MWCNTs, in particular. In addition, they exhibit a higher area to volume ratio, lower resistivity and higher mechanical stability than other carbon allotropic forms such as graphite and fullerenes. For these reasons, it is proved that the electrocatalytic activity of MWCNTs, combined with the polymeric matrix properties are very useful for MWCNT-based amperometric (bio)sensors construction.^{7,8,9}

Some parameters, such as the reinforcement scale, composite resistivity, background capacitance current, material stability and heterogeneous electron transfer rate are dependent on carbon load within the polymeric matrix.^{10,11} Thus, for the same polymer, depending on the carbon load, the nanocomposite electrodes can behave

similarly to a microelectrode array that takes place for compositions into percolation zone (NPC zone). Working with nanocomposite electrodes based on the NPC zone have shown enhanced properties such as better limits of detection and increase of the stability and repeatability of the analytical signal.^{12,13}

One of the main parameters used to determine the percolation behaviour and the conductivity of the nanocomposites is the length/diameter ratio of CNTs.^{14,15} However, the lack of homogeneity in the different commercial CNTs lots, which is mainly caused by the amounts of different metal impurities in the nanotubes, as well as the dispersion in their diameter/length.^{16,17} Under this context, it makes mandatory a careful characterization and optimization of both MWCNT/polymer composition ratio and the raw transducer material before being used for sensing purposes.

In most studies, the aspect ratio of the CNTs was calculated using the lengths and diameters given by the supplier. There are only few studies on the measurement of the MWCNTs length and diameter distributions.^{18,19} However, the purity of the raw CNTs is rarely analysed as they are purified directly prior to (bio)sensor nanocomposite fabrication. Thereby, it is unknown whether the purity of the raw MWCNT might affect both the electroanalytical behaviour of amperometric nanocomposite electrodes and the optimum MWCNT/epoxy composition ratio.

Most of the results that will be presented below have already been published as journal articles. These publications are listed follow and are collected in Appendix A.

– *Influence of raw carbon nanotubes diameter for the optimization of the load composition ratio in epoxy amperometric composite sensors.*

Journal of Materials Science (2015), 50 (2), 652-661.

J. Muñoz, J. Bartrolí, F. Céspedes and M. Baeza.

– *Effect of carbon nanotubes purification on electroanalytical response of near – percolation amperometric nanocomposite sensors.*

Journal of the Electrochemical Society (2015), 162 (8), B217–B224.

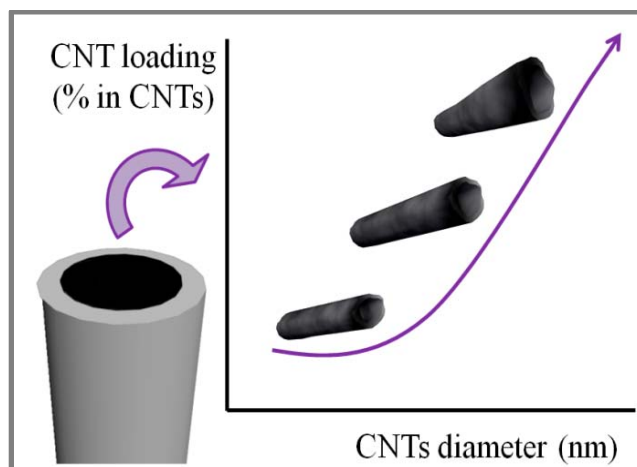
J. Muñoz, F. Céspedes and M. Baeza.

4.1 Results and Discussion

In this section is discussed the necessity to characterize the raw MWCNTs before being used as filler nanomaterials for their integration in nanocomposite sensors based on MWCNTs dispersed in epoxy resin. From an analytical point of view, the requirements to achieve a good electrode performance are high sensitivity, rapid response time, low limit of detection and electroanalytical reproducibility. These analytical parameters are related with some physical parameters such as material resistivity (R_{Ω}), heterogeneous electron transfer rate (R_{ct}) and double-layer capacitance (C_{dl}). For this reason, in this chapter it has been carried out an accurate characterization protocol to study these physical parameters for different MWCNT/epoxy electrode compositions with the goal of determining the optimum MWCNT loading nanocomposite regarding to the raw MWCNT nature.

For this aim, the nature of different commercial samples of MWCNTs was previously characterized by HR-TEM and TGA in order to determine their diameters, lengths and purities. In addition, XRF was used in order to identify and quantify the metal impurities contented on MWCNTs. Afterwards, the different samples of MWCNTs were classified in function of their physical parameters, resulting in two different studies: (i) effect of the raw MWCNTs diameter (§ 4.1.1) and (ii) effect of the raw MWCNTs purity (§ 4.1.2). Subsequently, the samples were used to fabricate different series of MWCNTs dispersed into epoxy resin varying the amount of conducting nanomaterial. Composition ratios were modelled by Percolation Theory and characterized by different electrochemical techniques including Cyclic Voltammetry (CV) and Electrochemical Impedance Spectroscopy (EIS). Morphological experiments were made by Confocal Microscopy 3D (CM3D), which provided information about the roughness of the electrode surface. Finally, the potentiality of this approach in terms of electroanalytical response was demonstrated by means of amperometric detection of ascorbic acid in water solution, which was used as a model analyte.

4.1.1 Effect of the raw MWCNTs diameter



Graphical Abstract I. MWCNT diameter as a key parameter to determine the optimum filler/polymer ratio.

The aim of this work was to study one of the physical properties of raw MWCNTs, concretely the diameter and its relation on the electroanalytical response of nanocomposite sensors based on MWCNTs. For this goal, three different commercial samples of MWCNTs with *a priori* distinctive diameters were used as conductor fillers and dispersed in an insulating polymer (the epoxy resin), in order to fabricate three different series of nanocomposite electrodes based on MWCNT/epoxy. Then, the electrodes were systematically characterized mainly applying different electrochemical techniques. After an accurate characterization, MWCNT diameter resulted to be a key parameter in the optimum MWCNT/epoxy composition ratio.

4.1.1.1 Physical characterization of MWCNTs

Diameter and length of the three different MWCNT samples (MWCNT-1, MWCNT-2 and MWCNT-3 following the specifications shown in Table 3.1 from § 3.1) were calculated from HR-TEM images (Figure 4.1). For making the measurements, a greater dispersion of these tubes was needed. After an accurate data compilation, an important difference between the experimental results and the specifications provided by the suppliers were found, as is shown in Table 4.1.

Both length and diameter values obtained through HR-TEM characterization were inferior to those specified by the manufacturers. Accordingly, length parameter was kept constant for the three MWCNTs samples.

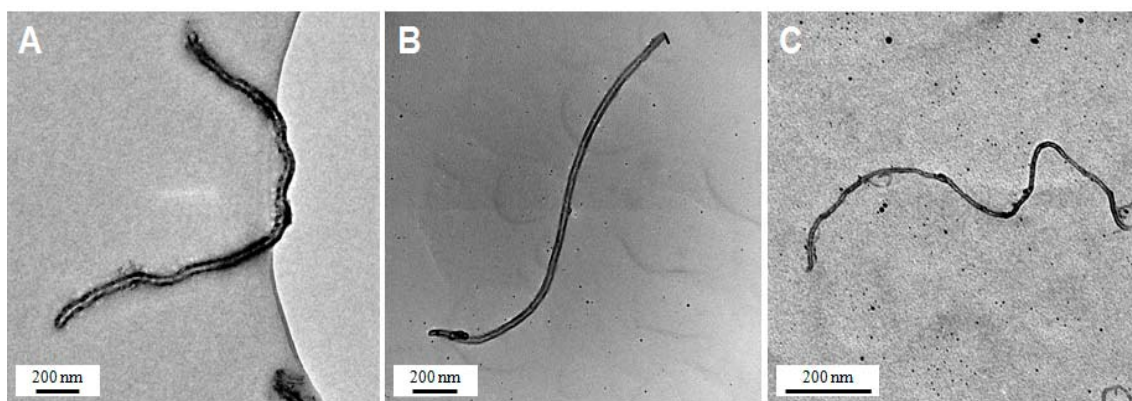


Figure 4.1 HR-TEM images of A) MWCNT-1, B) MWCNT-2 and C) MWCNT-3.

Regarding diameter, while MWCNT-1 was expected to be narrower than MWCNT-2, the result was contrary and the MWCNT-1 resulted to be the widest. MWCNT-3, which had a diameter value closer to the provided by Sigma Aldrich, resulted to be the narrowest.

On the other hand, TGA analysis reveals information about purity of MWCNT samples, as to percentage of carbon referred.²⁰ The background line is because of the metallic catalyst residues. In this case, the purity obtained by TGA for each MWCNT sample was slightly higher than the specified one (see Table 4.1).

In brief, length, diameter and purity values obtained by HR-TEM and TGA for the three samples of MWCNTs were different from the values given by the manufacturers. Considering length and purity experimental values were homogeneous for each MWCNTs sample, the study was focused on the effect of the diameter on the electroanalytical response of the nanocomposite sensors.

Table 4.1 Physical parameters of the different MWCNTs samples were obtained by HR-TEM (length and diameter) and TGA (purity) and compared with those given by the manufacturers (MFG).

MWCNTs samples	Diameter (nm)		Length (μm)		Purity (% in C)	
	TEM	MFG	TEM	MFG	TGA	MFG
MWCNT-1	35–55	10–20	0.5–1.5	1–2	> 97	>95%
MWCNT-2	30–45	10–30	0.5–2.0	5–15	> 99	>95%
MWCNT-3	8–15	6–9	0.5–2.5	5	> 98	>95%

4.1.1.2 Electrical characterization

The electrical properties of the different MWCNT/epoxy nanocomposite electrodes were adjusted by Percolation Theory,¹² as is shown in Figure 4.2. Each series of MWCNT/epoxy nanocomposites (at different composition ratios) were tested in order to estimate the maximum conductivity value of the nanocomposite materials with the minimum conductive particle loading, which is described as near-percolation zone (NPC).

The first series was MWCNT-1/epoxy nanocomposites (C1), the second one consists of MWCNT-2/epoxy nanocomposites (C2) and finally, the third series of nanocomposites was made dispersing MWCNT-3 into epoxy resin (C3).

While C1, C2 and C3 nanocomposites containing more than 20% of MWCNTs samples had a poor mechanical stability, those nanocomposites containing less than 1% exhibited resistivity values that tend to infinity. After the experiments, three different conductive regions were determined regarding the electrical behaviour: high resistance zone (HRC) and thus lowly conducting, near-percolation zone or second percolation zone (NPC) and low resistance zone (LRC) and thus highly conducting, which are represented in Figure 4.2 B.

Comparing the electrical differences between the three series of MWCNT/epoxy nanocomposites, a displacement in the near-percolation zone was observed. This fact is due to the differences of the MWCNTs diameter. For nanocomposites containing MWCNT-1, which have a greater diameter, an average range around 12% in sample was the optimum load to just fall on the second percolation threshold, as is shown in Figure 4.2 A. However, nanocomposites containing MWCNT-3, which had the lowest diameter, the average range that just fell on the NPC zone was around 5% in sample (see Figure 4.2 C).

Finally, for MWCNT-2, the average NPC composition was around 10% in sample, as can be seen in Figure 4.2 B. Thus, as diameter of raw MWCNTs decreases, a leftward displacement on the second percolation threshold zone was observed, due to the surface area increment for the same percentage of MWCNTs in the nanocomposite, as is shown in Table 4.2. Consequently, a lower load of MWCNTs is required for those nanocomposites containing the narrowest nanotubes (C3).

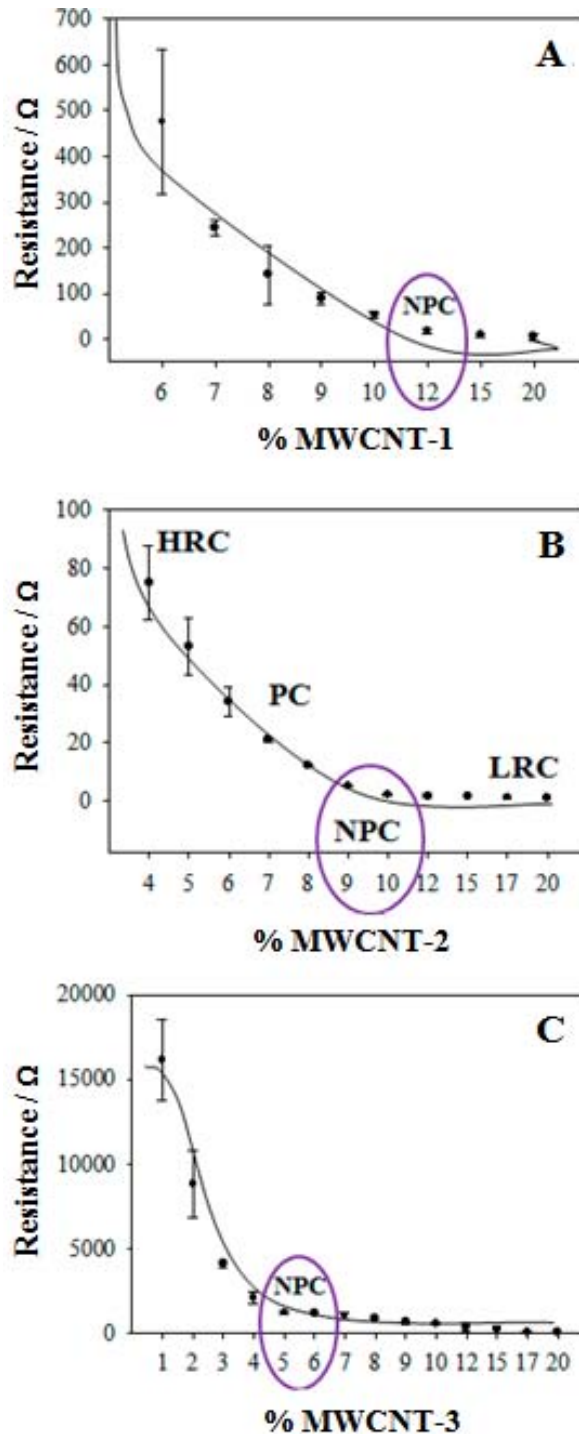


Figure 4.2 Percolation curve obtained for the rigid conducting nanocomposite electrodes based on the polymer epoxy and raw MWCNTs for A) C1, B) C2 and C) C3. In Figure 2B is described: HRC: high resistivity zone composites; PC: percolation zone composites; NPC: near-percolation zone composites and LRC: low resistivity zone composites. Experiments were calculated three times ($n=3$) with three different nanocomposite electrodes and are presented with their respectively 95% confidence interval.

In order to gain more insight in the relative electrochemical behaviour (wet conditions), different additional parameters were analyzed, which will be shown bellow.

4.1.1.3 Voltammetric experiments

CV was applied in order to electrochemically characterize the different series of MWCNT/epoxy nanocomposite electrodes. Fifteen different MWCNT/epoxy nanocomposite electrodes composition (from 1% to 20%) were fabricated. It is important to highlight that three electrodes were prepared at each loading concentration in order to evaluate the reproducibility of the handmade nanocomposite electrodes. Cyclic voltammograms were taken under the same experimental conditions (scan rate of $10 \text{ mV}\cdot\text{s}^{-1}$) for the three different series of MWCNT/epoxy nanocomposite electrode compositions in the presence of the benchmark $[\text{Fe}(\text{CN})_6]^{3-/4-}$ redox couple, which are shown in Figure 4.3. Different parameters such as peak height (I_p), peak separation potential (ΔE) and electroactive area (A) have been extracted from the cyclic voltammograms according to the modified Randles-Sevcik equation,²¹ which are summarized in Table 4.2.

According to voltammetric results, peak height increased with the MWCNT loading, due to an increase in the electroactive area. Simultaneously, a decrease of peak separation was also observed, related to an enhancement of the electron transfer rate. In addition, the exchange current (i_0) from Tafel plots (log current density vs. potential) has also been evaluated. i_0 is a parameter which provides information about the reversibility of the electron transfer process. From this value it is possible to evaluate the charge transfer resistance (R_{ct}) (see Equation 1.7 from § 1.4.1).

The trend observed in Table 4.2 is a decrease of this parameter which decreased loadings of MWCNTs; this observation indicates the strong relationship between electrochemical reactivity and the surface characteristics of the conducting material filler. As the carbon load increases, the probability of having more electroactive sites increases and hence also the electrode kinetics. Accordingly, low values in the charge-transfer resistance allows for increased the final electroanalytical capabilities of the electrode. By normalizing charge transfer resistance with respect the electroactive area ($R_{ct}\cdot A$), it is also possible to observe in Table 4.2 that this parameter is also decreasing with the increase of A . The parameter $R_{ct}\cdot A$ should be constant for conventional metal electrode interfaces. However, in the case of MWCNT-based nanocomposite electrodes, this is not expected as they are known to exhibit electrochemical anisotropy with higher electrode kinetics on edges and lower electron transfer rates on the walls or basal planes.^{22,23}

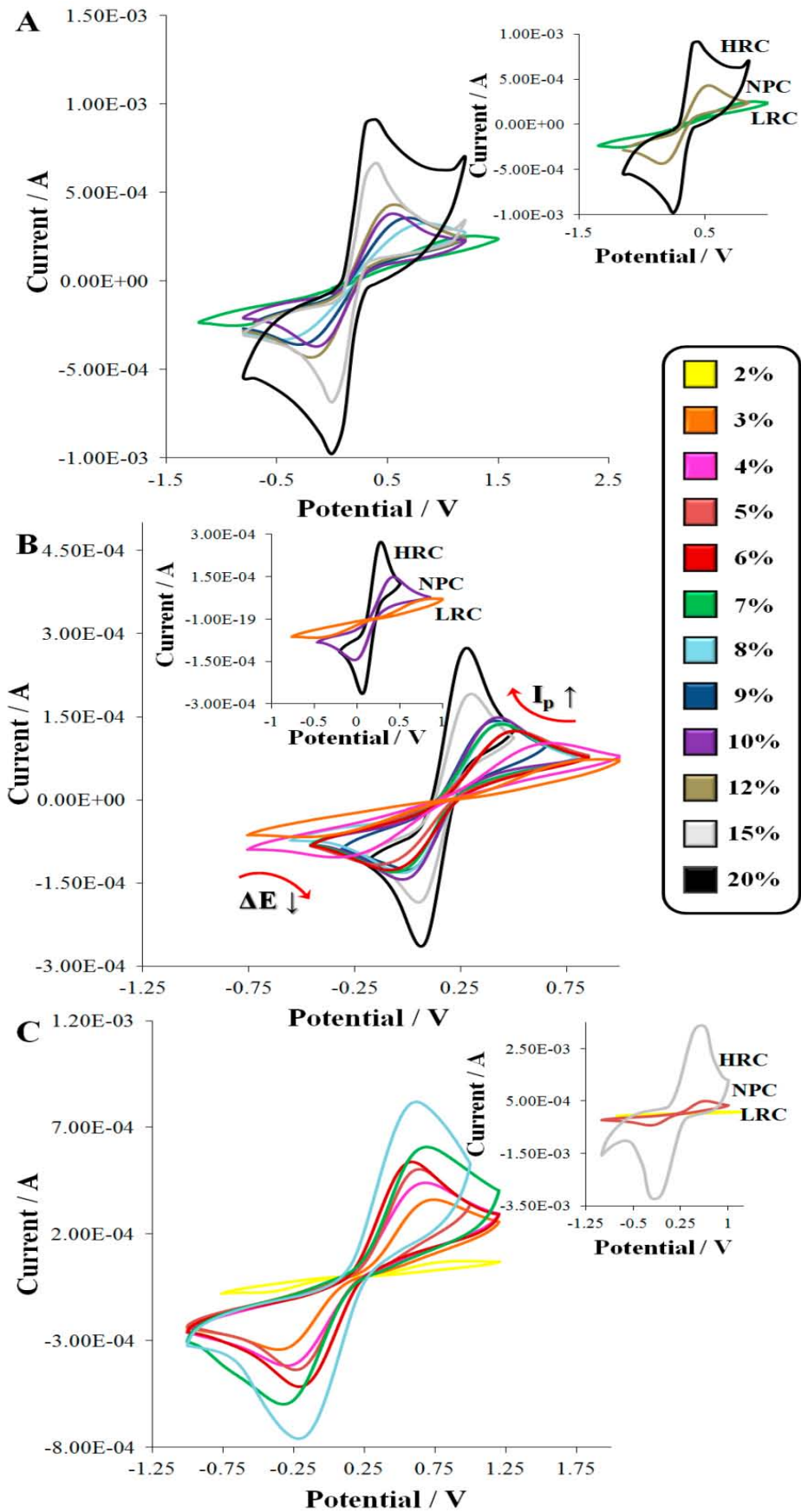


Figure 4.3 CV of A) C1, B) C2 and C) C3 electrodes recorded in a 0.1 M KCl containing 0.01 M $[\text{Fe}(\text{CN})_6]^{3-/4-}$ solution (scan rate: $10 \text{ mV} \cdot \text{s}^{-1}$). Inserts: comparison behaviours of HRC, NPC and LRC.

Table 4.2 Cyclic voltammetry parameters (i_0 , R_{ct} , I_p , A and ΔE) for the different nanocomposite compositions of the three series of MWCNT/epoxy electrodes. $R_{ct} \cdot A$ and $R_{ct}^{EIS} \cdot A$ correspond to the R_{ct} obtained by CV and EIS measurements, respectively, which are normalized with respect to the electroactive area.

MWCNTs samples	% CNTs	i_0 (μA)	R_{ct} ($k\Omega$)	I_p (μA)	A (cm^2)	ΔE (V)	$R_{ct} \cdot A$ ($\Omega \cdot cm^2$)	$R_{ct}^{EIS} \cdot A$ ($\Omega \cdot cm^2$)
MWCNT-1	5	2.75	9.2	178	0.11	5.94	970	60
	6	5.26	4.8	200	0.12	3.13	570	49
	7	11.5	2.2	269	0.16	2.30	351	40
	8	20.8	1.2	303	0.18	0.834	218	38
	9	34.1	0.74	351	0.21	0.734	154	40
	10	61.9	0.41	394	0.23	0.667	95	35
	12	73.4	0.35	441	0.26	0.634	90	31
	15	176	0.14	664	0.39	0.402	57	17
	20	334	0.076	938	0.55	0.399	42	11
MWCNT-2	4	4.05	6.3	91.4	0.17	0.871	1066	547
	5	13.7	1.9	122	0.23	0.580	426	392
	6	14.2	1.8	125	0.24	0.540	430	306
	7	14.4	1.8	123	0.23	0.534	422	301
	8	16.3	1.6	126	0.24	0.488	374	263
	9	24.7	1.0	126	0.24	0.470	237	141
	10	35.6	0.71	132	0.25	0.444	178	133
	15	26.1	0.97	143	0.27	0.491	234	187
	17	51.1	0.50	178	0.33	0.249	164	102
	20	103	0.25	263	0.49	0.229	121	99
MWCNT-3	4	14.3	1.7	355	0.21	1.08	372	802
	5	20.9	1.2	369	0.24	0.859	265	255
	6	41.0	0.61	455	0.27	0.825	166	244
	7	35.5	0.71	534	0.32	1.04	225	315
	8	74.0	0.34	626	0.37	1.06	171	208
	9	96.8	0.26	844	0.50	0.822	97	77
	10	262	0.097	1540	0.91	0.838	88	99
	12	354	0.072	1990	1.2	0.827	84	49
	15	878	0.029	2850	1.7	0.808	49	25
	17	1180	0.022	4060	2.4	0.744	52	14
	20	1830	0.014	5200	3.1	0.734	43	12

Comparing the three different series of MWCNT/epoxy nanocomposite electrodes, Figure 4.4 shows the cyclic voltammogram of the three NPC electrodes previously extracted from the percolation curve (12% for C1, 10% for C2 and 5% for C3). Non significant differences were observed in ΔE , A and I_p parameters, demonstrating that the optimum nanocomposites have similar electrochemical behaviours and that their performance depends on the raw MWCNTs diameter.

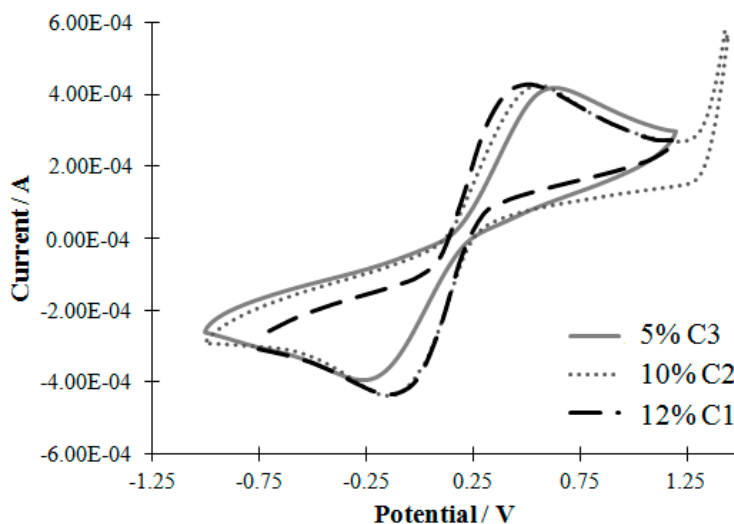
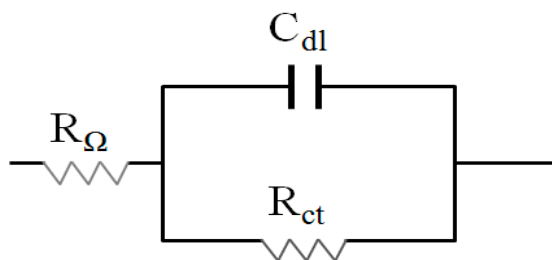


Figure 4.4 Cyclic voltammograms for the three optimum nanocomposite electrodes recorded in a 0.1 KCl containing $[\text{Fe}(\text{CN})_6]^{3-/4-}$ solution. Scan rate: $0.01 \text{ V}\cdot\text{s}^{-1}$.

Finally, another electrochemical technique (EIS) has been carried out in order to obtain resistance/impedance information about the different nanocomposite electrode compositions for each series. Furthermore, different electrochemical parameters were also used to compare the obtained results between both electrochemical techniques.

4.1.1.4 Impedimetric experiments

Ohmic resistance (R_Ω), charge transfer resistance (R_{ct}) and double-layer capacitance (C_{dl}) for nanocomposites with different MWCNT loadings were evaluated for the three series of MWCNT/epoxy nanocomposites by EIS technique. These parameters were obtained by fitting the impedance spectra to a simple equivalent circuit: $R_\Omega \cdot (R_{ct} \cdot C_{dl})$, using the equilibrium potential previously obtained by CV. This circuit, which is shown in Scheme 4.1, was sufficiently suitable to interpret the R_Ω , R_{ct} and C_{dl} values in terms of the interfacial phenomena that occur at the electrochemical cell.



Scheme 4.1 Equivalent circuit used for the impedance spectra fitting.

Figure 4.5 shows the Nyquist plot for each nanocomposite series in the frequency range between 0.1 Hz and 100 kHz (amplitude around 10 mV). In general, impedance behaviours of three series presented similar trends. Nanocomposites from HRC zone to NPC zone (<10% for C1, <9% for C2 and <5% for C3, percentage expressed in %MWCNTs), appeared to be dominated by a big diameter semicircle and only the kinetic-controlled electrode process was present in all the recorded frequency range. On the other hand, nanocomposites with lower resistivity and thus, between NPC zone and LRC zone (>10% of MWCNT loading for C1, >9% for C2 and >5% for C3) impedance values showed a kinetically controlled response representing again kinetic-controlled electrode process, through in some cases, the diffusion-controlled process started to be discerned at low frequencies (linear region after the semicircle).

R_{Ω} resistance is the one that has a direct relation with the dry resistance taken for the percolation plot of Figure 4.2. C1, C2 and C3 showed a R_{Ω} decrease at the same time that the MWCNT loaded increased, as shown in Figure 4.6 (black plots). This behaviour is in agreement with the obtained results in the percolation curve.

Concerning R_{ct} , this parameter is well known as a useful parameter reflecting the facility of electrode reaction, which can be measured by EIS from the semicircle diameter in the Nyquist plots.²⁴ From Figure 4.6, the light grey plots showed a decrease of R_{ct} parameter with carbon proportion because of the increase of electroactive sites, as has been discussed in the previous section. Due to the electrode kinetics of CNTs electrodes is dependents on the CNTs nature and structure, the electroactive area became different from a same percentage of MWCNTs, depending on the raw MWCNT nature; as a matter of fact it was the diameter for this study.

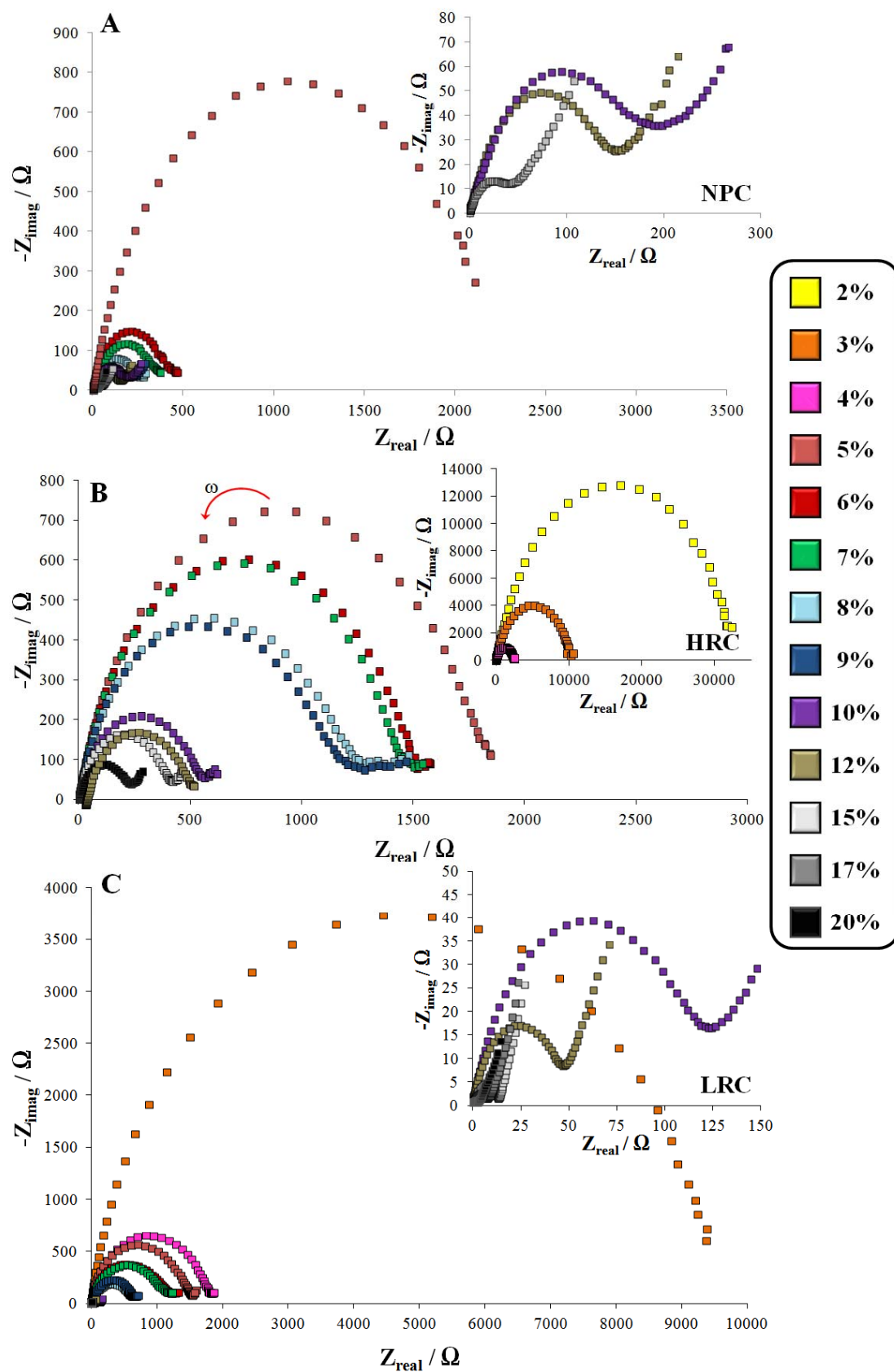


Figure 4.5 Impedance spectra of A) C1, B) C2 and C) C3 for the different MWCNT/epoxy electrode compositions in the presence of 0.1 m KCl containing 0.01 M $[\text{Fe}(\text{CN})_6]^{3-/4-}$. Insets: zoom of different conductive zones.

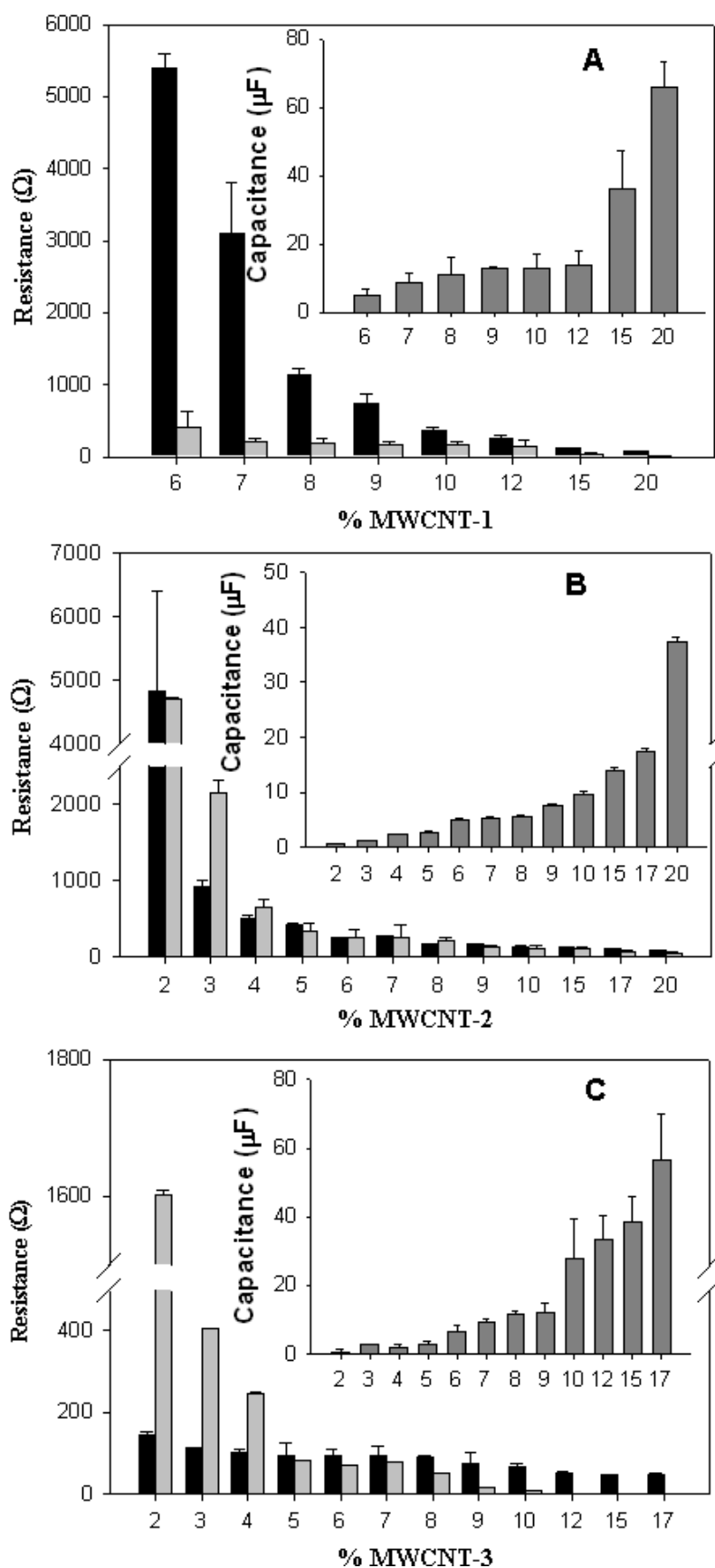


Figure 4.6 Values of ohmic resistance (R_{Ω} , black, ■), charge transfer resistance (R_{ct} , light gray, ■) and double-layer capacitance (C_{dl} , dark grey, ■), with their corresponding standard deviation for a) C1, b) C2 and c) C3. A redox solution of 0.01 M $[\text{Fe}(\text{CN})_6]^{3-/4-}$ containing 0.1 M KCl was used.

C_{dl} parameter is known to be directly related to the charging or background current and is inversely proportional to the signal to noise ratio. An increase of C_{dl} values was obtained for electrodes comprising high surface area of conducting material. From Figure 4.6 (dark grey plots) it is possible to observe a decrease of the double-layer capacitance values with the decrease of the MWCNT loadings. Accordingly, electrodes containing less carbon loads enhance the signal to noise ratio and consequently should decrease the analyte detection limits.

An electrode for electroanalytical purpose must have a rapid response time, low limit of detection and high sensitivity. According to the impedance results and taking that into account, the intervals between 10% and 12% of MWCNT-1 loading fulfil all these requirements for C1. Regarding C2 and C3, their optimum ratios were found around 9%–10% and 5%–6%, respectively. These results demonstrated that the optimum intervals of MWCNT/epoxy ratio, which are also in agreement with the obtained by percolation curve, were closely tied to raw MWCNTs nature. The benefit of working within these MWCNT/epoxy intervals led to an increase of the electrochemical reproducibility, assuring the compromise to work with electrodes with low resistivity and low signal-noise ratio.

4.1.1.5 Morphological studies

Roughness surfaces of near-percolation zone electrodes were compared for the three different MWCNT/epoxy nanocomposites (C1–NPC, C2–NPC and C3–NPC electrodes). Thus, the topography of each optimum nanocomposite was measured by CM3D. Figure 4.7 presents the most significant images obtained during the electrode surface study.

Based on the morphological values obtained by CM3D, which are shown in Table 4.3, it was determined that the three optimum electrode topographies were strongly similar, in spite of the differences with carbon loading. These results were the expected due to their active areas (A) are much similar, as it is shown in Table 4.2. Once again it is corroborated that the physical properties of raw nanotubes are crucial in the electrochemical response of the sensor. Under this context, it is necessary an optimum characterization and optimization of the nanocomposite composition ratio previously to be used as a transducer material

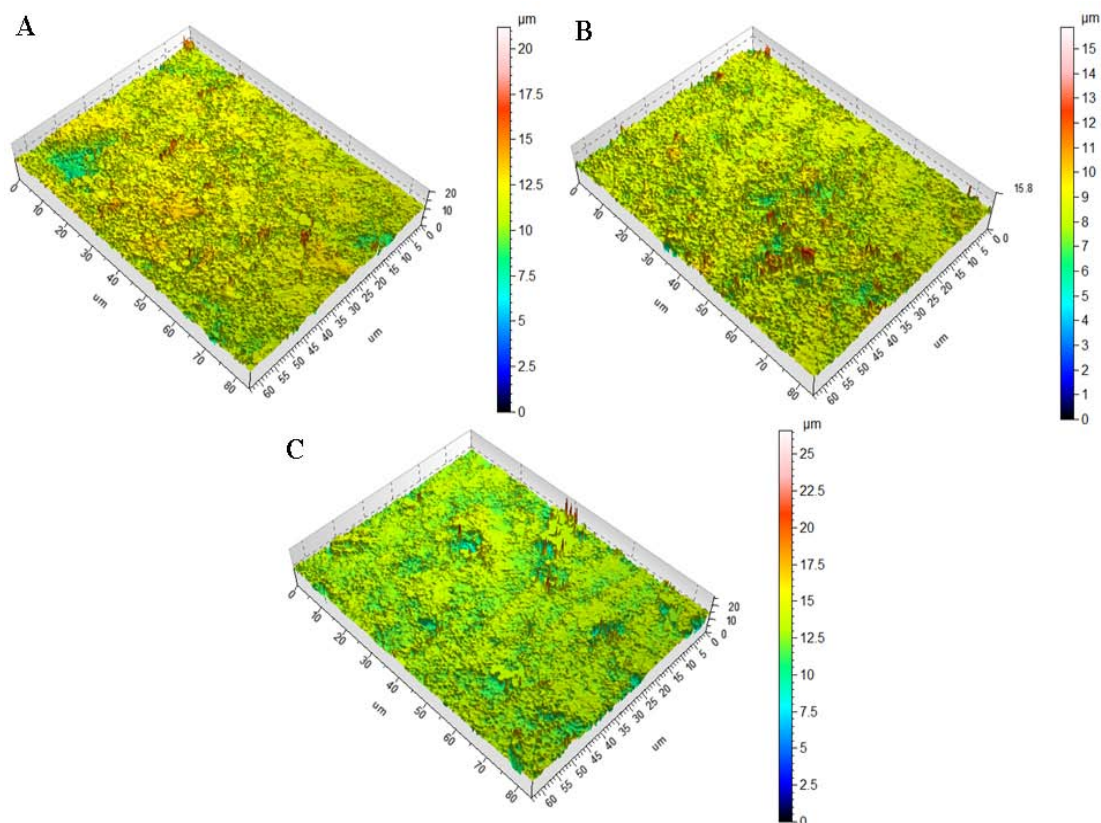


Figure 4.7 Topographic images of the A) C1–NPC, B) C2–NPC and C) C3–NPC electrodes were obtained with the 3D Optical Surface Metrology System Leica CM3D for the roughness study.

Table 4.3 Roughness values collected from surface analysis. Data are the mean and standard deviation (SD) from 57 profiles of three areas examined in each series (ISO 4287).

Electrodes	MWCNTs content (%)	R_a^a (μm)		R_q^b (μm)		R_z^c (μm)	
		Mean	SD	Mean	SD	Mean	SD
C1–NPC	12	0.559	0.208	0.812	0.212	4.899	1.616
C2–NPC	10	0.555	0.129	0.920	0.271	7.306	2.602
C3–NPC	5	0.579	0.175	0.809	0.286	5.516	2.830

^aArithmetical mean deviation of the assessed profile

^bThe root mean square deviation of the assessed profile

^cMaximum height of the profile

4.1.1.6 Electroanalytical performance

Ascorbic acid was used as a model analyte for evaluating the electroanalytical performance of the sensors. The MWCNT/epoxy nanocomposite response to the change of ascorbic acid concentration was evaluated by hydrodynamic amperometry. The analytical parameters as the detection limit (LOD) and sensitivity were evaluated for

each optimum nanocomposite sensor and compared with the most concentrated nanocomposites prepared (20% in carbon load), see Table 4.4. Furthermore, 20% in carbon load is the convectional composition used in the vast majority of previous studies reported by our research group.²⁵ Comparing optimum nanocomposite sensors with the ones which contain 20% in carbon load, the best LOD was obtained for the optimized-sensors, although the most concentrated nanocomposites prepared contain a higher number of transducer particles. This fact is because of a lower MWCNTs load results in a diminution of the signal to noise ratio (C_{dl}). In this way, sensors containing 20% in MWCNT-3 load could not be amperometrically stabilized due to their high value of C_{dl} . Thereby, 9% of MWCNT-3 was the highest carbon load which could be measured in this series. The LOD obtained for this composition was $0.68 \pm 0.03 \text{ mg}\cdot\text{L}^{-1}$, higher than the one obtained by the optimized composition. Comparing among series, the lowest LOD was obtained for the optimum C3–NPC sensor (0.042 ppm), which contains nanotubes with the narrowest diameter (MWCNT-3). On the other hand, C1–NPC and C2–NPC sensors presented the same LOD (0.070 ppm) due to their optimum loading are closely similar. These results showed again the C_{dl} effect on the amperometric measurements, obtaining the best results for the optimized-sensors.

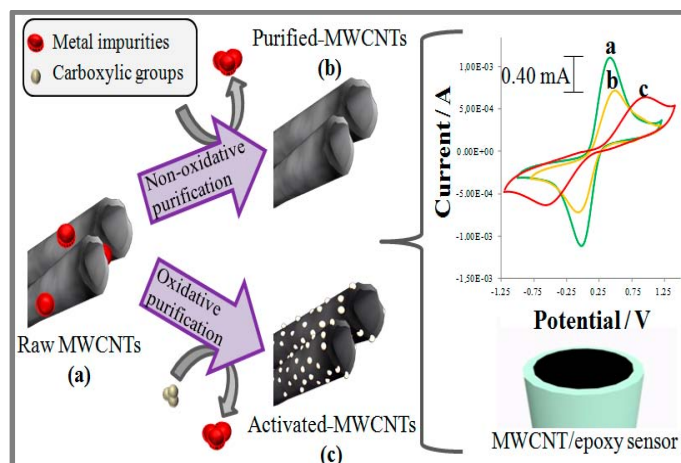
Finally, having made a meticulous characterization of the optimum composition interval of epoxy nanocomposite sensors based on different MWCNTs, it can be concluded that optimizing both the nature of the raw filler material as the filler/polymeric composition ratio, it is possible to obtain more efficient and sensitive electrochemical sensors which contain a more reproducible analytical signal.

Table 4.4 Amperometric values of ascorbic acid are shown for the optimized and non-optimized sensors. LOD was calculated with their respectively 95% confidence interval (n=3).

Analytical values	Sensors					
	C1		C2		C3	
	12%	20%	10%	20%	5%	20%
LOD ($\text{mg}\cdot\text{L}^{-1}$)	0.070 ± 0.002	0.34 ± 0.01	0.070 ± 0.004	0.26 ± 0.01	0.042 ± 0.004	*
Sensitivity ($\mu\text{A}\cdot\text{L}\cdot\text{mg}^{-1}$)	0.015	0.082	0.018	0.071	0.021	*
r^2 (n=14)	0.996	0.998	0.999	0.998	0.999	*

*C3 sensors containing 20% in MWCNT-3 were not able to be measure due to their high noise (C_{dl}).

4.1.2 Effect of the raw MWCNTs purity



Graphical Abstract II. Effect of the MWCNT purity on the electroanalytical signal.

This work focuses on the effect of MWCNTs purification methods for their application as conducting filler in the development of epoxy amperometric nanocomposite sensors based on different MWCNTs. For this purpose, three different MWCNTs samples with distinctive purities were characterized previously to nanocomposite incorporation using different tools. Then, composition ratios were characterized by different electrical, electrochemical and morphological techniques. After characterization results, it has been demonstrated that the purification method affects the electrochemical performance of the nanocomposite electrodes but not their optimum MWCNT/epoxy ratio, which kept unaltered. From an analytical point of view, sensors containing the non-modified MWCNTs interestingly presented the best electroanalytical response for the reference analyte (ascorbic acid).

4.1.2.1 Physical characterization of MWCNTs

The study of purity was made using three different samples of MWCNTs: raw MWCNTs, purified-MWCNTs and activated-MWCNTs (which was obtained from the acid oxidative oxidation of raw MWCNTs), following the specifications shown in Table 3.1 from § 3.1. Raw MWCNTs (90% in C given by manufacturer specifications) were chosen as raw carbon material. Purified-MWCNTs were obtained by a non-oxidative acidic treatment of raw MWCNTs, also according to the manufacturer. The second purification method consisted in subduing the raw MWCNTs under acid oxidative

conditions, obtaining the activated–MWCNTs by using a 3:1 mixture of concentrated $\text{H}_2\text{SO}_4/\text{HNO}_3$.²⁶ In order to keep the length/diameter ratio, 90 min of concentrated acid treatment in ultrasound bath was enough not to have an evident reduction of the length,²⁷ as can be seen in Figure 4.8.

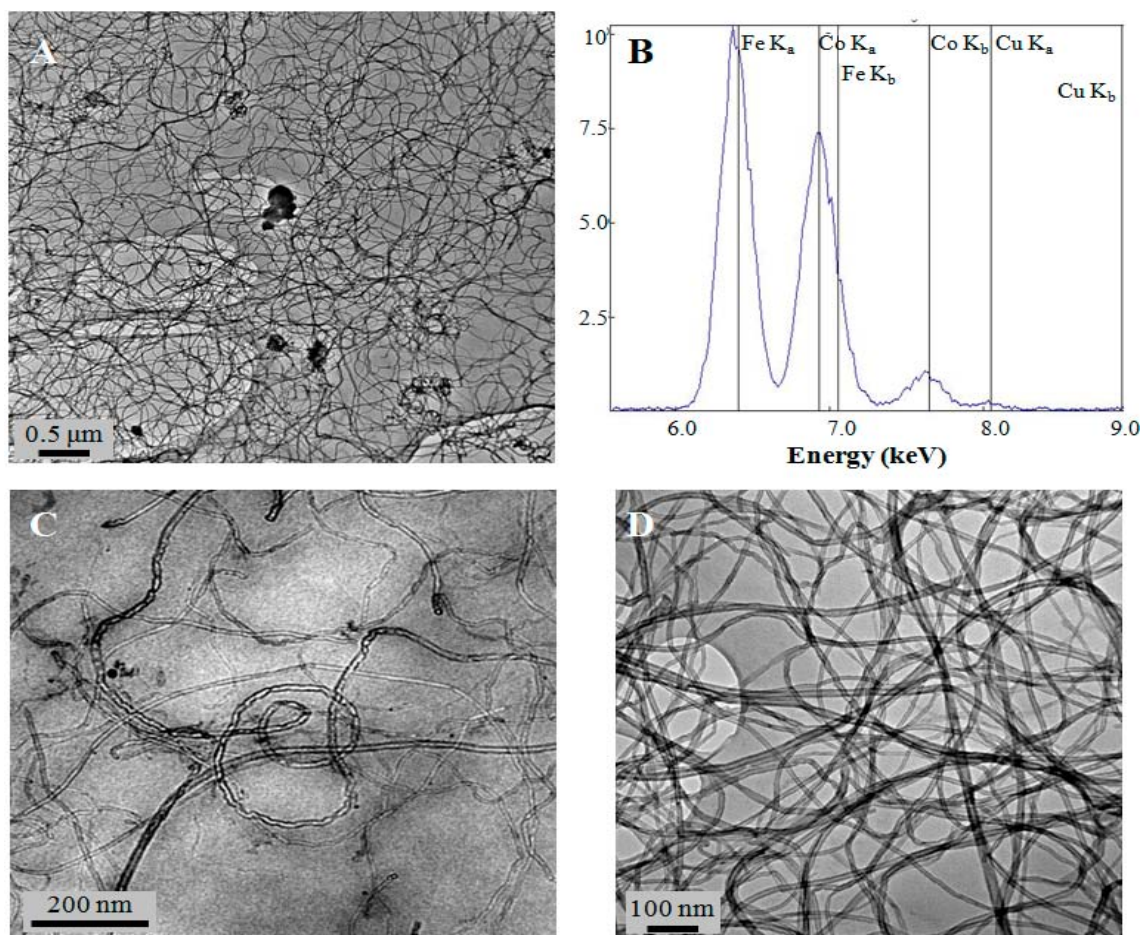


Figure 4.8 HR–TEM images of A) raw MWCNTs and B) its corresponding FP–RXF spectrum; C) purified–MWCNTs and D) activated–MWCNTs.

Purity characterization was carried out by TGA analysis. From Figure 4.9 it is possible to observe that the weight loss for the three MWCNTs took place in a single step, with a maximum of weight loss between 600 °C and 700 °C. The background line is attributed to metallic remaining. While raw MWCNTs analysis revealed 11.0% of metal oxide, purified–MWCNTs showed 98.0% in carbon content. These values are in concordance with the specifications were given by the manufacturer. Finally, 2.8% in metal oxide was obtained by activated–MWCNTs. Thereby, both purification methods showed a decrease of metal oxide content, as shown in Table 4.5.

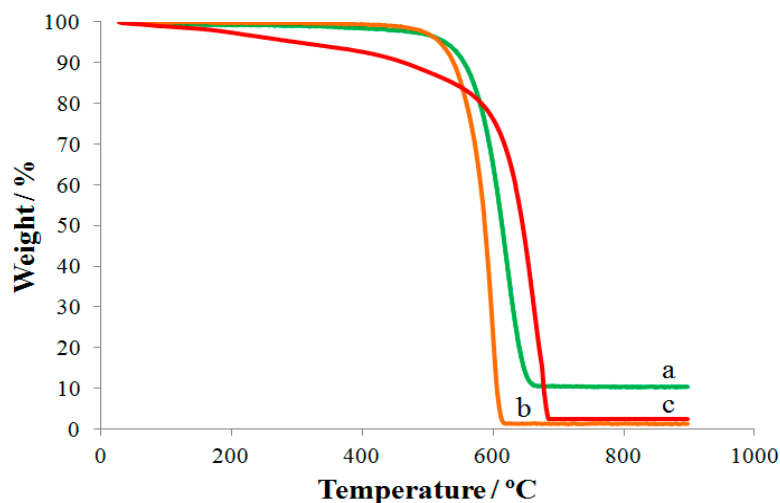


Figure 4.9 The TGA curve of the raw MWCNTs (a) before purification and (b) after purification by non-oxidative (c) and oxidative treatments.

It is important to emphasize that TGA provides only quantitative information on the presence of total metal content in CNT material. Figure 4.8 B also shows the FP-XRF analysis, which was carried out in order to quantify and identify the metal content on raw MWCNTs. Fe, Co and Cu metals were detected on the raw material. Fe and Co could be quantified, obtaining 15357 ± 227 ppm and 908 ± 16 ppm respectively, while only qualitative results could be reached for Cu.

Both diameter and length of the different MWCNT samples were measured using HR-TEM. The average lengths and diameters of the nanotubes are also shown in Table 4.5. After an accurate data compilation, certain differences between the experimental results and the specifications provided by the suppliers were detected, obtaining higher values in length as well as in diameter. According to TEM characterization, similar length and diameter have been obtained for the three studied MWCNTs. Thus, both parameters can be considered as constants and purity is the only study variable.

Table 4.5 Physical parameters of the three different MWCNT samples were studied by HR-TEM (length and diameter) and TGA (purity) and compared with those given by commercial suppliers (MFG).

MWCNTs samples	Diameter (nm)		Length (μm)		Purity (% in C)	
	TEM	MFG	TEM	MFG	ATG	MFG
Raw MWCNTs	10–20	9.5	1.5–2.5	1.5	89.0	>90
Purified-MWCNTs	8–16	9.5	1.5–2.5	1.5	98.0	>95
Activated-MWCNTs	8–18	-	1.5–2.0	-	97.2	-

Based on these results, this work is focused on the effect of the MWCNTs purification method on both the electrochemical and electroanalytical response of the nanocomposite electrodes as the optimum MWCNT/epoxy composition ratio. Furthermore, the influence of the metallic particles and the presence or not of carboxylic groups on MWCNTs surface by using different purification methods was also evaluated.

4.1.2.2 Electrical characterization

The electrical properties of the three series of MWCNT/epoxy nanocomposite electrodes were investigated by Percolation Theory, see Figure 4.10. In order to evaluate the electrical properties of such nanocomposites, the electrical resistance was tested by varying the carbon loading for every nanocomposite composition. The first series was raw MWCNT/epoxy nanocomposites (S1), the second one consists of purified-MWCNT/epoxy nanocomposites (S2) and finally, the third series of nanocomposites was made dispersing activated-MWCNTs into epoxy resin (S3). The percolation threshold for S1, S2 and S3 nanocomposites was achieved at 1%, 2% and 5%, respectively. In concordance with the results obtained in the section § 4.1.1.2, three different conductive regions regarding the electrical behaviour were observed, which are depicted in Figure 4.10 B.

Based on the electrical results, the variation of the resistivity for the three series of nanocomposites materials was negligible between NPC and LRC. To obtain the optimal analytical response is necessary a lower resistivity value which produces a higher sensitivity.¹²

Thus, in terms of resistivity, the nanocomposites lying in such interval are suitable for electroanalytical measurements. On the other hand, comparing the electrical differences between the three series of MWCNT/epoxy nanocomposites, a non-displacement in the NPC zone was observed (see Figure 4.10), given that the length/diameter ratio is practically a constant value, as is shown in Table 4.5. This observation is attributed to the same nature of the three MWCNT samples. Hence, values between 6% and 8% have been identified as the optimum interval of MWCNT load for each series, since these composition ranges are located into the NPC zone.

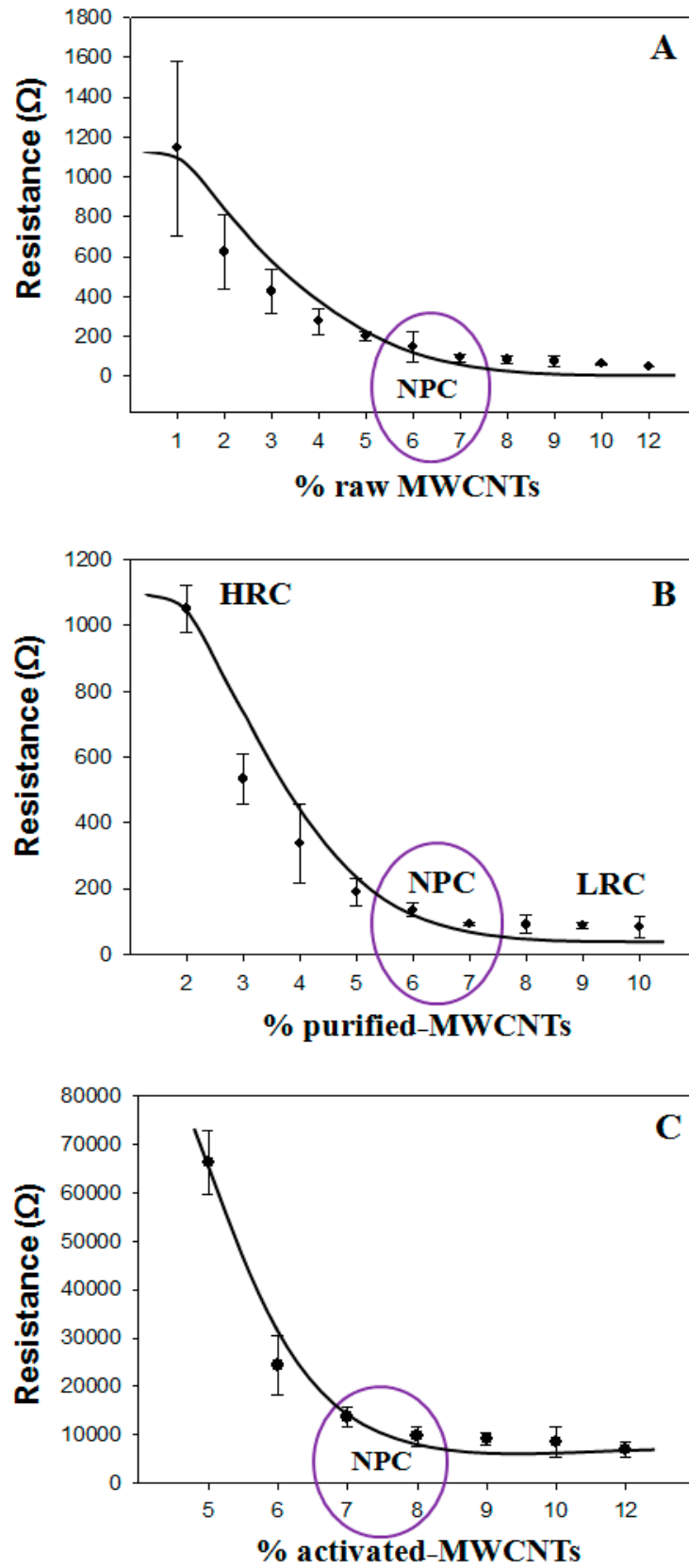


Figure 4.10 Percolation curve obtained for A) S1, B) S2 and C) S3. In figure B are described the three different conductive regions. HRC: high resistivity zone, NPC: near-percolation zone (highlighted) and LRC: low resistivity zone.

Finally, it is important to highlight that the optimum ratios are consistent with the expected results through the previous characterization of diameters (§ 4.1.1), demonstrating again that the diameter is the most important physical parameter which shifts the NPC zone.

4.1.2.3 Voltammetric experiments

NPCs of each series were electrochemically characterized by CV and compared one with other. Figure 4.11 shows the cyclic voltammograms for the three NPC electrodes containing raw MWCNTs (S1-NPC), purified-MWCNTs (S2-NPC) and activated-MWCNTs (S3-NPC). Some parameters, such as I_p , ΔE and A have been extracted from the cyclic voltammograms, which are shown in Table 4.6. The A was estimated from the peak-shaped voltammograms by using the modified Randles-Sevcik equation, which is appropriated for electron transfer-controlled processes.

According to CV results, the highest electroactive area was obtained for S1-NPC (0.51 cm^2) due to their major content of conductive material. Contrary, the lowest electroactive area was exhibited for S3-NPC electrodes (0.36 cm^2), mainly caused by the steric hindrance provided by carboxylic groups. Hence, the metal content in S1-NPC electrodes showed an electrocatalytic effect from an electrochemical point of view. This fact can also be observed in their I_p value, which was 35% and 43% higher than S2-NPC and S3-NPC electrodes, respectively. On the other hand, electrodes containing both purified-MWCNTs and activated-MWCNTs did not exhibit significant differences in their I_p values due to their same purity (see Table 4.5).

Table 4.6 Electrochemical and analytical values for the three NPC materials. LOD was calculated with their respectively 95% confidence interval (n=3), using ascorbic acid.

Electrode/ Sensor	I_p (mA)	A (cm^2)	ΔE (V)	LOD ($\text{mg}\cdot\text{L}^{-1}$)	Sensitivity ($\mu\text{A}\cdot\text{L}\cdot\text{mg}^{-1}$)	r^2 (n=12)
S1-NPC	1.11	0.51	0.50	0.014 ± 0.002	0.071	0.999
S2-NPC	0.72	0.42	0.57	0.042 ± 0.008	0.145	0.997
S3-NPC	0.64	0.36	1.52	0.07 ± 0.02	0.058	0.998

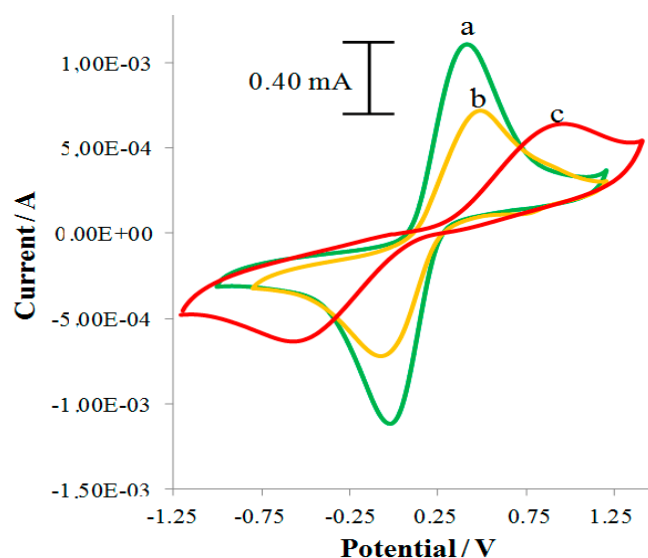


Figure 4.11 Cyclic voltammograms recorded in 0.01 M $[\text{Fe}(\text{CN})_6]^{3-/4-}$ for a) S1-NPC, b) S2-NPC and c) S3-NPC electrodes. Scan rate: $10 \text{ mV} \cdot \text{s}^{-1}$.

Furthermore, Figure 4.11 also revealed a change in ΔE from 0.50 V for S1-NPC electrodes to 1.52 V for S3-NPC electrodes due to the strong electrode surface modification provided by the incorporation of carboxylic groups. This increase of ΔE turns into a partial decrease in the system reversibility.²⁹ Contrary, S1-NPC and S2-NPC did not show a significant change in the ΔE value (0.50 V vs. 0.57 V), obtaining both a fast electron transfer process and a pair of well-defined and quasi-reversible redox peaks.

The voltammetric studies show proof-of-concept in respect of observed apparent electrocatalysis in the nanocomposite sensors containing raw MWCNTs, which is likely due to the role of metal impurities in the carbon nanotubes. While the edge-plane sites/defects on MWCNTs are mainly responsible of the electron transfer exchange for electrodes containing purified-MWCNTs and activated-MWCNTs (note the similar I_p values),³⁰ the significant I_p enhancement observed for the electrodes containing raw MWCNTs must derive from the issue of metal impurities in the carbon material.^{31,32}

4.1.2.4 Impedimetric experiments

R_Ω , R_{ct} and C_{dl} were also evaluated for the three series of MWCNTs/epoxy nanocomposite electrodes (S1, S2 and S3). These parameters were obtained by fitting the impedance spectra to a simple equivalent circuit: $R_\Omega \cdot (R_{ct} \cdot C_{dl})$, which is shown in Scheme 4.1.

As was mentioned above, it is important to achieve low R_{Ω} in order to assure high sensitivity and low response time of the nanocomposite electrodes. As it is depicted in Figure 4.12 (black plots), S1, S2 and S3 showed a R_{Ω} decrease at the same time as the MWCNT loading increased. While the obtained R_{Ω} values were similar for S1 and S2, S3 exhibited a significant increase, which can be attributed to the incorporation of carboxylic groups on the MWCNT surface. This activation modifies the electrode surface, incorporating a significant steric hindrance on its surface.

As in the previous section, R_{ct} parameter decreased with the increasing of MWCNT load (see Figure 4.12, light gray bars) because of the increment of electroactive sites on the electrode surface, demonstrating that electrodes with low R_{ct} are appropriated to be used in electrochemical measurements. In addition, EIS is also a powerful tool for studying the interface properties of the different series of MWCNT/epoxy nanocomposite electrodes and may provide information on the impedance changes of the interface of the electrode surface–electrolyte solution. Figure 4.13 presents the typical Nyquist plots for NPCs containing both raw MWCNTs as activated–MWCNTs. As can be observed, the R_{ct} values of S3-NPC electrodes were much higher than the S1-NPC electrodes, demonstrating an evident activation of their carbon surface with carboxylic groups.

Regarding C_{dl} parameter, Figure 4.12 (dark gray bars, inside) showed an increment of the C_{dl} values when the load of MWCNTs increases. Due to this parameter is directly related to the charging or background current and inversely proportional to the signal to noise ratio, high proportion of MWCNT loads increases the conducting areas, the surface roughness and porosity of the nanocomposites and consequently the background current increments remarkably.²⁸ While S1 and S2 electrodes presented similar values of C_{dl} , S3 electrodes exhibited slight decrease of C_{dl} values and hence, an enhancement of the signal to noise ratio what significantly reduces the background current.

According to the impedimetric results and taking into account the aim to maintain low resistances and a high signal to noise ratio, compositions between 6% and 8% of conductor material (NPC zone obtained by percolation curve) seems to fulfil the optimum conditions to obtain the properties required by an electrode for electroanalytical purposes, such as rapid response time, low limit of detection and high sensitivity.

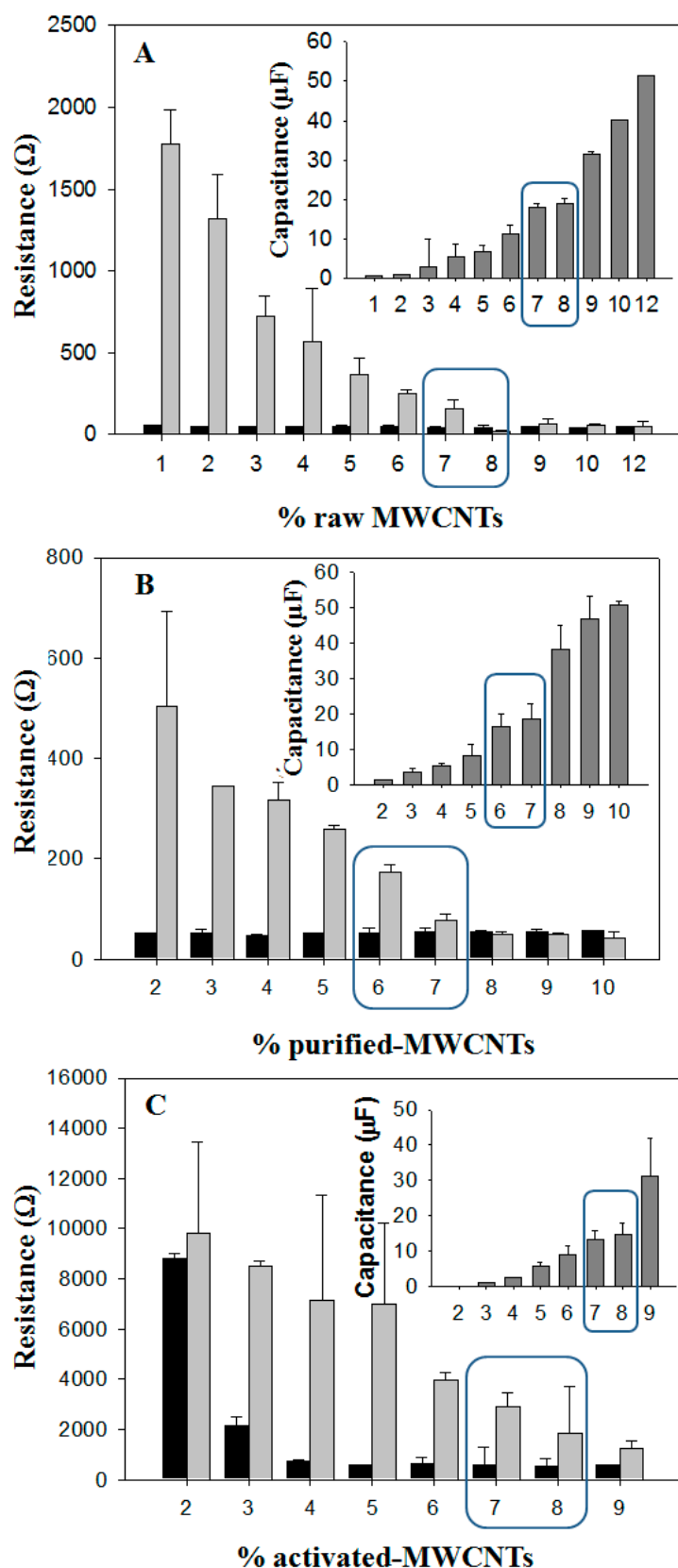


Figure 4.12 Values of ohmic resistance (black, ■), charge transfer resistance (light gray, ■) and double-layer capacitance (dark gray, ■) and their corresponding standard deviation (n=3) for A) S1, B) S2 and C) S3 obtained in a 0.01 M $[\text{Fe}(\text{CN})_6]^{3-}/[\text{Fe}(\text{CN})_6]^{4-}$ containing 0.1 M KCl solution. Highlighted the optimum nanocomposite ranges (NPC zone) for electroanalytical proposes.

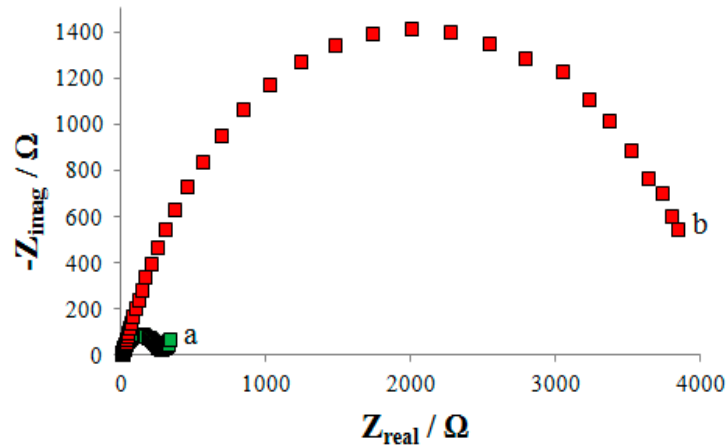


Figure 4.13 Nyquist plots of raw MWCNTs (a) before and (b) after acid oxidative treatment through a 3:1 mixture of concentrated $\text{H}_2\text{SO}_4/\text{HNO}_3$ acids in an ultrasound bath for 90 min. The experiments were carried out in a background solution of $0.1 \text{ M } [\text{Fe}(\text{CN})_6]^{4-/3-}$ containing 0.1 M KCl .

The fabricated composites in such interval depicted similar electrochemical performance. Furthermore, the use of the NPC electrodes presents the benefit that small variations in their composition during the hand-made fabrication process produce little changes in the electrochemical nanocomposite behaviour. Hence, the use of nanocomposite devices in such interval of composition present high reproducibility in the analytical response.

4.1.2.5 Morphological studies

Roughness surfaces of the three NPC electrodes have been compared by CM3D in order to complement the electrochemical results.³⁴ Figure 4.14 presents significant images obtained during the electrode surface study. Results presented in Table 4.7 show the effect of both the metal impurities and the carboxylic groups on the electrode roughness.

Table 4.7 Roughness values collected from surface analysis. Data are the mean and standard deviation (SD) from 57 profiles of three areas examined in each series (ISO 4287).

Electrodes	MWCNTs content (%)	R_a^a (μm)		R_q^b (μm)		R_z^c (μm)	
		Mean	SD	Mean	SD	Mean	SD
S1-NPC	7	0.87	0.33	1.29	0.57	9.09	4.62
S2-NPC	7	0.61	0.20	0.84	0.32	5.86	2.57
S3-NPC	8	0.54	0.08	0.72	0.12	4.25	1.06

^aArithmetical mean deviation of the assessed profile

^bThe root mean square deviation of the assessed profile

^cMaximum height of the profile

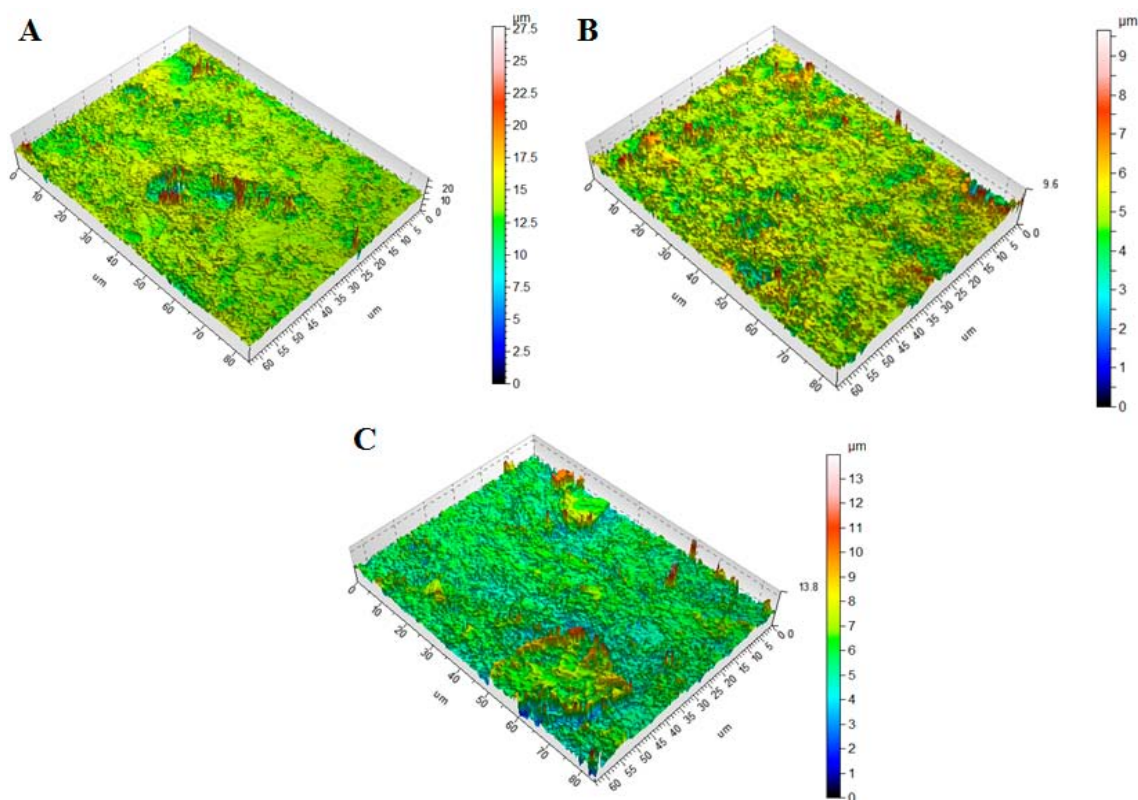


Figure 4.14 Topographic images of A) S1-NPC, B) S2-NPC and C) S3-NPC were obtained with the 3D Optical Surface Metrology System Leica CM3D for the roughness study.

According to confocal microscopy results, the presence of metal impurities significantly increased the roughness of the nanocomposite electrode, mainly due to the presence of more conducting material on the electrode surface. Thus, as can be seen in Table 4.7, S1-NPC presented an enhancement of the roughness surface around 30% respected to S2-NPC, which is in agreement with the improvement of the electroactive area (A) obtained by CV. However, as it was expected, S3-NPC showed a significant diminution of the roughness surface around 11% respected S2-NPC, which can be explained by the incorporation of carboxylic groups on the MWCNT walls.

4.1.2.6 Electroanalytical performance

The feasibility of the three NPC sensors was evaluated in terms of analytical response by hydrodynamic amperometry, using ascorbic acid as the model analyte (see Figure 4.15). The analytical parameters as the detection limit (LOD) and sensitivity were evaluated for the optimum range of composition of nanocomposite sensors for each series (NPC sensors), see Table 4.6.

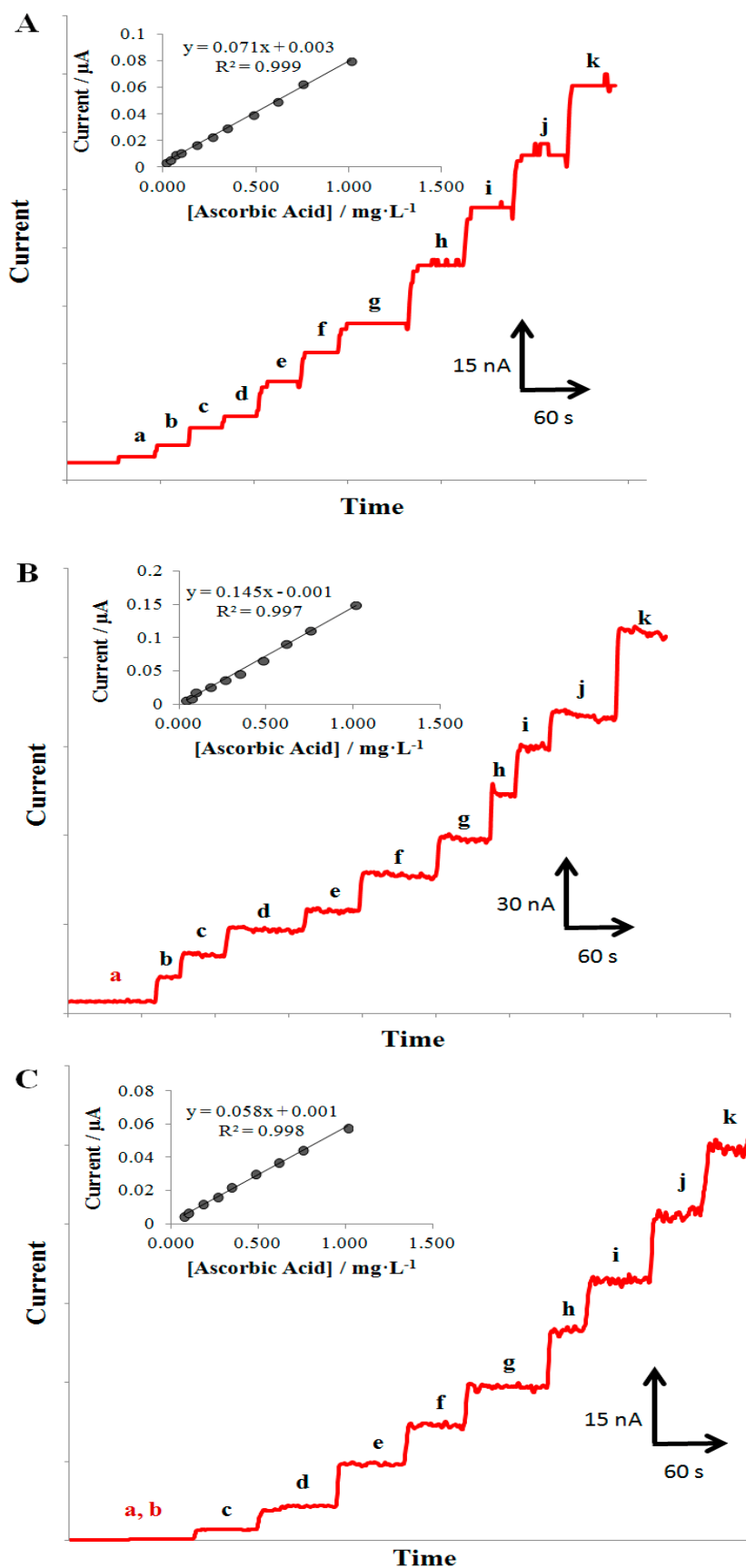


Figure 4.15 Dynamic responses of A) S1-NPC, B) S2-NPC and C) S3-NPC sensors to successive additions of ascorbic acid in a 0.10 M $\text{HNO}_3/\text{KNO}_3$ solution. Applied potential: 600 mV. Insert: their corresponding calibration curves in the range of (a to k) 0.014 to 1.014 $\text{mg}\cdot\text{L}^{-1}$.

Interestingly, the lower LOD was obtained for S1-NPC sensors, fact that verifies an electrocatalytic effect of the catalyst metal contained in the raw MWCNTs, improving the analytical response of the sensors to detect ascorbic acid. However, the less effective amperometric response was shown by S3-NPC sensors, in spite of providing a better signal to noise ratio (C_{dl}). This fact is related to the steric effects of the carboxylic groups on the sensor surface, which considerably decreased the electron transfer process on the sensor surface. S2-NPC sensors exhibited a better LOD regarding to those containing activated-MWCNTs, demonstrating that the non-aggressive acidic treatment benefits an enhanced of the final electroanalytical response of the sensor. On the other hand, S1-NPC sensors also exhibited a lower LOD in comparison with S2-NPC sensors in spite of providing a better sensitivity, demonstrating again the role of the metal impurities on the electrocatalytic detection of ascorbic acid.

Based on the electroanalytical results, the activation of carbon materials with carboxylic groups has proven to be neither necessary nor efficient to determine directly analytes by hydrodynamic amperometry.

The fact that the sensors containing raw MWCNTs presented an improvement in some physical parameters, such as higher electroactive area, faster electron transfer and a significant increment in the peak current height value compared to both pristine carbon materials (purified-MWCNTs and activated-MWCNTs) lead to enhanced high sensitivity, fast electrode response and low detection limits, as it has been demonstrated for the ascorbic acid detection. It is known that improving those parameters is possible to reduce the detection limits and thus, it is expected an improvement in detection limits for other types of analytes.^{33,34}

4.2 Conclusions

Several conclusions have been extracted from the results:

- Diameter, length and purity of the different MWCNTs samples have successfully compiled by different HR-TEM and TGA. Whereas purity is in good agreement with the manufacturer specifications, length and diameter strongly differed.

- Electrical experiments of the different MWCNT/epoxy nanocomposite materials were successfully modelled by percolation theory, demonstrating that the MWCNT diameter is a key parameter that determines the percolation behaviour of MWCNT-based nanocomposite materials, showing a leftward displacement on the NPC zone with increasing diameter. However, MWCNT purity does not provide significant changes in the NPC zone, remaining unaltered independent of the acidic treatment method used.
- EIS and CV are suitable techniques for the systematic characterization and optimization of the optimum MWCNT/epoxy composition regarding the nature of the raw MWCNT sample. Thus, the optimum MWCNT/epoxy composition ratios are from 5% in MWCNTs loading for the narrowest sample to 12% for the widest sample.
- The presented characterization protocol allows the optimization of MWCNT/epoxy composition ratios in terms of (i) R_{Ω} , which is related to the percolation resistivity; (ii) R_{ct} , directly related with the heterogeneous electron transfer rate and also depends on the surface electrochemical reactivity and (iii) C_{dl} , correlated to the background current. This protocol verified the optimum MWCNT/epoxy composition ratios, which are in concordance with the electrical results, and it is set as a consolidated characterization strategy of nanocomposite materials for the development of MWCNT-based electrochemical sensors.
- The optimized electrodes, which are those that just fall on the NPC zone, have provided an electroanalytical enhancement for the reference analyte used regarding to the ones non-optimized (standard composition: 20%) that contain the maximum load of conducting material permitted by the nanocomposite material without losing their mechanical properties.

- Comparing between different types of MWCNTs, sensors containing the narrowest MWCNTs shows lower LODs than the ones containing the widest. Regarding purification methods, MWCNTs treated by the oxidative treatment present the worst analytical response because of the incorporation of a steric hindrance effect caused by the –COOH groups on the tube surface. Interestingly, sensors containing non-purified MWCNTs exhibit the lowest LOD, demonstrating an electrocatalytic effect of the metal impurities contained in MWCNTs on the analytical response of ascorbic acid.

- Morphological experiments carried out by CM3D, which was novelty used for MWCNT-based nanocomposite electrodes studies, determined that the roughness values are directly related to the electroactive values obtained by CV, associating low roughness surface with low electroactive area.

4.3 References

1. Kroto, H. W.; Heath, J. R.; O'Brien, S. C.; Curl, R. F.; Smalley, R. E., C 60: buckminsterfullerene. *Nature* **1985**, *318* (6042), 162-163.
2. Iijima, S., Helical microtubules of graphitic carbon. *Nature* **1991**, *354* (6348), 56-58.
3. Chico, L.; Crespi, V. H.; Benedict, L. X.; Louie, S. G.; Cohen, M. L., Pure carbon nanoscale devices: nanotube heterojunctions. *Physical Review Letters* **1996**, *76* (6), 971-974.
4. Eatemadi, A.; Daraee, H.; Karimkhanloo, H.; Kouhi, M.; Zarghami, N.; Akbarzadeh, A.; Abasi, M.; Hanifehpour, Y.; Joo, S. W., Carbon nanotubes: properties, synthesis, purification, and medical applications. *Nanoscale Research Letters* **2014**, *9* (1), 1-13.
5. Penza, M.; Tagliente, M.; Aversa, P.; Re, M.; Cassano, G., The effect of purification of single-walled carbon nanotube bundles on the alcohol sensitivity of nanocomposite Langmuir–Blodgett films for SAW sensing applications. *Nanotechnology* **2007**, *18* (18), 185502.
6. Pearce, R.; Andersson, M.; Belmonte, J.; Gracia, I.; Stevens, M.; Buchholt, K.; Shaw, J.; Shaffer, M.; Spetz, A. L., A Comparison of the Gas Sensing Properties of Purified and Platinum Decorated Chemical Vapour Deposition Grown Multi Walled

Carbon Nanotubes. In *Smart Sensors and Sensing Technology*, Springer: 2008; pp 85-99.

7. Vashist, S. K.; Luong, J. H. T., Recent advances in electrochemical biosensing schemes using graphene and graphene-based nanocomposites. *Carbon* **2015**, *84* (0), 519-550.

8. Valentini, F.; Amine, A.; Orlanducci, S.; Terranova, M. L.; Palleschi, G., Carbon nanotube purification: preparation and characterization of carbon nanotube paste electrodes. *Analytical Chemistry* **2003**, *75* (20), 5413-5421.

9. Shi, J.; Wang, Z.; Li, H.-l., Electrochemical fabrication of polyaniline/multi-walled carbon nanotube composite films for electrooxidation of methanol. *Journal of Materials Science* **2007**, *42* (2), 539-544.

10. Krause, B.; Villmow, T.; Boldt, R.; Mende, M.; Petzold, G.; Pötschke, P., Influence of dry grinding in a ball mill on the length of multiwalled carbon nanotubes and their dispersion and percolation behaviour in melt mixed polycarbonate composites. *Composites Science and Technology* **2011**, *71* (8), 1145-1153.

11. McCreery, R. L., Advanced Carbon Electrode Materials for Molecular Electrochemistry. *Chemical Reviews* **2008**, *108* (7), 2646-2687.

12. Olivé-Monllau, R.; Baeza, M.; Bartrolí, J.; Céspedes, F., Novel Amperometric Sensor Based on Rigid Near-Percolation Composite. *Electroanalysis* **2009**, *21* (8), 931-938.

13. Carabineiro, S.; Pereira, M.; Nunes-Pereira, J.; Silva, J.; Caparros, C.; Sencadas, V.; Lanceros-Méndez, S., The effect of nanotube surface oxidation on the electrical properties of multiwall carbon nanotube/poly (vinylidene fluoride) composites. *Journal of Materials Science* **2012**, *47* (23), 8103-8111.

14. Bauhofer, W.; Kovacs, J. Z., A review and analysis of electrical percolation in carbon nanotube polymer composites. *Composites Science and Technology* **2009**, *69* (10), 1486-1498.

15. Jyotishkumar, P.; Logakis, E.; George, S. M.; Pionteck, J.; Häussler, L.; Haßler, R.; Pissis, P.; Thomas, S., Preparation and properties of multiwalled carbon nanotube/epoxy-amine composites. *Journal of Applied Polymer Science* **2013**, *127* (4), 3063-3073.

16. Castillo, F. Y.; Socher, R.; Krause, B.; Headrick, R.; Grady, B. P.; Prada-Silvy, R.; Pötschke, P., Electrical, mechanical, and glass transition behavior of polycarbonate-

based nanocomposites with different multi-walled carbon nanotubes. *Polymer* **2011**, *52* (17), 3835-3845.

17. Morcom, M.; Atkinson, K.; Simon, G. P., The effect of carbon nanotube properties on the degree of dispersion and reinforcement of high density polyethylene. *Polymer* **2010**, *51* (15), 3540-3550.

18. Song, W.; Windle, A. H., Isotropic-nematic phase transition of dispersions of multiwall carbon nanotubes. *Macromolecules* **2005**, *38* (14), 6181-6188.

19. Krause, B.; Boldt, R.; Pötschke, P., A method for determination of length distributions of multiwalled carbon nanotubes before and after melt processing. *Carbon* **2011**, *49* (4), 1243-1247.

20. McKee, G. S.; Vecchio, K. S., Thermogravimetric analysis of synthesis variation effects on CVD generated multiwalled carbon nanotubes. *The Journal of Physical Chemistry B* **2006**, *110* (3), 1179-1186.

21. Laoire, C. O.; Mukerjee, S.; Abraham, K.; Plichta, E. J.; Hendrickson, M. A., Elucidating the mechanism of oxygen reduction for lithium-air battery applications. *The Journal of Physical Chemistry C* **2009**, *113* (46), 20127-20134.

22. Montes, R.; Bartrolí, J.; Baeza, M.; Céspedes, F., Improvement of the detection limit for biosensors: Advances on the optimization of biocomposite composition. *Microchemical Journal* **2015**, *119*, 66-74.

23. Olivé-Monllau, R.; Esplandiú, M. J.; Bartrolí, J.; Baeza, M.; Céspedes, F., Strategies for the optimization of carbon nanotube/polymer ratio in composite materials: applications as voltammetric sensors. *Sensors and Actuators B: Chemical* **2010**, *146* (1), 353-360.

24. Bard, A. J.; Faulkner, L. R., *Electrochemical Methods: Fundamentals and Applications*. Wiley New York: 1980; Vol. 2.

25. Pumera, M.; Merkoçi, A.; Alegret, S., Carbon nanotube-epoxy composites for electrochemical sensing. *Sensors and Actuators B: Chemical* **2006**, *113* (2), 617-622.

26. Alvaro, M.; Aprile, C.; Ferrer, B.; Garcia, H., Functional molecules from single wall carbon nanotubes. Photoinduced solubility of short single wall carbon nanotube residues by covalent anchoring of 2, 4, 6-Triarylpyrylium units. *Journal of the American Chemical Society* **2007**, *129* (17), 5647-5655.

27. Ziegler, K. J.; Gu, Z.; Peng, H.; Flor, E. L.; Hauge, R. H.; Smalley, R. E., Controlled oxidative cutting of single-walled carbon nanotubes. *Journal of the American Chemical Society* **2005**, *127* (5), 1541-1547.

28. Palasantzas, G.; Backx, G. M. E. A., Roughness effects on the double-layer charge capacitance: the case of Helmholtz layer induced roughness attenuation. *Surface Science* **2003**, *540* (2–3), 401-406.

29. Wang, J., *Analytical Electrochemistry*. John Wiley & Sons: 2006.

30. Banks, C. E.; Davies, T. J.; Wildgoose, G. G.; Compton, R. G., Electrocatalysis at graphite and carbon nanotube modified electrodes: edge-plane sites and tube ends are the reactive sites. *Chemical Communications* **2005**, (7), 829-841.

31. Pumera, M.; Iwai, H., Metallic impurities within residual catalyst metallic nanoparticles are in some cases responsible for “electrocatalytic” effect of carbon nanotubes. *Chemistry–An Asian Journal* **2009**, *4* (4), 554-560.

32. Banks, C. E.; Crossley, A.; Salter, C.; Wilkins, S. J.; Compton, R. G., Carbon nanotubes contain metal impurities which are responsible for the “electrocatalysis” seen at some nanotube-modified electrodes. *Angewandte Chemie International Edition* **2006**, *45* (16), 2533-2537.

33. Muñoz, J.; Bastos-Arrieta, J.; Muñoz, M.; Muraviev, D.; Céspedes, F.; Baeza, M., Simple green routes for the customized preparation of sensitive carbon nanotubes/epoxy nanocomposite electrodes with functional metal nanoparticles. *RSC Advances* **2014**, *4* (84), 44517-44524.

34. Montes, R.; Bartrolí, J.; Céspedes, F.; Baeza, M., Towards to the improvement of the analytical response in voltammetric sensors based on rigid composites. *Journal of Electroanalytical Chemistry* **2014**, *733*, 69-76.

CHAPTER V

**Tunability of MWCNT/epoxy nanocomposite electrodes
with nanoparticles for sensing improvements**

CHAPTER V

Tunability of MWCNT/epoxy nanocomposite electrodes with nanoparticles for sensing improvements

Since their discovery in 1991, CNTs are extensively studied because of their potential applications in a large field of uses like emitter devices, nanoelectronics, chemical probes, energy storage and sensing. Their unique qualities make them extremely attractive for the development of MWCNT-based chemical (bio)sensors, in general, and electrochemical detection, in particular.^{1,2} Electrochemical (bio)sensors usually require chemical modifications (e.g. attachment of (bio)molecules, enzymes, NPs or catalysts) on the MWCNTs to improve the sensitivity and/or selectivity upon an specific analyte.^{3,4} However, the major drawback of CNTs is their low processability which may limit their applications. In spite of that, a well-known way to overcome this problem is (i) conjugation or addition of other materials to CNTs using different methods, which are mainly based on either the attachment of the different modifiers on the active sites of the sidewall and tips of CNTs or (ii) filling the cavity of CNTs using nanoscale materials.⁵ Both methods, however, require a previous surface activation with different functional groups (e.g. $-OH$, $-C=O$, $-COOH$), which can be easily grafted by acid oxidative treatments.⁶

Under this context, MWCNTs can be considered as feasible supports for different heterogeneous catalysts, including functional metal nanoparticles (FMNPs),⁷ metal oxide nanoparticles (MO-NPs)⁸ and quantum dots (QDs).⁹ Modified-MWCNTs electrodes combined with these NPs have shown excellent electrocatalytic activities due to the fast electron transfer ability of MWCNTs, which may include reductions in overpotentials, increments in the voltammetric peak heights that facilitate lower detection limits and enhanced sensitivities in analytical sensing coupled with little or no observed surface fouling.

In spite of these advantages, the surface modification of MWCNTs with the mentioned NPs usually involves thermal evaporation, electroless deposition or electrochemical deposition. Greener synthesis routes present aggregation of NPs on the walls of MWCNTs, limiting their application in electrochemical systems.^{10,11} Regarding this, the Intermatrix Synthesis (IMS) technique becomes a valid environmentally friendly nanoparticles preparation methodology thanks to the ion exchange properties of the support matrix (e.g. sulfonic resins, CNTs) for consecutive loading and reduction processes during their synthesis, providing an extra level of stability and a favourable distribution of these NPs on the final nanocomposite material.^{12,13}

A slightly modified version of this chapter has been published as journal articles. These publications are listed follow and are collected in Appendix A and B.

– *Simple green routes for the customized preparation of sensitive carbon nanotubes/epoxy nanocomposite electrodes with Functional Metal Nanoparticles.*

RSC Advances (2014), 4 (84), 44517–44524.

J. Muñoz, J. Bastos-Arrieta, M. Muñoz, D. Muraviev, F. Céspedes and M. Baeza.

– *Modified multiwall carbon nanotubes/epoxy nanocomposite sensors with CuO nanoparticles for electrocatalytic detection of free chlorine.*

Microchemical Journal (2015), 122, 189–196.

J. Muñoz, F. Céspedes and M. Baeza.

– *CdS-QDs as a scattering nanomaterial of carbon nanotubes in polymeric nanocomposite sensors for microelectrode array behaviour.*

Submitted at Journal of Materials Science (2015).

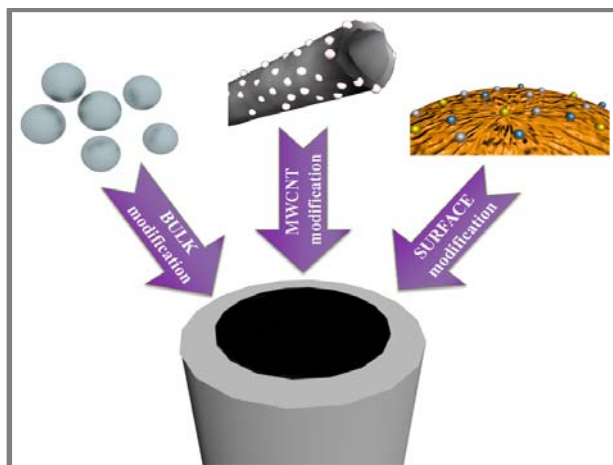
J. Muñoz, J. Bastos-Arrieta, M. Muñoz, D. Muraviev, F. Céspedes and M. Baeza.

5.1 Results and Discussion

Having been optimized the MWCNT/epoxy composition ratios regarding to the nature of the raw MWCNT samples, the next step consisted of enhancing the analytical performance of these electrochemical nanocomposite sensors introducing some electrocatalytical effect by the incorporation of different NPs. For this goal, a simple methodology for synthesizing a wide range of different NPs has been developed. IMS was used as a green technique to design three different routes for MWCNT/epoxy nanocomposite electrodes modification, which offer a customized way for the preparation of sensitive amperometric sensors. Accordingly, in this chapter is reported not only a novel, simple, effective and environmentally friendly methodology for the incorporation of different NPs, including Ag-, Au- and Pd-NPs, as well as CdS-QDs and CuO-NPs in MWCNT/epoxy nanocomposite electrodes but also their contribution to improve the electrochemical and electroanalytical skills on electrochemical sensors.

Microscopy tools verified the incorporation of NPs in/into/on the MWCNT/epoxy composite matrix. EDS and TGA analysis determined qualitatively and quantitatively the amount of NPs. Electrochemical techniques such as EIS, CV and LSV were carried out to characterize the electrochemical performance of the modified-electrodes regarding to the type of NPs incorporation. Analytical improvements of these modified-sensors have been demonstrated for different analytes in means of electrocatalytical effect, such as: (i) decreasing overpotentials (§ 5.1.1); (ii) scattering material, involving dispersion of the conducting microzones through the insulating polymer (§ 5.1.2) and (iii) enhancements on current height peaks (§ 5.1.3).

5.1.1 Customized preparation of modified-nanocomposite electrodes with Functional Metal Nanoparticles



Graphical Abstract III. Routes for nanocomposite electrodes functionalization with FMNPs.

In this section is reported novel, simple, effective and green methodologies for the incorporation of a wide range of different FMNPs in MWCNT/epoxy nanocomposite sensors in order to enhance their electroanalytical performance. Presented methodologies are based on the use of the IMS technique for the customized preparation of modified MWCNT/epoxy nanocomposite electrodes with different FMNPs by three different routes: (i) Route A: *in situ* functionalization of MWCNTs surface; (ii) Route B: incorporation and dispersion in bulk of FMNPs (in powder form) and (iii) Route C: electrode surface modification by drop-attachment (Graphical Abstract III). The electrocatalytic behaviour of these FMNPs on the analytical response of the modified-nanocomposite sensors was demonstrated for hydrogen peroxide detection, using as model working electrodes those modified with Au-NPs and Pd-NPs in a 3:2 ratios.

5.1.1.1 Physical characterization of FMNPs incorporated by Route A

Firstly, the feasibility of the IMS technique to incorporate a wide range of FMNPs on the MWCNTs walls (Route A) was studied, including Ag-, Au-, Cu-, Pd- and Pt-NPs. The new obtained nanomaterial is FMNPs@MWCNTs. From Figure 5.1 it is possible to observe a favourable distribution of these FMNPs on the MWCNTs surface. In addition to the distribution of the FMNPs, it was also observed a homogenous size distribution over MWCNTs surface and no FMNPs agglomeration was detected.

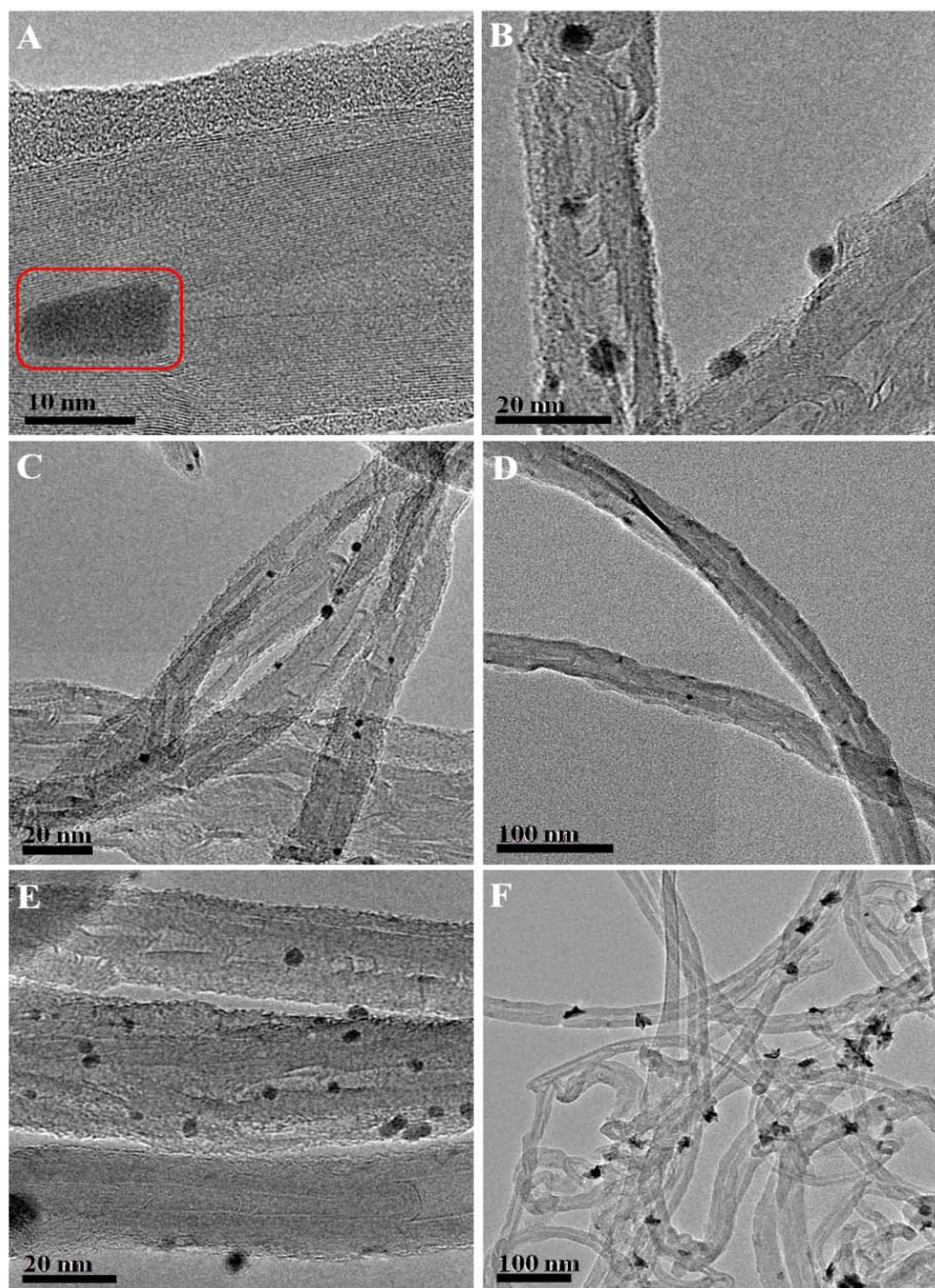


Figure 5.1 HR-TEM images of (A) raw MWCNTs, where metal catalyst impurity is highlighted, and different modified-MWCNTs containing (B) Ag-NPs, (C) Au-NPs, (D) Cu-NPS, (E) Pd-NPs and (F) Pt-NPs.

The quantification of the metal content in each FMNPs@MWCNTs sample was carried out by TGA analysis (see Table 5.1). The residue at the end of analysis corresponds to the total metal content. The amount of metal impurities of raw MWCNTs after acidic treatment was 2% in catalyst. When the different types of FMNPs@MWCNTs were analyzed, this 2% of catalyst remaining was subtracted in order to quantify the FMNPs content.

Table 5.1 Metal content of modified-MWCNTs with different NPs were obtained by TGA analysis.

FMNPs@ MWCNTs	TGA (% in FMNPs)
Raw MWCNTs	98% in C
Ag-NPs@MWCNTs	5.6
Au-NPs@MWCNTs	6.6
Cu-NPs@MWCNTs	7.0
Pd-NPs@MWCNTs	1.7
Pt-NPs@MWCNTs	8.5

It is important to emphasize that TGA provides only quantitative information on the presence of total metal content in CNT material. Under this context, EDS analysis is needed for the qualitative determination of the metal composition. EDS was a successful tool to differentiate the FMNPs attached on the MWCNTs walls from the catalyst remaining from the industrial synthesis of the raw MWCNTs. An example of EDS is shown in Figure 5.2 for Ag-NPs@MWCNTs.

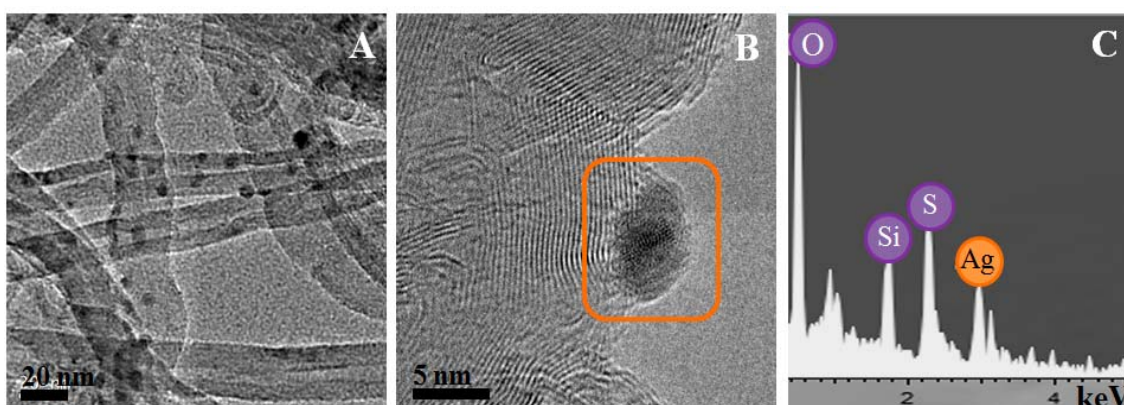


Figure 5.2 HR-TEM images of (A) Ag-NPs@MWCNTs, (B) Ag-NPs@MWCNTs amplification and (C) the corresponding EDS spectra from (B).

5.1.1.2 Impedimetric experiments of modified-electrodes by Route A

The effect of MWCNTs surface modification with different FMNPs on the electrochemical response of nanocomposite electrodes was studied by EIS and CV. Their results were also compared with the electrodes containing raw MWCNTs.

Impedimetric studies are depicted in Figure 5.3. Nyquist plots show an optimum kinetically controlled response for these electrodes based on FMNPs@MWCNTs/epoxy

nanocomposites. Different electrochemical values are presented in Table 5.2. From Table 5.2 it is possible to observe a general slight decrease of R_{Ω} for FMNPs@MWCNTs/epoxy nanocomposite electrodes respect to the ones non-modified (raw MWCNTs). This is because the ohmic resistance is more controlled by the solution resistance for nanocomposites containing a higher load of conductor material.¹⁴ However, MWCNTs/epoxy electrodes containing Pt–NPs presented an increase of R_{Ω} , which can be attributed to their morphology (see Figure 5.1).

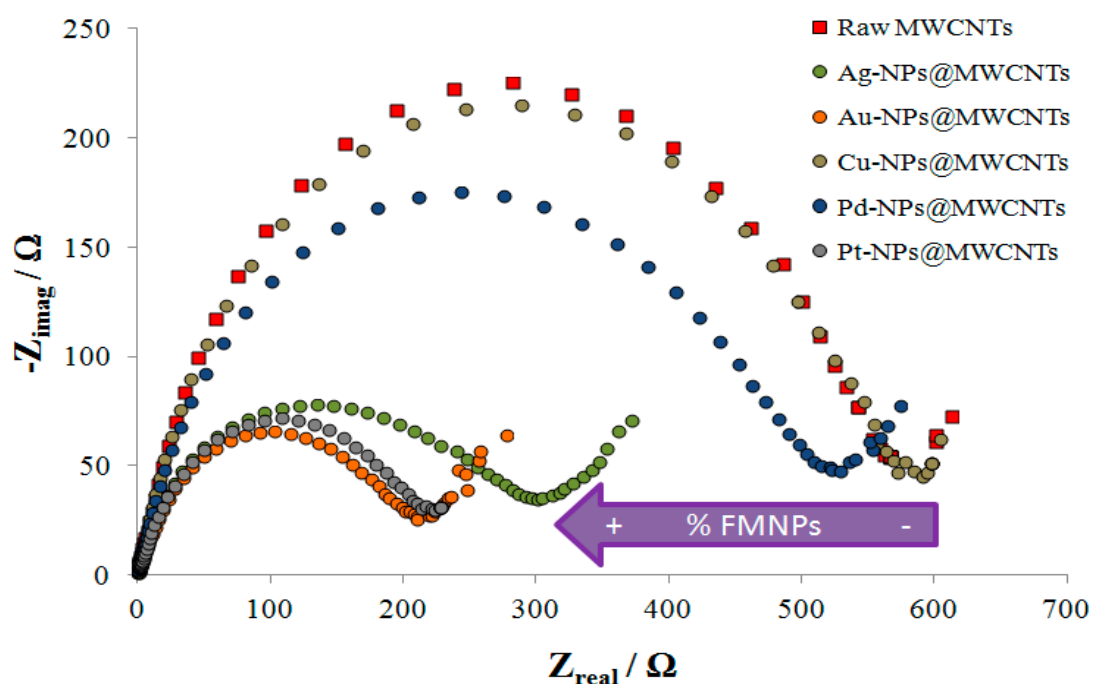


Figure 5.3 Nyquist plots of nanocomposite electrodes containing either raw MWCNTs or FMNPs@MWCNTs. Experiments were carried out in a 0.1 M solution containing 0.01 M $[\text{Fe}(\text{CN})_6]^{4-/3-}$.

Regarding R_{ct} , a decrease of this value with the amount of FMNPs incorporation on the MWCNTs surface was observed (see Table 5.2). As the conductor material load increases, the probability of having more electroactive sites increases, as well as the electrode kinetics. Accordingly, while electrodes containing Pt–NPs (8.5% by TGA) presented the highest decrease of R_{ct} (from 530.0 Ω to 173.7 Ω), those containing Pd–NPs (1.7% by TGA) showed the lowest decrease (from 530.0 Ω to 501.0 Ω). However, electrodes containing Cu–NPs presented higher R_{ct} values than the ones non-modified, which could be attributed to their rapid trend to oxidize.

Table 5.2 Characterization of modified-nanocomposites sensors containing different FMNPs@MWCNTs. Electrochemical parameters were extracted by EIS, using a 0.1 M KCl solution containing 0.01 M $[\text{Fe}(\text{CN})_6]^{3-/4-}$.

FMNPs@ MWCNTs	R_{Ω} (Ω)	R_{ct} (Ω)	C_{dl} (μF)
Raw MWCNTs	138.0	530.0	9.02
Ag-NPs@MWCNTs	113.5	464.0	6.34
Au-NPs@MWCNTs	131.2	173.3	7.95
Cu-NPs@MWCNTs	136.5	599.0	5.22
Pd-NPs@MWCNTs	111.3	501.0	7.11
Pt-NPs@MWCNTs	221.2	173.7	8.63

The fact that nanocomposite electrodes with low charge resistances (R_{Ω} and R_{ct}) are more appropriate to be used in electroanalytical measurements suggests that the use of nanocomposites containing FMNPs guarantees fast electron exchange. However, the enhanced kinetics is usually accompanied by an increase of the background current. As a consequence, it is important to consider the remaining impedance parameter represented by the double-layer capacitance, (C_{dl}) which is directly related to the charge or background current and, consequently with the achieved detection limit.

As was described in Chapter IV, C_{dl} parameter exhibited higher values for electrodes with high surface area of conducting material. However, when FMNPs are incorporated on MWCNTs surface, their electrocatalytic effect causes a significant decrease of the C_{dl} value, reducing the background current (see Table 5.2).

Thereby, impedance results demonstrated an improvement of the electrochemical parameters when MWCNTs/epoxy nanocomposite electrodes were functionalized with FMNPs, resulting in lower resistances (R_{Ω} and R_{ct}) and higher signal to noise ratio (C_{dl}). This functionalization improves properties that an electrode must have, such as rapid response time, low limit of detection and high sensitivity. This statement was demonstrated for the amperometric detection of hydrogen peroxide, using as a model working electrode a modified-MWCNTs/epoxy nanocomposite sensor containing Au-NPs@MWCNTs and Pd-NPs@MWCNTs in a 3:2 ratio. According to results obtained from Chapter IV, a 10% (w/w) of filler material was dispersed within the epoxy resin.

5.1.1.3 Electroanalytical evaluation of Au–/Pd–NPs modified-sensors by Route A

The electroanalytical study was focused on modified-nanocomposite sensors containing 10% of a mix of Au–NPs@MWCNTs and Pd–NPs@MWCNTs in a 3:2 ratio into the polymeric matrix. The electrocatalytic effect of these noble metals in the oxidation of hydrogen peroxide has already been studied.^{15,16}

Previously to amperometric studies, LSV was used to determine the optimum hydrogen peroxide oxidation potential based on the working electrodes used (Au–/Pd–NPs@MWCNTs/epoxy and raw MWCNTs/epoxy nanocomposite electrodes). The linear voltammograms show the characteristics shoulders of the oxidation curve of hydrogen peroxide (see Figure 5.4).

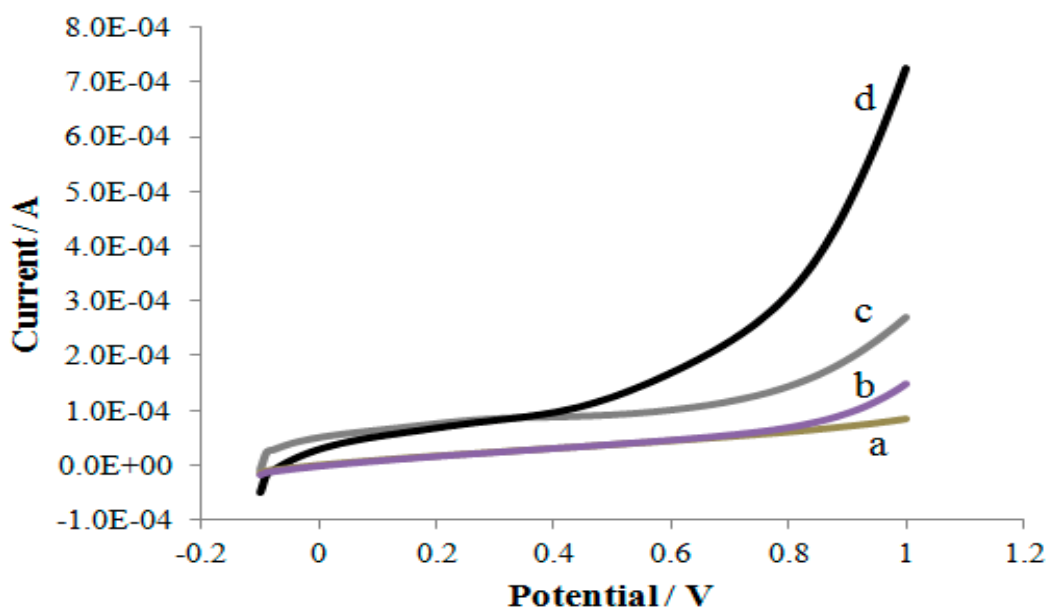


Figure 5.4 LSV of nanocomposite electrodes containing either raw MWCNTs (a to b) or Au–/Pd–NPs@MWCNTs (c to d) in the absence (a and c) and in the presence (b and d) of $2 \text{ mg}\cdot\text{L}^{-1}$ of H_2O_2 at pH 7.0.

Different concentrations of hydrogen peroxide ranged from $0 - 2 \text{ mg}\cdot\text{L}^{-1}$ were added in 10.0 mL of PBS at pH 7.0. LSV characterization also demonstrated a significant electrocatalytic effect of these FMNPs on the nanocomposite electrodes, showing a reduction in the oxidation potential of the system, being 900 mV for the non-modified electrode and 700 mV for the modified-electrode with Au–NPs and Pd–NPs. The polarization potential was used to evaluate the electroanalytical response of hydrogen peroxide in the same experimental conditions.

The electroanalytical response of these modified-sensors has also been compared with the one of sensors bases on non-modified MWCNTs with FMNPs. Both LOD and LOQ were obtained by hydrodynamic amperometry, see Table 5.3. If sensors containing raw MWCNTs demonstrated electrochemical response for the oxidation of hydrogen peroxide, a substantially enhanced after incorporation of Au–NPs and Pd–NPs into the composite material was observed, mainly due to the significant improvement of the C_{dl} (from 9.02 to 6.50 μF , corresponding to a decrease around 30%). This enhancement was traduced on a LOD of $0.027 \text{ mg}\cdot\text{L}^{-1}$, a decade of concentration less in comparison to the sensor containing raw MWCNTs.

Table 5.3 Impedimetric and amperometric comparative of the three modified-nanocomposite electrodes with Au–NPs and Pd–NPs are presented. EIS experiments were recorded in a 0.1 M KCl solution containing 0.01 M $[\text{Fe}(\text{CN})_6]^{3-/4-}$. Amperometric experiments were carried out in a PBS buffer pH 7.0 solution. Analytical parameters are shown with their respectively 95% confident interval (n=3).

Electrode resulting	R_{Ω} (Ω)	R_{ct} (Ω)	C_{dl} (μF)	LOD ($\text{mg}\cdot\text{L}^{-1}$)	LOQ ($\text{mg}\cdot\text{L}^{-1}$)	Sensitivity ($\mu\text{A}\cdot\text{L}\cdot\text{mg}^{-1}$)
Raw	138.0	530.0	9.02	0.095 ± 0.002	0.190 ± 0.002	0.0151 ± 0.0003
Route A	137.9	246.6	6.50	0.027 ± 0.001	0.068 ± 0.001	0.066 ± 0.001
Route B	116.4	462.3	6.32	0.027 ± 0.002	0.041 ± 0.001	0.037 ± 0.002
Route C	269.1	1303.0	3.28	0.014 ± 0.001	0.027 ± 0.002	0.031 ± 0.002

According with the good results obtained by Route A, the next step consisted in extended the IMS technique to modify MWCNT/epoxy nanocomposite electrodes with FMNPs. For this aim, two additional routes (Route B and Route C) were developed with the finality to demonstrate which is the most suitable way to modify MWCNT–based nanocomposite electrodes with FMNPs. These results are presented below (see § 5.1.1.4).

5.1.1.4 Alternative routes for electrodes modification: A comparative electrochemical and electroanalytical study

The methodology to integrate these FMNPs (concretely Au–NPs and Pd–NPs) as part of the transducer material has been focus of study. Accordingly, two additional forms to incorporate Au–NPs and Pd–NPs were tested in order to optimize the electrochemical

and thus, the final electroanalytical response of modified-(MWCNTs/epoxy) nanocomposite electrodes for amperometrically sensing the hydrogen peroxide.

Table 5.3 also shows the comparative electrochemical and electroanalytical studies of the modified-electrodes regarding to the three different routes of FMNPs incorporation: (i) *In situ* functionalization of MWCNTs surface, RA, (ii) Dispersion and incorporation within the polymeric matrix (in bulk) of powder FMNPs, RB and (iii) Electrode surface modification by drop-attachment, RC. As it can be observed, modified-electrodes by RA (RA-electrodes) presented a significant increase of the electroanalytical values obtained by EIS and hydrodynamic amperometry in comparison with the non-modified electrodes. For modified-electrodes by RB (RB-electrodes), the FMNPs were incorporated in bulk as powder form in the same proportion that TGA analysis determined for RA (see Table 5.1). EIS parameters showed to be similar for both routes, providing the same LOD. Furthermore, RB-electrodes presented also a lower LOQ than RA-electrodes. Whereas in RA the FMNPs are incorporated on the surface of the transducer material, and hence their incorporation is limited by the presence of carboxylic groups on the MWCNTs surface, the advantage of RB is the tunability of functionalization.

In addition, both routes were compared with the ones obtained by RC (RC-electrodes). The main disadvantage of this last route is that the sensor surface is not renewable. Thus, the FMNPs must be reincorporated when the electrode is polished; thereby, these electrodes presented a non homogeneous and reproducible modified-surface (see Figure 5.5). In spite of those operational inconvenient, the best LOD and LOQ were obtained for RC-electrodes.

Finally, CV was used as a complementary tool to extract further information about the electrochemical performance of the four different nanocomposite electrodes studied in this work (electrodes containing raw MWCNTs and RA-electrodes, RB-electrodes and RC-electrodes).

Figure 5.6 shows their typical cyclic voltammograms, which were recorded in a 0.01 M $[\text{Fe}(\text{CN})_6]^{3-/4-}$ solution containing 1.0 M KCl at a scan rate of 10 $\text{mV}\cdot\text{s}^{-1}$. Different parameters such as peak separation potential ΔE and peak height I_p have been extracted from the cyclic voltammograms following the Randles-Sevcik equation.

According to these results, electrodes modified with Au-NPs and Pd-NPs by the three different routes presented an enhancement of I_p independently of the route of FMNPs incorporation.

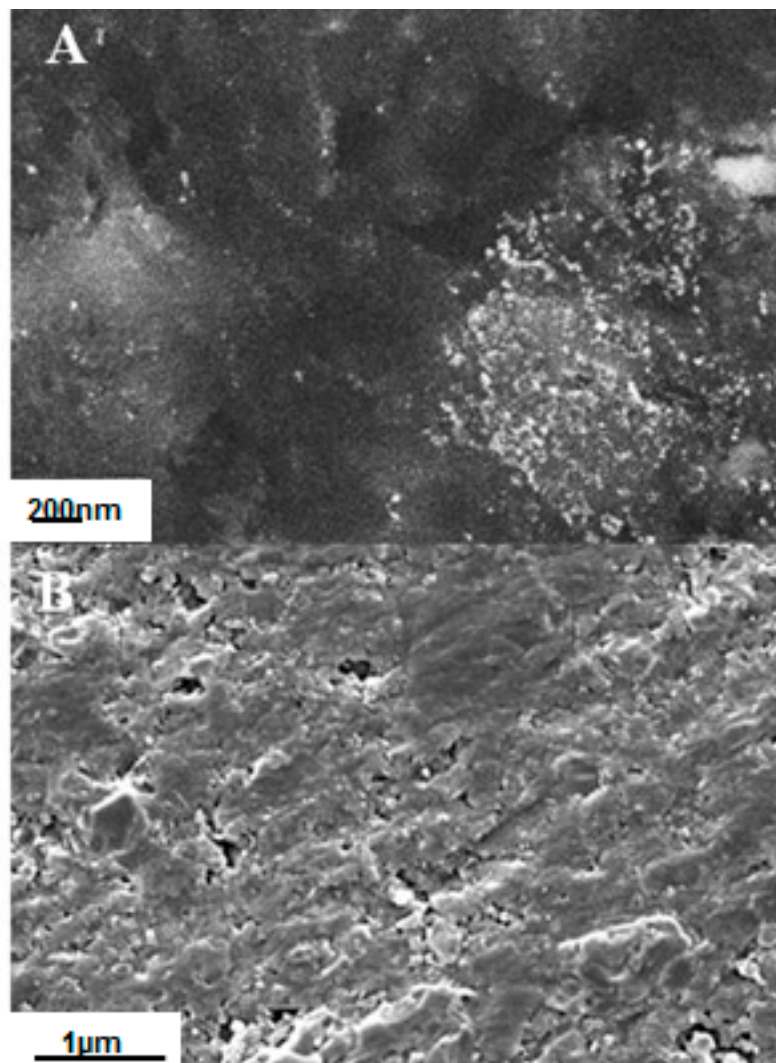


Figure 5.5 SEM images obtained for A) modified-nanocomposite electrode modified by RC (RC-electrode) and B) raw MWCNT/epoxy nanocomposite electrode.

The maximum increase of I_p , which was around 75%, was observed for the nanocomposite electrodes modified by RA; RB-electrodes showed a similar behaviour, since both electrodes contains the same amount of FMNPs. Nevertheless, electrodes prepared by RC presented the minimum increase of I_p , which may be associated due to the lower amount of FMNPs (only on the electrode surface). Therefore, I_p increases with FMNPs load, which leads to an increase of the electroactive area.

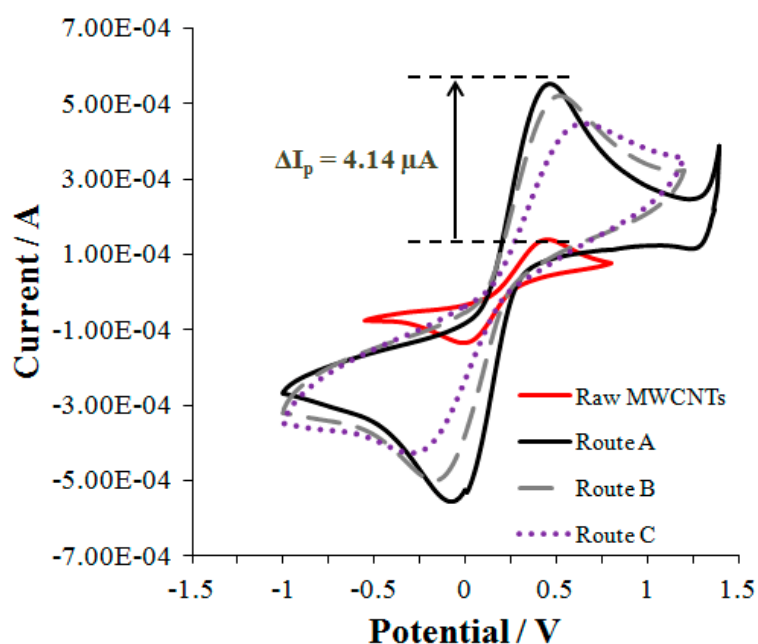
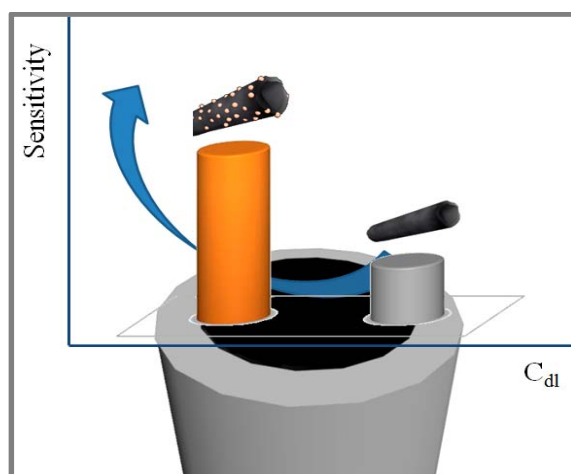


Figure 5.6 Cyclic voltammograms of the four types of nanocomposite electrodes studied. CV experiments were recorded in a 0.1 M KCl solution containing 0.01 M $[\text{Fe}(\text{CN})_6]^{3-/4-}$ at a scan rate of 10 $\text{mV}\cdot\text{s}^{-1}$.

Simultaneously, a comparison of the ΔE was also evaluated for all electrodes (see Figure 5.6). While RA-electrodes presented a non significant increase of ΔE (from 0.48 V to 0.51 V), which can be explained by the total contain of conducting nanomaterial into the epoxy matrix is the same (10% of Au-/Pd-NPs@MWCNTs regarding to 10% raw MWCNTs into the nanocomposite material), RB-electrodes showed a higher increase of ΔE (from 0.48V to 0.63 V). Finally, RC-electrodes exhibited the highest ΔE increase, until 0.94 V because of the previously activation of the electrode surface with carboxylic groups under acidic conditions for FMNPs incorporation, providing a significant steric hindrance on its surface.

5.1.2 CdS quantum dots as a scattering nanomaterial in MWCNT-based nanocomposite sensors for microelectrode array behaviour



Graphical Abstract IV. Electroanalytical improvements after CdS-QDs incorporation.

The goal of this work is focused on evaluating the direct electrochemical effect of semiconducting nanocrystals, as CdS-QDs, on the electroanalytical response of MWCNT-based amperometric nanocomposite electrodes (Graphical Abstract IV). Since these CdS-QDs modified-electrodes presented favourable improvements in different physical parameters, such as peak current height, electroactive area, limit of detection, sensitivity and emphasizing the double-layer capacitance value compared to the non-modified sensors. Different topographic, morphological and electrical characterizations were carried out to determine the contribution of these semiconducting nanocrystals in the nanocomposite properties. According to the results, a scattering effect of the CdS-QDs on the MWCNTs contained in epoxy nanocomposite electrodes was observed, conferring them a microelectrode array behaviour. This performance, which is directly related to the electrochemical and electroanalytical enhancement, provides to the CdS-QDs modified-sensor the capability to determine low concentrations of analytes.

5.1.2.1 Physical characterization of CdS-QDs nanocrystals

IMS technique provided a favourable distribution of CdS-QDs on the MWCNTs surface, as shown in the HR-(S)TEM images, Figure 5.7. Moreover, CdS-QDs are well separated from each other and do not form any visible agglomerates.

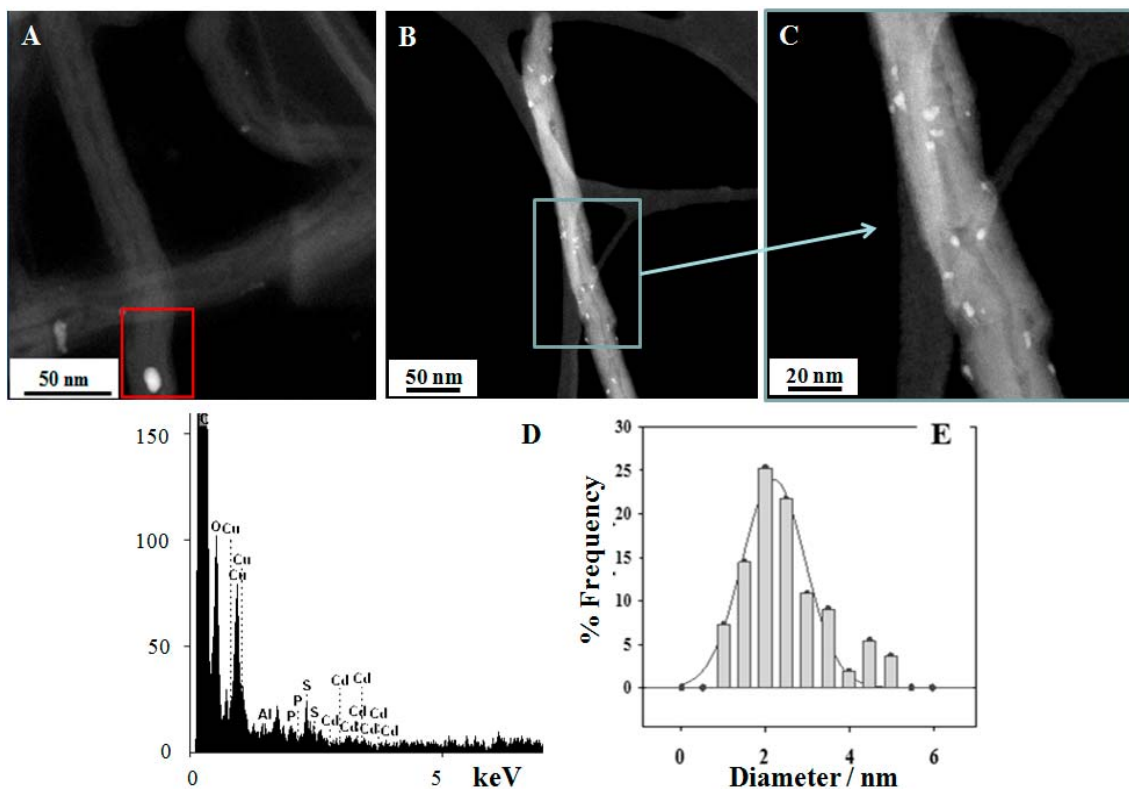


Figure 5.7 A) HR-(S)TEM of raw MWCNTs (inset shows a catalyst metal particle); B) HR-(S)TEM of CdS-QDs@MWCNTs; C) amplification of B) and D) its corresponding EDS spectrum. Finally, E) shows size distribution histogram for CdS-QDs on MWCNTs.

The identification and quantification of the metal content in each case was accomplished by EDS spectra (Figure 5.7 D) and TGA analysis, respectively, differentiating the QDs from the catalyst metal remaining from the industrial synthesis of the raw MWCNTs. While TGA analysis of raw MWCNTs showed a metal impurity content of 2.0%, TGA analysis of CdS-QDs@MWCNTs determined that IMS technique provides 11.0% of CdS-QDs content.

As TGA provides only quantitative information on the presence of total metal content in CNT material, EDS analysis is needed for the qualitative determination of the metal composition. EDS spectra determined that the raw MWCNTs contain different metals as catalyst particles, mainly Fe and Ni. These catalysts are located into the walls of the MWCNTs. The QDs nanocrystals were differentiated from the catalyst particles by the EDS analysis of CdS-QDs@MWCNTs. After a study of more than 200 nanoparticles, the average diameter of CdS-QDs nanocrystals obtained was 2.3 ± 0.4 nm, as is shown in Figure 5.7 E.

According to the characterization of CdS–QDs, the fact that these semi-conducting nanocrystals were well distributed over the surface of the MWCNTs led to the idea of studying the electrochemical characteristics of this nanomaterial as a component of electrochemical sensors, concretely as amperometric CdS–QDs@MWCNTs/epoxy nanocomposite sensors. Hydrogen peroxide and ascorbic acid were chosen as the model analytes for this aim.

In order to probe the electrochemical behaviour of the CdS–QDs@MWCNTs/epoxy nanocomposite electrodes, different electrochemical techniques, such as CV and EIS were carried out in a 0.01 M $[\text{Fe}(\text{CN})_6]^{3-/4-}$ solution containing 0.1 M KCl. The results will be discussed below.

5.1.2.2 Voltammetric experiments

CV studies were performed for the CdS–QDs@MWCNTs/epoxy nanocomposite electrodes. The obtained results were also compared to the non-modified electrodes (MWCNTs/epoxy nanocomposite electrodes) in order to observe if these semi-conducting nanocrystals cause some effect on the electrochemical response of the final nanocomposite electrodes. Based on the previous results shown in § 4.1.1, the content of filler materials (raw MWCNTs and CdS–QDs@MWCNTs) in this polymeric matrix was fixed to 10%.¹⁷ Figure 5.8 shows the typical cyclic voltammograms of the two different electrodes studied. Different parameters such as I_p , ΔE and A have been extracted from the cyclic voltammograms, which are reported in Table 5.4. The electroactive area was estimated from the peak-shaped voltammograms by using the equation for electron transfer-controlled processes.¹⁸

Table 5.4 CV characterization of the two nanocomposite electrodes studied. The redox probe $[\text{Fe}(\text{CN})_6]^{3/4-}$ contained in a 0.1 M KCl solution was used for CV (scan rate 10 $\text{mV}\cdot\text{s}^{-1}$) experiments.

Electrode Containing	I_p (mA)	A (cm^2)	ΔE (V)
Raw MWCNTs	0.139	0.25	0.48
CdS-QDs@MWCNTs	0.509	0.84	0.62

In agreement with CV results, CdS–QDs@MWCNTs/epoxy nanocomposite electrodes exhibited an enhancement of I_p , which was around 73%, indicating that the CdS–QDs well enhanced the surface area of the modified-nanocomposite electrodes as well as the electroactivity and, consequently, their conductivity. Thereby, the incorporation of CdS–QDs on the MWCNT surface increased the electroactive area (A) of the electrode from 0.25 cm² to 0.84 cm². From Figure 5.8 it is also possible to observe a change in ΔE from 0.48 V to 0.62 V for the CdS–QDs modified-electrodes, which can be explained by the incorporation of semi-conducting nanocrystals in the nanocomposite matrix.

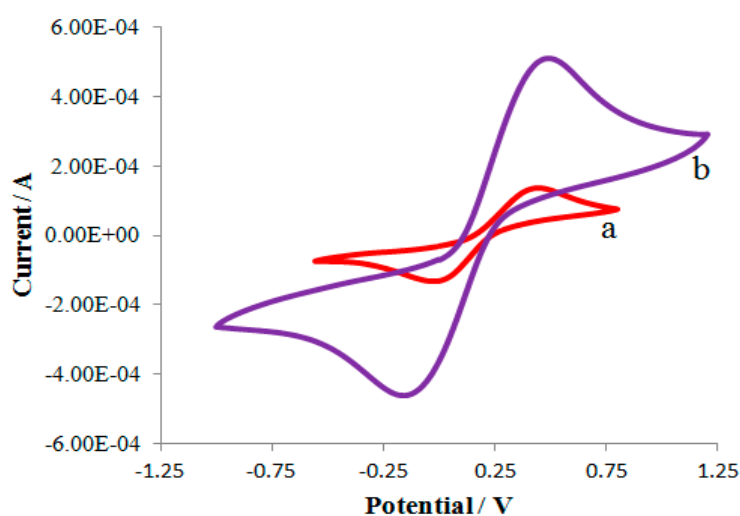


Figure 5.8 CV recorded in a 0.1 M KCl solution containing 0.01 M $[\text{Fe}(\text{CN})_6]^{3-/4-}$ for (a) raw MWCNTs/epoxy and (b) CdS–QDs@MWCNTs nanocomposite electrodes. Scan rate: 10 mV·s⁻¹.

Finally, CV was also used to verify if there is any release of CdS–QDs from MWCNTs to the media during the use of CdS–QDs@MWCNTs/epoxy nanocomposite electrodes. For this aim, different consecutive voltammograms were carried out, as is shown in Figure 5.9 A.

Four voltammograms were performed in 0.1 M KCl media, the first one without presence of Fe^{2+} and the following with increasing Fe^{2+} concentration. None peak was observed when the voltammogram was recorded without presence of Fe^{2+} , indicating that any redox reaction providing by the CdS–QDs took place. These results demonstrated the stability of the CdS–QDs on the MWCNT surface and consequently in the nanocomposite electrode.

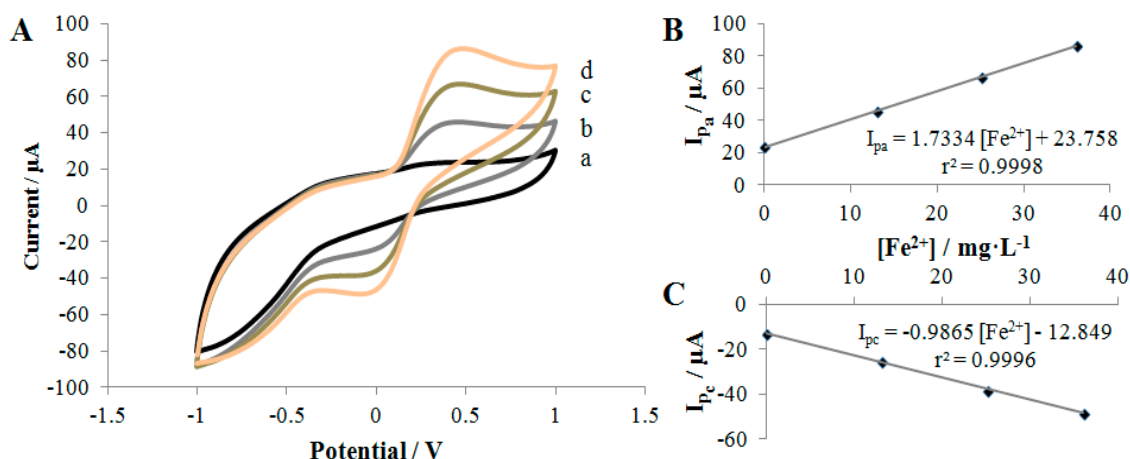


Figure 5.9 A) Cyclic voltammogram of CdS–QDs@MWCNTs/epoxy nanocomposite electrodes in (a) absence and in (b) presence of 13 ppm, (c) 25 ppm and (d) 37 ppm of $[\text{Fe}^{2+}]$. Linear relationship between B) I_{p_a} vs. $[\text{Fe}^{2+}]$ and C) I_{p_c} vs. $[\text{Fe}^{2+}]$. CV was recorded at $50 \text{ mV}\cdot\text{s}^{-1}$ in a 0.1 M KCl solution.

Then, the feasibility of this electrode in terms of electrochemical response and system reversibility was studied in front of different $[\text{Fe}^{2+}]$, as is also shown in Figure 5.9 A. The corresponding calibration curves for I_p (anodic and cathodic) vs. $[\text{Fe}^{2+}]$ depicted in Figures 5.9 B–C showed a linear and good correlation coefficient. This fact demonstrated that the presented electrodes are suitable to be used for electroanalytical purposes.

5.1.2.3 Impedimetric experiments

R_{Ω} , R_{ct} and C_{dl} were evaluated for the two nanocomposite electrodes studied in this section (see Table 5.5) These parameters were obtained by fitting the impedance spectra to a simple equivalent circuit: $R_{\Omega}\cdot(R_{ct}\cdot C_{dl})$.

Nyquists plots presented in Figure 5.10 shows, on the one hand, an optimum kinetically controlled response for both nanocomposite electrodes, demonstrating a fast electron exchange. However, as was expected, an increase of R_{ct} with the incorporation of CdS–QDs on the MWCNTs surface was observed (from 530Ω to 858.5Ω) because of the incorporation of semi-conducting nanocrystals in the nanocomposite, confirming again the modification of the nanocomposite electrode. On the other hand, R_{Ω} values kept constant during the measurements (around 140 ohms) for both nanocomposite electrodes.

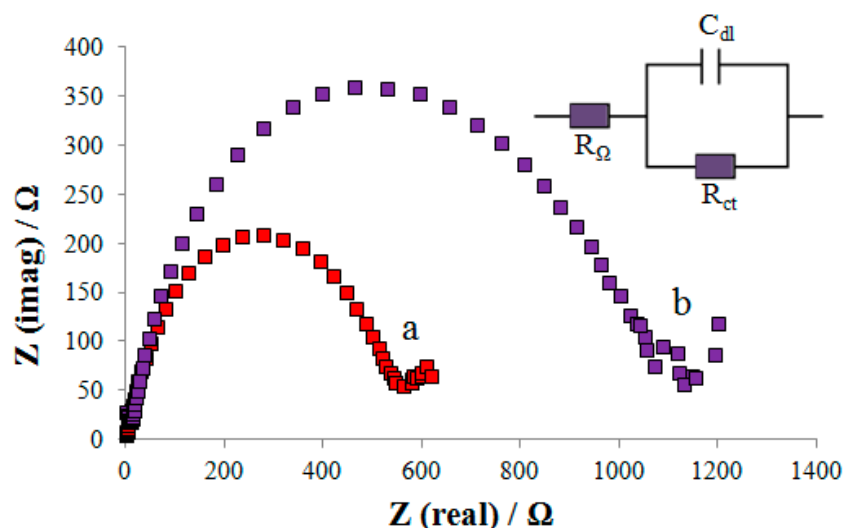


Figure 5.10 Nyquist plots for (a) raw MWCNTs/epoxy and (b) CdS-QDs@MWCNTs nanocomposite electrodes. Impedance spectra was carried out in a 0.1 M KCl solution containing 0.01 M $[\text{Fe}(\text{CN})_6]^{3-/4-}$. The inset shows the equivalent circuit used for the impedance spectra fitting.

Regarding C_{dl} value, an evident decrease of the C_{dl} value was observed for the CdS-QDs@MWCNTs/epoxy nanocomposite electrodes (from 9.02 μF to 1.55 μF), which corresponded to a decrease around 80%. This important decrease of C_{dl} value makes the signal to noise ratio increase and consequently, it is expected an improvement in the detection limits.

Table 5.5 Electrochemical impedance spectroscopy characterization of the two nanocomposite electrodes studied. The redox probe $[\text{Fe}(\text{CN})_6]^{3-/4-}$ in a 0.1 M KCl solution was used.

Electrode Containing	R_{Ω} (Ω)	R_{ct} (Ω)	C_{dl} (μF)
Raw MWCNTs	138.0	530.0	9.02
CdS-QDs@MWCNTs	141.9	858.5	1.55

Based on EIS results, an improvement of the electrochemical values was obtained for the modified-electrodes with CdS-QDs. The electrochemical enhancement of the CdS-QDs@MWCNTs/epoxy nanocomposite electrodes showed by CV and EIS seemed to provide the properties that a sensor must have, such as rapid response time, low limit of detection and high sensitivity. To assess these properties, the electroanalytical performance of these modified-sensors has been evaluated by hydrodynamic amperometry for the detection of hydrogen peroxide and ascorbic acid.

5.1.2.4 Morphological studies

CSAFM and CM3D techniques were carried out in order to understand the electrochemical results obtained for the nanocomposite electrodes containing CdS–QDs@MWCNTs.

CSAFM technique was used to obtain qualitative information about the size, shape and distribution of the conducting material in the modified-nanocomposite structure. Figure 5.11 presents significant images obtained during the electrode surface study. Based on these results, it was determined that the presence of CdS–QDs in the nanocomposite increased the distance between the conductive channels, in spite of containing the same load of conducting material. However, the raw MWCNTs/epoxy nanocomposite material showed closer conductive channels.

CSAFM results allowed the observation of different surface features. While the raw MWCNTs/epoxy nanocomposite material had the filler particles more proximal one with other, the surface of the modified-electrodes with CdS–QDs showed an extra separation between the conductive microzones where the transfer is produced. Whereas for electrodes with less separation particles presents a behaviour more proximal to a macroelectrode where principally the linear diffusion is contemplated, for electrodes with a microelectrode array behaviour the radial diffusion is usually given. Therefore, the greater distance between conducting fillers leads to a significant radial diffusion increase. This fact also provides an increase of the mass transfer, which favours positively the electroanalytical signal because C_{dl} decreases and consequently the limit of detection improves.¹⁹

Furthermore, the separation of the conductive zones observed on the modified-electrodes with CdS–QDs caused, on the one hand, a R_{ct} enhancement and, on the other, a decrease in the background current, resulting from a decrease of the C_{dl} , as reported in Table 5.5. The improvement of the C_{dl} must provide a diminution on the LOD, fact that will be demonstrated in the electroanalytical studies.²⁰

In addition, roughness surfaces of CdS–QDs@MWCNT/epoxy nanocomposite electrodes and raw MWCNTs/epoxy nanocomposite electrodes were also compared by CM3D, see Figure 5.12.

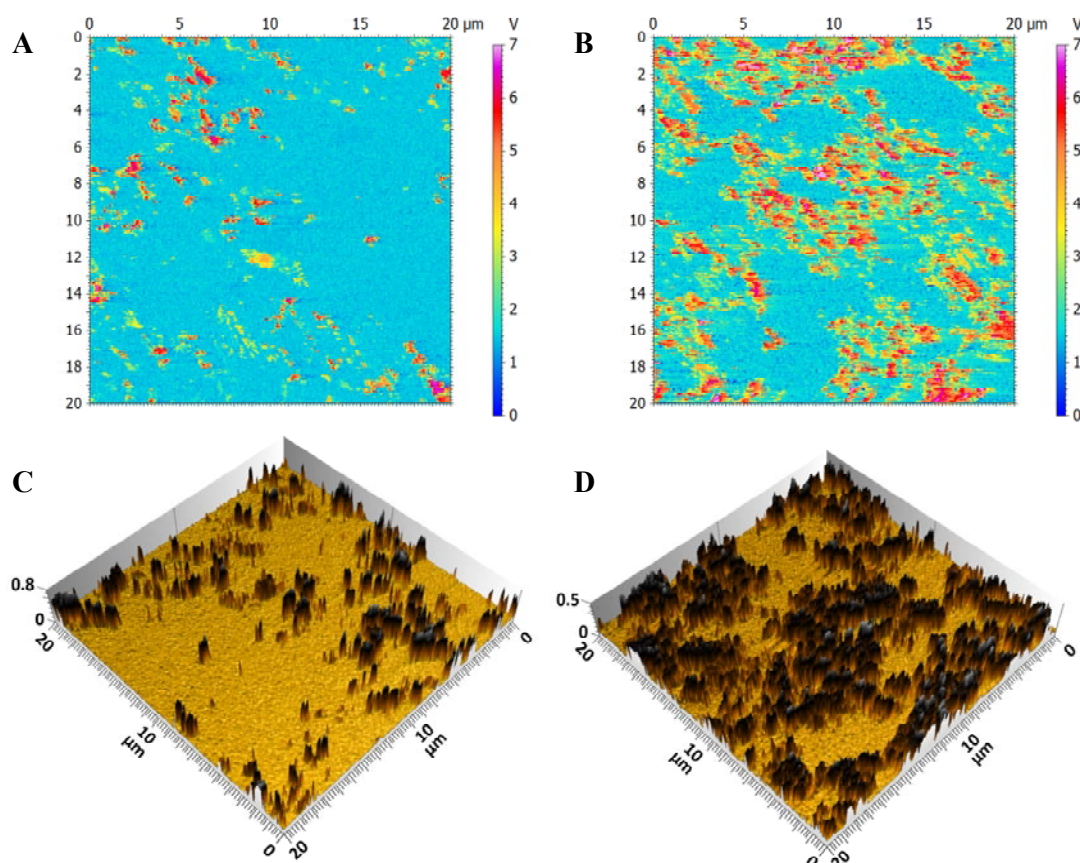


Figure 5.11 Topographical CSAFM images with their corresponding conductance mapping for nanocomposite electrodes containing A) CdS-QDs@MWCNTs and B) raw MWCNTs. C) and D) correspond to 3D conductance image from A) and B), respectively.

Figure 5.12 presents significant images obtained during the electrode surface study. According to confocal microscopy results shown in Table 5.6, the incorporation of these semi-conducting nanocrystals on the conductor material significantly modified the roughness of the MWCNT-based epoxy nanocomposites, resulting in an increment of around 75% compared with the surface of the one non-modified, fact that could explain the electroactive area enhancement, which was also around 70% (see Table 5.4). If the electrode roughness increases, the probability of more conductive material exposed on the electrode surface also increases, and hence its electroactive area.

Based on topographic results, CSAFM and CM3D results corroborated that the electrochemical enhancement of the CdS-QDs nanocomposite electrodes is mainly based on the dispersion of the conductive microzones, conferring a microelectrode array behaviour more emphasized than that observed from the non-modified electrodes.

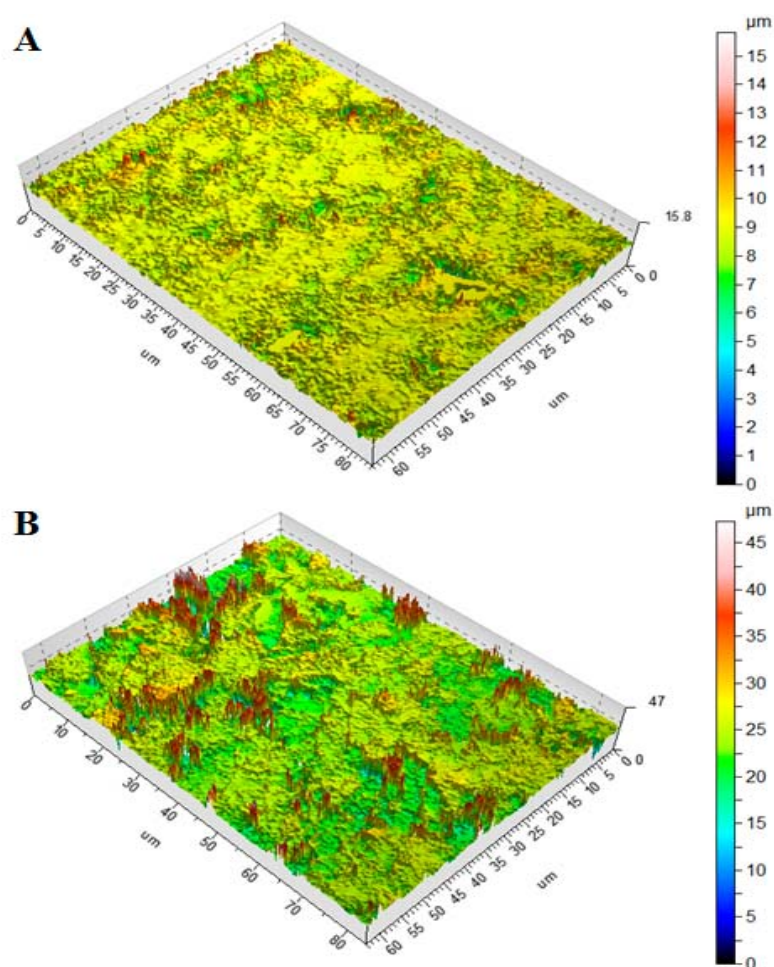


Figure 5.12 Topographic images of nanocomposite electrodes containing A) raw MWCNTs and B) CdS-QDs@MWCNTs were obtained with the 3D Optical Surface Metrology System Leica CM3D for the roughness study.

Table 5.6 Roughness values collected from surface analysis. Data are the mean and standard deviation (SD) from 57 profiles of three areas examined in each series (ISO 4287).

Electrodes Containing	R_a^a (μm)		R_q^b (μm)		R_z^c (μm)	
	Mean	SD	Mean	SD	Mean	SD
Raw MWCNTs	0.555	0.129	0.920	0.271	7.31	2.60
CdS-QDs@MWCNTs	2.24	0.55	3.34	0.97	21.82	6.70

^aArithmetical mean deviation of the assessed profile

^bThe root mean square deviation of the assessed profile

^cMaximum height of the profile

Finally, the potentiality of this approach in terms of electroanalytical response has been evaluated by means of amperometric detection of ascorbic acid and hydrogen peroxide, both used as reference analytes.

5.1.2.5 Polarization potential determination

Previously to amperometric performance, the polarization potentials based on the working sensor used were obtained by LSV, as presented in Figure 5.13. The polarization potentials obtained were 900 mV for hydrogen peroxide detection and 600 mV for ascorbic acid detection.

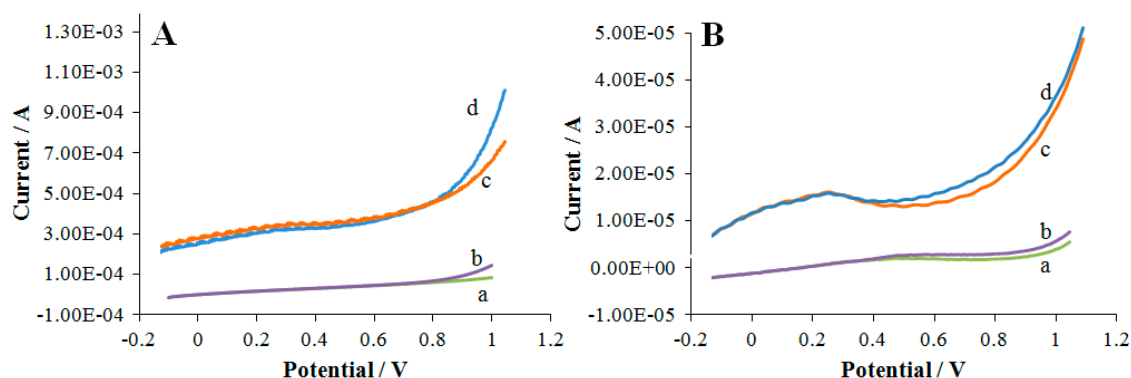


Figure 5.13 LSV of sensors containing raw MWCNTs (a-b) and CdS-QDs@MWCNTs (c-d). LSV corresponding to absence (a and c) and in presence (b and d) of analytes. LSV carried out under A) 30 μM of hydrogen peroxide in a PBS solution at pH 7.0 and B) 11 μM of ascorbic acid in a 0.01 M $\text{KNO}_3/\text{HNO}_3$ solution. Scan rate: $10 \text{ mV}\cdot\text{s}^{-1}$.

According to LSV results, no significant differences on the polarization potential peaks were observed between non-modified and CdS-QDs modified-sensors. Accordingly, variations in overpotentials could not be shown from LSV experiments.

5.1.2.6 Electroanalytical performance

The feasibility of these modified-sensors in terms of analytical response has been evaluated for the oxidation of hydrogen peroxide and ascorbic acid, both used as reference analytes. If the raw sensors demonstrated a suitable electroanalytical response for the oxidation of both analytes, the modified-sensors with CdS-QDs exhibited a clear enhanced of its response, as is depicted in Figure 5.14. In addition, this enhanced of sensitivity was translated into an important LOD decrease (see Table 5.7).

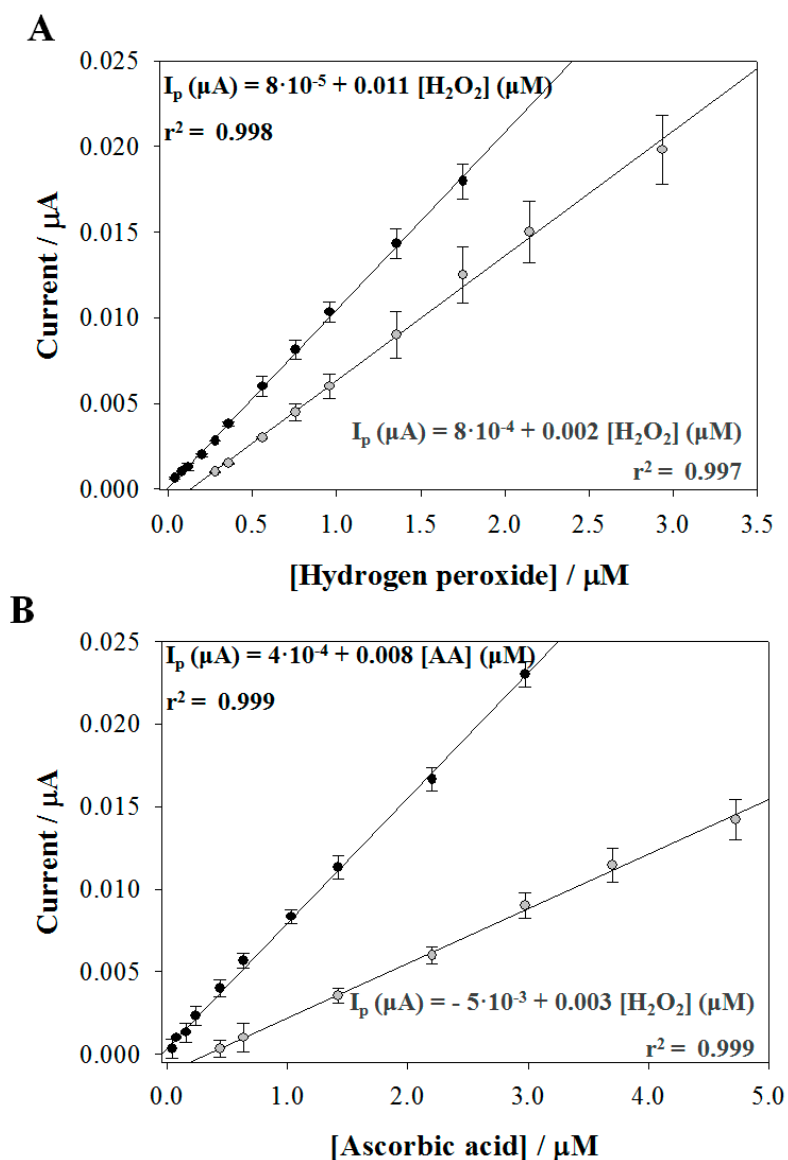


Figure 5.14 Calibration curves of I_p vs. concentration of A) hydrogen peroxide in a PBS solution at pH 7.0 and B) ascorbic acid in a 0.01 M $\text{KNO}_3/\text{HNO}_3$ solution for (●) CdS-QDs@MWCNTs/epoxy and (○) raw MWCNTs/epoxy sensors, which are represented with their corresponding error bars ($n=3$).

For hydrogen peroxide detection, the LOD obtained with the CdS-QDs modified-sensors is $0.040 \pm 0.002 \mu\text{M}$, more than 1.4 decades of concentration less than the non-modified sensors, whose LOD was $2.80 \pm 0.06 \mu\text{M}$. LOQ improved as well, obtaining $0.200 \pm 0.003 \mu\text{M}$ compared to $5.59 \pm 0.06 \mu\text{M}$ obtained for raw MWCNTs/epoxy nanocomposite sensors, being more than 1.5 decades of concentration better. In regard to ascorbic acid detection, the LOD and LOQ obtained for the CdS-QDs@MWCNTs modified-sensors were $0.067 \pm 0.004 \mu\text{M}$ and $0.159 \pm 0.001 \mu\text{M}$, respectively. Comparing these values with the ones obtained by the non-modified sensors (see Table 5.7), the presence of CdS-QDs improved around 2 orders of magnitude the LOD and 1

order of magnitude the LOQ. In addition, a significant enhancement of sensitivity for the CdS–QDs modified-sensors was also observed (see Table 5.7).

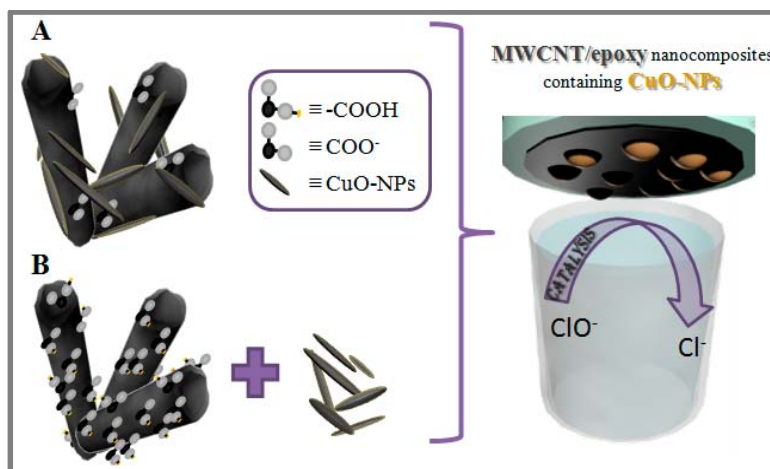
In agreement with the results expected from electrochemical and morphological characterizations, the electroanalytical enhancement of sensors containing CdS–QDs is mainly attributed to the improved dispersion of the conductive microzones through the insulating polymeric matrix, which decreases the C_{dl} value. This value is directly related to the decrease of the background current and hence, improves the signal-to-noise ratio and LODs. Accordingly, the simply incorporation of CdS–QDs in the MWCNT–based bulky system makes possible to obtain advanced electrochemical nanocomposite sensors with a behaviour more similar to a microelectrode array than those non-modified.

Table 5.7 Electroanalytical comparison between CdS-QDs@MWCNTs/epoxy and MWCNT/epoxy nanocomposite sensors. LOD and LOQ which their respectively 95% confidence interval (n=3) were obtained by hydrodynamic amperometry for: hydrogen peroxide analyte in PBS at pH 7.0 and ascorbic acid analyte in 0.01 M KNO₃/HNO₃.

Analyte	Sensors containing	LOD (μM)	LOD (μM)	Sensitivity (μA·μM ⁻¹)
Hydrogen peroxide	Raw MWCNTs	2.80 ± 0.06	2.80 ± 0.06	0.002
	CdS–QDs@MWCNTs	0.040 ± 0.002	0.040 ± 0.002	0.011
Ascorbic acid	Raw MWCNTs	0.400 ± 0.003	1.51 ± 0.02	0.003
	CdS–QDs@MWCNTs	0.067 ± 0.004	0.159 ± 0.001	0.008

Finally, LSV studies also confirmed that the sensing improvements of the CdS–QDs@MWCNTs/epoxy nanocomposite sensors are only related to the greater dispersion of the conductor microzones and no shifts in their polarization potentials respected to the non-modified sensors were found.

5.1.3 Electrocatalytical activity of CuO nanoparticles for free chlorine amperometric detection



Graphical Abstract V. Routes for CuO–NPs incorporation on the device for the electrocatalytic determination of free chlorine.

The benefits of using CuO–NPs, which have electrocatalytic activity for the decomposition of hypochlorite solutions, for the amperometric detection of free chlorine are reported. NaClO is a compound registered in the Toxic Substances Control Act (TSCA) Chemical Substance Inventory that is frequently used for water disinfection and purification, including drinking water, swimming pool water, treated wastewater for non-potable reuse and others. The sum of Cl_2 , HClO and ClO^- is known in hydrochemistry as free chlorine and its concentration can be expressed as mass of Cl_2 per liter. Accordingly, in this section it has been exploited the catalytic effect of CuO–NPs through their incorporation as a modifier agent in the optimum MWCNT/epoxy nanocomposite composition (Graphical Abstract V) to develop sensitive devices capable to amperometrically detect traces of free chlorine.

5.1.3.1 Physical characterization of CuO–NPs

Concerning CuO–NPs@MWCNTs obtained by Route A, HR–TEM images from Figure 5.15 (B to C) provided that the CuO–NPs were coated homogeneously on the walls of the MWCNTs and no agglomeration of CuO–NPs was detected. The identification of the copper (II) oxide was accomplished by EDS spectra (Figure 5.15 D) and TGA analysis, differentiating the CuO–NPs from the catalyst remaining from the industrial synthesis of the raw MWCNTs. The amount of metal impurities of raw MWCNTs after

acidic treatment was 2.0%. When the CuO–NPs@MWCNTs were analyzed, this 2.0% of metal impurities was subtracted in order to quantify the content of CuO–NPs. The CuO–NPs content on the MWCNTs surface results 9.1%. On the other hand, Figure 5.15 E shows the local view of CuO–NPs product formed by Route B, which indicates that the product consists of small particles with ellipsoidal shape. Its EDS spectra also determined the presence of CuO–NPs (Figure 5.15 F).

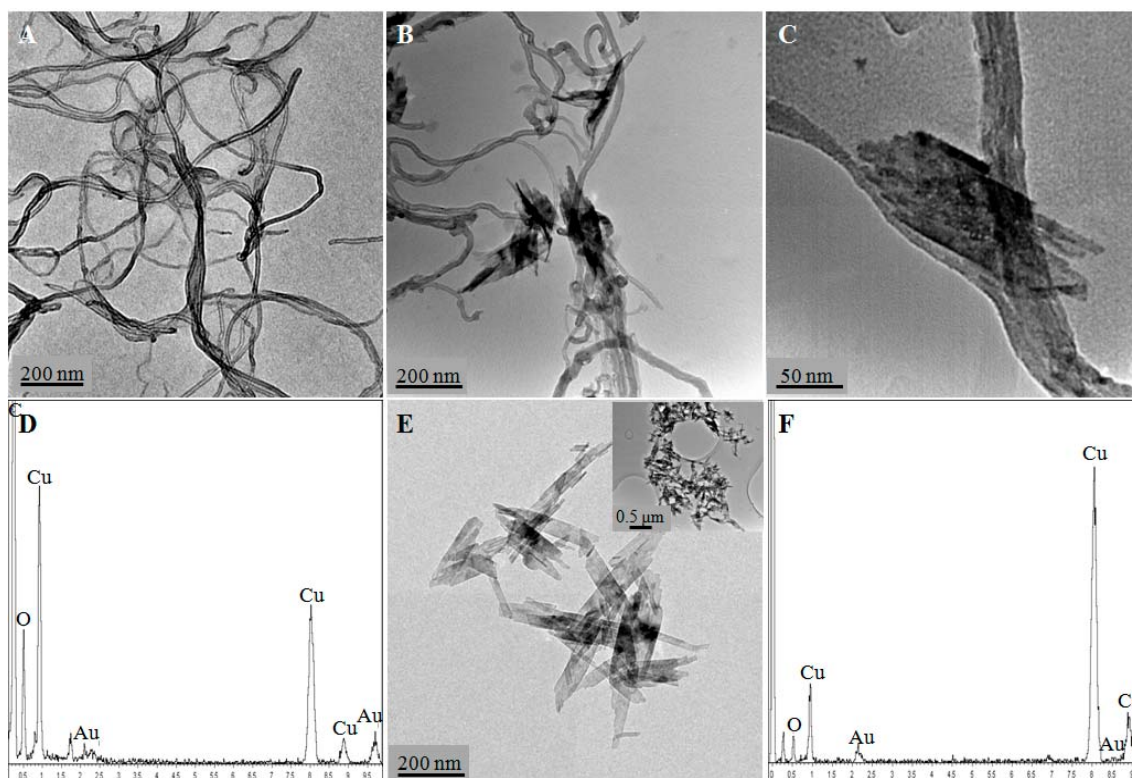


Figure 5.15 HR–TEM images of A) raw MWCNTs; B) CuO–NPs@MWCNT; C) amplification of a single CuO–NPs@MWCNTs; D) EDS spectra of CuO–NPs@MWCNT; E) CuO–NPs and low magnification image (insert); F) EDS spectra of CuO–NPs.

According to TGA and EDS results and taking into account the dispersion of CuO–NPs on the MWCNTs surface observed in HR-TEM images, 0.91% of CuO–NPs were incorporated in the MWCNT/epoxy nanocomposite electrodes by two different routes as a catalyst component. The electrocatalytic effect of the CuO–NPs on reduction of free chlorine was electrochemically studied by CV and EIS and verified for analytical application by hydrodynamic amperometry. In addition, the electrochemical and electrocatalytic behaviour of the CuO–NPs in the nanocomposite sensors were compared with the ones non-modified (raw MWCNT/epoxy nanocomposite electrodes).

5.1.3.2 Voltammetric experiments

As is shown in Figure 5.16, the electrocatalytic performance of the MWCNT/epoxy (curve a), CuO–NPs@MWCNT/epoxy (curve b) and CuO–NPs/MWCNT/epoxy (curve c) nanocomposite electrodes toward the reduction of NaClO in acidic medium (pH 5.5) was demonstrated by CV (scan rate of $50 \text{ mV}\cdot\text{s}^{-1}$). Voltammograms were carried out in absence (experiment control) and in presence of $0.6 \text{ mg}\cdot\text{L}^{-1}$ free chlorine.

Experimental control presented in Figure 5.16 A (curves b and c) shows two pairs of well-defined anodic and cathodic peaks at both MWCNT/epoxy nanocomposite electrodes containing CuO–NPs, which is believed to be due to the redox reactions of CuO–NPs. The first pair of well-defined peaks (E_{a1}/E_{c1}) was found between $+0.56 \text{ V}$ (E_{c1}) and $+0.66 \text{ V}$ (E_{a1}) for CuO–NPs@MWCNT/epoxy nanocomposite electrodes and $+0.60 \text{ V}$ (E_{c1}) and $+0.65 \text{ V}$ (E_{a1}) for CuO–NPs/MWCNT/epoxy nanocomposite electrodes. Both waves might correspond to a Cu(II)/Cu(III) redox couple similar to the previous reports.²¹ Another pair of well-defined redox peaks (E_{a2}/E_{c2}) could be observed: oxidation peak about $+0.07 \text{ V}$ and $+0.13 \text{ V}$ and reduction peak about -0.08 V and -0.09 V for CuO–NPs@MWCNT/epoxy and CuO–NPs/MWCNT/epoxy nanocomposite electrodes, respectively, which might correspond to a Cu(I)/Cu(II) redox couple. These peaks evidence the presence of CuO–NPs on the nanocomposite electrode surface.

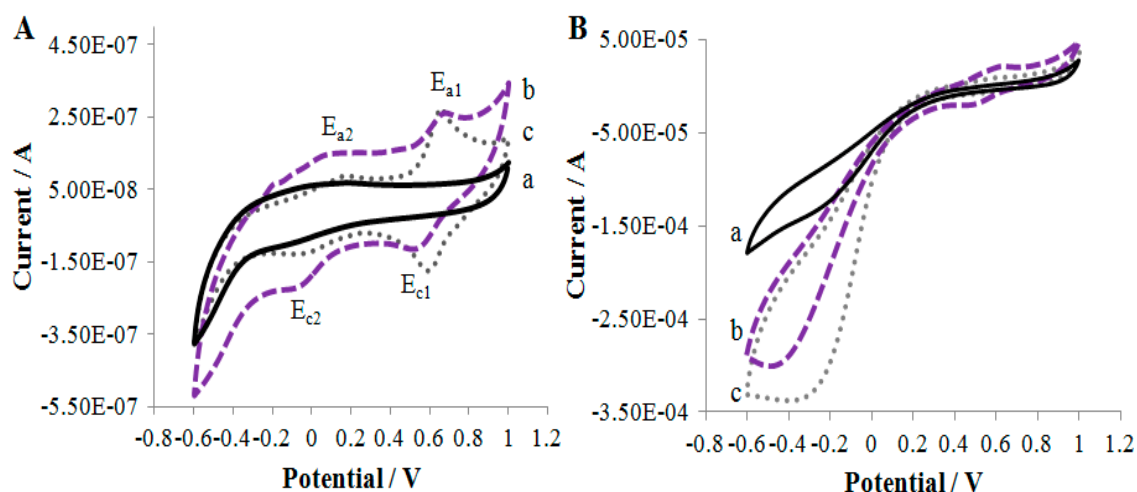


Figure 5.16 Cyclic voltammograms of nanocomposite electrodes containing a) raw MWCNT/epoxy; b) CuO–NPs@MWCNT/epoxy and c) CuO–NPs/MWCNT/epoxy in the absence A) and in the presence B) of $0.6 \text{ mg}\cdot\text{L}^{-1}$ free chlorine. All voltammograms were recorded in 10.0 mL 0.1 M KCl containing PBS at pH 5.5 solution. Scan rate: $50 \text{ mV}\cdot\text{s}^{-1}$.

On the other hand, as is shown in Figure 5.16 B, the two modified-electrodes with CuO-NPs (curves b and c) present a remarkable catalytic current cathodic peak (I_{pc}) at -0.35 V, more emphasized for the CuO-NPs/MWCNT/epoxy nanocomposite electrodes. This fact is mainly caused by the higher accessibility of CuO-NPs on the electrode surface when they are incorporated by Route B. The I_{pc} increased demonstrated the electrocatalytic behaviour of the CuO-NPs in the presence of ClO^- . Compared to the raw MWCNT/epoxy nanocomposite electrodes, nanocomposite electrodes containing CuO-NPs displayed a substantial negative shift of the cathodic peak potential (from -0.1 V to -0.35 V), which suggests a high electrocatalytic activity of the nanocomposite electrodes containing CuO-NPs in the direct reduction of ClO^- . The overpotential shifted negatively, which can be attributed to a kinetic effect by an increase in the electroactive area and the rate of electron transfer from ClO^- to the nanocomposite electrodes containing CuO-NPs.²²

In addition, CV technique was also used to determine the electroactive area (A) of the nanocomposite electrodes, as well as the separation potential (ΔE) and the peak height (I_p), according to the modified Randles-Sevcik equation.²³ The electrochemical experiments, which were carried out in 10.0 mL of 0.1 M KCl solution containing 0.01 M $[Fe(CN)_6]^{3-/4-}$, are presented in Table 5.8. The calculated values of A were 0.25 cm², 1.27 cm² and 2.84 cm² for raw MWCNT/epoxy, CuO-NPs@MWCNT/epoxy and CuO-NPs/MWCNT/epoxy nanocomposite electrodes, respectively. These results confirmed the improvement of the electroactive area with the incorporation of CuO-NPs in the nanocomposite material, independently of the route of CuO-NPs incorporation. The highest value of A was obtained for the modified-electrodes by Route B, which improved around 90% vs. the ones non-modified and 55% vs. the ones modified by Route A. These results revealed that the CuO-NPs are more exposed on the electrode surface when they were incorporated as a powder form by Route B.

Simultaneously, a comparison of the ΔE was evaluated for all electrodes. As can be also seen in Table 5.8, the incorporation of CuO-NPs in both routes presented a slight decrease of ΔE , from 0.48 V to 0.12 V and 0.24 V, for modified-electrodes obtained by Route A and Route B, respectively. This enhancement of ΔE is mainly contributed by the electrocatalytic activity of the copper (II) oxide nanoparticles.

Table 5.8 Electrochemical parameters obtained by CV in a 0.1 M KCl solution containing 0.01 M $[\text{Fe}(\text{CN})_6]^{3-/4-}$ at $50 \text{ mV}\cdot\text{s}^{-1}$ for the three nanocomposite electrodes studied.

Nanocomposite Electrode	A (cm^2)	I_p (mA)	ΔE (V)
Raw MWCNT/epoxy	0.25	0.132	0.48
CuO-NPs@MWCNT/epoxy	1.27	0.680	0.12
CuO-NPs/MWCNT/epoxy	2.84	1.52	0.24

5.1.3.3 Impedimetric experiments

Before probing the electrocatalytic properties of the modified-nanocomposite electrodes with CuO-NPs towards hypochlorite reduction, the electrodes were characterized to know their resistance/impedance by EIS technique. The resultant values are summarized in Table 5.9.

The Nyquist plots present in Figure 5.17 A exhibited a well defined semicircle for electrodes containing raw MWCNT and CuO-NPs@MWCNTs. However, the spectrum of the modified-electrodes obtained by Route B included two segments. The first segment at higher frequency range, seen as circular portion, is due to an electron transfer limited process. The second one at lower frequency range, the linear portion is due to the diffusion controlled process (Figure 5.17 B).

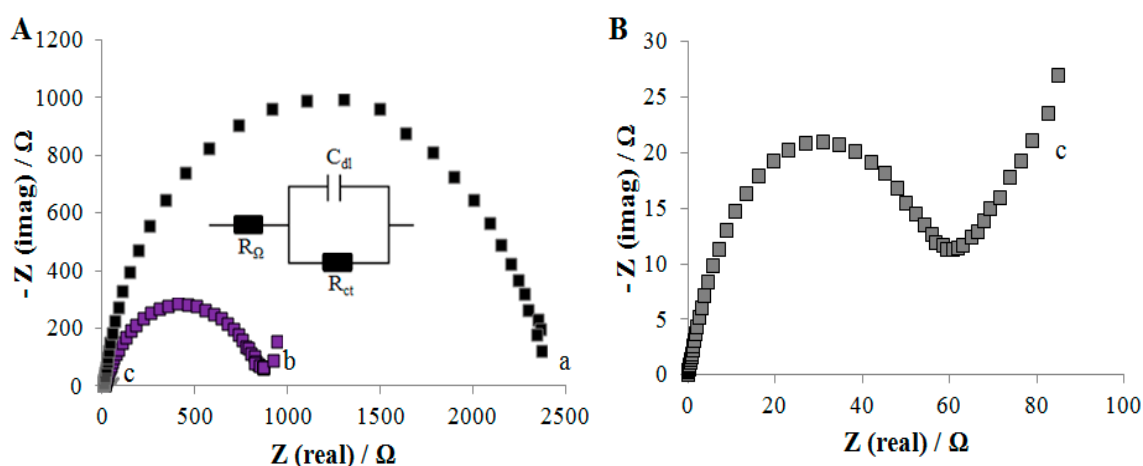


Figure 5.17 A) Electrochemical impedance spectra of nanocomposite electrodes containing a) Raw MWCNT/epoxy; b) CuO-NPs@MWCNT/epoxy and c) CuO-NPs/MWCNT/epoxy examined in a 0.1 M KCl solution containing 0.01 M $[\text{Fe}(\text{CN})_6]^{3-/4-}$. The insert shows the equivalent circuit used for the impedance spectra fitting. B) Magnification of the c) from spectra A.

Nanocomposite electrodes containing CuO–NPs showed a R_{Ω} decrease at the same time that their electroactive areas increased. Thus, while raw MWCNT/epoxy nanocomposite electrode presented an ohmic resistance value of 126.7 Ω , CuO–NPs@MWCNT/epoxy and CuO–NPs/MWCNTs/epoxy nanocomposite electrodes presented lower ohmic resistance values (92.6 Ω and 13.7 Ω , respectively). Accordingly, the lower R_{Ω} values exhibited for both modified nanocomposite materials with CuO–NPs verified that CuO–NPs acts as an electron mediator.²⁴

Concerning R_{ct} , both modified-nanocomposite electrodes with CuO–NPs exhibited a smaller semicircle compared to the raw MWCNT/epoxy nanocomposite electrode (see Figure 5.17 A), indicating a lower resistance of electron transfer, as is shown in Table 5.9. This fact is mainly caused for the electrocatalytic effect provided by the CuO–NPs.

Finally, C_{dl} value is also an important parameter which is directly related with the signal-to-noise ratio. A decrease of resistance values should be accompanied by an increase in the aforementioned parameter. In spite of that, the strong resistance decrease observed for the electrodes containing CuO–NPs more than compensates the slightly significant increase of their background current, as is shown in Table 5.9.

According to impedimetric results, the significant decrease of R_{Ω} and R_{ct} for the CuO–NPs/MWCNT/epoxy nanocomposite electrode suggested that when the nanoparticles were incorporated in powder form (Route B), they were more accessible on the electrode surface, emphasizing their electrocatalytic activity. These results indicated the role of CuO–NPs in the enhancement of the electron transfer process. In addition, the significant R_{ct} and R_{Ω} decrease in the presence of CuO–NPs resulted in an effective charge transfer, leading to an enhanced electrocatalytic activity for degradation of NaClO, and hence to detect low concentrations of free chlorine.

Table 5.9 Electrochemical parameters obtained by EIS in a 0.1 M KCl solution containing 0.01 M $[\text{Fe}(\text{CN})_6]^{3-/4-}$ at $50 \text{ mV}\cdot\text{s}^{-1}$ for the three nanocomposite electrodes studied.

Nanocomposite Electrode	R_{Ω} (Ω)	R_{ct} (Ω)	C_{dl} (μF)
Raw MWCNT/epoxy	126.7	2360	12.3
CuO–NPs@MWCNT/epoxy	92.6	976.4	54.7
CuO–NPs/MWCNT/epoxy	13.7	84.9	78.1

5.1.3.4 Electroanalytical performance

The feasibility of both CuO-NPs containing nanocomposite sensors in terms of analytical response has been amperometrically evaluated for the determination of free chlorine under stirring conditions (constant stirring) at -0.35 V vs. Ag/AgCl. The working potential was taken from the voltammograms depicted in Figure 5.16.

If the raw MWCNT/epoxy nanocomposite sensor demonstrated a great electroanalytical response for the detection of free chlorine in water,^{25,26} the nanocomposite sensors containing CuO-NPs exhibited a substantially enhanced of its response, also accompanied by an electrocatalytic effect, as shown in Table 5.10.

Table 5.10 Amperometric parameters recorded in a PBS solution (pH 5.5) for modified-nanocomposite electrodes with CuO-NPs and compared with the ones obtained for raw MWCNT/epoxy nanocomposite sensors. LOD and LOQ with their respectively 95% confidence interval (n=3).

Nanocomposite sensors	LOD ($\mu\text{g}\cdot\text{L}^{-1}$)	LOQ ($\mu\text{g}\cdot\text{L}^{-1}$)	Sensitivity ($\text{nA}\cdot\text{L}\cdot\text{mg}^{-1}$)
Raw MWCNT/epoxy [25]	20 ± 10	-	-150
CuO-NPs@MWCNT/epoxy	4.4 ± 0.1	8.8 ± 0.2	-432.5
CuO-NPs/MWCNT/epoxy	0.6 ± 0.1	1.1 ± 0.1	-446.2

For nanocomposite sensors containing CuO-NPs@MWCNTs, the calibration curve for the free chlorine sensor is shown in Figure 5.18 A. The LOD obtained for these sensors exhibited an enhancement in the LOD of 0.9 decades of concentration less than the raw MWCNT/epoxy nanocomposite sensors. Figure 5.18 B also shows the calibration curve for the free chlorine detection obtained by CuO-NPs/MWCNT/epoxy nanocomposite sensors. As in the previous case, the electroanalytical parameters obtained for these modified-sensors also improved respected to those non-modified. The LOD and LOQ of these sensors were $0.6 \mu\text{g}\cdot\text{L}^{-1}$ and $1.1 \mu\text{g}\cdot\text{L}^{-1}$, respectively. Thus, the LOD obtained for these sensors was 1.2 decades of concentration better than the one non-modified.

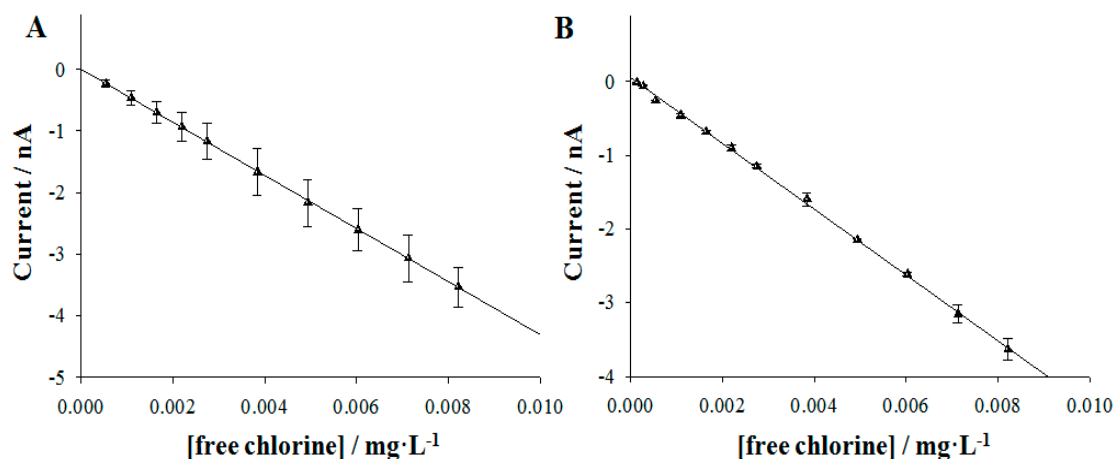


Figure 5.18 Calibration curve of I_p vs. concentration of free chlorine at modified electrodes by A) Route A and B) Route B. The calibration curves are represented with their corresponding error bars expressed as a standard deviation of $n=3$ measurements. Amperometric experiments were carried out in a PBS solution at pH 5.5.

The LOD of both CuO–NPs containing MWCNT/epoxy nanocomposite sensors was obviously better than that of those using MWCNTs, glassy carbon and other modified-sensors which contain different NPs as working electrodes, which are summarized in Table 5.11. This can be attributed to the CuO–NPs loading on MWCNTs arrays, which significantly increase the electrocatalytic active areas and promote electron transfer in the reduction of hypochlorite.

Table 5.11 Comparison of sensing abilities for free chlorine determination with different electrodes.

Electrodes	Analytes	E_{app} (V)	Reaction	LOD ($\mu\text{g}\cdot\text{L}^{-1}$)	Ref.
Pt, Au, GCE	Cl	+1.1	Oxidation	1988	[27]
Nano Au-PEDOT/GCE	HClO	0.0	Reduction	71	[28]
Gold thin-film	Cl	+0.35	Oxidation	398	[29]
MWCNT/epoxy	Cl	-0.1	Reduction	398	[25]
Boron Doped Diamond	Cl	+1.4	Oxidation	16	[30]
Modified by Route A	Cl	-0.35	Reduction	4.4	This work
Modified by Route B	Cl	-0.35	Reduction	0.6	This work

Based on the electroanalytical results, the best electroanalytical and electrocatalytical responses were obtained for the sensors in which the CuO–NPs were incorporated by Route B. These results can be explained since the CuO–NPs were more exposed on the sensor surface, increasing their electrocatalytic activity for the detection of free chlorine.

5.1.3.5 Specificity, Stability and Reproducibility of modified-sensors by Route B

In order to study the selectivity of the sensor which presented the best electroanalytical response (the CuO–NPs/MWCNT/epoxy nanocomposite sensors), different usual ions present in water at high concentrations were evaluated in terms of analytical response. These ions usually co-exist with free chlorine in water. Accordingly, the electroanalytical response of the possible interfering species was also evaluated at this sensor, as is shown in Figure 5.19. Therefore, the effect of Na^+ , K^+ , Ca^{2+} , NO_3^- , Cl^- , and SO_4^{2-} under the presence of free chlorine was studied. Hydrodynamic amperometric response of CuO–NPs/MWCNT/epoxy nanocomposite sensors was monitored in a 0.1 M KCl solution containing PBS (pH 5.5). The interference experiment was carried out by successive injection of 0.1 mM NaClO and 1.0 mM interfering species.

Figure 5.19 shows the current response of (a) the background current and after the subsequently addition of different aliquots of (b) 0.1 mM NaClO, (c) 0.1 mM NaClO, (d) 1.0 mM NaCl, (e) 1.0 mM KCl, (f) 1.0 mM KNO_3 , (g) 1.0 mM K_2SO_4 , (h) 1.0 mM CaSO_4 and (i) 0.1 mM NaClO. A well-defined NaClO responses were observed (peaks b to c), while insignificant responses were observed for interfering species (peaks d to h). Thus, the current response increased only for NaClO, even in the presence of 1.0 mM Na^+ , 4.0 mM K^+ , 1.0 mM Ca^{2+} , 1.0 mM NO_3^- , 2.0 mM Cl^- and 2.0 mM SO_4^{2-} . It is important to highlight that these concentrations are similar to those commonly found in tap water and recreational water. Furthermore, the similar phenomenon for the addition (i) was also found.

After interference studies, it can be concluded that small amount of different usually ions presented in water samples, such as Na^+ , K^+ , Ca^{2+} , NO_3^- , Cl^- , and SO_4^{2-} can be neglected. In other words, the present sensing system apparently exhibit excellent selectivity for the detection of free chlorine in water.

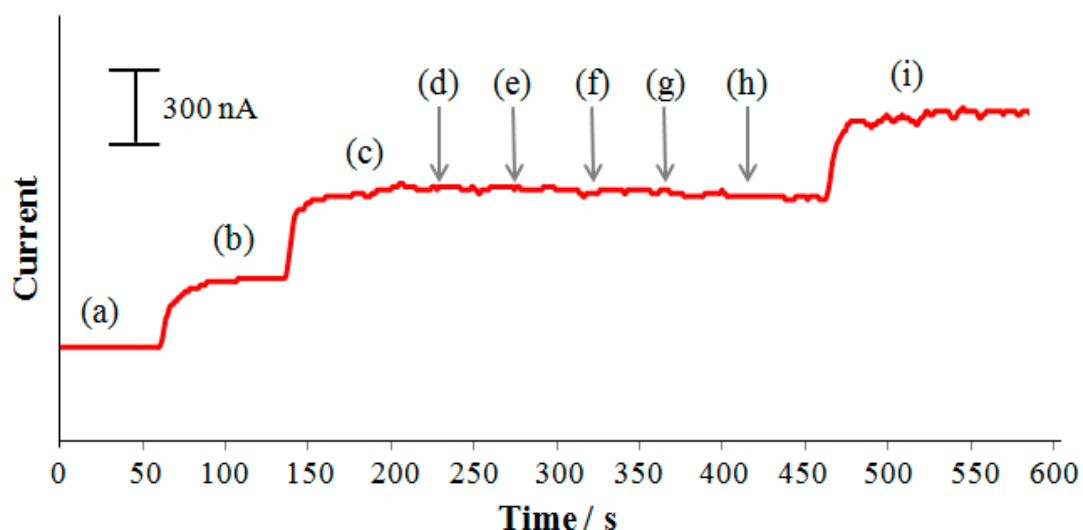


Figure 5.19 Amperometric response of CuO–NPs/MWCNT/epoxy nanocomposite sensor recorded in a PBS solution at pH 5.5. The interference experiment shows the current response for (a) blank, (b) a + 0.1 mM NaClO, (c) b + 0.1 mM NaClO, (d) c + 1.0 mM NaCl, (e) d + 1.0 mM KCl, (f) e + 1.0 mM KNO₃, (g) f + 1.0 mM K₂SO₄, (h) g + 1.0 mM CaSO₄ and (i) h + 0.1 mM NaClO, respectively. $E_{app} = -0.35$ V vs. Ag/AgCl.

Afterwards, the stability and reproducibility of the CuO–NPs/MWCNT/epoxy nanocomposite sensors were also evaluated. On the one hand, to investigate the stability of the sensor, five successive measurements of free chlorine were carried out using one sensor. The relative standard deviation (RSD) was 1.9%, indicating that the sensor was stable. On the other hand, three different sensors were prepared and evaluated in order to compare their amperometric current responses. The measurements, which were carried out in triplicate ($n=3$), yielded an RSD of 1.1%, confirming that the preparation method was highly reproducible.

Finally, multiple calibration experiments were carried out with these three CuO–NPs/MWCNT/epoxy nanocomposite sensors within a 7-day period in order to make an estimation of the loss of sensitivity to both short and long time (see Table 5.12). The mean value of the calibration plots carried out the first working day was used as the control sensitivity value. Successive calibration plots were performed during 7 consecutive days. During this period, the sensor was exposed to air without renewing its surface. Regarding this results, it is important to highlight that a simple approach was implemented with the aim of keeping the electrode surface active for longer without needing to renew its surface. This pretreatment consisted of applying, before each calibration, a +1.23 V vs. Ag/AgCl fix potential during 30 s. After 7 days, the current

response of the CuO–NPs/MWCNT/epoxy nanocomposite sensor was approximately 96.5% of its original counterpart, which can be mainly attributed to the chemical stability of the CuO–NPs. The results demonstrated that the simple procedure explained above enables the sensor to be used for at least 7 days without having significant differences in sensitivity, keeping its original properties (RSD of 1.3%). Furthermore and according to previous reports, these results also demonstrate that the CuO–NPs do not show any degradation under the presence of NaClO during repeated uses and thus, keep their catalytic activity for the electrocatalytic detection of free chlorine in water.³¹

Table 5.12 Variation of the CuO–NPs/MWCNT/epoxy nanocomposite sensor sensitivity upon carrying out successive free chlorine calibration experiments for a 7-day period time. Sensitivity values expressed with their respectively 95% confidence interval (n=3) was obtained by hydrodynamic amperometry in a 0.1 M KCl solution containing PBS (pH 5.5); $E_{app} = -0.35$ V vs. Ag/AgCl.

Day	Sensitivity (nA·L·mg ⁻¹)	r ² (n=12)
1	-446 (±) 12	0.999
2	-436 (±) 16	0.998
5	-440 (±) 17	0.997
7	-433 (±) 12	0.999

5.2 Conclusions

Different conclusions have been extracted from these results:

- Three different routes have been carried out to functionalize MWCNT/epoxy nanocomposite electrodes with a wide range of NPs, including FMNPs, QDs and MO–NPs.
- IMS has successfully been used as an environmentally friendly technique to develop a customized way to modify MWCNT–based nanocomposite electrodes. Modified-electrodes present different electrochemical and analytical improvements regardless of the route of NPs incorporation.

- Different microscopy, thermogravimetric and spectroscopic tools have allow the characterization, identification and quantification of the modified (nano)materials containing NPs.
- Electrochemical techniques have enabled the identification of the different electrocatalytical activities regarding to the type of NPs incorporated, differentiating three different electrocatalytical effects: (i) FMNPs (Au–NPs and Pd–NPs) provide decreases in overpotentials for sensing hydrogen peroxide; (ii) CdS–QDs acts as scattering material, involving dispersion of the conducting microzones through insulating polymer and decreasing LODs and (iii) CuO–NPs enhances the current height peaks in the determination of free chlorine.
- Morphological techniques are powerful tools to characterize the micro/macroelectrode behaviour of MWCNT–based nanocomposite materials. Both CSAFM and CM3D techniques demonstrated that CdS–QDs act as a scattering material sensors based on MWCNT/epoxy, resulting in a great dispersion of their conductive microzones. This fact offers them an improvement in the microelectrode array behaviour, obtaining more sensitive devices capable to detect lower LODs of different analytes regarding to those non-modified.
- Modified nanocomposite sensors containing CuO–NPs present many attractive analytical characteristics such as valuable electrocatalytic activity, high sensitivity, strong stability, good reproducibility and selectivity, as well as quick response for free chlorine determination. This fact is mainly attributed to the improvement of electroactive surface area and synergistic electrocatalytic activity resulting from the combination of MWCNTs and CuO–NPs, resulting in a sensor suitable to determine traces in the order of parts per billion ($\mu\text{g}\cdot\text{L}^{-1}$), around a decade of concentration less than the obtained by the raw MWCNT/epoxy nanocomposite sensor.

5.3 References

1. Wang, J.; Musameh, M., Carbon nanotube/teflon composite electrochemical sensors and biosensors. *Analytical Chemistry* **2003**, *75* (9), 2075-2079.
2. Pumera, M.; Merkoçi, A.; Alegret, S., Carbon nanotube-epoxy composites for electrochemical sensing. *Sensors and Actuators B: Chemical* **2006**, *113* (2), 617-622.
3. Chen, R. J.; Bangsaruntip, S.; Drouvalakis, K. A.; Kam, N. W. S.; Shim, M.; Li, Y.; Kim, W.; Utz, P. J.; Dai, H., Noncovalent functionalization of carbon nanotubes for highly specific electronic biosensors. *Proceedings of the National Academy of Sciences* **2003**, *100* (9), 4984-4989.
4. Shim, M.; Shi Kam, N. W.; Chen, R. J.; Li, Y.; Dai, H., Functionalization of carbon nanotubes for biocompatibility and biomolecular recognition. *Nano Letters* **2002**, *2* (4), 285-288.
5. Sepahvand, R.; Adeli, M.; Astinchap, B.; Kabiri, R., New nanocomposites containing metal nanoparticles, carbon nanotube and polymer. *Journal of Nanoparticle Research* **2008**, *10* (8), 1309-1318.
6. Eatemadi, A.; Daraee, H.; Karimkhanloo, H.; Kouhi, M.; Zarghami, N.; Akbarzadeh, A.; Abasi, M.; Hanifehpour, Y.; Joo, S. W., Carbon nanotubes: properties, synthesis, purification, and medical applications. *Nanoscale Research Letters* **2014**, *9* (1), 1-13.
7. Kim, B.; Sigmund, W. M., Functionalized multiwall carbon nanotube/gold nanoparticle composites. *Langmuir* **2004**, *20* (19), 8239-8242.
8. Yang, J.; Jiang, L.-C.; Zhang, W.-D.; Gunasekaran, S., A highly sensitive non-enzymatic glucose sensor based on a simple two-step electrodeposition of cupric oxide (CuO) nanoparticles onto multi-walled carbon nanotube arrays. *Talanta* **2010**, *82* (1), 25-33.
9. Liu, Q.; Lu, X.; Li, J.; Yao, X.; Li, J., Direct electrochemistry of glucose oxidase and electrochemical biosensing of glucose on quantum dots/carbon nanotubes electrodes. *Biosensors and Bioelectronics* **2007**, *22* (12), 3203-3209.
10. Nikoobakht, B.; El-Sayed, M. A., Preparation and growth mechanism of gold nanorods (NRs) using seed-mediated growth method. *Chemistry of Materials* **2003**, *15* (10), 1957-1962.
11. Murphy, C. J.; Jana, N. R., Controlling the aspect ratio of inorganic nanorods and nanowires. *Advanced Materials* **2002**, *14* (1), 80.

12. Muraviev, D. N., Inter-matrix synthesis of polymer stabilised metal nanoparticles for sensor applications. *Contributions to Science* **2005**, *3* (1), 19.
13. Ruiz, P.; Muñoz, M.; Macanás, J.; Muraviev, D. N., Intermatrix Synthesis of Polymer–Copper Nanocomposites with Tunable Parameters by Using Copper Comproportionation Reaction. *Chemistry of Materials* **2010**, *22* (24), 6616-6623.
14. Rassaei, L.; Marken, F.; Sillanpää, M.; Amiri, M.; Cirtiu, C. M.; Sillanpää, M., Nanoparticles in electrochemical sensors for environmental monitoring. *TrAC Trends in Analytical Chemistry* **2011**, *30* (11), 1704-1715.
15. Balasubramanian, K.; Burghard, M., Chemically functionalized carbon nanotubes. *Small* **2005**, *1* (2), 180-192.
16. Cespedes, F.; Valero, F.; Martinez-Fabregas, E.; Bartroli, J.; Alegret, S., Fermentation monitoring using a glucose biosensor based on an electrocatalytically bulk-modified epoxy-graphite biocomposite integrated in a flow system. *Analyst* **1995**, *120* (8), 2255-2258.
17. Muñoz, J.; Bartrolí, J.; Céspedes, F.; Baeza, M., Influence of raw carbon nanotubes diameter for the optimization of the load composition ratio in epoxy amperometric composite sensors. *Journal of Materials Science* **2015**, *50* (2), 652-661.
18. Pacios, M.; Del Valle, M.; Bartroli, J.; Esplandiu, M., Electrochemical behavior of rigid carbon nanotube composite electrodes. *Journal of Electroanalytical Chemistry* **2008**, *619*, 117-124.
19. Esplandiu, M. J.; Baeza, M.; Olivé-Monllau, R.; Céspedes, F.; Bartrolí, J., Development of Tunable Nanocomposites Made from Carbon Nanotubes for Electrochemical Applications. *Advances in Composite Materials for Medicine and Nanotechnology*, Dr. Brahim Attaf (Ed.) **2011**.
20. O'Hare, D.; Macpherson, J. V.; Willows, A., On the microelectrode behaviour of graphite–epoxy composite electrodes. *Electrochemistry Communications* **2002**, *4* (3), 245-250.
21. Pourbaix, M., Atlas d'équilibres électrochimiques à 25 °C. Gauthier-Villars. Editeur, Paris **1963**.
22. Zhuang, Z.; Su, X.; Yuan, H.; Sun, Q.; Xiao, D.; Choi, M. M., An improved sensitivity non-enzymatic glucose sensor based on a CuO nanowire modified Cu electrode. *Analyst* **2008**, *133* (1), 126-132.

23. Laoire, C. O.; Mukerjee, S.; Abraham, K.; Plichta, E. J.; Hendrickson, M. A., Elucidating the mechanism of oxygen reduction for lithium-air battery applications. *The Journal of Physical Chemistry C* **2009**, *113* (46), 20127-20134.
24. Ye, J. S.; Cui, H. F.; Liu, X.; Lim, T. M.; Zhang, W. D.; Sheu, F. S., Preparation and characterization of aligned carbon nanotube–ruthenium oxide nanocomposites for supercapacitors. *Small* **2005**, *1* (5), 560-565.
25. Olivé-Monllau, R.; Pereira, A.; Bartrolí, J.; Baeza, M.; Céspedes, F., Highly sensitive CNT composite amperometric sensors integrated in an automated flow system for the determination of free chlorine in waters. *Talanta* **2010**, *81* (4–5), 1593-1598.
26. Olivé-Monllau, R.; Martínez-Cisneros, C. S.; Bartrolí, J.; Baeza, M.; Céspedes, F., Integration of a sensitive carbon nanotube composite electrode in a ceramic microanalyzer for the amperometric determination of free chlorine. *Sensors and Actuators B: Chemical* **2011**, *151* (2), 416-422.
27. Koderá, F.; Umeda, M.; Yamada, A., Determination of free chlorine based on anodic voltammetry using platinum, gold, and glassy carbon electrodes. *Analytica Chimica Acta* **2005**, *537* (1), 293-298.
28. Tsai, T.-H.; Lin, K.-C.; Chen, S.-M., Electrochemical synthesis of poly (3, 4-ethylenedioxythiophene) and gold nanocomposite and its application for hypochlorite sensor. *International Journal of Electrochemical Science* **2011**, *6*, 2672-2687.
29. Olivé-Monllau, R.; Orozco, J.; Fernández-Sánchez, C.; Baeza, M.; Bartrolí, J.; Jimenez-Jorquera, C.; Céspedes, F., Flow injection analysis system based on amperometric thin-film transducers for free chlorine detection in swimming pool waters. *Talanta* **2009**, *77* (5), 1739-1744.
30. Murata, M.; Ivandini, T. A.; Shibata, M.; Nomura, S.; Fujishima, A.; Einaga, Y., Electrochemical detection of free chlorine at highly boron-doped diamond electrodes. *Journal of Electroanalytical Chemistry* **2008**, *612* (1), 29-36.
31. Kim, K.-W.; Lee, E.-H.; Chung, D.-Y.; Moon, J.-K.; Shin, H.-S.; Kim, J.-S.; Shin, D.-W., Manufacture characteristics of metal oxide–hydroxides for the catalytic decomposition of a sodium hypochlorite solution. *Chemical Engineering Journal* **2012**, *200*, 52-58.

CHAPTER VI

**Towards to the electroanalytical enhancement of
graphene–polymer nanocomposite (bio)sensors**

CHAPTER VI

Towards to the electroanalytical enhancement of graphene– polymer nanocomposite (bio)sensors

During the past few decades the electrochemical properties of different carbon paste electrodes were studied in detail.^{1,2,3} Nanocomposite materials based on different forms of carbon nanostructure material (e.g. graphite, CNTs and graphene) as conductive phase have played a leading role in the analytical electrochemistry field, particularly in sensor devices.^{5,6,7}

Because of their good conductivity, thermal stability and excellent mechanical strength, graphene and its derivatives are important filler materials for polymer nanocomposites. From an electrochemical point of view, graphene-based nanocomposite materials possess important characteristics, such as large specific surface area, excellent conductivity and availability for surface functionalization.^{8,9} As another important member of graphene family, graphene oxide (GO) and reduced graphene oxide (rGO) are more electrochemically active as compared to pristine graphene owing to the oxygen-containing reactive sites at edges and in the basal plane.^{10,11} In spite of this fact, electrodes based on rGO exhibit a higher sensitivity and electrocatalytic activity than most GO-based electrodes, due to the higher conductivities associated with the increased level of in-plane sp^2 hybridization.^{12,13}

As was mentioned above, the properties and performances of carbon-based polymer nanocomposites not only depends on the quality of the filler material and polymer matrix, but performance will also depend on its dispersity and the ratio of filler to the matrix.¹⁴ The electrical conductivity is one of the most important changes when graphene-based nanocomposites are prepared because of in this systems, the bulk conductivity of the insulating polymers increases by several orders of magnitude when an appropriate amount of graphene is added, following normally a percolation behaviour.¹⁵ As is known, depending on the conductive load, nanocomposites can

behave as microelectrode arrays, which provide efficient mass transport of the electroactive species due to radial diffusion on the spaced carbon particles, favouring the sensitive electroanalysis of a variety of reagents.^{16,17,18} Under this context, the optimization of the carbon loading in the nanocomposite materials is again a key point for improving their electrochemical properties and analytical applications.

Another point of consideration is the feasibility of GO to be used as support for different heterogeneous catalysts, including different functional metal nanoparticles (FMNPs).¹⁹ To date, graphene-based hybrid nanomaterials have become a hot research topic in material science because the hybridization can be an effective strategy to enhance the functionality of materials,²⁰ and the integration of nanomaterials on graphene sheets potentially paves a new way to enhance their electronic, chemical and electrochemical properties.²¹

A slightly modified version of this chapter has been submitted as journal articles.

– *Characterization protocol to improve the electroanalytical response of graphene–polymer nanocomposite sensors.*

Submitted at Composite Science and Technology (2015)

J. Muñoz, L.J. Brennan, F. Céspedes, Y.K. Gun'ko and M. Baeza

– *Near-percolation nanocomposite sensor based on modified-graphene for the sensitive electrochemical biorecognition of Thyroxine.*

Submitted at Chemical Communication (2015)

J. Muñoz, M. Riba-Moliner, L.J. Brennan, Y.K. Gun'ko, F. Céspedes, A. González-Campo and M. Baeza

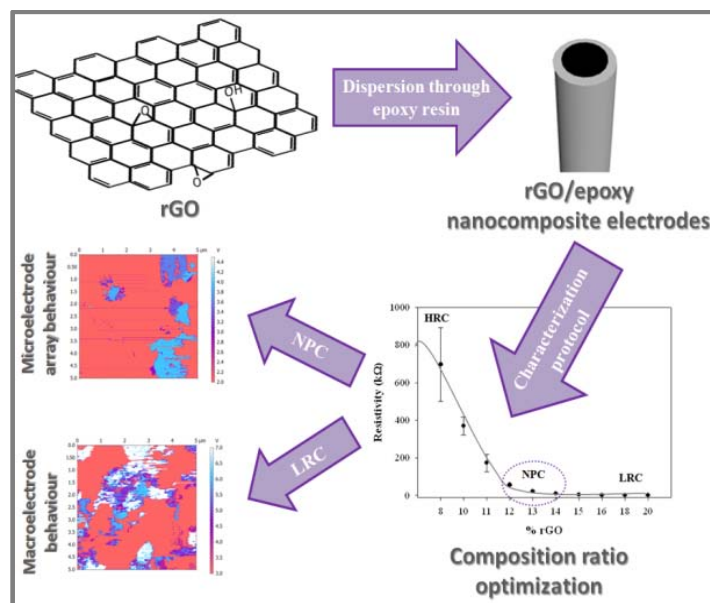
6.1 Results and Discussion

As was discussed above, the requirements to achieve good electrode performance are high sensitivity, a rapid response time and a low limit of detection. In Chapter IV it has been demonstrated that these requirements are related to some of the physical parameters such as material resistivity, heterogeneous electron transfer rate and double-layer capacitance. Accordingly, the main goal of this work is based on developing optimized graphene-based epoxy nanocomposite electrodes for their use in electroanalysis.

For this aim, the characterization protocol carried out to optimize MWCNT/epoxy nanocomposite sensors (see Chapter IV) has been extended for those based on rGO/epoxy. Thus, the already described electrical, electrochemical, physical and microscopic techniques have been implemented in § 6.1.1 in order to achieve the best electrode performance.

Having found the optimum nanocomposite composition, the next step consisted in developing a novel device for thyroxin (T_4) sensing. For this aim, GO was functionalized with Au-NPs, obtaining a new hybrid nanomaterial, Au-NPs@rGO, which was used as a support nanomaterial to attach a specific molecule for T_4 biorecognition. Concretely, the per-6-thiol- β -cyclodextrin (β -CD-SH) was chosen as a recognition agent, that once attached to the filler nanomaterial, it was dispersed within epoxy resin for the construction of a sensitive nanocomposite sensor which was used in § 6.1.2 for the sensitive detection of T_4 . Finally, different NPs incorporation routes, which were developed in Chapter V, has been also studied and discussed in this section in order to find the best sensing performance.

6.1.1 Characterization protocol to achieve the optimum graphene–polymer ratio for electrochemical sensing applications



Graphical Abstract VI. Use of Near-percolation nanocomposite sensors for electroanalytical improvements

In this section, the optimum graphene/polymer composition ratio has been studied in order to improve the electroanalytical signal of nanocomposite sensors based on graphene. For this aim, GO was previously synthesized, using the Hummers method, and consequently reduced with ascorbic acid before its dispersion in epoxy matrix with the aim of evaluating different rGO/epoxy nanocomposite electrodes compositions (from 8% to 20% in rGO loading) for amperometric purposes. Loadings of rGO were systematically varied and measured the bulk and dry state resistivity of the resulting nanocomposite electrode using various tools. Finally, the benefits of using optimized devices (NPC sensors) were demonstrated in terms of analytical performance, using ascorbic acid as a model analyte for its amperometric detection.

6.1.1.1 Physical characterization of GO and rGO

HR-TEM was employed to monitor the extent of exfoliation of GO after dispersion in H₂O using ultrasonication. TEM images from Figure 6.1 (A to B) clearly show the effect of oxidation on the dispersibility of the material in water from the bulk graphite. Finally, Figure 6.1 C shows a representative image of the rGO, which was obtained after GO reduction with ascorbic acid.

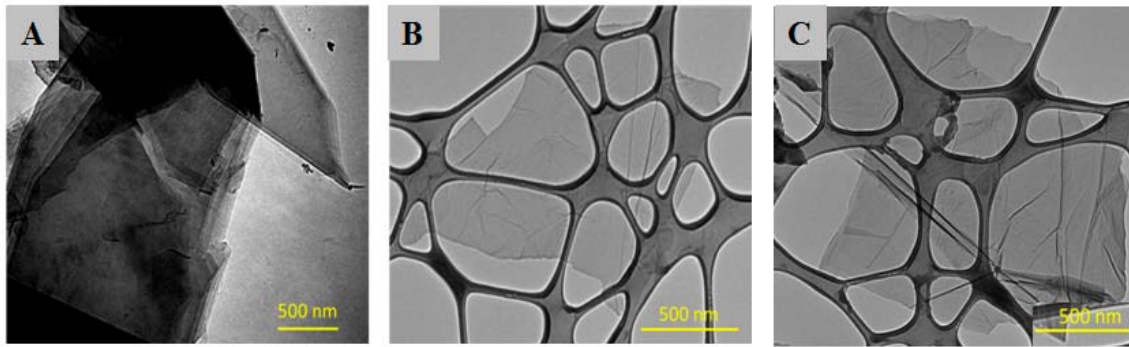


Figure 6.1 HR-TEM images recorded for A) graphite, B) GO and C) rGO deposited onto Lacey carbon grids from aqueous suspension.

UV-vis absorbance spectra recorded for GO and rGO can be seen in Figure 6.2. The main spectroscopic features associated with optical absorption in GO are due to electronic transitions within C=C bonds (231 nm) and -C=O bonds (~ 300 nm). After reduction has taken place, the band associated with -C=O functionality is removed from the spectra while the band located at 231 nm due to in-plane -C=C bonds shifts to the red (267 nm). This shift is known to be associated with the increased in-plane hybridization of the rGO²² and agrees well with the findings on the bibliography.^{23,24}

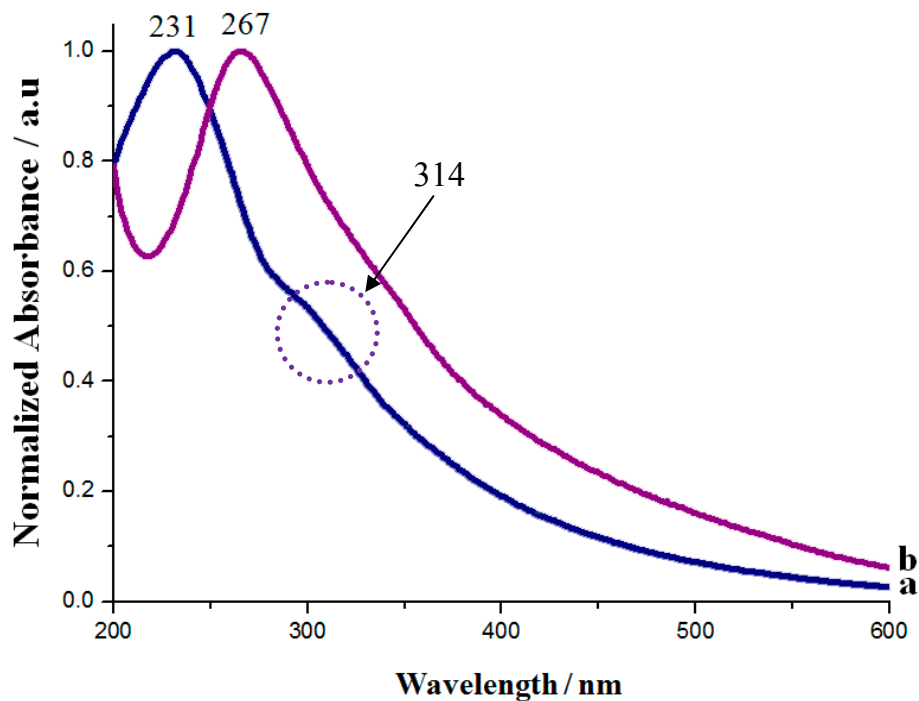


Figure 6.2 UV-vis spectra recorded for aqueous suspensions of a) GO and b) rGO.

Raman spectroscopy is an extremely useful technique for analysis of carbon based materials. Changes in the positions, shapes and relative intensities of the strong Raman bands can be employed to gain an insight into the structural properties of the carbon material under investigation. Figure 6.3 shows the Raman spectra recorded for A) graphite, B) graphene oxide and C) reduced graphene oxide after deposition from aqueous suspensions onto Si/SiO₂ (300 nm) substrates. The Raman spectra shown are composed of 2 peaks. The disorder band (D band) located at ~1330 cm⁻¹ and the graphitic band (G band) located at ~1580 cm⁻¹.

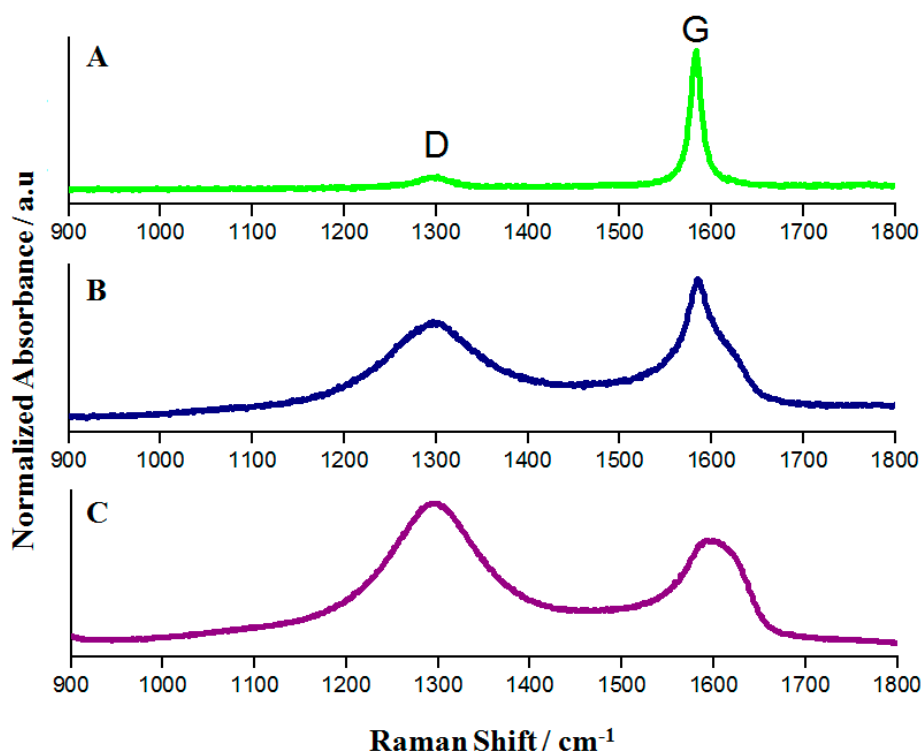


Figure 6.3 Raman spectra recorded for A) graphite, B) GO and C) rGO deposited on Si/SiO₂ (300 nm) substrates.

A large increase in the intensity of the D band can be observed upon oxidation of the graphite to the graphene oxide. This increase in intensity is due to the increased level of disorder in the material, as the oxidation process leads to the formation of sp³ hybridized carbon domains at the expense of the sp² hybridized graphitic structure. This oxidation also causes the G band of GO band to red shift (1578 – 1582 cm⁻¹). This shift has been associated with the isolation of carbon-carbon double bonds in the lattice, which causes resonance at a higher frequency.²⁵

The ratio of the relative intensities of the G and D bands (I_D/I_G) is seen to increase once GO is reduced to rGO, using ascorbic acid. GO exhibits an I_D/I_G of 0.70, while this ratio increases to 1.34 once the material is reduced. It has been suggested that the increase in I_D/I_G after the reduction is related to a decrease in the average size of the sp^2 domains which are smaller in size, but more numerous in number, compared to those present in GO.^{26,27}

According with these results, it can be concluded that GO was successfully synthesized from graphite and then efficiently reduced with ascorbic acid to obtain the rGO, which was used as a filler nanomaterial for the construction of different nanocomposite electrodes based on rGO/epoxy.

6.1.1.2 Electrical characterization

The electrical properties of rGO/epoxy nanocomposite electrodes were investigated applying the well-known percolation theory applied along this Thesis.²⁸ The percolation curve was constructed by varying the rGO loading in the epoxy matrix. It is important to highlight that three equal electrodes were prepared at each loading concentration in order to evaluate the reproducibility of the hand-made nanocomposite electrodes. While nanocomposites containing less than 8% of rGO presented insulating properties with resistivity values $\sim \infty$, those containing more than 20% of rGO gave poor mechanical stability. As is shown in Figure 6.4, resistivity decreases rapidly below the percolation threshold to a minimum value (from 700 k Ω to 10 k Ω), where variations in resistivity are negligible. After the experiments and in concordance with the electrical results obtained sections § 4.1.1 and § 4.1.2 for MWCNT-based nanocomposites, three different conductive regions were determined regarding the electrical behaviour (see Figure 6.4): HRC: High resistivity zone nanocomposites, and thus lowly conducting; NPC: Near-percolation zone nanocomposites and LRC: Low resistivity zone nanocomposites, and thus highly conducting. According to the results, the variation of the resistivity was negligible between 13% and 20% of rGO loading, demonstrating that the nanocomposites lying between such intervals are suitable for electroanalytical measurements.

Finally, Figure 6.4 also shows a significant decrease in the standard deviation of the resistivity values when the rGO/epoxy composition ratio reached the NPC zone. Taking these observations into account, it can be concluded that the similar reproducibility in the electrode handmade fabrication is remarkably similar for compositions comprised between LRC zone and NPC zone.

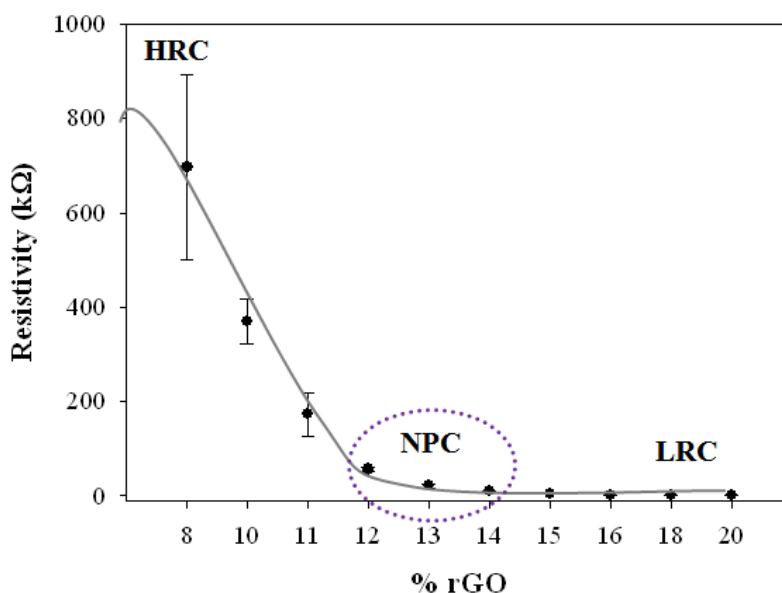


Figure 6.4 Percolation curve obtained for the rigid conducting nanocomposite electrodes based on rGO/epoxy, where the rGO load varies between 8% and 20%. The trend follows the percolation theory, showing three different conductive regions: High resistance zone (HRC), near-percolation zone or second percolation composite zone (NPC) and low resistance zone (LRC). Experimental error was estimated as a standard deviation ($n=3$).

6.1.1.3 Voltammetric experiments

CV was applied in order to electrochemically characterize the different rGO/epoxy nanocomposite electrodes. Ten different rGO/epoxy nanocomposite electrodes composition (from 8% to 20%) were fabricated. Cyclic voltammograms were taken under the same experimental conditions (scan rate of $50 \text{ mV}\cdot\text{s}^{-1}$) for the different nanocomposite electrode compositions in the presence of the benchmark $[\text{Fe}(\text{CN})_6]^{3-/4-}$ redox couple, which are shown in Figure 6.5. Different parameters such as I_p , ΔE and A have been extracted from the cyclic voltammograms, which are summarized in Table 6.1. The electroactive area can be calculated in terms of peak current (I_p , A) and scan rate (v , $\text{V}\cdot\text{s}^{-1}$) according to the modified Randles-Sevcik equation,²⁹ which is adequate for electron transfer-controlled processes.³⁰ According to voltammetric results (see

Table 6.1), peak height increased with the increase of rGO loading, due to an increase in the electroactive area. Simultaneously, a decrease of peak separation was also observed, related to an enhancement of the electron transfer rate.

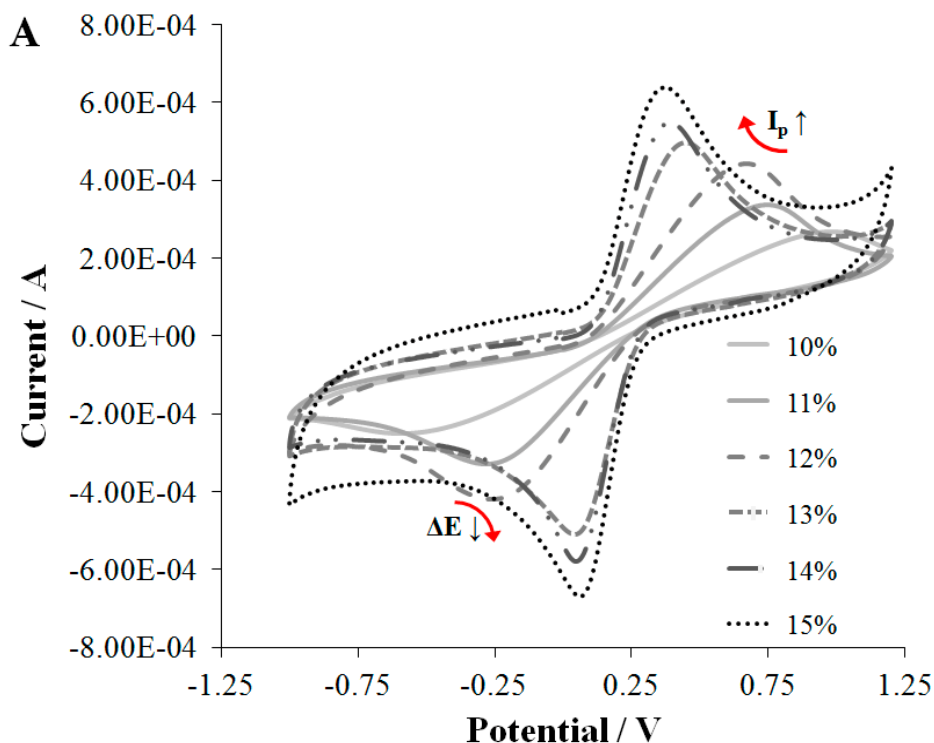


Figure 6.5 Cyclic voltammograms recorded in a 0.1 M KCl containing 0.01 M $[\text{Fe}(\text{CN})_6]^{3-/4-}$ solution for the different rGO/epoxy nanocomposite compositions. Scan rate: $50 \text{ mV} \cdot \text{s}^{-1}$.

In addition, the exchange current (i_0) from Tafel plots (log current density vs. potential) has also been evaluated. i_0 is a parameter which provides information about the reversibility of the electron transfer process. From this value it is possible to evaluate the charge transfer resistance (R_{ct}). The trend observed is a decrease of this parameter which decreased loadings of rGO (see Table 6.1); this observation indicates again the strong relationship between electrochemical reactivity and the surface characteristics of the conducting material. By normalizing charge transfer resistance with respect the electroactive area ($R_{ct} \cdot A$), it is possible to observe in Table 6.1 that this parameter is also decreasing with the increase of A . As was mentioned above in Chapter IV, the changes in $R_{ct} \cdot A$ values are due to the electrochemical anisotropy of the carbon filler nanomaterial.^{31,32}

Table 6.1 Summary of different CV parameters obtained from the different nanocomposite compositions: i_0 , R_{ct} , I_p , A and ΔE . $R_{ct} \cdot A$ and $R_{ct}^{EIS} \cdot A$ corresponds to the R_{ct} obtained by voltammetric and EIS measurements, respectively, and were normalized with respect to the electroactive area.

% rGO	i_0 (μA)	R_{ct} ($k\Omega$)	I_p (μA)	A (cm^2)	ΔE (V)	$R_{ct} \cdot A$ ($\Omega \cdot cm^2$)	$R_{ct}^{EIS} \cdot A$ ($\Omega \cdot cm^2$)
8	18.7	1.4	250	0.21	1.57	283	134
10	21.3	1.2	260	0.22	1.44	259	95
11	38.0	0.67	330	0.28	1.02	184	94
12	61.6	0.41	419	0.35	0.93	144	120
13	155	0.16	511	0.43	0.41	70	121
14	189	0.13	580	0.48	0.34	65	90
15	236	0.11	669	0.56	0.31	60	93
16	273	0.093	699	0.58	0.31	54	54
18	303	0.084	717	0.60	0.31	50	27
20	309	0.082	788	0.66	0.35	54.1	26

Finally, another electrochemical technique (EIS) has been carried out in order to obtain resistance/impedance information about the different nanocomposite electrode compositions evaluated during this study. Furthermore, different electrochemical parameters were also used to compare the obtained results between both electrochemical techniques.

6.1.1.4 Impedimetric experiments

Every rGO/epoxy nanocomposite electrode composition was also impedimetrically characterized by EIS. Following the same procedure used in the previous chapters, it has been applied a model circuit to describe individual elements based on the physical electrochemistry system, such as the aforementioned solution resistance (R_{Ω}), charge transfer resistance (R_{ct}) and double-layer capacitance (C_{dl}). In addition, for rGO-based nanocomposite electrodes, a fourth element was necessary to be included in the system in order to obtain an optimum fitting. Accordingly, Warburg impedance (Z_w), which arises from mass-transfer limitations and can be used to measure effective diffusion coefficients, was also incorporated in the system, resulting the well-known Randles circuit (see Figure 6.6, inset). As is shown in Figure 6.6, the impedance behaviour is mainly dominated by a semicircle, representing kinetic-controlled electrode process.

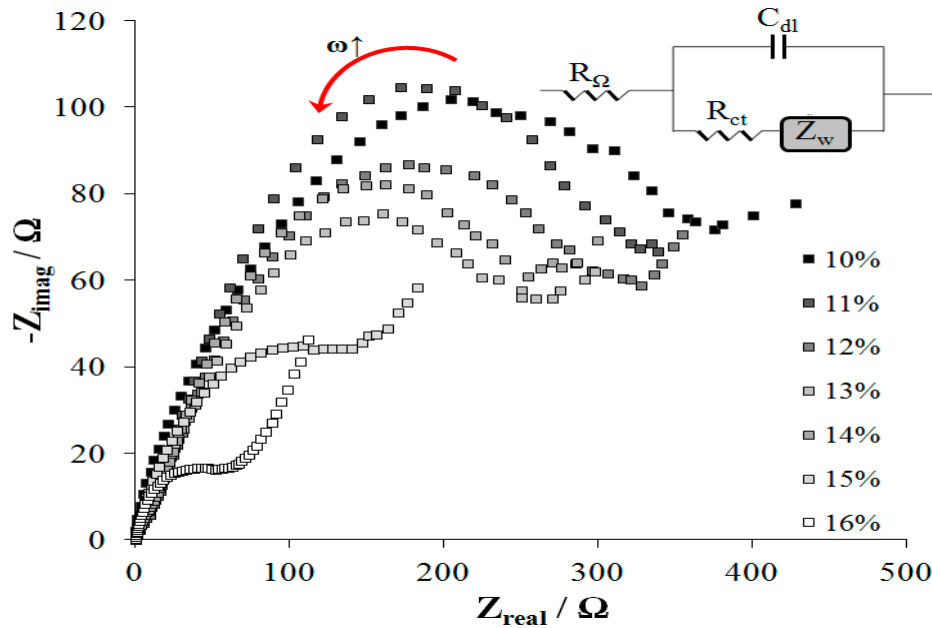


Figure 6.6 Electrochemical impedance spectra of rGO/epoxy nanocomposite electrodes containing different rGO loads were examined in a 0.1 M KCl containing 0.01 M $[\text{Fe}(\text{CN})_6]^{3-/4-}$ solution. The insert shows the equivalent circuit used for the impedance spectra fitting (Randles circuit).

Thus, nanocomposites containing low rGO loading, from HRC zone ($< 8\%$) to NPC zone ($\geq 14\%$), appeared to be dominated by a big diameter semicircle, demonstrating that only the kinetic-controlled electrode process were present in the recorded frequency range. However, for nanocomposites containing high rGO loading, from NPC zone to LRC zone ($> 15\%$), the impedance behaviour was dominated by a small diameter semicircle and the diffusion-controlled process started to be discerned in some cases at low frequencies.

The parameter R_Ω is the one that has a direct relation with the dry resistance taken for the percolation plot of Figure 6.4. As is shown in Figure 6.7 A, the variation of the ohmic resistance as a function of the rGO composition and it can be seen that the R_Ω values decreased with increased rGO loading. This is due the fact that at low carbon loads (less than 14% of rGO loading), the ohmic resistance is dominated by the nanocomposite resistance whereas at higher carbon loads (more than 15% of rGO loading), the ohmic resistance decreases to low values and it is more dominated by the solution resistance. According to these results, this behaviour is in accordance with those obtained by percolation curve.

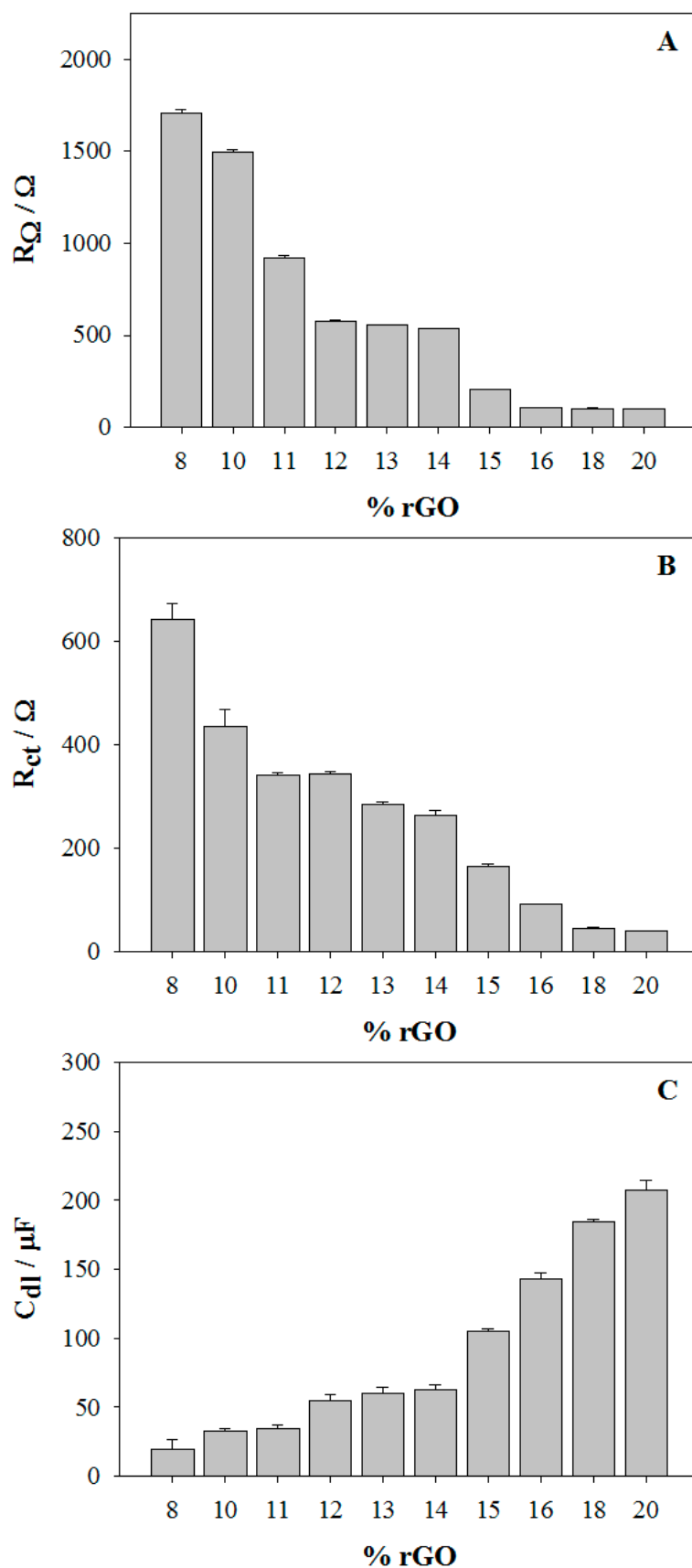


Figure 6.7 Values of A) ohmic resistance, B) charge transfer resistance and C) double-layer capacitance, with their corresponding standard deviation for the different rGO loading electrodes, using the redox probe $[\text{Fe}(\text{CN})_6]^{3-/4-}$ contained in a 0.1 M KCl solution.

Concerning R_{ct} , Figure 6.7 B, nanocomposites between NPC zone and LPC zone presented lower charge R_{ct} values, demonstrating that the nanocomposites with low charge transfer resistances are the most appropriate to be used in electrochemical measurements. Normalizing the EIS R_{ct} values with respect to the A ($R_{ct}^{EIS} \cdot A$), it is possible to observe that there is also a decrease in the value when the electroactive area increases, following the observed tendency in voltammetric performance (see Table 6.1). From the comparison of the normalized R_{ct} values extracted from CV with the ones obtained by EIS (R_{ct}^{EIS}), it can be concluded that the values agree quite well, being more similar for the HRC range of compositions. According to these results, the use of near-percolation nanocomposite electrodes guarantees a fast electron exchange.

Finally, C_{dl} can be determined nearly exclusively by the exposed carbon on the electrode surface. In general, nanocomposites contain only a fraction of conductive area exposed to the solution and the other fraction is occupied by the insulating polymer. Thus, high proportion of rGO loading should increase the conducting area, the surface roughness and porosity of the nanocomposites.³³ This behaviour can be observed in Figure 6.7 C, showing an increase of the C_{dl} value with the increase loading of the rGO.

According to the impedance results and taking this into consideration, the interval between 12% and 14% of rGO loading is considered the optimum to obtain the best electroanalytical response. In addition, the fabricated nanocomposites in this interval range show similar electrochemical performance. Consequently, the use of these nanocomposites in this interval range shows that small variations in the nanocomposite composition during the hand-made fabrication process produces changes in their overall electrochemical behaviour and therefore the nanocomposite material presents an excellent reproducibility for analytical purposes.

6.1.1.5 Morphological studies

CSAFM and CM3D techniques were carried out in order to confirm the electrochemical and electroanalytical results obtained for optimized (NPC) and non-optimized or conventionally used (LRC) electrodes, which contain 13% and 20% in rGO loading, respectively.

Firstly, the CSAFM technique was used in order to obtain qualitative information about the size, shape and distribution of the conducting nanomaterial in the nanocomposite structures. Figure 6.8 (A to B) presents the most significant images obtained during the surface study of the NPC and LRC electrodes. After the surface study, it was observed that a low percentage of rGO dispersed into the polymer matrix generates nanocomposites with larger distances between the conductive channels. However, a higher rGO percentage produces nanocomposites with closer conductive channels.

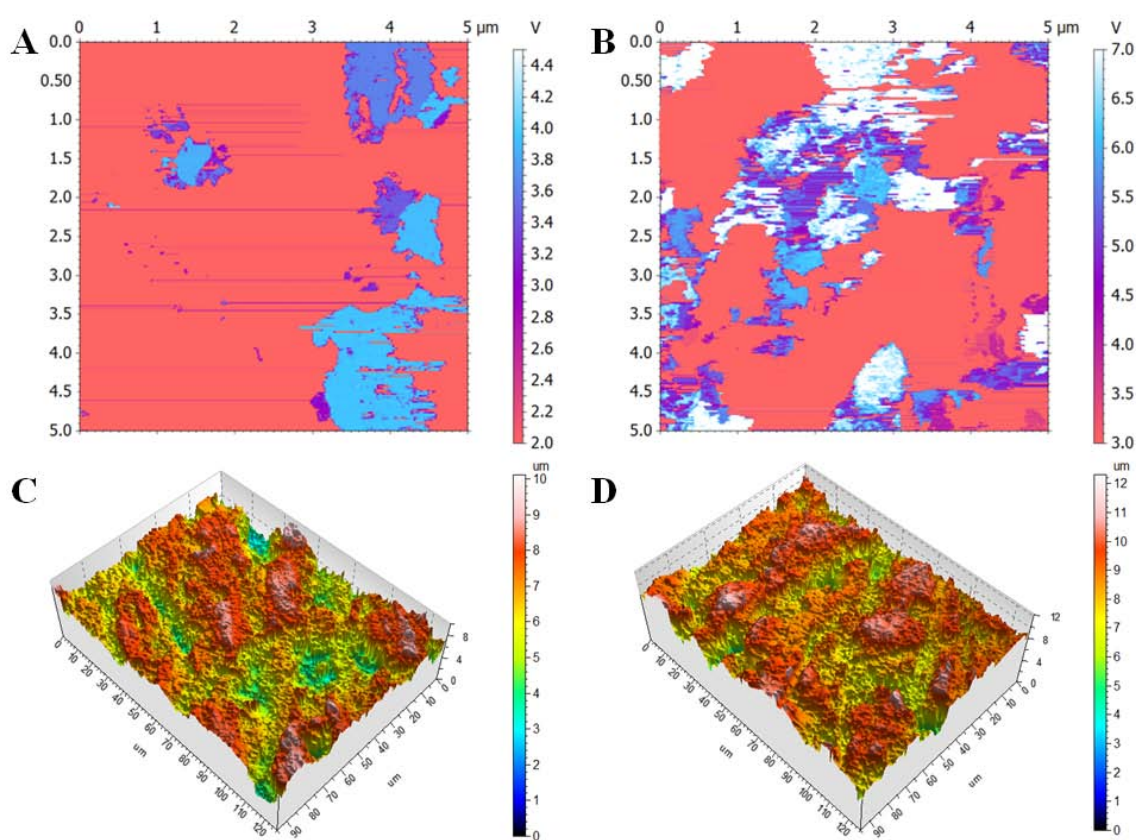


Figure 6.8 Conductance mapping obtained by CSAFM for A) NPC and B) LRC and their corresponding topographic images (C to D) obtained by CM3D.

According to conductive results, CSAFM images allow the observation that even though both materials have a similar microelectrode appearance, the NPC surface (Figure 6.8 A) includes many separated conductive microzones on its surface where the electronic transfer is produced. This fact offers the electrode the possibility to generate radial diffusion where the electroactive species diffuse on its surface by the Edge effect.³⁴ However, for the LRC electrodes (Figure 6.8 B) the linear diffusion seems to

be predominated because the conductive zones are closer with each other. Due to the random structure of the presented nanocomposites, the distance between conductive microzones are not easy to control. Nevertheless, this morphological characterization makes it possible to slightly control the distance between the conductive microzones by a decrease or an increase of the rGO loading.

Afterwards, surface roughnesses of both rGO/epoxy nanocomposite electrodes were also compared by CM3D. Figure 6.8 (C to D) presents significant images obtained during the electrode surface study. When the electrode roughness increases, the probability of more conductive material exposed on the electrode surface also increases and consequently, its electroactive area (A). Confocal results, which are summarized in Table 6.2, presented for LRC electrodes (Figure 6.8 D) a roughness value 34% higher than the optimized-electrodes (NPC electrodes, Figure 6.8 C). These results are consistent with the A values obtained by CV (Table 6.1), where an increment of 35% in A was also achieved for the LRC electrodes.

Finally, CSAFM and CM3D results corroborated that the electroanalytical enhancement of the nanocomposite electrodes with optimized compositions is mainly based to the dispersion of the conductor microzones, conferring behaviours much closer to a microelectrode array. In addition, it has also been demonstrated that through optimization of the graphene/polymer electrode composition it is possible to improve some electroanalytical features, resulting in more effective sensors.

Table 6.2 Roughness values collected from surface analysis. Data are the mean and standard deviation (SD) from 57 profiles of three areas examined in each series (ISO 4287).

Electrodes	rGO (%)	R_a^a (μm)		R_q^b (μm)		R_z^c (μm)	
		Mean	SD	Mean	SD	Mean	SD
NPC	13	0.50	0.11	0.63	0.14	2.57	0.55
LRC	20	0.76	0.12	0.93	0.14	3.71	0.63

^aArithmetical mean deviation of the assessed profile

^bThe root mean square deviation of the assessed profile

^cMaximum height of the profile

6.1.1.6 Electroanalytical performance

Ascorbic acid was used as a model analyte for evaluating the electroanalytical characteristics of the rGO/epoxy nanocomposite sensors, see Figure 6.9. Measurements were carried out at 600 mV *vs.* Ag/AgCl fixed potential, which was previously determined by LSV. The graphene nanocomposite response to changes in concentration of ascorbic acid was evaluated by hydrodynamic amperometric measurements (constant stirring). Different parameters, such as LOD, LOQ and sensitivity were evaluated for the optimum nanocomposite composition (13%) and compared to that obtained with the highest rGO loading, which lose its physical and mechanical stability (20%). Analytical parameters are summarized in Table 6.3. It is worthy to highlight that three different sensors for each nanocomposite composition were evaluated in order to estimate their reproducibility.

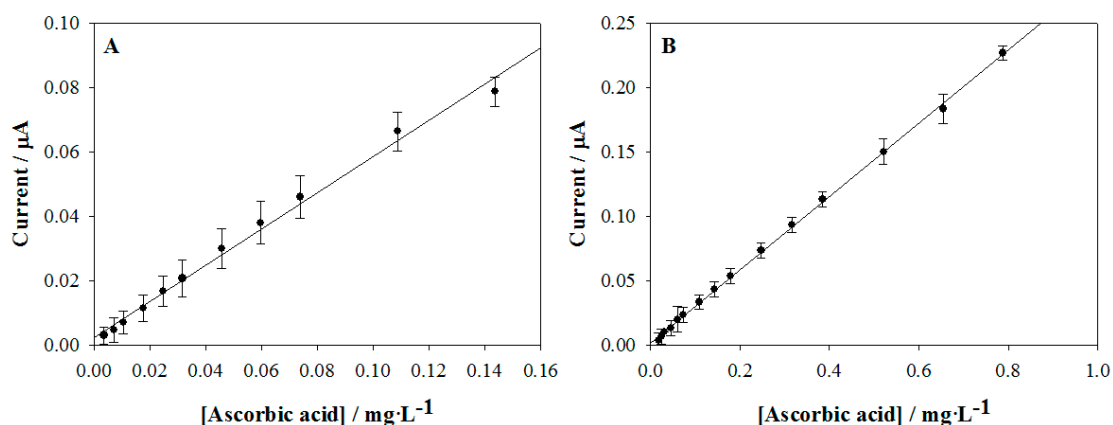


Figure 6.9 Calibration curve of I_p vs. concentration of ascorbic acid for A) NPC and B) LRC. Experimental data are represented with their corresponding error bars ($n=3$) and estimated as a standard deviation. Amperometric analyses were carried out in a 0.01 M $\text{KNO}_3/\text{HNO}_3$ background electrolyte solution; working potential: 600 mV.

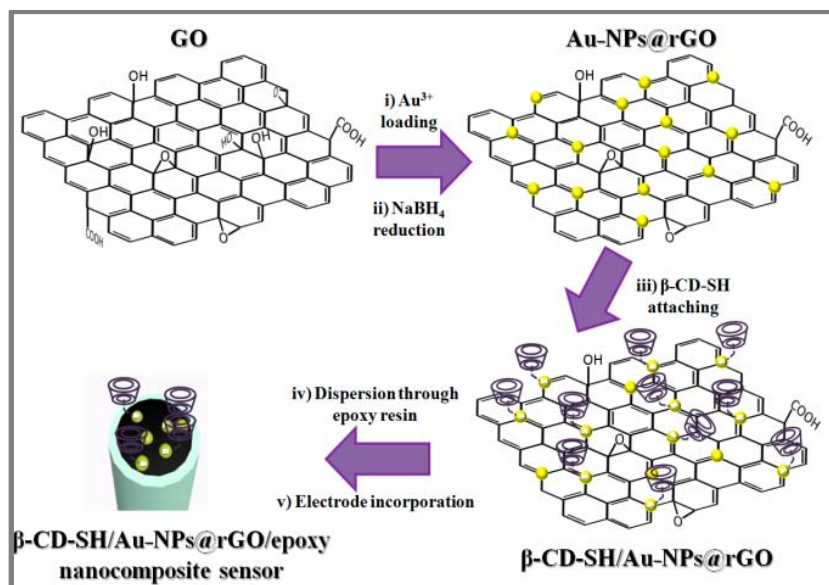
Amperometric results demonstrated that when the rGO loading increases from 13% to 20%, both LOD and LOQ showed a remarkable increase, although the nanocomposites with higher rGO loading contain higher number of transducer particles. These results can be explained since a lower rGO load becomes in a diminution of the signal to noise ratio (C_{dl}), resulting in an 83% and 72% improvement in LOD and LOQ, respectively. Accordingly, these results suggest that an rGO loading of 13% is an optimal composition, since it can achieve a good sensitivity but more importantly, lower limits of detection.

Table 6.3 Amperometric parameters of 13% and 20% of rGO nanocomposite electrodes for ascorbic acid determination in a 0.01 M KNO₃/HNO₃ background electrolyte solution. Working potential: 600 mV vs. Ag/AgCl. LOD and LOQ were calculated three times (n=3) and they are presented with their respectively 95% confidence interval.

Sensor containing	LOD ($\mu\text{g}\cdot\text{L}^{-1}$)	LOQ ($\mu\text{g}\cdot\text{L}^{-1}$)	Sensitivity ($\mu\text{A}\cdot\text{L}\cdot\text{mg}^{-1}$)	r^2 (n=13)
13%	3 ± 2	7 ± 5	0.609	0.999
20%	18 ± 8	25 ± 8	0.284	0.999

Comparing these results with those previously obtained for optimum graphite/epoxy composite sensors (NPC sensors, which contain 15%–16% in graphite loading),¹⁷ better LOD has been obtained with the presented graphene-based nanocomposite sensors. Thus, while graphite-based NPC sensors presented a LOD of $17 \mu\text{g}\cdot\text{L}^{-1}$ for ascorbic acid, this parameter was significantly enhanced for graphene-based NPC sensors. It should be noted that this value is similar to the obtained by the non-optimized rGO-based nanocomposite electrode (LRC electrode), as can be observed in Table 6.3. This fact resulted in an improvement of 0.8 decades of concentration for the model analyte.¹⁷ Under this context, the simple bulk graphite modification for synthesizing the rGO nanomaterial presents important benefits from an analytical point of view, resulting enhanced nanocomposite sensors because of they provide lowest LODs.

6.1.2 Modified graphene-based nanocomposite sensor for the sensitive biorecognition of Thyroxine



Graphical Abstract VII. Simple green methodology to obtain a sensitive biorecognition nanocomposite device for the T_4 detection.

This work reports a new strategy for modifying graphene-based electrochemical nanocomposite sensors for the sensitive amperometric detection of Thyroxine (T_4) using supramolecular chemistry by an inclusion complex with β -Cyclodextrin (β -CD). T_4 is an important biological hormone of iodoamino acid derivative of thyronine, produced in the thyroid gland. Currently, immunoassay methods and high performance liquid chromatography are often used for its determination. These methods are complicated and require expensive instruments. Under this context, electrochemical techniques are facile and easy to automate. Some carbon-based electrodes have also been studied for the determination of T_4 . Nevertheless, graphene-based electrodes have not been directly used for this aim. Accordingly, it is reported the first nanocomposite sensor based on modified-graphene for the sensitive biorecognition of T_4 which exhibits the lowest LOD regarding to those electrochemical methods previously described in literature.

6.1.2.1 Physical characterization of hybrid nanomaterials

Firstly, the feasibility of the GO loading with Au^{3+} and its subsequent reduction through a $NaBH_4$ solution to generate the $Au-NPs@rGO$ nanomaterial was studied. HR-TEM and UV-vis absorbance spectroscopy were employed for this aim.

Figure 6.10 shows different HR-TEM images of GO, Au-NPs@rGO and β -CD-SH/Au-NPs@rGO, respectively. Figure 6.10 A determined that GO was successfully synthesized from the bulk graphite. Figure 6.10 B–C shows a clearly deposition of Au-NPs upon the graphene sheets by loading with Au^{3+} and subsequently *in situ* reduction with NaBH_4 . In addition, a favourable distribution of these nanoparticles on the graphene surface is also observed, as well as a homogeneous size distribution over its surface, without agglomerations of Au-NPs.

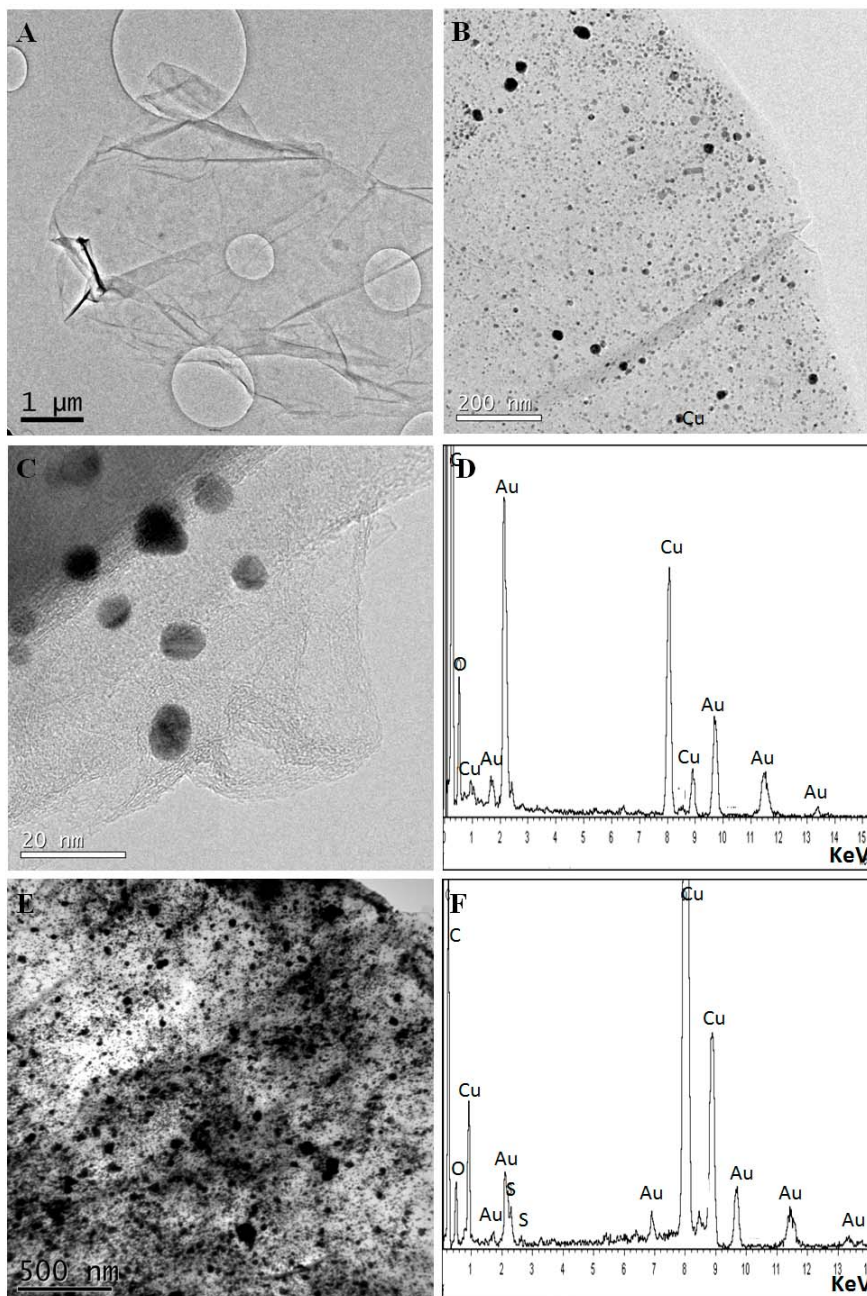


Figure 6.10 HR-TEM images of A) GO; B) Au-NPs@rGO; C) Au-NPs@rGO magnification and D) its corresponding EDS. E) β -CD-SH/Au-NPs@rGO and F) its corresponding EDS spectra.

EDS spectra of Au-NPs@rGO was also carried out in order to determine qualitatively the presence of Au-NPs on the graphene sheets (Figure 6.10 D). Finally, the Au-NPs@rGO was used as a supporting nanomaterial for the attachment of the specific biorecognition agent, the β -CD-SH. The strength of the gold-thiol interactions provided the basis to obtain a robust hybrid-nanomaterial, the β -CD-SH/Au-NPs@rGO, which is shown in Figure 6.10 E. Its EDS spectra (Figure 6.10 F), demonstrated the presence of Au and S on the graphene sheets, verifying the successful attachment of the biorecognition agent on the Au-NPs surface.

At the same time, UV-vis spectra recorded for GO and Au-NPs@rGO can be seen in Figure 6.11. As was explained in § 6.1.1.1, the main spectroscopic features associated with optical absorption in GO are the electronic transitions within $-C=C$ bonds (232 nm) and $-C=O$ bonds (~ 300 nm). After reduction took place under Au^{3+} loading with $NaBH_4$ for Au-NPs@rGO formation, the band associated with $-C=O$ functionality is removed from the spectra while the band located at 232 nm due to in-plane $-C=C$ bonds shifts to the red (268 nm).²⁴ Furthermore, a second band located at 522 nm was observed in the Au-NPs functionalized nanomaterial, which is associated to Au-NPs plasmon band,³⁵ indicating the presence of Au-NPs on the nanostructured carbon material.

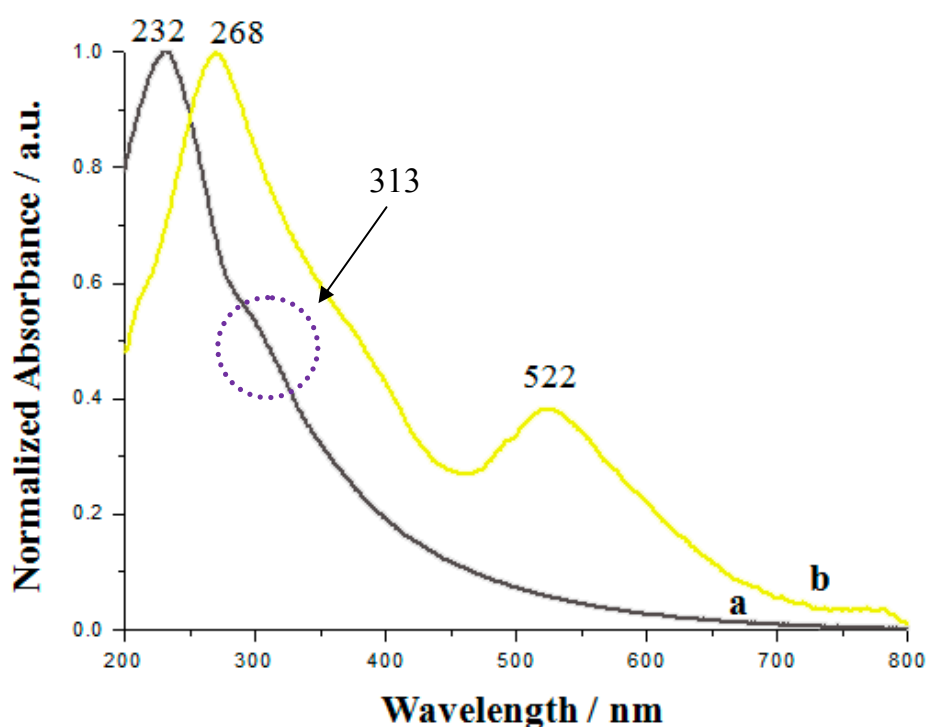


Figure 6.11 Uv-vis spectra recorded for aqueous suspension of a) rGO and b) Au-NPs@rGO.

In agreement with the characterization results, GO was efficiently loaded with Au³⁺ and then *in situ* reduced with NaBH₄ in order to obtain the Au–NPs@rGO nanomaterial, which was used as a support nanomaterial for the successfully incorporation of the thiolated biorecognition agent for electrochemical sensing purposes.

In addition, the quantification of both gold metal content and biorecognition agent was carried out by TGA analysis. Accordingly, TGA results determined an amount of 23.6% in Au–NPs and 12.5% in β–CD-SH deposited on the graphene sheets. Thus, these results verified that an important number of biorecognition agent could be attached on the Au–NPs@rGO surface for obtaining the β–CD-SH/Au–NPs@rGO hybrid-nanomaterial, which will be used as a conducting filler for polymer-based nanocomposite sensors fabrication. This is an amazing result because Au–NPs@rGO loading so many β–CD molecules will have a good opportunity to develop the supramolecular biorecognition and enrichment ability previously at electrochemical detection.

6.1.2.2 Voltammetric studies at the biorecognition electrode

In concordance with the electrical results found in § 6.1.1, 13% of conducting filler hybrid-nanomaterial was dispersed within epoxy resin for NPC–electrodes construction. Having found the optimum composition ratio, the electrochemical responses of 10 μM T₄ in a 0.1 M HCl solution³⁶ at the β–CD-SH/Au–NPs@rGO/epoxy nanocomposite electrode were recorded by CV. On the one hand, Figure 6.12 A shows a pair of well-defined anodic and cathodic peaks (E_{a1}/E_{c1}), which are believed to be due to the redox reaction of Au–NPs. This pair of peaks (E_{a1}/E_{c1}) was found around +0.55 V *vs.* Ag/AgCl (E_{a1}) and +0.40 V *vs.* Ag/AgCl (E_{c1}), corresponding to the formation and subsequent reduction of gold oxide, respectively.³⁷ On the other hand, the electrochemical behaviour of T₄ at the surface of the presented electrode is also shown in Figure 6.12. A well-defined oxidation peak (E_{a2}) appeared at around +0.85 V *vs.* Ag/AgCl for the β–CD-SH/Au–NPs@rGO/epoxy nanocomposite electrode, which is in concordance with the previously reported carbon-based electrodes in this acidic medium.³⁸

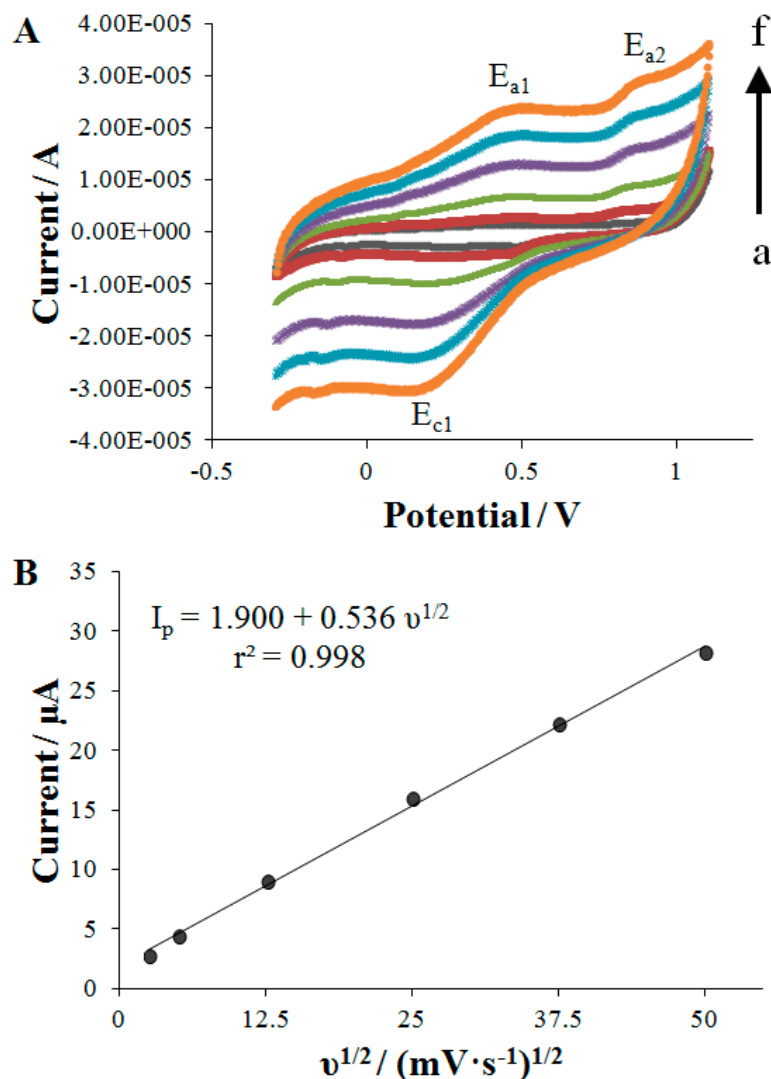


Figure 6.12 A) Influence of scan rate from a) $10 \text{ mV} \cdot \text{s}^{-1}$ to b) $100 \text{ mV} \cdot \text{s}^{-1}$ for $10 \mu\text{M}$ of T_4 sensing at the $\beta\text{-CD-SH/Au-NPs@rGO/epoxy}$ nanocomposite electrode. B) Anodic peak currents vs. square root of the scan rates. CV experiments were carried out in a 0.1 M HCl solution.

Finally, Figure 6.12 A also depicts the influence of scan rate ($10\text{--}100 \text{ mV} \cdot \text{s}^{-1}$) on the electrochemical response of T_4 . The peak current is dependent upon the electrochemical response of T_4 on the electrode surface. Multiple CVs confirmed the irreversibility oxidation of T_4 , which also occur in nature, since no reverse peaks were observed. After the successive voltammetric cycles, the anodic current response for T_4 gradually decreased, indicating that the reduction product blocked the electrode surface and, consequently, the possibility to determine more T_4 present in the solution. Furthermore, the anodic peak currents varied linearly with the square root of the scan rates, as is shown in Figure 6.12 B, indicating a diffusion-controlled process of the oxidation of T_4 .

6.1.2.3 Electrochemical behaviour of the different graphene-based electrodes

Prior to sensing of T_4 , different graphene-epoxy nanocomposite electrodes were electrochemically characterized for their material composition, see Figure 6.13. Thereby, rGO/epoxy, Au-NPs@rGO/epoxy and β -CD-SH/Au-NPs@rGO/epoxy nanocomposite electrodes were fabricated in order to compare their electrochemical performance. As was mentioned above, 13% of conducting nanofiller material was dispersed within epoxy resin for NPC-electrode construction (see § 6.1.1). Cyclic voltammograms were taken under the same experimental conditions (scan rate of $50 \text{ mV}\cdot\text{s}^{-1}$, which was found as the optimal from Figure 6.12) in the presence of the benchmark $[\text{Fe}(\text{CN})_6]^{3-/4-}$ redox couple since it is very sensitive to the electrode surface characteristics. Comparing to the bare rGO/epoxy nanocomposite electrode, it is possible to observe a peak height increased with the incorporation of Au-NPs due to their electrocatalytic effect. However, when the recognition agent (β -CD-SH) was attached upon these nanoparticles, current height value significantly decreased mainly caused by the steric hindrance of these molecules on the electrode surface, as well as its insulating behaviour. In spite of that, the β -CD-SH/Au-NPs@rGO/epoxy nanocomposite electrode still maintains an excellent electrochemical performance.

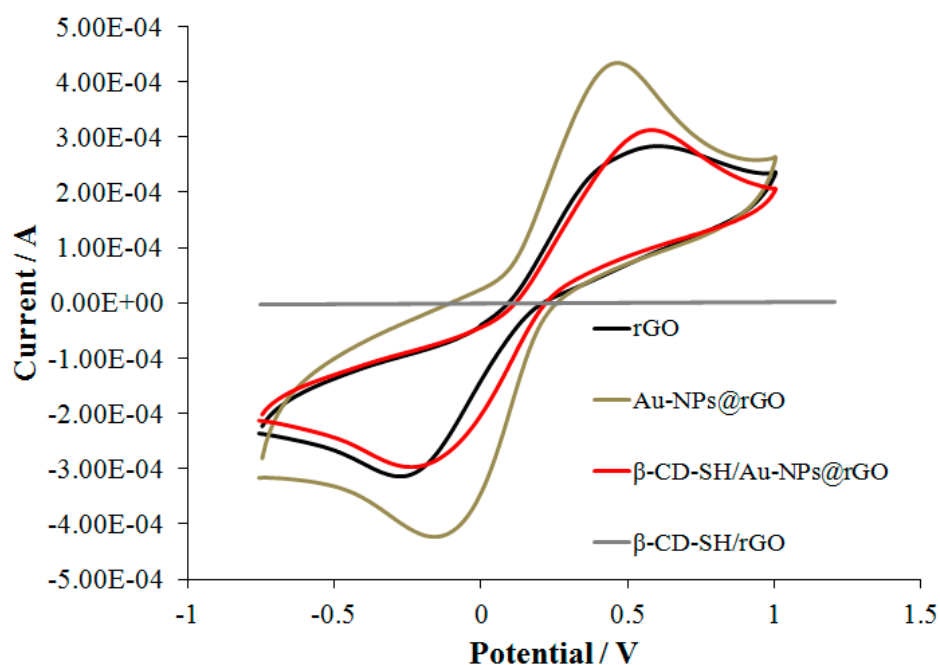


Figure 6.13 CV of the different graphene-based nanocomposite electrodes in a 0.1 M KCl containing 0.01 M $[\text{Fe}(\text{CN})_6]^{3-/4-}$. Scan rate: $50 \text{ mV}\cdot\text{s}^{-1}$.

Simultaneously, a fourth nanocomposite material, the β -CD-SH/rGO/epoxy electrode was also fabricated in order to demonstrate the importance of the Au-NPs as a supporting nanotemplate for the biorecognition agent through the graphene layers. As it is shown in Figure 6.13, the introduction of the same amount of β -CD-SH obtained by TGA in powder form (see § 6.1.2.1) resulted in a strong loss of conductivity. These results may be explained since the β -CD-SH can directly interact with the conducting rGO filler and blocked the conducting transfer, obtained a similar behaviour of GO, which is a non-conductor material. Under this context, the introduction of the Au-NPs is a must to keep the conduction of the nanocomposite device.

Finally, the importance to introduce the β -CD-SH as a biorecognition agent in the nanocomposite system has been also verified in terms of T_4 oxidation detection. For this aim, the three different conducting graphene-epoxy nanocomposite electrodes (rGO/epoxy, Au-NPs@rGO/epoxy and β -CD-SH/Au-NPs@rGO/epoxy) were electrochemically characterized by CV under the presence of $10 \mu\text{M}$ T_4 in a 0.1 M HCl solution, as is shown in Figure 6.14.

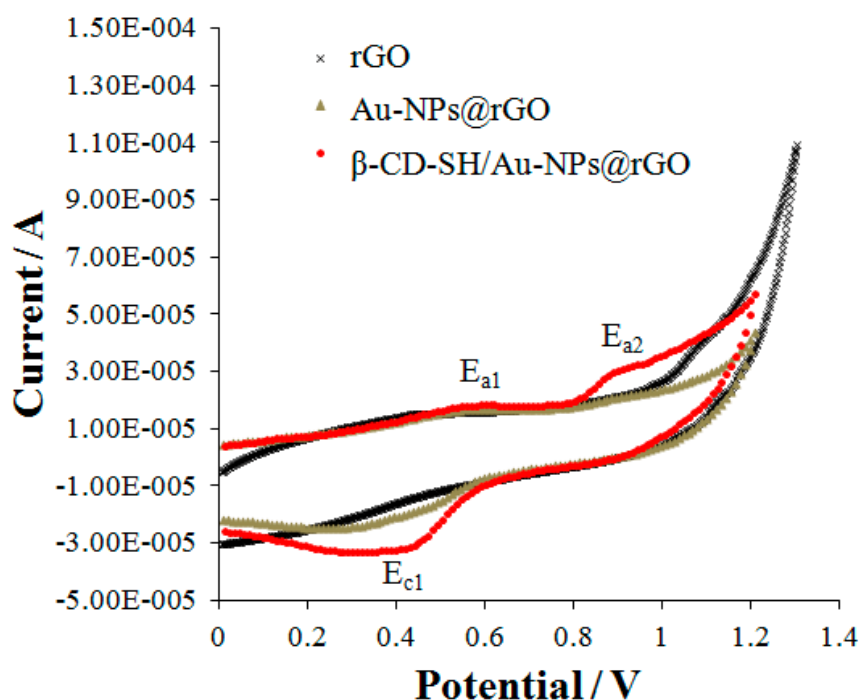


Figure 6.14 CV of the different graphene-based nanocomposite electrodes under the presence of $10 \mu\text{M}$ of T_4 in a 0.1 M HCl solution. Scan rate: $50 \text{ mV} \cdot \text{s}^{-1}$.

While both electrodes containing Au–NPs (Au–NPs@rGO/epoxy and β –CD–SH/Au–NPs@rGO/epoxy nanocomposite electrodes) presents a pair of well-defined anodic and cathodic peaks (E_{a1}/E_{c1}), which may be attributed to the oxidation and the consequently reduction of the Au–NPs, the bare rGO/epoxy nanocomposite electrode does not show this pair of peaks, as was expected. These results confirm again the successful deposition of the Au–NPs on the graphene sheets for Au–NPs@rGO/epoxy and β –CD–SH/Au–NPs@rGO/epoxy electrodes fabrication. In addition, whereas the introduction of the biorecognition agent on the device considerable increases the current signal of the T_4 oxidation (E_{a2}) at the β –CD–SH/Au–NPs@rGO/epoxy electrode, the response of T_4 on the bare rGO/epoxy and Au–NPs@rGO/epoxy electrode surfaces appeared weak and broad. This increase on the oxidation peak current indicated that there was a strong supramolecular interaction between the biorecognition agent and the T_4 , obtaining then a 40% improvement in the signal in comparison to the electrodes without the biorecognition agent. Thereby, the presented biorecognition system based on supramolecular interaction between β –CD and T_4 has been used for amperometric sensing.

6.1.2.4 Electroanalytical performance at the biorecognition sensor

It is worthy to note that the CV method for the determination of T_4 presented the limitation of surface fouling by adsorption during the pre-concentration process. In order to develop more accurate methods for detection of T_4 , hydrodynamic amperometric experiments were carried out, enabling a more sensitive technique rather than the CV methodology. Therefore, an amperometric calibration curve for the β –CD–SH/Au–NPs@rGO/epoxy sensor in a 0.1 M HCl solution with subsequent additions of a 1.0 μ M T_4 aliquots was performed. The polarization potential applied was +0.85 V, following the results obtained from Figure 6.12.

As is depicted in Figure 6.15, the calibration curve obtained was, I_p (nA) = $-2.458 + 2.485 [T_4]$ (nM), with $r^2 = 0.999$ (n=9), together with a LOD of 1.00 ± 0.02 nM and a LOQ of 2.00 ± 0.03 nM. LOD and LOQ were calculated three times (n=3) and they are presented with their respectively 95% confidence interval.

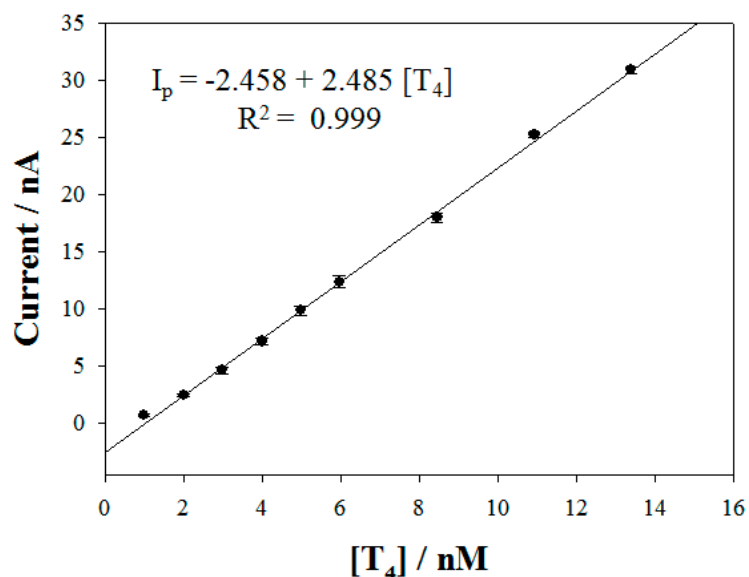


Figure 6.15 Calibration curve obtained from the representation of I_p vs. $[T_4]$ was carried out by hydrodynamic amperometry in a 0.1 M HCl solution; E_{app} : +0.85 V.

The LOD of the novel nanocomposite sensor containing the biorecognition agent β -CD was obviously improved regarding to those previously referenced electrodes using another carbon materials (modified or not) as working electrodes, which are summarized in Table 6.4. This analytical enhancement may be attributed from the combination of two factors: the 2D nanofiller material and the biorecognition agent, promoting electron transfer in the oxidation of T_4 on the electrode surface.

Table 6.4 Comparison of sensing performance for T_4 determination with different carbon-based electrochemical electrodes previously referenced.

Electrodes	Tool	Redox potential (V)	LOD (nM)	References
PHE mediated CPE	CV	0.78 / Ox.	2500	[36]
PVP modified CPE (in CTAB media)	CV	0.42 / Ox.	80	[39]
MWCNTs-DHP film modified GCE	DPV	0.80 / Ox.	6.5	[40]
Edge-Plane PGE	CV	0.82 / Ox.	3.0	[38]
Unmodified SPCE	DPV	0.30 / Ox.	3.0	[41]
β -CD-SH/Au-NPs@rGO contained in CPE	Amperometry	0.85 / Ox.	1.0	This work

6.1.2.4 Stability and Reproducibility

The stability and reproducibility of the biorecognition system were also evaluated. Firstly, to investigate the stability of the sensors, five successive measurements of 10 nM T₄ were made at the same sensor, refreshed after each measurement by successive CV sweeps between -0.3 and +1.2 V vs. Ag/AgCl at scan rate of 50 mV·s⁻¹. After five successive amperometric experiments carried out under the same experimental conditions, the relative standard deviation (RSD) was 4.6%. Secondly, three different β-CD-SH/Au-NPs@rGO/epoxy sensors were prepared and evaluated in order to compare their amperometric current responses. For this aim, 10 nM T₄ was evaluated in three different nanocomposite electrodes. The resulting RSD was 0.6%, confirming that the preparation method was highly reproducible.

Finally, multiple calibration experiments were also performed with these three nanocomposite sensors after polishing in order to estimate the reproducibility of the electrode surface. Contrary to most studies in which the (bio)recognition agents are attached on the electrode surface, in the presented work the biorecognition agent is dispersed the polymeric matrix and consequently is fixed in bulk. Experiments after five polishing processes demonstrated that the β-CD-SH/Au-NPs@rGO hybrid-nanomaterial was homogeneously well dispersed within the epoxy matrix, and no significant differences in sensitivity were observed (RSD of 3.8%). Therefore, thanks to surface regeneration by simple polishing, a homogeneous distribution of the modifier agents in the nanocomposite would be obtained after each polishing, which guarantees that a reproducible electrode surface is obtained and the properties of the biorecognition system are maintained.

Finally, these results allow the presented biorecognition system to be comfortably integrated as a detector in an automated flow analyzer, for example based on flow injection analysis (FIA) for the rapid and *in situ* detection of T₄, which might be applied in interesting clinical, pharmacological and biomedicine investigations.

6.2 Conclusions

After experiments, some conclusions have been extracted from these results:

- GO was successfully synthesized from graphite and then efficiently reduced with ascorbic acid to obtain the rGO, which was used as a filler nanomaterial for the construction of different nanocomposite electrodes based on rGO/epoxy.
- The simple bulk graphite exfoliation for synthesizing the graphene 2D nanomaterial (rGO) presents important benefits from an analytical point of view, resulting enhanced nanocomposite sensors with lower LODs for the studied reference analyte.
- Electrical (percolation curve) and electrochemical (CV and EIS) tools have used for first time to determine the optimum rGO/polymer composition ratio, which is that composition that just falls in the NPC zone.
- The optimization of the nanocomposite composition ratio has allowed the improvement of different electroanalytical parameters in graphene-based nanocomposite sensors, such as detection limits, quantification limits, sensitivity, stability and reproducibility of the analytical signal.
- Morphological studies have corroborated that a lower loading of conductor filler nanomaterial regarding to the maximum loading gives to the electrode an optimum separation of conductor microzones in the final nanocomposite device (rGO/epoxy) is obtained, obtaining a microelectrode array behaviour.
- GO has been successfully modified and reduced by Au^{3+} loading for the *in situ* incorporation of Au-NPs on the GO sheets, obtaining the new Au-NPs@rGO hybrid-nanomaterial, which was used as a template for the incorporation of a thiolated biorecognition agent, the β -CD-SH.
- For first time, the new β -CD-SH/Au-NPs@rGO filler hybrid-nanomaterial was integrated in a polymeric nanocomposite for the sensitive amperometric biorecognition of T_4 . Experiments demonstrated an excellent electrochemical response of the presented NPC-based sensors, obtaining the best LOD compared to those electrochemical electrodes found in literature.

6.3 References

1. Švancara, I.; Vytřas, K.; Barek, J.; Zima, J., Carbon paste electrodes in modern electroanalysis. *Critical Reviews in Analytical Chemistry* **2001**, *31* (4), 311-345.
2. Downard, A. J., Electrochemically assisted covalent modification of carbon electrodes. *Electroanalysis* **2000**, *12* (14), 1085-1096.
3. Zima, J.; Švancara, I.; Barek, J.; Vytřas, K., Recent advances in electroanalysis of organic compounds at carbon paste electrodes. *Critical Reviews in Analytical Chemistry* **2009**, *39* (3), 204-227.
4. Adams, R., Carbon paste electrodes. *Analytical Chemistry* **1958**, *30* (9), 1576-1576.
5. Alegret, S.; Céspedes, F.; Martínez-Fàbregas, E.; Martorell, D.; Morales, A.; Centelles, E.; Muñoz, J., Carbon-polymer biocomposites for amperometric sensing. *Biosensors and Bioelectronics* **1996**, *11* (1), 35-44.
6. Wang, J.; Musameh, M., Carbon nanotube/teflon composite electrochemical sensors and biosensors. *Analytical Chemistry* **2003**, *75* (9), 2075-2079.
7. Al-Mashat, L.; Shin, K.; Kalantar-Zadeh, K.; Plessis, J. D.; Han, S. H.; Kojima, R. W.; Kaner, R. B.; Li, D.; Gou, X.; Ippolito, S. J., Graphene/polyaniline nanocomposite for hydrogen sensing. *The Journal of Physical Chemistry C* **2010**, *114* (39), 16168-16173.
8. Shao, Y.; Zhang, S.; Engelhard, M. H.; Li, G.; Shao, G.; Wang, Y.; Liu, J.; Aksay, I. A.; Lin, Y., Nitrogen-doped graphene and its electrochemical applications. *Journal of Materials Chemistry* **2010**, *20* (35), 7491-7496.
9. Chen, D.; Tang, L.; Li, J., Graphene-based materials in electrochemistry. *Chemical Society Reviews* **2010**, *39* (8), 3157-3180.
10. Martín, A.; Escarpa, A., Graphene: the cutting-edge interaction between chemistry and electrochemistry. *TrAC Trends in Analytical Chemistry* **2014**, *56*, 13-26.
11. Liu, Y.; Dong, X.; Chen, P., Biological and chemical sensors based on graphene materials. *Chemical Society Reviews* **2012**, *41* (6), 2283-2307.
12. Shin, H. J.; Kim, K. K.; Benayad, A.; Yoon, S. M.; Park, H. K.; Jung, I. S.; Jin, M. H.; Jeong, H. K.; Kim, J. M.; Choi, J. Y., Efficient reduction of graphite oxide by sodium borohydride and its effect on electrical conductance. *Advanced Functional Materials* **2009**, *19* (12), 1987-1992.

13. Fan, Y.; Liu, J.-H.; Yang, C.-P.; Yu, M.; Liu, P., Graphene–polyaniline composite film modified electrode for voltammetric determination of 4-aminophenol. *Sensors and Actuators B: Chemical* **2011**, *157* (2), 669-674.

14. Salavagione, H. J.; Díez-Pascual, A. M.; Lázaro, E.; Vera, S.; Gómez-Fatou, M. A., Chemical sensors based on polymer composites with carbon nanotubes and graphene: the role of the polymer. *Journal of Materials Chemistry A* **2014**, *2* (35), 14289-14328.

15. Balogun, Y. A.; Buchanan, R. C., Enhanced percolative properties from partial solubility dispersion of filler phase in conducting polymer composites (CPCs). *Composites Science and Technology* **2010**, *70* (6), 892-900.

16. McCreery, R. L., Carbon electrodes: structural effects on electron transfer kinetics. *Electroanalytical Chemistry* **1991**, *17*, 221-374.

17. Montes, R.; Bartrolí, J.; Céspedes, F.; Baeza, M., Towards to the improvement of the analytical response in voltammetric sensors based on rigid composites. *Journal of Electroanalytical Chemistry* **2014**, *733*, 69-76.

18. Muñoz, J.; Bartrolí, J.; Céspedes, F.; Baeza, M., Influence of raw carbon nanotubes diameter for the optimization of the load composition ratio in epoxy amperometric composite sensors. *Journal of Material Science* **2015**, *50* (2), 652-661.

19. Goncalves, G.; Marques, P. A.; Granadeiro, C. M.; Nogueira, H. I.; Singh, M.; Gracio, J., Surface modification of graphene nanosheets with gold nanoparticles: the role of oxygen moieties at graphene surface on gold nucleation and growth. *Chemistry of Materials* **2009**, *21* (20), 4796-4802.

20. Jasuja, K.; Berry, V., Implantation and growth of dendritic gold nanostructures on graphene derivatives: electrical property tailoring and Raman enhancement. *ACS Nano* **2009**, *3* (8), 2358-2366.

21. Fang, Y.; Guo, S.; Zhu, C.; Zhai, Y.; Wang, E., Self-Assembly of Cationic Polyelectrolyte-Functionalized Graphene Nanosheets and Gold Nanoparticles: A Two-Dimensional Heterostructure for Hydrogen Peroxide Sensing. *Langmuir* **2010**, *26* (13), 11277-11282.

22. Li, D.; Müller, M. B.; Gilje, S.; Kaner, R. B.; Wallace, G. G., Processable aqueous dispersions of graphene nanosheets. *Nature Nanotechnology* **2008**, *3* (2), 101-105.

23. Fernandez-Merino, M.; Guardia, L.; Paredes, J.; Villar-Rodil, S.; Solis-Fernandez, P.; Martinez-Alonso, A.; Tascon, J., Vitamin C is an ideal substitute for hydrazine in the reduction of graphene oxide suspensions. *The Journal of Physical Chemistry C* **2010**, *114* (14), 6426-6432.
24. Zhang, J.; Yang, H.; Shen, G.; Cheng, P.; Zhang, J.; Guo, S., Reduction of graphene oxide via L-ascorbic acid. *Chemical Communications* **2010**, *46* (7), 1112-1114.
25. Ferrari, A.; Robertson, J., Interpretation of Raman spectra of disordered and amorphous carbon. *Physical Review B* **2000**, *61* (20), 14095.
26. Tuinstra, F.; Koenig, J. L., Raman spectrum of graphite. *The Journal of Chemical Physics* **1970**, *53* (3), 1126-1130.
27. Stankovich, S.; Dikin, D. A.; Piner, R. D.; Kohlhaas, K. A.; Kleinhammes, A.; Jia, Y.; Wu, Y.; Nguyen, S. T.; Ruoff, R. S., Synthesis of graphene-based nanosheets via chemical reduction of exfoliated graphite oxide. *Carbon* **2007**, *45* (7), 1558-1565.
28. Scher, H.; Zallen, R., Critical density in percolation processes. *The Journal of Chemical Physics* **1970**, *53* (9), 3759-3761.
29. Laoire, C. O.; Mukerjee, S.; Abraham, K.; Plichta, E. J.; Hendrickson, M. A., Elucidating the mechanism of oxygen reduction for lithium-air battery applications. *The Journal of Physical Chemistry C* **2009**, *113* (46), 20127-20134.
30. Banerjee, S.; Hemraj-Benny, T.; Wong, S. S., Covalent surface chemistry of single-walled carbon nanotubes. *Advanced Materials* **2005**, *17* (1), 17-29.
31. Montes, R.; Bartrolí, J.; Baeza, M.; Céspedes, F., Improvement of the detection limit for biosensors: Advances on the optimization of biocomposite composition. *Microchemical Journal* **2015**, *119*, 66-74.
32. Olivé-Monllau, R.; Esplandiu, M. J.; Bartrolí, J.; Baeza, M.; Céspedes, F., Strategies for the optimization of carbon nanotube/polymer ratio in composite materials: applications as voltammetric sensors. *Sensors and Actuators B: Chemical* **2010**, *146* (1), 353-360.
33. Palasantzas, G.; Backx, G., Roughness effects on the double-layer charge capacitance: the case of Helmholtz layer induced roughness attenuation. *Surface Science* **2003**, *540* (2), 401-406.
34. Banks, C. E.; Davies, T. J.; Wildgoose, G. G.; Compton, R. G., Electrocatalysis at graphite and carbon nanotube modified electrodes: edge-plane sites and tube ends are the reactive sites. *Chemical Communications* **2005**, (7), 829-841.

35. Huang, J.; Zhang, L.; Chen, B.; Ji, N.; Chen, F.; Zhang, Y.; Zhang, Z., Nanocomposites of size-controlled gold nanoparticles and graphene oxide: formation and applications in SERS and catalysis. *Nanoscale* **2010**, 2 (12), 2733-2738.

36. Raj, M. A.; John, S. A., Assembly of gold nanoparticles on graphene film via electroless deposition: spontaneous reduction of Au³⁺ ions by graphene film. *RSC Advances* **2015**, 5 (7), 4964-4971.

37. Khafaji, M.; Shahrokhian, S.; Ghalkhani, M., Electrochemistry of Levo-Thyroxine on Edge-Plane Pyrolytic Graphite Electrode: Application to Sensitive Analytical Determinations. *Electroanalysis* **2011**, 23 (8), 1875-1880.

38. Chitravathi, S.; Kumara Swamy, B. E.; Chandra, U.; Mamatha, G. P.; Sherigara, B. S., Electrocatalytic oxidation of sodium levothyroxine with phenyl hydrazine as a mediator at carbon paste electrode: A cyclic voltammetric study. *Journal of Electroanalytical Chemistry* **2010**, 645 (1), 10-15.

39. He, Q.; Dang, X.; Hu, C.; Hu, S., The effect of cetyltrimethyl ammonium bromide on the electrochemical determination of thyroxine. *Colloids and Surfaces B: Biointerfaces* **2004**, 35 (2), 93-98.

40. Wu, K.; Ji, X.; Fei, J.; Hu, S., The fabrication of a carbon nanotube film on a glassy carbon electrode and its application to determining thyroxine. *Nanotechnology* **2004**, 15 (3), 287.

41. Das, A.; Sangaranarayanan, M., Electroanalytical Sensor Based on Unmodified Screen-Printed Carbon Electrode for the Determination of Levo-Thyroxine. *Electroanalysis* **2014**.

CHAPTER VII

**General Conclusions and
Future Perspectives**

CHAPTER VII

General Conclusions and Future Perspectives

Nanocomposite (bio)sensors based on nanostructured carbon materials, such as carbon nanotubes (CNTs) and graphene, have experienced a huge advance over recent years due mainly to the significant advantages provided by these materials. Nevertheless, characterization and optimization of each component constituting these nanocomposites have remained in the background. A large number of objectives were outlined in the presented thesis, which are based fundamentally on defining new approaches and establishing new characterization protocols with the goal of developing more efficient nanocomposite (bio)sensors from an electrochemical point of view. This study builds on the many similarities shared by composites with microelectrode arrays, referring to their electrochemical characteristics. Assuming as a starting point that both the analytical quality as the reproducibility of CNT-based amperometric nanocomposite (bio)sensors depend on the nature of the raw CNT sample, in this work it has been demonstrated that the optimization of the electrochemical transducer is decisive for obtaining an improved analytical response of the final sensor. In addition, achieved the optimum composition, the inclusion of different nanoparticles (NPs) in/on/into the composite matrix is able to considerably enhance their electroanalytical performance thanks to the resulting electrocatalytic effect, favouring the development of more sensitive and selective devices and widening the field of potential analytical applications.

7.1 General Conclusions

Based on the results obtained in this thesis, it has been demonstrated the importance of optimizing the composition ratio of each component contained in the composite material aimed at developing enhanced electrochemical transducers for sensing purposes. The implementation of a valid characterization protocol to optimize the nanocomposite composition ratio has been feasible through the systematic application

of electrical, electrochemical, spectroscopic, morphological and analytical techniques. Throughout the work performed, diverse techniques such as Electrochemical Impedance Spectroscopy (EIS), Cyclic Voltammetry (CV), Current Sensing Atomic Force Microscopy (CSAFM) and Confocal Microscopy 3D (CM3D), have enabled the optimization of different types of MWCNTs dispersed within epoxy resin (Epo-Tek H77), before and after their functionalization with different NPs.

EIS technique has provided to be a powerful tool to characterize the optimum composition ratio in nanocomposite electrodes based on nanostructured carbon materials for electrochemical sensing approaches. Impedance spectra provide relevant information about: (i) ohmic resistance (R_{Ω}), parameter which is related to the percolation resistivity, (ii) charge transfer resistance (R_{ct}), which is inversely proportional with the heterogeneous electron transfer rate and also depends on the electrochemical surface reactivity of the electrodes and especially (iii) double-layer capacitance (C_{dl}), which is directly related to the charging or background current and thus, it is a parameter that must be reduced to enhance the signal-to-noise ratio.

These physical parameters are relevant on the final electroanalytical response of the nanocomposite material and thus, they allow a proper evaluation to discern the composition which satisfies the analytical requirements demanded for an electrochemical (bio)sensor, such as high sensitivity, fast response and low limit of detection. Both electrical and electrochemical studies are in agreement with the optimum composition ratio, which is the one that falls on the near-percolation zone (the NPC zone) because this composition presents an agreement between low resistances and low signal-to-noise ratios.

The implementation of various tools to characterize the physical properties of the different MWCNTs samples, including length, diameter and purity, has determined that the obtained values were strongly different from the ones provided by the suppliers, being this difference more emphasized in length and diameter. The application of the characterization protocol developed during this Thesis on different series of MWCNT-based nanocomposite electrodes with distinctive MWCNTs nature has demonstrated that while the MWCNT diameter is a key parameter which modifies the percolation behaviour and electrochemical response, the MWCNT purity does not provide significant changes in optimum composition ratio, remaining unaltered independent of

the acidic treatment method applied. In addition, the acidic treatments used for MWCNT purification have proven to be neither necessary nor efficient to determine directly analytes by electrochemical techniques, obtaining better analytical responses when the non-purified MWCNTs were used.

The optimum nanocomposite composition ratios (NPC zone) obtained by the electrical characterization were also confirmed by electrochemical techniques and demonstrated that these strongly depends on the MWCNTs nature. Therefore, an optimum characterization of the raw carbon material before being applied for amperometric (bio)sensors is a must to achieve improved devices from an electroanalytical point of view.

MWCNTs dispersed in an inert matrix provide attractive electrochemical properties since the polymeric matrix, together with the MWCNTs, confer mechanical robustness and high electric conductivity to the final nanocomposite electrode. Moreover, their high malleability before being hardened makes them an easy incorporation of a variety of NPs and recognition agents.

Intermatrix Synthesis (IMS) technique has been proposed as a potential environmentally friendly route to functionalize the optimum composition of MWCNT/epoxy nanocomposite electrodes with a wide range of nanoparticles (NPs) to obtain sensitive amperometric sensors. The proposed synthesis methodology offers a customized preparation of modified-nanocomposite electrodes by three different routes: (i) *in situ* functionalization of MWCNTs surface previously to construction of nanocomposite; (ii) incorporation and dispersion of powder NPs within nanocomposite matrix (in bulk) and (iii) *in situ* functionalization of nanocomposite electrode surface. These methodologies allow the modified-electrodes to be used as sensitive amperometric nanocomposite sensors, showing an enhancement on some physical parameters, such as higher peak heights and electroactive areas, lower resistances and excellent signal-to-noise ratio compared to those non-modified.

Modifications of MWCNT-based nanocomposite electrodes with different types of NPs, such as Functional Metal Nanoparticles (FMNPs), Quantum Dots (QDs) and Metal Oxide Nanoparticles (MO-NPs) have been successfully obtained by IMS technique. They present, respectively, the following electrocatalytic performance: (i) a decrease in

overpotentials; (ii) higher distances between conductor microzones through the insulating polymer, behaving as a microelectrode array and (iii) an enhancement on current height peaks. Those electrocatalytic effects became in more effective sensors which involve lower LODs for their corresponding analytes.

In this sense, the incorporation of different types of NPs demonstrated a great electrocatalytic effect to determine different analytes. While a 3:2 ratio of Au–NPs and Pd–NPs incorporated in MWCNT/epoxy nanocomposite sensors demonstrated an enhanced response to determine hydrogen peroxide, the catalytic activity of the CuO–NPs in the modified-nanocomposite sensors for free chlorine detection was suitable to determine traces in the order of parts per billion ($\mu\text{g}\cdot\text{L}^{-1}$), around a decade of concentration less than the obtained by the non-modified sensors. On the other hand, the incorporation of CdS–QDs attached upon MWCNTs opens a new way to obtain advanced hand-made microelectrode array nanocomposites where the separation of the conductive microzones can be generated by their incorporation, resulting in more sensitive sensors capable to detect traces of different analytes, such as hydrogen peroxide and ascorbic acid.

On the other hand, graphene oxide (GO) was successfully synthesized from the natural graphite powder and reduced by ascorbic acid in order to obtain the reduced graphene oxide (rGO), which was used for first time in our research group as a conducting nanofiller material for the fabrication of electrochemical sensors based on epoxy nanocomposites. In order to demonstrate the feasibility of this synthesis, different spectroscopic tools, such as UV-vis and Raman, were employed as complementary techniques to those already used for MWCNTs characterization.

Under this context, the leading characterization protocol developed for the optimization of MWCNT-based nanocomposite sensors could be applied for the new 2D nanofiller material (rGO). The optimum rGO/epoxy composition ratio was found between 12% and 14%, higher than those nanocomposite materials based on 1D nanomaterials (MWCNTs), which their composition ratios varied between 5% and 12% depending on the nature of the raw MWCNT sample. Based on previous works developed in our research group, this optimum composition is lower than those composites based on 3D carbon material (graphite) as conducting filler, where their optimum composition ratio is located around 15% in graphite. Accordingly, the

optimum composition zone (or NPC zone) was shifted to higher loads of (nano)filler material with increasing the dimensions of the (nano)structured carbon material.

Gold Nanoparticles (Au-NPs) decorating nanostructured carbon materials have demonstrated to be a consistent support for attaching thiolated molecules, which may be used as (bio)recognition agents. The strength of the gold-thiol interactions provided the basis to fabricate a robust hybrid-nanomaterial, the β -CD-SH/Au-NPs@rGO. This novel nanofiller material has been successfully used for the sensitive biorecognition of Thyroxine (T_4). Contrary to many research works where the (bio)recognition agent is directly incorporated on the electrode surface, the fact that the biorecognition agent contained on the nanofiller hybrid-material is incorporated within the polymeric matrix provides some attractive benefits as a renewable sensor surface by a simple polishing procedure. The supramolecular interaction between biorecognition agent and analyte (β -CD and T_4 , respectively) together with the graphene on the sensing surface favours the transfer of electrons between electroactive species, obtaining the most sensitive electrochemical sensor for T_4 detection with the lowest LOD if it is compared to different carbon-based electrochemical sensors found in literature.

7.2 Future Perspectives

The exploitation of carbon nanotubes as well as graphene in the design of electrochemical (bio)sensors is still in its beginnings. Future efforts should aim at better understanding the structural-electrochemical reactivity of their respective modified-sensors and the factors that govern the electron-transfer kinetics of these attractive devices.

In addition, the presented Thesis opens up an attractive perspective in the characterization, optimization and functionalization of nanocomposite sensors based on different nanostructured carbon materials. It has been built a consistent characterization protocol to optimize MWCNT/epoxy and rGO/epoxy electrochemical nanocomposite (bio)sensors for improving their electroanalytical performance as well as simple green routes for their tunability. Under this context, it is believed that this Thesis will allow for extension of this approach for various polymeric matrices as well as other 1D and 2D nanomaterials related to the carbon nanotubes and graphene family.

The future applications of the developed nanocomposite sensors based on CNTs and graphene require further developments in the following directions:

- A further characterization of the modified devices containing NPs should be carried out in order to determine the optimum NPs composition in the nanocomposite materials for improving their electrochemical response (sensitivity, detection limit, stability, etc.) towards to the studied analytes, as well as other analytes of interest.
- Enhance the electroanalytical response of the new modified-sensors for the detection of the studied analytes as well as the optimization of the amount of modifiers (NPs, recognition agents...) integrated in the transducer material for sensing improvements.
- Integration of the developed devices in an automated flow injection analysis system (FIA) to evaluate the electrochemical response so as to improve the sensitivity and operational stability using a minimum volume of sample for future applications in medicine and environmental studies. This integration will open up an automate system which may obtain information in real time and *in situ*.

ANNEX A

Accepted Publications

Influence of raw carbon nanotubes diameter for the optimization of the load composition ratio in epoxy amperometric composite sensors

J. Muñoz · J. Bartrolí · F. Céspedes ·
M. Baeza

Received: 5 August 2014 / Accepted: 22 September 2014 / Published online: 7 October 2014
© Springer Science+Business Media New York 2014

Abstract In this work, it is reported the necessity to characterize the raw carbon materials before their application in composite electrodes based on multiwall carbon nanotubes (MWCNTs) dispersed in epoxy resin for the development of improved amperometric sensors. These sensors must contain an optimum MWCNT/epoxy ratio for their best electroanalytical response. The main drawback in MWCNTs composite materials resides in the lack of homogeneity of the different commercial nanotubes largely due to different impurities content, as well as dispersion in their diameter/length ratio and state of aggregation. The optimal composite electrode composition takes into account the high electrode sensitivity, low limit of detection, fast response, and electroanalytical reproducibility. These features depend on carbon nanotube physical properties as the diameter. Three different commercial carbon nanotubes with different diameters were characterized by transmission electron microscopy and the results were significantly different from the ones provided by the manufacturers. Then, the three MWCNTs were used for the MWCNT/epoxy sensors construction. After an accurate electrochemical characterization by cyclic voltammetry and electrochemical impedance spectroscopy, they were employed as working electrodes using ascorbic acid as a reference analyte. Percolation theory was applied in order to verify the electrochemical results. It is demonstrated that the optimum interval load of raw carbon material in the optimized-composite electrodes closely depends on the MWCNTs diameter, needing 5 % in carbon content for the

narrowest MWCNTs containing composite electrodes versus 12 % for the widest MWCNTs.

Introduction

Composite materials based on different forms of carbon as conductive phase, dispersed in polymeric matrix, have enabled important advances in the analytical electrochemistry field, particularly in (bio)sensor devices [1–5].

During the past decades, the electrochemical properties of different carbon paste electrodes have been studied in detail [6–8]. Recently, it has been developed different composite materials based on different types of polymeric matrices, obtaining interesting electrochemical applications by using graphite powder as conductive phase [1, 9–11].

Currently, high interest is focused on composites based on carbon nanotubes (CNTs), because of their remarkable electrical, thermal, and mechanical properties. Furthermore, they exhibit a higher area to volume ratio, lower resistivity and higher mechanical and chemical stability than other carbon allotropic forms such as graphite and fullerenes [12–15]. For these reasons, it is proved that the electrocatalytic activity of CNTs, focused on multiwall carbon nanotubes (MWCNTs), combined with the polymeric matrix properties are very useful for CNT-based amperometric (bio)sensors construction [3, 16, 17], especially for the detection of compounds such as total cholesterol [18], glucose [19], ascorbic acid [20, 21], chlorine [22], and hydrogen peroxide [23, 24].

Some parameters, such as the composite resistivity, the background capacitance current, the material stability, and the heterogeneous electron transfer rate, depend on carbon load within the polymeric matrix [25]. Regarding to the background capacitance current, the electrode capacitance

J. Muñoz · J. Bartrolí · F. Céspedes · M. Baeza (✉)
Departament de Química, Facultat de Ciències, Edifici C-Nord,
Universitat Autònoma de Barcelona, Cerdanyola del Vallès
(Bellaterra), 08193 Barcelona, Spain
e-mail: mariadelmar.baeza@uab.cat

value is directly related to the amount of exposed carbon [26]. Besides, depending on the carbon load, composite electrodes can behave in the same way as microelectrodes array [27, 28]. The carbon load depends on the physical properties of raw CNTs. The lack of homogeneity in the different commercial CNTs is largely due to the metal impurities content and the high dispersion in their diameter/length [29]. One of the main parameters used to determine the percolation behavior and the conductivity of the composites is the length/diameter ratio of CNTs [30–33]. In most studies, the aspect ratio of the CNTs was calculated using the lengths and diameters given by the manufacturer. There are only few studies on the measurement of the MWCNTs length and diameter distributions [34–38]. The low electrochemical reproducibility of (bio)sensors is due to the poor homogeneity of raw MWCNTs. Consequently, a careful characterization and optimization of the raw conductor material results mandatory [26, 39, 40].

Therefore, the aim of this work was to study one of the physical properties of raw MWCNTs, concretely the diameter [41] and its relation in the electrochemical response of the sensor in order to obtain the optimum MWCNT/polymer ratio in composite materials in function of the raw conductor material for their application in amperometric (bio)sensors. Accordingly, three different commercial MWCNTs with a priori distinctive diameters and resin epoxy have been used to fabricate three series of composites from 1 to 20 % in MWCNTs load for each of them.

Finally, the benefits of using this approach in terms of analytical performance are demonstrated by the detection of ascorbic acid as reference analyte.

Experimental

Chemicals and reagents

Three different commercial MWCNTs were used in this research. MWCNT-1 was provided by HELIX Material Solutions (Richardson, TX, USA) and its physical properties are >95 % of carbon purity, 10–20 nm of length and 1–2 μm on diameter. The physical properties of MWCNT-2, provided by SES Research (Houston, TX, USA), were >95 % of carbon purity, 10–30 nm of outer diameter and has about 5–15 μm of length. Finally, MWCNT-3 from Sigma-Aldrich (St. Louis, MO, USA) has >95 % of carbon purity, about 6–9 nm of outer diameter and 5 μm of length. All of them were produced using a chemical vapor deposition (CVD) method. Epotek H77A and its corresponding hardener Epotek H77B, from Epoxy Technology (Billerica, MA, USA), were used as polymeric matrix. All solutions

were prepared using deionised water from a Milli-Q system (Millipore, Billerica, MA, USA). Potassium ferricyanide/ferrocyanide (99.8 %), ascorbic acid (99.5 %), potassium nitrate (99.0 %), potassium chloride (99.5 %), and nitric acid (65 %) were purchased from Sigma-Aldrich (St. Louis, MO, USA).

Apparatus and procedure

Cyclic voltammetry (CV) and electrochemical impedance spectroscopy (EIS) studies were carried out in a conventional three-electrode cell powered by an electrochemical system consisting of a potentiostat/galvanostat Autolab system (PGSTAT 30 and FRA boards, Eco Chemie, Utrecht, The Netherlands). The system was run on a PC using GPES and FRA 4.9 software. The measurements were made in a 10.0 mL of 0.1 M KCl containing 0.01 M $\text{K}_3[\text{Fe}(\text{CN})_6]/\text{K}_4[\text{Fe}(\text{CN})_6]$ under quiescent condition. The kinetic processes of those species are strongly dependent on the state of the electrode surface. The experiments were performed at room temperature (25 °C). For impedance measurements, a frequency range of 100 kHz–0.1 Hz was employed. The signal amplitude to perturb the system was 10 mV and the equilibrium time was 15 s. Cyclic voltammograms were taken at the same experimental condition (10 mV/s of scan rate). A single junction reference electrode Ag/AgCl Orion 900100 (Thermo Electron Corporation, Beverly, MA, USA) and a platinum-based electrode 52-671 (Crison Instruments, Alella, Barcelona, Spain) were used as reference and auxiliary, respectively. The MWCNT/epoxy composite electrodes, prepared following the conventional methodology previously established [9], were employed as working electrodes. Finally, the MWCNT composite response changing a concentration of ascorbic acid was evaluated by hydrodynamic amperometric measurements using an amperometer LC-4C (Bio Analytical Systems INC., West Lafayette, IN, USA). Ascorbic acid was used as an analyte for evaluating the electroanalytical characteristics of sensors. Measurements were carried out at 600 mV fixed potential.

Diameter and length of the different raw MWCNTs were estimated from transmission electron microscopy (TEM) images, using a JEM-1400 unit with an acceleration voltage of 120 kV. A ~ 1 mg of MWCNTs was dispersed in 5 mL of acetone as organic solvent and then placed in ultrasound bath for 1 h. Finally, a drop of this solution was placed on a grid and let it dry before TEM analysis. Both distributions were compiled from at least 100 tubes. Measurements of composites topography were made by Confocal Microscopy 3D (CM3D). A Leica DCM 3D unit to 150 \times magnifications was used for measuring fifty-seven profiles in three different areas for each optimum composite electrode (ISO 4287). Electrical resistance measurements were performed by means of a digital

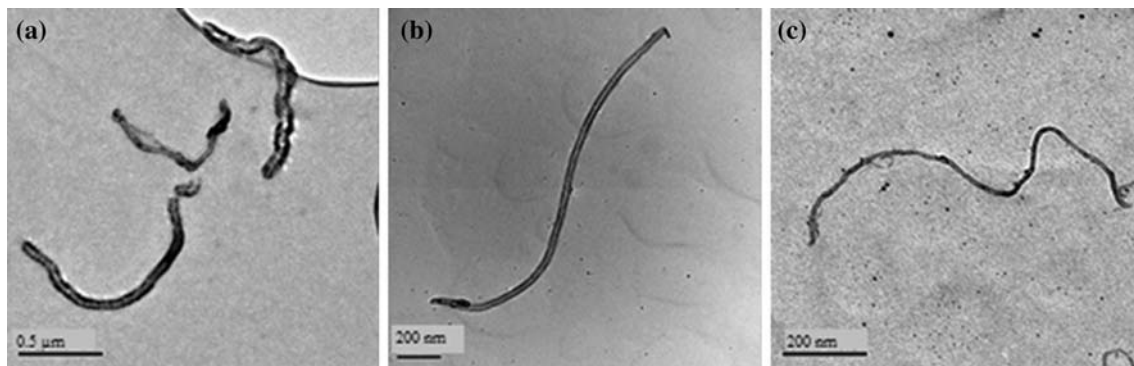


Fig. 1 TEM images for **a** MWCNT-1, **b** MWCNT-2, and **c** MWCNT-3

multimeter (Fluke, Everett, WA, USA). Lastly, the carbon content was evaluated by thermogravimetric analysis (TGA) [42], using a Netzsch instrument, model STA 449 F1 Jupiter[®]. A ~20 mg of sample was heated to 1000 °C at 10 °C/min, using flow of air. The mass of the sample was continuously measured as a function of temperature and the rate of weight loss (d.t.g.) was automatically recorded.

Composite preparation

A resin Epotek H77 and its corresponding hardener compound were mixed in the ratio of 20:3 (w/w). Three series of MWCNT/epoxy composites were prepared by loading different amounts of CNTs, from 1 to 20 % (w/w) into the epoxy resin before hardening. The composites were homogenized for 1 h. The mixture was blended thoroughly and placed in the hollow end of a PVC tube to form the body of the electrode [9]. The composite paste thickness in the electrode was 3 mm. Then, the composite paste electrodes were allowed to harden during 24 h at 80 °C [5]. Afterward, composite electrodes surfaces were polished with different sandpapers of decreasing grain size. The final electrode dimensions were 28 mm² of physical circular area. The three series of MWCNT/epoxy composites were made in the same way but modifying the MWCNT nature. Thus, the first series was MWCNT-1/epoxy composites and they contain MWCNT-1, C1. The second series consists of MWCNT-2/epoxy composites, C2. Finally, the third series of composites was made dispersing MWCNT-3 into epoxy resin, C3.

Results and discussion

Physical properties characterization of raw MWCNTs

Diameter and length of the three different MWCNTs (MWCNT-1, MWCNT-2, and MWCNT-3) were calculated

Table 1 Physical parameters of raw MWCNTs were studied and compared with values given by the manufacturers (MFG)

MWCNTs	Purity (% in C)		Length (μm)		Diameter (nm)	
	TGA	MFG	TEM	MFG	TEM	MFG
HELIX [MWCNT-1]	>97	>95	0.5–1.5	1.0–2.0	35–55	10–20
SES Research [MWCNT-2]	>99	>95	0.5–2.0	1.0–15	30–45	10–30
Sigma-Aldrich [MWCNT-3]	>98	>95	0.5–2.5	>5.0	8–15	6–9

Purity was obtained by TGA analysis; TEM was utilized for determining length and diameter

from TEM images (Fig. 1). For the measurements, a greater dispersion of these tubes was needed. After an accurate data compilation, an important difference between the experimental results and the specifications provided by the manufacturers were found as it is shown in Table 1.

Firstly, it was observed a shorter MWCNT length than the specified one by the manufacturers which were above 5 μm for MWCNT-3 and above 1 μm for the rest. Both lower and upper length limit values obtained by TEM images were shorter than the specified by the manufactures, as shown in Table 1. Thus, 0.5 μm was the estimated lower length limit value for the three kinds of MWCNTs. Regarding to the upper length, 1.5, 2.0, and 2.5 μm were the values obtained for MWCNT-1, MWCNT-2, and MWCNT-3, respectively.

Secondly, the diameter was another characteristic that shows really different results as well. MWCNT-1 and MWCNT-2 obtained superior diameters for both lower and upper limit. Moreover, while MWCNT-1 was expected to be narrower than MWCNT-2, the result was contrary and MWCNT-1 became the widest. Finally, MWCNT-3 had the diameter value closer to the provided by Sigma-Aldrich, emerging the narrowest.

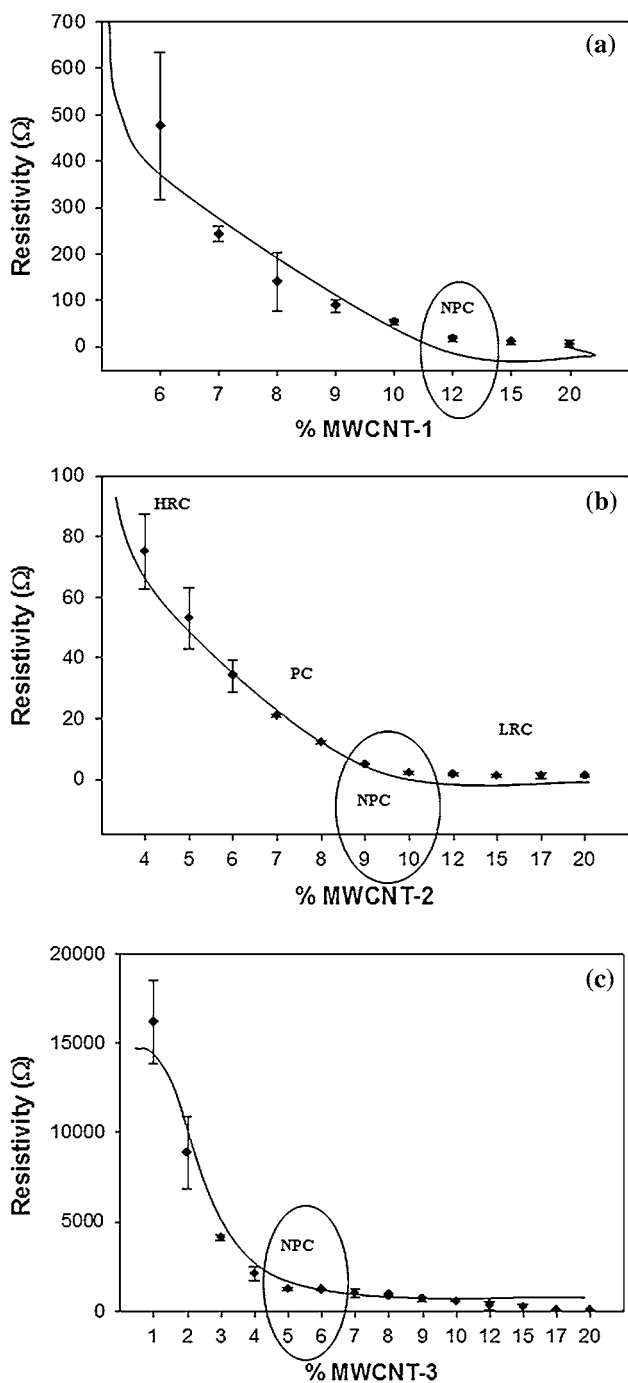


Fig. 2 Percolation curve obtained for the rigid conducting composites based on the polymer epoxy and raw MWCNTs for **a** C1, **b** C2, and **c** C3. **b** describes *HRC* High resistivity zone composites, and thus lowly conducting; *PC* percolation zone composites, *NPC* Near-percolation zone composites, and *LRC* Low resistivity zone composites, and thus highly conducting

On the other hand, TGA analysis reveals information about purity of MWCNTs, as to percentage of carbon referred. It has been observed that all the carbon was oxidized to CO₂ at 600 °C in air atmosphere [43]. The

background line is because of the metallic catalyst residues. In this case, the purity obtained by TGA for each MWCNT was slightly higher than the specified one.

In brief, length, diameter, and purity values obtained by TEM and TGA for all studied MWCNTs were different from the values given by the manufacturers. Considering length and purity experimental values were homogeneous for each MWCNT, the study was focused on the effect of the diameter in the electroanalytical response of the composite sensors.

Electrical characterization

The electrical properties of the MWCNT composite electrodes were investigated by percolation theory [22]. In order to estimate the maximum conductivity value of the composite materials with the minimum conductive particle loading, each series of MWCNT/epoxy composites was tested following the experimental procedure previously presented. While C1, C2, and C3 composites contained more than 20 % of MWCNTs had a poor mechanical stability, those composites contained less than 1 % exhibited resistivity values that tend to infinity. Analytically, a lower resistivity value produces a higher sensitivity. The percolation threshold (PT) zone was achieved around 1 % in conductor material because at this point the first conductive network is formed throughout the matrix. Resistivity decreases rapidly below PT by several orders of magnitude to a minimum value, where variations in resistivity are negligible. It is important to highlight that MWCNTs loading has to be high enough to guarantee a conducting pathway and sufficiently low bulk resistivity. Due to this fact, the study was based on the zone right below PT zone, see Fig. 2. After the experiments, three different conductive regions (Fig. 2b) were determined regarding the electrical behavior: high resistance zone composite (HRC), near-percolation zone or second percolation zone composite (NPC), and low resistance zone composite (LRC).

Comparing the electrical differences between the three series of MWCNT/epoxy composites, a displacement in the NPC is observed in Fig. 2. This fact is due to the differences of the MWCNTs diameter. For composites loaded with MWCNT-1 which have a greater diameter, around 12 % in MWCNTs was the needed load to fall on the second PT, Fig. 2a. However, composites containing MWCNT-3 had the lowest diameter and the first point that fell on the NPC was around 5 % in MWCNTs, Fig. 2c. Finally, for MWCNT-2, the first composition that fell on the second PT zone was 10 % in MWCNTs, as it is shown in Fig. 2b. Thus, as diameter of raw MWCNTs decreases, a leftward displacement on the second PT zone was observed, due to the increase of surface area for the same percentage of MWCNTs in the composite, see Table 2.

Table 2 Electrochemical impedance spectroscopy data of 0.01 M $\text{Fe}(\text{CN})_6^{3-/4-}$ in 0.1 M KCl are showed by optimum composites and composites with maximum charge (20 % in MWCNTs load)

R_{Ω} ($C_{dl} \cdot R_{ct}$)/Values	C1		C2		C3	
	12 %	20 %	10 %	20 %	5 %	20 %
R_{Ω} (Ω)	248.0	71.4	137.1	97.9	95.5	47.9
R_{ct} (Ω)	145.6	20.17	530.0	203.3	1169.0	3.9
C_{dl} (μF)	14.0	65.9	9.0	37.3	2.8	318.1
A (cm^2)	0.26	0.55	0.25	0.49	0.24	3.07
LOD (ppm)	0.070 ± 0.002	0.34 ± 0.01	0.070 ± 0.004	0.26 ± 0.01	0.042 ± 0.004	*

A was extracted by CV and LOD was obtained by hydrodynamic amperometry for ascorbic acid detection, ($n = 3$)

* 20 % C3 was not able to be measured due to the high C_{dl}

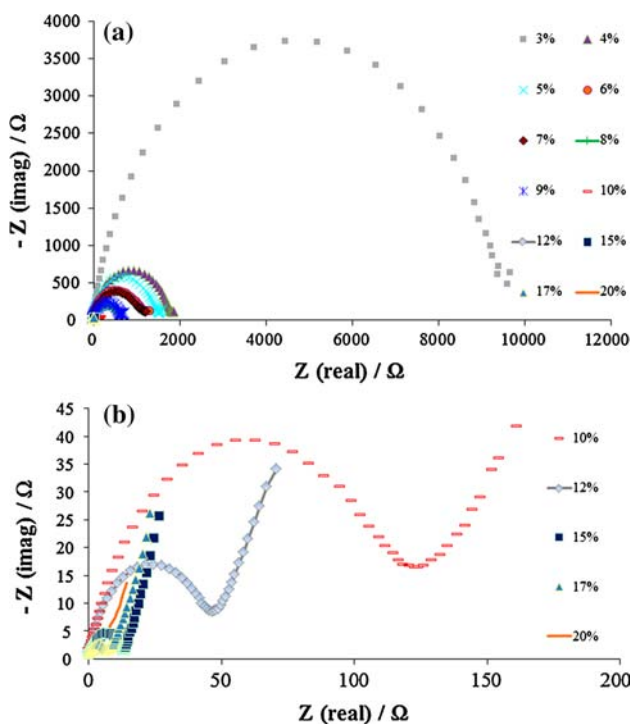


Fig. 3 Impedance spectra for different MWCNT-3 loading electrodes (C3) in the presence of 0.01 M $[\text{Fe}(\text{CN})_6]^{3-/4-}$ and 0.1 M KCl. $R_{\Omega} \cdot (R_{ct} \cdot C_{dl})$ were the equivalent circuit used for the impedance spectra fitting. MWCNT-3 containing electrodes **a** from 3 to 20 % in nanotubes and **b** zoom of the low impedance composite electrodes (from 10 to 20 %)

Consequently, a lower load of MWCNTs is required for those composites that contain the narrowest nanotubes (C3).

Electrochemical impedance spectroscopy measurements

Ohmic resistance (R_{Ω}), charge transfer resistance (R_{ct}), and double-layer capacitance (C_{dl}) for composites with different MWCNT loadings were evaluated for the three series

of MWCNT/epoxy composites by EIS technique. These parameters were obtained by fitting the impedance spectra to a simple equivalent circuit: $R_{\Omega} \cdot (R_{ct} \cdot C_{dl})$, using the equilibrium potential previously obtained by CV. This circuit was sufficiently suitable to interpret the R_{Ω} , R_{ct} , and C_{dl} values in terms of the interfacial phenomena that occur at the electrochemical cell, Fig. 3. If in a previous study was demonstrated a general trend of these physical parameters as a function of MWCNT loading [26], in this work is attempted to obtain the relation between raw MWCNTs diameter and the electrochemical response of the composite electrodes.

Accordingly, 15 different compositions of MWCNT/epoxy composite electrodes were studied for each series by changing the MWCNT loading from 1 to 20 %. For each MWCNT composition, three equal electrodes were prepared and evaluated in order to obtain the reproducibility of the composites. From NPC to LRC (>10 % of MWCNT loading for C1, >9 % for C2, and >5 % for C3, percentage expressed in MWCNTs content) appeared to be dominated by a big diameter semicircle and only the kinetic-controlled electrode process was present in the recorded frequency range. An example of this behavior is shown in Fig. 3 for MWCNT-3/epoxy composite electrodes (C3).

R_{Ω} parameter, which is dependent on the ionic concentration, the type of ions and also the electrode area, consists of the solution resistance in series with the contact or the ohmic composite resistance. C1, C2, and C3 showed a R_{Ω} decrease at the same time that the MWCNT loaded increased, as shown in the black plots in Fig. 4. Whereas at low carbon loads the ohmic resistance is dominated by

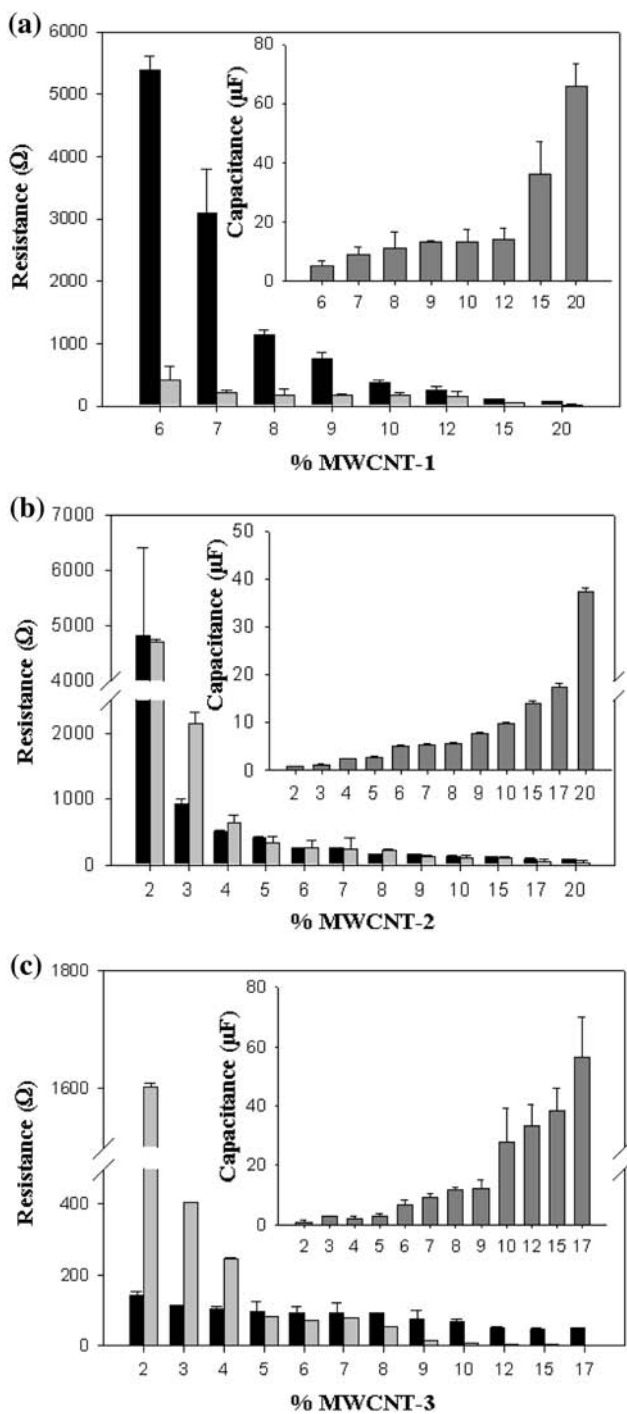


Fig. 4 Values of ohmic resistance (R_{Ω} , black square), charge transfer resistance (R_{ct} , light gray square), and double-layer capacitance (C_{dl} , dark gray square), with their corresponding standard deviation ($n = 3$) for **a** C1, **b** C2, and **c** C3. The redox probe $[\text{Fe}(\text{CN}_6)]^{3-}/[\text{Fe}(\text{CN}_6)]^{4-}$ was used

ohmic composite resistance, at higher carbon loads the ohmic resistance is more dominated by the solution resistance.

Concerning R_{ct} , this parameter is well known as a useful parameter reflecting the facility of electrode reaction,

which can be measured by EIS from the semicircle diameter in the Nyquist plots [44]. Moreover, the charge transfer resistance was inversely proportional to the heterogeneous charge transfer rate and also affected the sensitivity and response time of the electrode. From Fig. 4, the light gray plots show the decrease of R_{ct} with the increasing of MWCNTs load because of the rise of electroactive sites. This increase also exhibits an enhancement on the electrodes kinetics. It is known that the electrode kinetics of CNTs electrodes is dependent on the CNTs nature and structure. Thus, the electroactive area becomes different from a same percentage of MWCNTs, depending on the raw MWCNTs nature; as a matter of fact it was the diameter for this study. However, electroactive area was very similar for MWCNT/epoxy near-percolation composites, motivating to think that they should have a similar electroanalytical behavior, see Table 2. This fact demonstrated again the importance of characterizing both raw carbon material and CNT/resin ratio in order to make the best electrochemical sensor. Moreover, it was observed that composites with low charge transfer resistances were the most appropriate to be used in electrochemical measurements. According to the results, composites between NPC and LRC presented lower charge transfer values. The use of near-percolation composite electrodes guarantees a fast electron exchange. In spite of the enhanced kinetics, high load of conducting material can increase the background current and smear the Faradaic signal response, especially when the electroactive species are present in low concentration. As a consequence, it is important to consider the remaining impedance parameter represented by the double-layer capacitance which is directly related to the charging or background current.

An increase of C_{dl} values was obtained for electrodes comprising high surface area of conducting material. In general, composites contain only a fraction of conductive area exposed to the solution and the other fraction is occupied by the insulating polymer. The electrode capacitance, which is determined nearly exclusively by the exposed carbon, becomes low and because of that the background current decreases. This fact enhances the signal to noise ratio and consequently decreases the analyte detection limits (LOD). The decrease of the double-layer capacitance values with the decrease of the MWCNT loadings can be observed in Fig. 4 (dark gray plots).

An electrode for electroanalytical purpose must have a rapid response time, low limit of detection, and high sensitivity. According to the impedance results and taking that into account, the interval between 10 and 12 % of MWCNT-1 loading fulfill all these requirements for MWCNT-1/epoxy composites, C1. For C2, the optimum ratio was between 9 and 10 % of MWCNT-2. Those intervals are similar because of the proximity of their

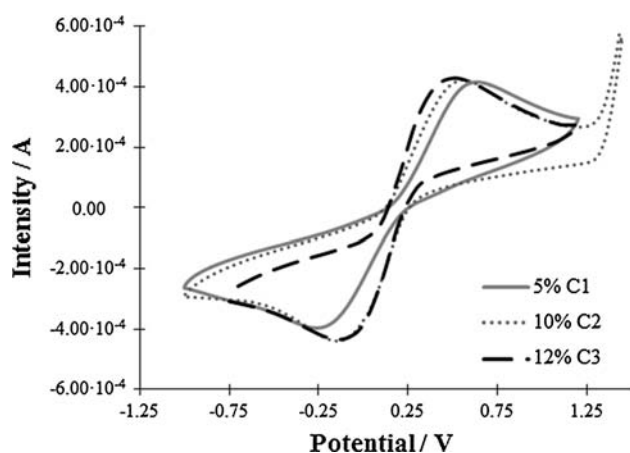


Fig. 5 Cyclic voltammogram for three optimum composite electrodes recorded in 0.01 M $\text{Fe}(\text{CN})_6^{3-/4-}$ and 0.1 M KCl. Scan rate 10 mV/s

diameter. Finally, an interval around 5–6 % in MWCNT-3 load was considered the optimum to obtain the best electroanalytical response for MWCNT-3/epoxy composites, C3. These results demonstrated that the optimum interval of MWCNT/epoxy ratio was closely tied to raw MWCNTs nature.

It is worthy to highlight that the manufactured composites in the optimum carbon load intervals mentioned above presented similar electrochemical performance. The benefit of working within these intervals led to an increase of the electrochemical reproducibility. Furthermore, it is assured the compromise to work with electrodes with low resistivity and high signal-noise ratio.

Finally, it was observed that the optimum interval of MWCNT/epoxy ratio for each series was in agreement with the obtained results in the percolation curve.

Cyclic voltammetry characterization

CV was used in order to obtain the equilibrium electrode potential of each composite composition, necessary parameter to make EIS measurements. Moreover, it was also used to compare the results obtained with the EIS technique. Different parameters were calculated at the same experimental conditions from the cyclic voltammograms, such as the equilibrium electrode potential (E_{eq}), peak separation potential (ΔE), and peak current (I_p). The relative electroactive area (A) was estimated from the peak-shaped voltammograms by quantifying the peak current with the use of this relationship, $I_p = 3.01 \cdot 10^5 n^{3/2} (\alpha D_{\text{red}} v)^{1/2} A C_{\text{red}}^*$ [45], which is appropriate for electron transfer-controlled processes, Table 2. An increase of the peak current with the MWCNT loading was

observed for each series, due to an increase of the electroactive area, together with a decrease of peak separation related to an enhancement of the electron transfer rate. Figure 5 shows the cyclic voltammogram of the three optimized carbon load composites previously selected for each series (5 % for C1, 10 % for C2, and 12 % for C3). Non-significant changes of ΔE and I_p were observed, demonstrating again that the optimum composites have the same electrochemical behavior and that their performance depends on the raw MWCNTs diameter.

Morphological characterization

Roughness surfaces of NPC electrodes were compared for the three different MWCNT/epoxy composites. Thus, the topography of each optimum composite was measured by CM3D. Figure 6 presents the most significant images obtained during the electrode surface study. Based on these results showed in Table 3, it was determined that the three optimum electrode topographies were strongly similar, in spite of the differences with carbon loading. These results were the expected due to their electroactive areas (A) are much similar, as it is shown in Table 2. Once again it is corroborated that the physical properties of raw nanotubes are crucial in the electrochemical response of the sensor.

Electroanalytical performance

Ascorbic acid was used as a reference analyte for evaluating the electroanalytical characteristics of sensors. The MWCNT/epoxy composite response to the change of ascorbic acid concentration was evaluated by hydrodynamic amperometric measurements. The analytical parameters as the LOD and sensitivity were evaluated for the optimum composite electrode composition of each series and compared with the most concentrated composites prepared (20 % in carbon load), see Table 2. Furthermore, 20 % in carbon load is the convectional composition used in the vast majority of previous studies reported by our research group [5, 46]. Comparing optimum composite sensors with the ones which contain 20 % in carbon load, the best LOD was obtained for optimized-composite sensors, although the most concentrated composites prepared contain a higher number of transducer particles. A lower MWCNTs load results in a increase of the signal to noise ratio, C_{dl} . C3 sensors containing 20 % in carbon load could not be amperometrically stabilized due to their high value of C_{dl} . 9 % of MWCNT-3 was the highest carbon load which could be measured in this series. The LOD obtained for this electrode composition was 0.68 ppm, higher than optimized-composite electrode composition (5 % for C3).

On the other hand, comparing among series, the lower LOD was obtained for the optimum composite composition

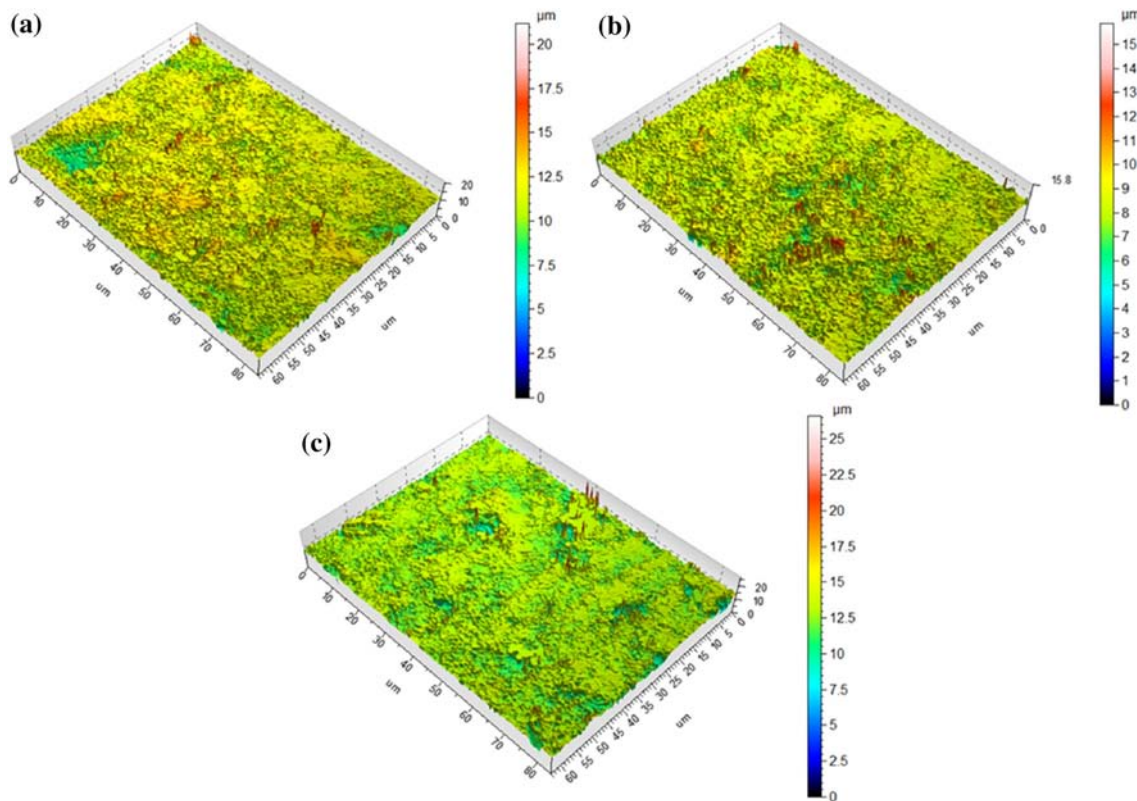


Fig. 6 Topographic images of the optimum **a** C1 **b** C2, and **c** C3 composites for each series were obtained with the 3D Optical Surface Metrology System Leica CM3D for the roughness study

Table 3 Roughness values collected from surface analysis

Electrodes	R_a^a		R_q^b		R_z^c	
	Mean	SD	Mean	SD	Mean	SD
12 % C1	0.559	0.208	0.812	0.212	4.899	1.616
10 % C2	0.555	0.129	0.920	0.271	7.306	2.602
5 % C3	0.579	0.175	0.809	0.286	5.516	2.830

Data are the mean and standard deviation (SD) from 57 profiles of three areas examined in each series (ISO 4287)

- ^a Arithmetical mean deviation of the assessed profile
- ^b The root mean square deviation of the assessed profile
- ^c Maximum height of the profile

which contains nanotubes with the narrowest diameter (MWCNT-3). MWCNT-1 and MWCNT-2 optimum composites loading are closely similar that the same LOD was obtained. These results showed again the C_{dl} effect on the amperometry measurements. Finally, in agreement with the percolation theory and the electrochemical results, the best sensor for each series of MWCNTs in terms of LOD is the one which just falls on second PT zone: 5 % for C1, 10 % for C2, and 12 % for C3.

Conclusions

Purity and dimensions of raw MWCNTs (in powder form) were studied and compared with the provided values by the manufacturers. While the carbon content is in good agreement with the manufacturer specifications, the length is significantly shorter and the diameter is proved to be strongly different. Considering the purity and length as constant parameters, the diameter value could be considered as the only variable. One of the most important parameters that determines the composite conductivity and the percolation behavior of the MWCNTs is the aspect ratio. Thus, a leftward displacement on the NPC could be observed, only needing 5 % in carbon load the narrowest MWCNT containing composites (MWCNT-3) in comparison with 12 % for the widest, MWCNT-1. Therefore, the CNT diameter is a key parameter to optimize the composite ratio, needing less carbon load for the narrowest nanotubes.

The electrochemical measurements (EIS and CV) were in concordance with the results achieved by electrical experiments (PT), obtaining the same optimum MWCNT/epoxy ratio for each series. A minimum LOD for 5 % MWCNT-3/epoxy electrode was obtained when it was used

as a working electrode for ascorbic acid detection as reference analyte, due to the C_{dl} value turned out to be the lowest and this parameter is directly connected with the signal to noise ratio. On the other hand, non-optimized composites (20 % in carbon load) presented a higher LOD, showing the necessity of optimizing the MWCNT/polymer ratio. Accordingly, an optimum characterization of the raw carbon material before their application for amperometric sensors is required to obtain an optimal composite electrode composition which contains high sensitivity, low limit of detection, fast response, and electroanalytical reproducibility.

Acknowledgements We are sincerely grateful to all our associates cited throughout the text for making this publication possible. J. Muñoz thanks Universitat Autònoma de Barcelona (UAB) for the award of PIF studentship.

References

- Céspedes F, Martínez-Fàbregas E, Alegret S (1996) New materials for electrochemical sensing I. Rigid conducting composites. *Trends Anal Chem* 15:296–304
- Zhao Q, Gan Z, Zhuang Q (2002) Electrochemical sensors based on carbon nanotubes. *Electroanalysis* 14:1609–1613
- Vashist SK, Zheng D, Al-Rubeaan K, Luong JHT, Sheu F-S (2011) Advances in carbon nanotube based electrochemical sensors for bioanalytical applications. *Biotechnol Adv* 29:169–188
- Yang X, Feng B, He XL, Li FP, Ding YL, Fei JJ (2013) Carbon nanomaterial based electrochemical sensors for biogenic amines. *Microchim Acta* 180:935–956
- Pumera M, Merkoçi A, Alegret S (2006) Carbon nanotube-epoxy composites for electrochemical sensing. *Sensors Actuat B: Chem* 113:617–622
- Švancara I, Vytrás K, Barek J, Zima J (2001) Carbon paste electrodes in modern electroanalysis. *Crit Rev Anal Chem* 31:311–345
- Zima J, Švancara I, Barek J, Vytrás K (2009) Recent advances in electroanalysis of organic compounds at carbon paste electrodes. *Crit Rev Anal Chem* 39:204–227
- Navratil T, Barek J (2009) Analytical applications of composite solid electrodes. *Crit Rev Anal Chem* 39:131–147
- Alegret S, Morales A, Céspedes F et al (1996) Hydrogen peroxide amperometric biosensor based on a peroxidase-graphite-epoxy biocomposite. *Anal Chim Acta* 332:131–138
- Lermo A, Fabiano S, Hernández S et al (2009) Immunoassay for folic acid detection in vitamin-fortified milk based on electrochemical magneto sensors. *Biosens Bioelectron* 24:2057–2063
- Orozco J, Fernández-Sánchez C, Mendoza E, Baeza M, Céspedes F, Jiménez-Jorquera C (2008) Composite planar electrode for sensing electrochemical oxygen demand. *Anal Chim Acta* 607:176–182
- Wang D, Li Z-C, Chen L (2006) Templated synthesis of single-walled carbon nanotube and metal nanoparticle assemblies in solution. *J Am Chem Soc* 128:15078–15079
- Gao C, Li W, Morimoto H, Nagaoka Y, Maekawa T (2006) Magnetic carbon nanotubes: synthesis by electrostatic self-assembly approach and application in biomanipulations. *J Phys Chem B* 110:7213–7220
- Balashubramanian K, Burghard M (2005) Chemically functionalized carbon nanotubes. *Small* 1:180–192
- Guadagno L, De Vivo B, Di Bartolomeo A et al (2011) Effect of functionalization on the thermo-mechanical and electrical behavior of multi-wall carbon nanotube/epoxy composites. *Carbon* 49:1919–1930
- Valentini F, Amine A, Orlanducci S, Terranova ML, Palleschi G (2003) Carbon nanotube purification: preparation and characterization of carbon nanotube paste electrodes. *Anal Chem* 75:5413–5421
- Shi J, Wang Z, Li H-I (2007) Electrochemical fabrication of polyaniline/multi-walled carbon nanotube composite films for electrooxidation of methanol. *J mater sci* 42:539–544
- Solanki PR, Kaushik A, Ansari AA, Tiwari A, Malhotra B (2009) Multi-walled carbon nanotubes/sol-gel-derived silica/chitosan nanobiocomposite for total cholesterol sensor. *Sensors Actuat B: Chem* 137:727–735
- Noonan M (2005) Glucose biosensor based on carbon nanotube epoxy composites. *Nanosci Nanotechnol* 5:1694–1698
- Liu M, Wen Y, Xu J et al (2011) An amperometric biosensor based on ascorbate oxidase immobilized in poly(3,4-ethylenedioxythiophene)/multi-walled carbon nanotubes composite films for the determination of L-ascorbic acid. *Anal Sci* 27:477–482
- Liu Y, Su Z, Zhang Y et al (2013) Amperometric determination of ascorbic acid using multiwalled carbon nanotube-thiolated polyaniline composite modified glassy carbon electrode. *J Electroanal Chem* 709:19–25
- Olivé-Monllau R, Baeza M, Bartrolí J, Céspedes F (2009) Novel amperometric sensor based on rigid near-percolation composite. *Electroanalysis* 21:931–938
- Shobha Jeykumari DR, Ramaprabhu S, Sriman Narayanan S (2007) A thionine functionalized multiwalled carbon nanotube modified electrode for the determination of hydrogen peroxide. *Carbon* 45:1340–1353
- Liang M, Jin F, Liu R et al (2013) Enhanced electrochemical detection performance of multiwall carbon nanotubes functionalized by aspartame. *J Mater Sci* 48:5624–5632
- McCreery RL (2008) Advanced carbon electrode materials for molecular electrochemistry. *Chem Rev* 108:2646–2687
- Olivé-Monllau R, Esplandiú MJ, Bartrolí J, Baeza M, Céspedes F (2010) Strategies for the optimization of carbon nanotube/polymer ratio in composite materials: applications as voltammetric sensors. *Sensors Actuat B: Chem* 146:353–360
- Arrigan DW (2004) Nanoelectrodes, nanoelectrode arrays and their applications. *Analyst* 129:1157–1165
- Weisshaar DE, Tallman DE (1983) Chronoamperometric response at carbon-based composite electrodes. *Anal Chem* 55:1146–1151
- Castillo FY, Socher R, Krause B et al (2011) Electrical, mechanical, and glass transition behavior of polycarbonate-based nanocomposites with different multi-walled carbon nanotubes. *Polymer* 52:3835–3845
- Martin C, Sandler J, Shaffer M et al (2004) Formation of percolating networks in multi-wall carbon -nanotube-epoxy composites. *Composites Sci Technol* 64:2309–2316
- Li J, Ma PC, Chow WS, To CK, Tang BZ, Kim JK (2007) Correlations between percolation threshold, dispersion state, and aspect ratio of carbon nanotubes. *Adv Funct Mater* 17:3207–3215
- Jiang M-J, Dang Z-M, Xu H-P, Yao S-H, Bai J (2007) Effect of aspect ratio of multiwall carbon nanotubes on resistance-pressure sensitivity of rubber nanocomposites. *Appl Phys Lett* 91:072907-1–072907-3
- Pegel S, Pötschke P, Petzold G, Alig I, Dudkin SM, Lellinger D (2008) Dispersion, agglomeration, and network formation of multiwalled carbon nanotubes in polycarbonate melts. *Polymer* 49:974–984
- Song W, Windle AH (2005) Isotropic-nematic phase transition of dispersions of multiwall carbon nanotubes. *Macromolecules* 38:6181–6188

35. Krause B, Boldt R, Pötschke P (2011) A method for determination of length distributions of multiwalled carbon nanotubes before and after melt processing. *Carbon* 49:1243–1247
36. Rosca ID, Hoa SV (2009) Highly conductive multiwall carbon nanotube and epoxy composites produced by three-roll milling. *Carbon* 47:1958–1968
37. Chen Z, Appenzeller J, Knoch J, Lin Y-m, Avouris P (2005) The role of metal-nanotube contact in the performance of carbon nanotube field-effect transistors. *Nano Lett* 5:1497–1502
38. Krause B, Villmow T, Boldt R, Mende M, Petzold G, Pötschke P (2011) Influence of dry grinding in a ball mill on the length of multiwalled carbon nanotubes and their dispersion and percolation behaviour in melt mixed polycarbonate composites. *Composites Scie Technol* 71:1145–1153
39. Zhao H, O'Hare D (2008) Characterization and Modeling of Conducting Composite Electrodes. *J Phys Chem C* 112:9351–9357
40. Carabineiro S, Pereira M, Nunes-Pereira J et al (2012) The effect of nanotube surface oxidation on the electrical properties of multiwall carbon nanotube/poly (vinylidene fluoride) composites. *J Mater Sci* 47:8103–8111
41. Cadek M, Coleman J, Ryan K et al (2004) Reinforcement of polymers with carbon nanotubes: the role of nanotube surface area. *Nano Lett* 4:353–356
42. Mansfield E, Kar A, Hooker SA (2010) Applications of TGA in quality control of SWCNTs. *Anal Bioanal Chem* 396:1071–1077
43. Pang LS, Saxby JD, Chatfield SP (1993) Thermogravimetric analysis of carbon nanotubes and nanoparticles. *J Phys Chem* 97:6941–6942
44. Bard AJ, Faulkner LR (1980) *Electrochemical methods: fundamentals and applications*. Wiley, New York
45. Pacios M, Del Valle M, Bartroli J, Esplandiu M (2008) Electrochemical behavior of rigid carbon nanotube composite electrodes. *J Electroanal Chem* 619:117–124



Effect of Carbon Nanotubes Purification on Electroanalytical Response of Near-Percolation Amperometric Nanocomposite Sensors

J. Muñoz, F. Céspedes, and M. Baeza^z

Departament de Química, Facultat de Ciències, Edifici C-Nord, Universitat Autònoma de Barcelona,
08193 Cerdanyola del Vallès (Bellaterra), Spain

This work focuses on the effect of multiwall carbon nanotubes (MWCNTs) purification methods for their application as conductive materials in the development of MWCNTs/epoxy amperometric nanocomposite (bio)sensors. For this purpose, three different MWCNTs samples with distinctive purities were characterized by Thermogravimetric Analysis, X-Ray Fluorescence Spectroscopy and Transmission Electron Microscopy. Subsequently, the samples were used to fabricate three different series of MWCNTs dispersed into resin epoxy. These series contained from 1% to 12% of the MWCNT sample. Composition ratios were modelled by percolation theory and characterized by different electrochemical techniques including Cyclic Voltammetry and Electrochemical Impedance Spectroscopy. After accurate electrical and electrochemical characterization, it has been demonstrated that the purification method affects the electrochemical behavior of the nanocomposite electrodes; however the optimum MWCNT/epoxy ratio was not modified. Furthermore, morphological experiments corroborated that the electrochemical performance of the electrodes closely depends on the physical properties of the different MWCNTs used. The optimized-sensors (near-percolation sensors) were tested by hydrodynamic amperometry, using ascorbic acid as a model analyte. Interestingly, the sensors containing non-purified MWCNTs exhibited the best electroanalytical response. This fact demonstrates the beneficial effects of metal impurities being present in MWCNTs to enhance the analytical response of MWCNT-based amperometric nanocomposite (bio)sensors.

© 2015 The Electrochemical Society. [DOI: 10.1149/2.0531508jes] All rights reserved.

Manuscript submitted January 16, 2015; revised manuscript received April 16, 2015. Published May 19, 2015.

Following the discovery of fullerene C₆₀ by Kroto¹ and the subsequent first observation of a real carbon nanotube by Iijima,² research into carbon based nanomaterials and their potential applications has expanded rapidly.³ However, the first evidence for nano-sized carbon tubes is believed to have been published in 1952 by Radushkevich and Lukyanovich.⁴ CNTs may be fabricated using a variety of methods such as arc discharge methods,⁵ laser ablation⁶ and chemical vapor deposition.⁷ Such fabrication processes usually require a metal catalyst and result in the production of CNTs containing metal impurities and require extensive post-synthetic treatment.⁸ CNTs represent an important group of nanomaterials⁹ with attractive electronic,¹⁰ thermal¹¹ and mechanical¹² properties. These remarkable properties make them interesting for developing CNT nanocomposites, providing a highly accessible surface area, low resistance and a high mechanical and chemical stability. Due to these properties, their performance had been found to be superior to the other kinds of carbon materials in terms of reaction rates and reversibility.¹³ Nanocomposites based on CNTs have demonstrated a variety of applications^{14,15} including the fabrication of electrochemical (bio)sensors.^{16,17} These materials exhibit several electrocatalytic properties, which may include reductions in overpotentials, increments in the voltammetric peak heights that facilitate lower detection limits and enhanced sensitivities in analytical sensing coupled with little or no observed surface fouling. The benefits of CNTs, specifically multiwall carbon nanotubes (MWCNTs) combined with polymeric matrix properties, have proven to be very useful for the construction of MWCNT-based amperometric sensors and biosensors.^{18,19,20} These sensors have shown extensive use for the detection of compounds such as glucose,²¹ hydrogen peroxide,^{22,23} ascorbic acid²⁴ and free chlorine.²⁵ Some parameters, such as the reinforcement scale, composite resistivity, background capacitance current, material stability and heterogeneous electron transfer rate are dependent on carbon load within the polymeric matrix.^{26,27} Thus, for the same polymer, depending on the carbon load, the nanocomposite electrodes can behave similarly to a microelectrode array that takes place for compositions into percolation zone. The carbon load in these nanocomposites is dependent upon the physical properties of the raw CNTs which is known to vary in length, diameter and degree of aggregation between different CNT suppliers.^{27,28} One of the main parameters used to determine the percolation behavior and the conductivity of the nanocomposites is the length/diameter ratio of

CNTs.^{29,30} Consequently, a careful characterization and optimization of the raw transducer material is mandatory before being used for sensing purposes.^{31,32} Working with nanocomposite electrodes based on the near-percolation composition zone have shown enhanced properties such as better limits of detection, wider lineal range and increase of the stability and repeatability of the analytical signal.³³

The purity of the raw CNTs is rarely analyzed as they are purified directly prior to (bio)sensor nanocomposite fabrication.^{34,35} Therefore, it is unknown whether the purity of the raw MWCNT might affect both the electroanalytical behavior of amperometric nanocomposite electrodes and the optimum MWCNT/epoxy composition ratio. CNT synthesis inherently leads to the production of not only CNTs but also other carbonaceous bi-products such as amorphous carbon, fullerenes, nanocrystalline graphite and transition metals (Fe, Ni, Co, Cu) which were used as catalysts for growth.³⁶ These non-nanotube materials frequently hinder the advantageous properties of CNTs and limit their optimal performance in applications as new functional devices with enhanced sensing characteristics. Purification methods attempt to remove any unwanted carbon and metal impurities without damaging the MWCNTs as it is generally believed that the accurate purification of the raw carbon materials results in a greater analytical response for amperometric detection.^{37,38}

Within this context, this article reports several MWCNTs purification methods and their influence on both the MWCNT/epoxy composition ratio and the electroanalytical response of the MWCNTs/epoxy amperometric nanocomposite sensors. Accordingly, three different MWCNTs (non-purified and purified with/without carboxylic groups on the surface) were dispersed into epoxy resin in order to fabricate three different series of nanocomposites from 1% to 12% load of MWCNTs for each one of them. For the purposes of this research, not only an optimum characterization of the nanocomposite materials was carried out but also the raw MWCNTs samples were characterized before nanocomposite fabrication. The benefits of using this approach in terms of near-percolation nanocomposites and analytical performance are demonstrated by hydrodynamic amperometry, using ascorbic acid as the model analyte.

Experimental

Filler, matrix materials and reagents.— Three different MWCNTs materials have been directly incorporated into epoxy matrix. The nanotubes were produced in a large-scale CVD process. Two MWCNTs,

^zE-mail: mariadelmar.baeza@uab.cat

Nanocyl NC7000 and Nanocyl NC3100 nanotubes, which are named raw MWCNTs and purified-MWCNTs, respectively, were obtained from Nanocyl S.A. (Sambreville, Belgium) with specifications of approximately 10 nm diameter and 1.5 μm length. The purity was reported to be 90% and 95%, respectively. The third carbon material resulted from the purification and activation of the raw MWCNTs with carboxylic groups (named activated-MWCNTs), using a 3:1 mixture of concentrated $\text{H}_2\text{SO}_4/\text{HNO}_3$ acids in ultrasound bath for 90 min.³⁹ The purity of the final activated material (activated-MWCNTs) is 97.2% in carbon. Epotek H77A and its corresponding hardener Epotek H77B were obtained from Epoxy Technology (Billerica, MA, USA) and used as polymeric matrix. All solutions were prepared using deionised water from a Milli-Q system (Millipore, Billerica, MA, USA). Potassium ferricyanide/ferricyanide (99.8%), ascorbic acid (99.5%), potassium nitrate (99.0%), potassium chloride (99.5%), sulfuric acid (96%) and nitric acid (65%) were purchased from Sigma-Aldrich (St. Louis, MO, USA).

Apparatus.— Electrochemical Impedance Spectroscopy (EIS) study was performed using a potentiostat/galvanostat Autolab system (PGSTAT 30 and FRA boards, Eco Chemie, Utrecht, The Netherlands) with a three-electrode configuration. The system was run on a PC using GPES and FRA 4.9 software. An AgCl covered silver wire and a platinum-based electrode 52–671 (Crison Instruments, Alella, Barcelona, Spain) were used as reference and auxiliary electrodes, respectively. The MWCNT/epoxy nanocomposites were employed as working electrodes.

Electroanalytical experiments were carried out by hydrodynamic amperometry, using an amperometer LC-4C 4C (Bio Analytical Systems INC., West Lafayette, IN, USA) under three-electrode configuration as well. In this case, a simple junction reference electrode Ag/AgCl Orion 900100 (Thermo Electron Corporation, Beverly, MA, USA) was used as reference electrode.

Electrical resistance measurements were performed by means of a digital multimeter (Fluke, Everett, WA, USA). Transmission Electron Microscopy (TEM) images were obtained with a JEM-1400 unit with an acceleration voltage of 120 kV. Measurements of nanocomposites topography were made by Confocal Microscopy 3D (CM3D). A Leica DCM 3D unit to 150x magnifications was used for measuring fifty-seven profiles in three different areas for each optimum nanocomposite electrode (ISO 4287). Thermogravimetric Analysis (TGA) was carried out using a Netzsch instrument; model STA 449 F1 Jupiter. Field-Portable X-Ray Fluorescence Spectroscopy (FP-XRF) values were obtained using Alpha-6500R (Innov-X Systems Inc., Woburn, MA, USA).

Procedure.— Impedance and voltammetric measurements were made under quiescent condition in 10.0 ml of a 0.1 M potassium chloride (KCl) solution containing 0.01 M potassium ferricyanide/ferricyanide, $[\text{Fe}(\text{CN})_6]^{3-/4-}$. The experiments were performed at room temperature (25°C). For impedance measurements, a frequency range of 0.1 Hz to 100 kHz was employed at redox equilibrium potential, which was previously obtained by CV. The signal amplitude to perturb the system was 10 mV and the equilibrium time was 15 s. Finally, MWCNT nanocomposite response against different concentrations of analyte was evaluated by hydrodynamic amperometry. A daily-prepared 0.01 M ascorbic acid solution was used as stock solution. Standard solutions were prepared by dilution of the stock solution. A 10.0 ml 0.01 M $\text{HNO}_3/\text{KNO}_3$ solution was used as a background electrolyte in amperometric detection of ascorbic acid. Amperometric measurements were carried out at 600 mV fixed potential under stirring conditions (rotation speed: 1100 rpm).

The carbon content was evaluated by TGA.⁴⁰ Approximately 20 mg sample was heated to 1000°C at 10°C/min, using air flow. The mass of the sample was continuously measured as a function of temperature and the rate of weight loss (d.t.g.) was automatically recorded. Diameter and length of the three different MWCNTs were estimated from TEM images. For these measurements, ~1 mg of MWCNTs was dispersed in 5 ml of acetone as organic solvent and

then placed in ultrasound bath for 60 min. Finally, a drop of the solution was placed on a grid and let it dry before TEM analysis. Both distributions were compiled from at least 100 tubes. Lastly, FP-XRF was used in order to quantify and identify the metal remaining of the raw MWCNTs. Around 500 mg of sample was needed to carry out the analysis.

Nanocomposite electrodes preparation.— A resin Epotek H77 and its corresponding hardener compound were mixed in a 20:3 (w/w) ratio.⁴¹ Three series of MWCNT/epoxy nanocomposites were prepared by loading different amounts of CNTs, from 1% to 12% (w/w) into the epoxy resin before hardening. The nanocomposites were homogenized for 1 h. The mixture was blended thoroughly and placed in the hollow end of a 6 mm intern-diameter PVC tube to form the body of the electrode. The nanocomposite paste electrode thickness in the electrode was 3 mm. The composite paste electrodes were allowed to harden during 24 h at 80°C.⁴⁰ Then, electrode surfaces were polished using different sandpapers of decreasing grain size. The final electrode dimensions were 28 mm² of physic area. The three series of MWCNT/epoxy nanocomposites were made in the same way. While the nature of the three MWCNT samples is the same (from commercial raw MWCNTs), the purity was modified by a) a non-oxidative purified method (commercial purified-MWCNTs) and b) an oxidative active-purified method with carboxylic groups (activated-MWCNTs). According to this scheme, the first series was raw MWCNT/epoxy nanocomposites, S1; the second series consisted of purified-MWCNT/epoxy nanocomposites, S2; and finally, the third series of nanocomposites was made dispersing activated-MWCNTs into epoxy resin, S3.

Results and Discussion

Physical properties characterization of MWCNTs.— The study of purity was made using raw MWCNTs (90% in C given by manufacturer specifications) as raw carbon material. Purified-MWCNTs were obtained by a non-oxidative acidic treatment of raw MWCNTs, also according to the manufacturer. The second purification method consisted in subduing the raw MWCNTs under acid oxidative conditions, obtaining the activated-MWCNTs by using a 3:1 mixture of concentrated $\text{H}_2\text{SO}_4/\text{HNO}_3$.⁴² It is well-known that oxidative acid treatment not only removes the rest of the metallic impurities present in raw carbon nanotubes but also shortens the nanotube length by oxidatively cutting the nanotube at defects of the graphene layer with formation of carboxylic acid terminated tips.⁴³ In order to keep the length/diameter ratio, 90 min of concentrated acid treatment in ultrasound bath was enough not to have an evident reduction of the length, as can be seen in Figure 1 (A, C, D).

TGA analysis offers quantitative information regarding purity of the different samples of MWCNTs. It was observed that the weight loss for the three MWCNT samples took place in a single step; with a maximum of weight loss around 600°C.⁴⁴ The background line is attributed to metallic remaining. While raw MWCNTs analysis revealed 11.0% of metal oxide, purified-MWCNTs showed 98.0% in carbon content. These values are in concordance with the specifications which were given by the manufacturer. Finally, 2.8% in metal oxide was obtained by activated-MWCNTs. As is shown in Table I, both purification methods presented a decrease of metal oxide content. It is important to emphasize that TGA provides only quantitative information on the presence of total metal content in CNT material. Figure 1B shows the FP-XRF analysis, which was carried out in order to quantify and identify the metal content on the raw MWCNTs. Fe, Co and Cu metals were detected on the raw material. While Fe and Co could be quantified, obtaining 15357 ± 227 ppm and 908 ± 16 ppm respectively, only qualitative results could be reached for Cu (see Figure 1B).

Both diameter and length of the three different MWCNT samples were measured using HR-TEM. The average lengths and diameters of the nanotubes are also shown in Table I. For the measurements, a greater dispersion of these nanotubes was needed. After careful data

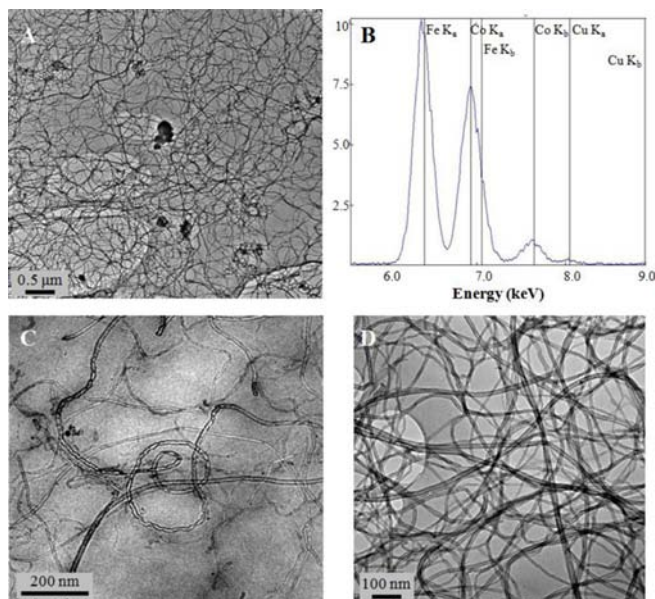


Figure 1. TEM images of A) raw MWCNTs and B) its corresponding FP-RXF spectrum; C) purified-MWCNTs and D) activated-MWCNTs.

compilation, certain differences between the experimental results and the specifications provided by the manufacturer were detected, obtaining higher values in length and diameter. According to TEM characterization, similar length and diameter were obtained for the three MWCNT samples (see Table I). Thus, both parameters could be considered as constants, being the purity the only variable studied. Based on these results, this work was focused on the effect of the MWCNTs purification method on both the electrochemical and electroanalytical response of the nanocomposite electrodes as the optimum MWCNT/epoxy composition ratio. Furthermore, the influence of the metallic particles and the presence or not of carboxylic groups on MWCNTs surface were also evaluated.

Electrical characterization.— The electrical properties of the MWCNT/epoxy nanocomposite electrodes were investigated by percolation theory, see Figure 2. Each series of MWCNT/epoxy nanocomposites were tested in order to estimate the maximum conductivity value of the nanocomposite materials with the minimum conductive particle loading, which is described as near-percolation zone. S1, S2 and S3 nanocomposites containing more than 12% of MWCNTs exhibited a poor mechanical stability. However, those nanocomposites which contain less than 1%, 2% and 5% for S1, S2 and S3 respectively, showed insulating properties with $R \approx \infty$. It is important to highlight that MWCNT loading has to be high enough to guarantee a conducting pathway and sufficiently low bulk resistivity. As is shown in Figure 2B, three different conductive regions regarding the electrical behavior could be observed: high resistance composite zone (HRC), near-percolation composite zone or second percolation composite zone (NPC) and low resistance composite zone (LRC).

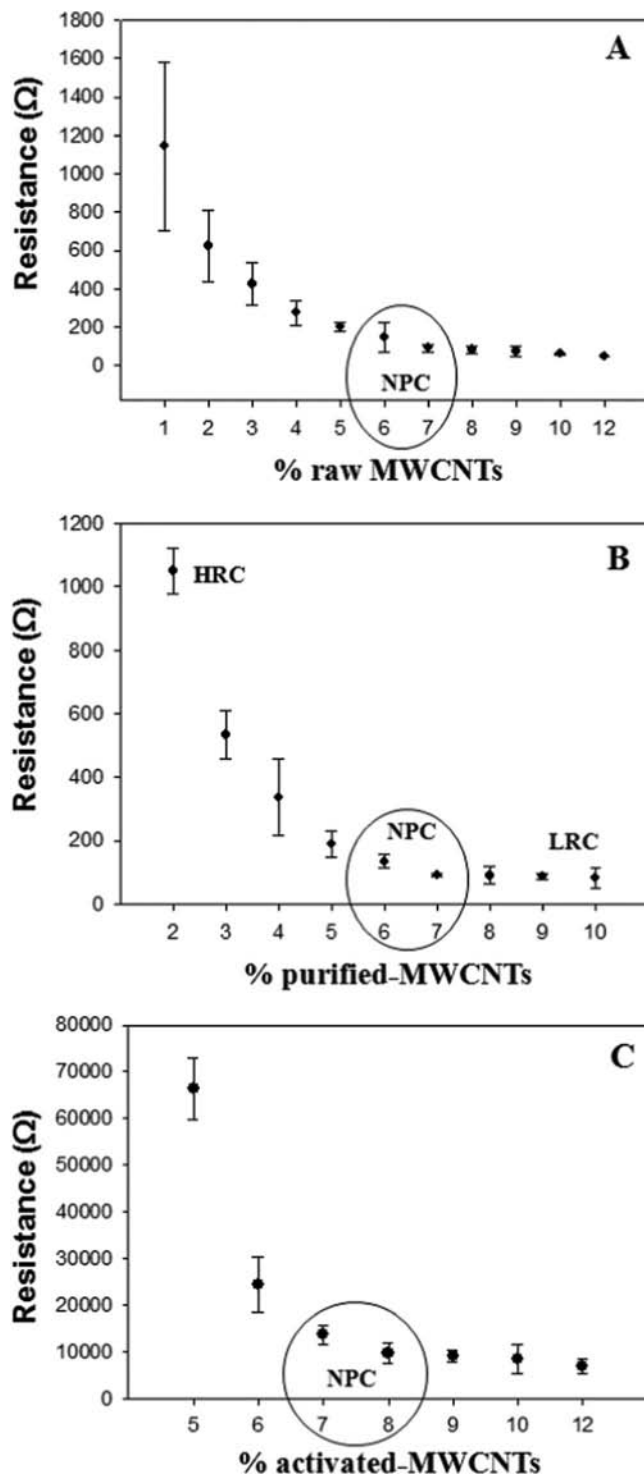


Figure 2. Percolation curve obtained for A) S1, B) S2 and C) S3. In figure B are described the three different conductive regions. HRC: high resistivity zone, NPC: near-percolation zone (highlighted) and LRC: low resistivity zone.

Table I. Physical parameters of three MWCNT samples were studied and compared with values given by the commercial supplier (MFG). Purity was obtained by TGA and TEM results were used to determine length and diameter.

MWCNT sample	Length (μm)		Diameter (nm)		Purity (% in C)	
	MFG	TEM	MFG	TEM	MFG	TGA
Raw MWCNTs	1.5	1.5 – 2.5	9.5	10 – 20	> 90	89.0
Purified-MWCNTs	1.5	1.5 – 2.5	9.5	8 – 16	> 95	98.0
Activated-MWCNTs	-	1.5 – 2.0	-	8 – 18	-	97.2

A2

Based on the electrical results shown in Figure 2, the variation of the resistivity for the three series of nanocomposite materials was negligible between NPC (MWCNT loading > 7%) and LRC (12% of MWCNT loading). To obtain the optimal analytical response is necessary a low resistivity value which produces a high sensitivity.³³ Thus, in terms of resistivity, nanocomposites lying in such interval are suitable for electroanalytical measurements.

Comparing the electrical differences between the three series of MWCNT/epoxy nanocomposite electrodes, a non-displacement in the NPC zone was observed (see Figure 2), given that the length/diameter ratio is practically a constant value, as is shown in Table I. This observation is attributed to the same nature of the three MWCNT samples.³² Hence, values between 6% and 8% were identified as the optimum MWCNT load for each series, since these composition ranges are located into the NPC zone.

Impedimetric characterization.— Ohmic resistance (R_{Ω}), charge transfer resistance (R_{ct}) and double-layer capacitance (C_{dl}) were evaluated for the three series of MWCNTs/epoxy nanocomposite electrodes (S1, S2 and S3), which contain different carbon load (from 1% to 12% for each series). For each MWCNT composition, three equal electrodes were prepared and evaluated in order to obtain reproducibility values of the nanocomposites electrodes. These parameters were obtained by fitting the impedance spectra to a simple equivalent circuit: $R_{\Omega} \cdot (R_{ct} \cdot C_{dl})$.³² This circuit was sufficiently suitable to interpret the R_{Ω} , R_{ct} and C_{dl} values in terms of the interfacial phenomena that occur at the electrochemical cell.

R_{Ω} comprises the resistance of the solution plus any contact resistance, which depends on the ionic concentration, the type of electrolyte, the electrode area and the dry resistance of the nanocomposite. In order to assure the sensitivity and low response time of the nanocomposite electrodes, it is important to achieve low R_{Ω} . S1, S2 and S3 showed a R_{Ω} decrease at the same time that the MWCNT loading increased, as shown in Figure 3 (black plots). While the obtained R_{Ω} values were similar for S1 and S2, S3 exhibited a significant increase, which may be attributed to the incorporation of carboxylic groups on the MWCNT surface. This activation modifies the electrode surface, incorporating a significant steric hindrance on its surface.

R_{ct} parameter reflects the electrode tendency to chemical reaction, which can be measured by EIS from the semicircle diameter in the Nyquist plots.⁴⁵ Light gray bars in Figure 3 presented a decrease of R_{ct} with the increasing of MWCNTs load. As the carbon load increases, the probability of having more electroactive sites also increases and hence, the electrode kinetics. Therefore, nanocomposites with low R_{ct} are appropriated to be used in electrochemical measurements. According to the results, nanocomposites between NPC and LRC presented lower charge transfer values. In addition, the electron transfer resistance of S3 electrodes were much higher than S1 and S2 electrodes, which are not functionalized with carboxylic groups. This fact demonstrated an evident activation of their carbon surface with carboxylic groups. Thus, the introduction of carboxylic groups contributes to a worsening of the electrical conductivity on the electrodes, mainly caused by steric hindrance of the carboxylic groups. Finally, significant differences from an electron-transfer kinetic were not observed between S1 and S2.

C_{dl} parameter is known to be directly related to the charging or background current and is inversely proportional to the signal to noise ratio. It should exhibit increased values for electrodes with high surface area of conducting material.³² The increase of the background current smears the faradaic signal response, especially when the electroactive species are presented in low concentrations. Thus, when the load of MWCNTs increases, the C_{dl} value also increases, as can be observed in Figure 3 (dark gray bars). Therefore, high proportions of MWCNT loads increase the conducting areas, the surface roughness and porosity of the nanocomposites and, consequently, the background current increments remarkably.⁴⁶ While S1 and S2 electrodes showed similar values of C_{dl} , S3 electrodes (Figure 3C inside) exhibited lower values of C_{dl} and hence, an enhancement of the signal to noise ratio what reduces the background current.

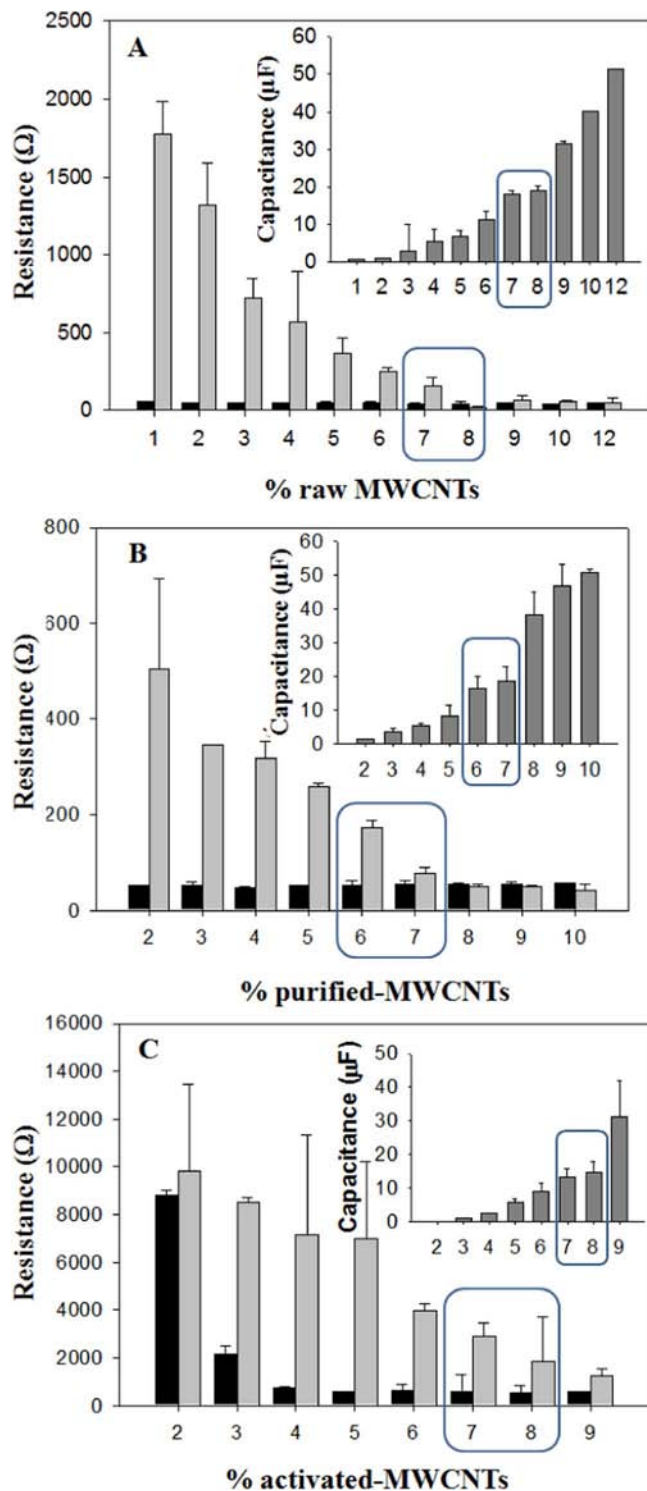


Figure 3. Values of ohmic resistance (R_{Ω} , black, ■), charge transfer resistance (R_{ct} , light gray, ■) and double-layer capacitance (C_{dl} , dark gray, ■) and their corresponding standard deviation ($n = 3$) for A) S1, B) S2 and C) S3. The redox probe $[\text{Fe}(\text{CN})_6]^{3-}/[\text{Fe}(\text{CN})_6]^{4-}$ was used. The optimum MWCNT/epoxy range for electroanalytical purposes is highlighted.

According to the impedance results and taking into account the aim to maintain low resistances and high signal to noise ratio, the composition range between 6% and 8% of conductor material (NPC zone obtained by percolation curve) seems to fulfil the optimum conditions to obtain the most sensitive sensors for each series. Consequently, the NPCs were chosen to continue with the rest of the electroanalytical studies.

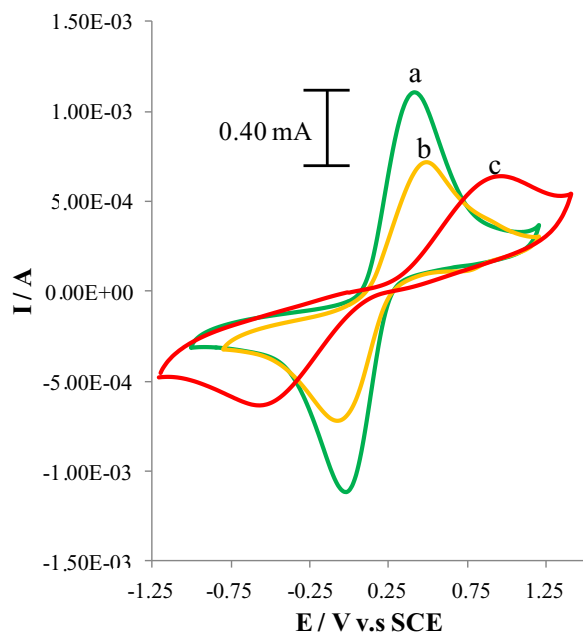


Figure 4. Cyclic voltammograms recorded in 0.01 M $[\text{Fe}(\text{CN})_6]^{3-/4-}$ for a) S1-NPC, b) S2-NPC and c) S3-NPC electrodes. Scan rate: $0.01 \text{ V} \cdot \text{s}^{-1}$.

Voltammetric characterization.— NPCs electrodes of each series (with 7% of conductive material in all cases) were also electrochemically characterized by CV and compared one with other. Figure 4 shows the cyclic voltammograms for the three NPC electrodes containing raw MWCNTs (7% for S1-NPC), purified-MWCNTs (7% for S2-NPC) and activated-MWCNTs (8% for S3-NPC). Different parameters such as peak height (I_p), peak separation potential (ΔE) and electroactive area (A) have been extracted from the cyclic voltammograms, which are shown in Table II. The A was estimated from the peak-shaped voltammograms by using the following equation (Equation 1) for electron transfer-controlled processes:¹⁴

$$I_p = 3.01 \times 10^5 \cdot n^{3/2} (\alpha D_{\text{ox}} \nu)^{1/2} A \cdot C_{\text{ox}}^* \quad [1]$$

where α represents the charge transfer coefficient ($\alpha = 0.5$), D_{ox} corresponds to the diffusion coefficient of the reduced species ($D_{\text{ox}} = 6.32 \times 10^{-6} \text{ cm}^2 \cdot \text{s}^{-1}$), ν represents the scan rate ($\nu = 0.01 \text{ V} \cdot \text{s}^{-1}$), A is the electroactive area and C_{ox}^* is the bulk concentration of the electroactive species ($C_{\text{ox}}^* = 0.01 \text{ M}$). According to CV results, the highest electroactive area was obtained for S1-NPC (0.51 cm^2) due to their major content of conductive material. Contrary, the lowest electroactive area was exhibited for S3-NPC electrodes (0.36 cm^2), mainly caused by the steric hindrance provided by carboxylic groups. Hence, the metal content showed an electrocatalytic effect from an electrochemical point of view. This fact can also be observed in their I_p values, which were 35% and 43% higher than S2-NPC and S3-NPC electrodes, respectively. On the other hand, electrodes containing both purified-MWCNTs and activated-MWCNTs did not exhibit significant differences in their I_p values due to their same purity (see Table I). Furthermore, Figure 4 also revealed a change in ΔE from 0.50 V for S1-NPC electrodes to 1.52 V for S3-NPC electrodes because of the

strong electrode surface modification provided by the incorporation of carboxylic groups. This increase of ΔE turns into partial decrease in the system reversibility.⁴⁷ Contrary, S1-NPC and S2-NPC did not show a significant change in the ΔE value (0.50 V vs. 0.57 V), obtaining both a fast electron transfer process and a pair of well-defined and quasi-reversible redox peaks.

The voltammetric studies show proof-of-concept in respect of observed apparent electrocatalysis in the nanocomposite electrodes containing raw MWCNTs, which is likely due to the role of metal impurities in the carbon nanotubes. While the edge-plane sites/defects on MWCNTs are mainly responsible of the electron transfer exchange for electrodes containing purified-MWCNTs and activated-MWCNTs (note the similar I_p values),⁴⁸ the significant I_p enhancement observed for the electrodes containing raw MWCNTs must derive from the issue of metal impurities in the carbon material. These results are in agreement with our previous studies, where the electrocatalytic effect of modified-electrodes with different functional metal nanoparticles, such as Ag, Au, Cu, Pd and Pt nanoparticles, was verified, using hydrogen peroxide as the model analyte.²²

According to CV results shown in Table II, whereas the S1-NPC electrodes seem to be good bet for analytical purposes due to the suggested electrocatalytic effect of their metallic particles, S3-NPC electrodes are expected to be the worst due to the high steric hindrance provided by the carboxylic groups.

Electroanalytical performance.— The feasibility of the three NPC sensors was evaluated in terms of analytical response by hydrodynamic amperometry, using ascorbic acid as the model analyte (see Figure 5). Some analytical parameters such as the detection limit (LOD) and sensitivity were evaluated for the optimum range of composition of nanocomposite sensors for each series, see Table II. LOD was estimated three times by the $S/N = 3$ criterion.⁴⁹ Interestingly, the lower LOD was obtained for the S1-NPC sensors, which contain raw MWCNTs ($0.014 \pm 0.002 \text{ mg} \cdot \text{L}^{-1}$). These results verified an electrocatalytic effect of the catalyst metal contained in the raw MWCNTs, improving their analytical response to detect ascorbic acid. However, the less effective amperometric response was shown by the S3-NPC sensors ($0.07 \pm 0.02 \text{ mg} \cdot \text{L}^{-1}$), in spite of providing a better signal to noise ratio (C_{dl}). This fact is related to the steric effects of the carboxylic groups on the sensor surface, which considerably decreased the electron transfer process on the sensor surface. S2-NPC sensors exhibited a better LOD ($0.042 \pm 0.008 \text{ mg} \cdot \text{L}^{-1}$) regarding to those containing activated-MWCNTs (S3-NPC), demonstrating that the non-aggressive acidic treatment benefits an enhanced electroanalytical response. On the other hand, S1-NPC sensors also exhibited a lower LOD in comparison with S2-NPC sensors in spite of providing a better sensitivity, demonstrating again the role of the metal impurities on the electrocatalytic detection of ascorbic acid.

Based on electroanalytical results shown in Table II, the activation of carbon materials with carboxylic groups has proven to be neither necessary nor efficient to determine directly analytes by hydrodynamic amperometry. The fact that the sensors containing raw MWCNTs presented an improvement in some physical parameters, such as higher electroactive area (A), faster electron transfer (R_{ct}) and a significant increment in the peak current height (I_p) value compared to both pristine carbon materials (purified-MWCNTs and activated-MWCNTs) lead to enhanced high sensitivity, fast electrode response and low detection limits, as it has been demonstrated for the ascorbic

Table II. Electrochemical values (I_p , A and ΔE) were obtained by CV in a 0.01 M $[\text{Fe}(\text{CN})_6]^{3-/4-}$ solution (scan rate: $0.01 \text{ V} \cdot \text{s}^{-1}$). Analytical parameters (LOD and sensitivity) were studied by hydrodynamic amperometry for the ascorbic acid detection, using a 0.10 M $\text{HNO}_3/\text{KNO}_3$ solution. LOD was calculated which their respectively 95% confidence interval ($n = 3$).

Electrode/Sensor	I_p (mA)	A (cm^2)	ΔE (V)	LOD ($\text{mg} \cdot \text{L}^{-1}$)	Sensitivity ($\mu\text{A} \cdot \text{L} \cdot \text{mg}^{-1}$)
S1-NPC	1.11	0.51	0.50	0.014 ± 0.002	0.071
S2-NPC	0.72	0.42	0.57	0.042 ± 0.008	0.145
S3-NPC	0.64	0.36	1.52	0.07 ± 0.02	0.058

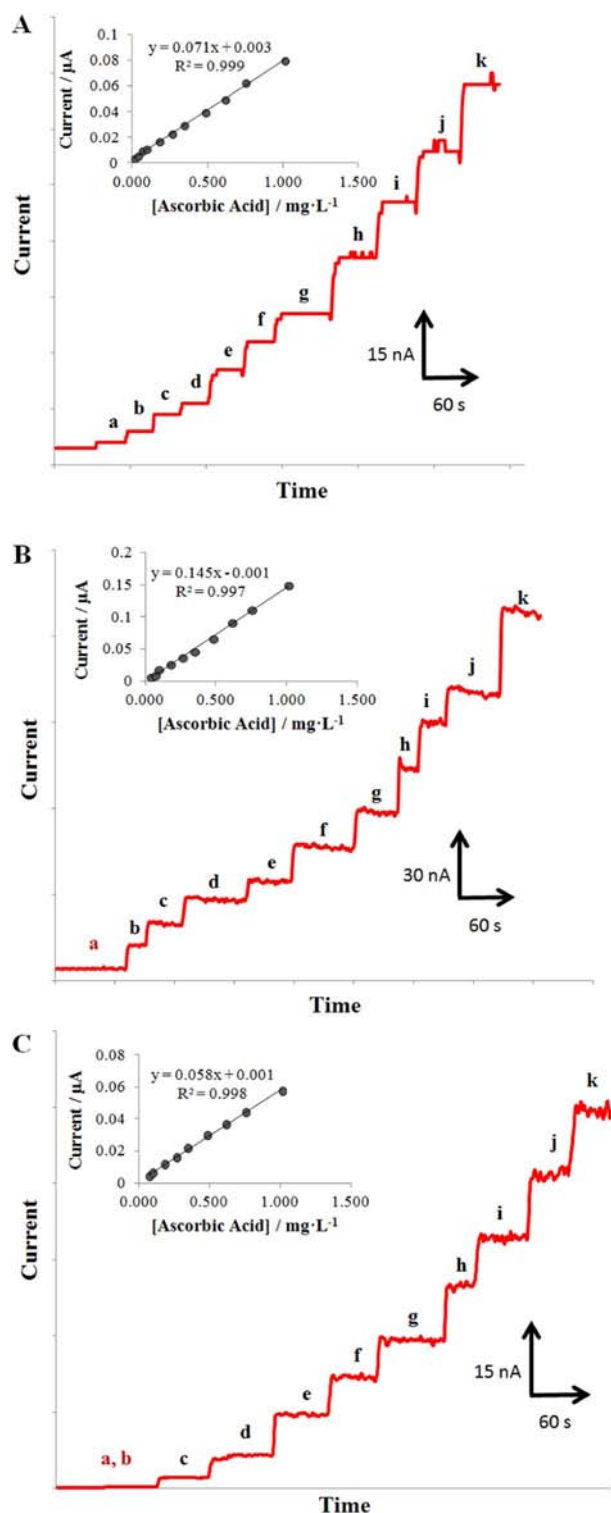


Figure 5. Dynamic responses of A) S1-NPC, B) S2-NPC and C) S3-NPC sensors to successive additions of ascorbic acid in a 0.10 M $\text{HNO}_3/\text{KNO}_3$ solution. Applied potential: 600 mV. Insert: their corresponding calibration curves in the range of (a to k) 0.014 to 1.014 $\text{mg} \cdot \text{L}^{-1}$.

acid detection. It is known that improving those physical parameters, it is possible to reduce the detection limits. Thereby, an improvement in detection limits is expected for other types of analytes.^{22,50}

Morphological characterization.— Roughness surfaces of the three near-percolation nanocomposite electrodes have been compared by confocal microscopy in order to complement the electrochemi-

Table III. Roughness values collected from surface analysis. Data are the mean and standard deviation (SD) from 57 profiles of three areas examined in each nanocomposite (ISO 4287).

Electrodes	R_a^a (μm)		R_q^b (μm)		R_z^c (μm)	
	Mean	SD	Mean	SD	Mean	SD
S1-NPC	0.87	0.33	1.29	0.57	9.09	4.62
S2-NPC	0.61	0.20	0.84	0.32	5.86	2.57
S3-NPC	0.54	0.08	0.72	0.12	4.25	1.06

^aAritmetical mean deviation of the assessed profile.

^bThe root mean square deviation of the assessed profile.

^cMaximum height of the profile.

cal results. The topographic experiment reveals qualitative information about the surface characteristics of MWCNT/epoxy nanocomposite electrodes. The measurements were carried out by CM3D. Figure 6 presents significant images obtained during the electrode surface study. Results presented in Table III show the effect of both the metal impurities and the carboxylic groups on the electrode roughness.

According to confocal microscopy results, the presence of metal impurities significantly increased the roughness of the nanocomposite electrode, mainly due to the presence of more conducting material on the electrode surface. Thus S1-NPC presented an enhancement of the roughness surface around 30% respected to S2-NPC, which is in agreement with the improvement of the electroactive area (A) obtained by CV. However, as it was expected, S3-NPC showed a significant diminution of the roughness surface around 11% respected S2-NPC, which can be explained by the incorporation of carboxylic groups on the MWCNT walls. This decrease is also in agreement with the A values obtained by CV.

Finally, CM3D results corroborated that the electrochemical behavior of MWCNT-based nanocomposite electrodes closely depends on the morphology of their surface, which in turn also depends on the purity of the MWCNT samples. For the same MWCNT load, the presence of metal impurities provides an enhancement on the conductive phase, which were responsible to improve the electroanalytical features of the sensors (see Table II). However, the purification of the MWCNT by an oxidative treatment (activated-MWCNTs) leads a decrease on the electroanalytical response of the sensors, mainly due to the diminution of conducting material on the electrode surface.

Conclusions

Three different MWCNTs with different physical properties, such as purity and oxidative activation or none of their surfaces have been subject of study. They were used to fabricate, characterize and hence optimize MWCNTs/epoxy nanocomposite electrodes in function of the MWCNT nature. EIS and CV techniques, as well as electron microscopy, thermogravimetry, electrical, morphological and amperometric techniques were used to carry out this aim. TGA analysis determined the total content of metal impurities on the MWCNTs. TEM characterization did not provide a significant change in the length/diameter ratio of the MWCNTs after purification treatments. Electrical results showed that NPC zone remained unaltered from 6% to 8% of conductor material, independent of the acidic treatment method used. The electrochemical measurements carried out by CV and EIS were in concordance with the electrical results, since the same optimum range MWCNT/epoxy composition ratio was obtained for each series. Optimized-sensors (or NPC sensors) were used as working electrodes to determine amperometrically ascorbic acid. The electroanalytical characterization interestingly exhibited the lowest LOD for sensors containing raw MWCNTs. Thus, an electrocatalytic metal effect on the analytical response for ascorbic acid became apparent. On the other hand, the highest LOD was obtained for sensors

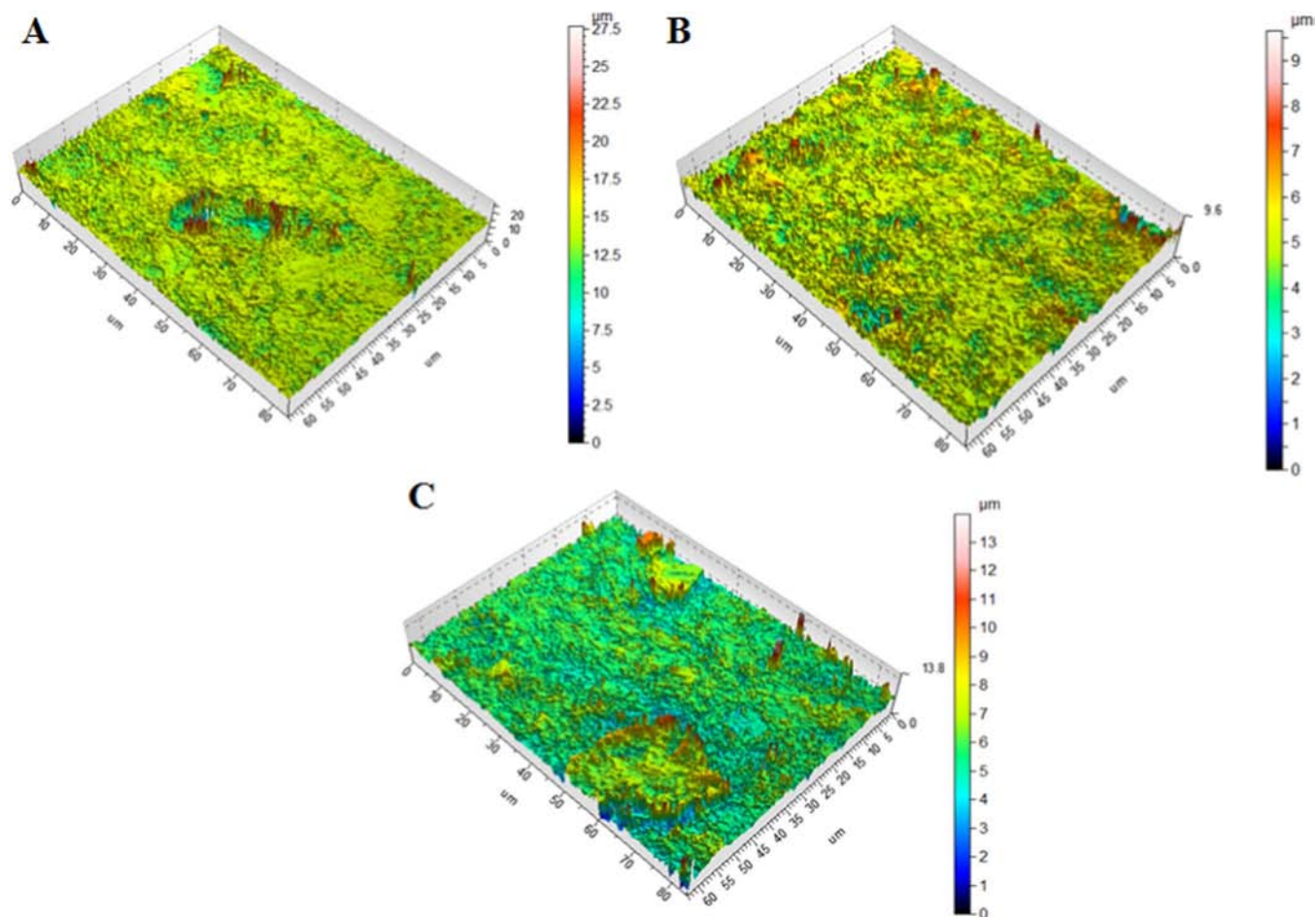


Figure 6. Topographic images of A) S1-NPC, B) S2-NPC and C) S3-NPC were obtained with the 3D Optical Surface Metrology System Leica CM3D for the roughness study.

containing activated-MWCNTs, mainly caused by the steric hindrance of these groups on the sensor surface. Comparing the two purification methods, the non acid oxidative treatment improved the analytical response of the sensors because of the lack of carboxylic groups on the carbon surface. The morphological experiments confirmed that the electrochemical and electroanalytical response of the MWCNT-based nanocomposite sensors closely depends on the MWCNTs nature.

Accordingly, this study opens the way to use the electrocatalytic effects of the metallic impurities of the raw MWCNTs for their application as NPC amperometric nanocomposite (bio)sensors to determine directly low concentrations of different analytes. Finally, this work shows a new perspective in the characterization and optimization of MWCNT-based electrochemical nanocomposite (bio)sensors which will allow extending this approach to another kind of carbon nanomaterials.

Acknowledgment

This work was supported by the project CTQ2012-36165. J. Muñoz thanks Universitat Autònoma de Barcelona (UAB) for the award of PIF studentship.

References

- H. W. Kroto, J. R. Heath, S. C. O'Brien, R. F. Curl, and R. E. Smalley, C 60: buckminsterfullerene. *Nature*, **318**(6042), 162 (1985).
- S. Iijima, Helical microtubules of graphitic carbon. *Nature*, **354**(6348), 56 (1991).
- M. Pumera and A. Escarpa, Nanomaterials as electrochemical detectors in microfluidics and CE: Fundamentals, designs, and applications. *Electrophoresis*, **30**(19), 3315 (2009).
- L. Radushkevich and V. Lukyanovich, About the structure of carbon formed by thermal decomposition of carbon monoxide on iron substrate. *J. Phys. Chem. (Moscow)*, **26**, 88 (1952).
- M. Glerup, J. Steinmetz, D. Samaille, O. Stephan, S. Enouz, A. Loiseau, S. Roth, and P. Bernier, Synthesis of N-doped SWNT using the arc-discharge procedure. *Chemical Physics Letters*, **387**(1), 193 (2004).
- Y. Zhang, H. Gu, and S. Iijima, Single-wall carbon nanotubes synthesized by laser ablation in a nitrogen atmosphere. *Applied physics letters*, **73**(26), 3827 (1998).
- M. Hashempour, A. Vicenzo, F. Zhao, and M. Bestetti, Effects of CVD direct growth of carbon nanotubes and nanofibers on microstructure and electrochemical corrosion behavior of 316 stainless steel. *Materials Characterization*, **92**(0), 64 (2014).
- T.-J. Park, S. Banerjee, T. Hemraj-Benny, and S. S. Wong, Purification strategies and purity visualization techniques for single-walled carbon nanotubes. *Journal of Materials Chemistry* **16**(2), 141 (2006).
- R. H. Baughman, A. A. Zakhidov, and W. A. de Heer, Carbon nanotubes—the route toward applications. *Science* **297**(5582), 787 (2002).
- T. W. Ebbesen, H. J. Lezec, H. Hiura, J. W. Bennett, H. F. Ghaemi, and T. Thio, Electrical conductivity of individual carbon nanotubes. *Nature* **382**(6586), 54 (1996).
- G. Chai and Q. Chen, Characterization Study of the Thermal Conductivity of Carbon Nanotube Copper Nanocomposites. *Journal of Composite Materials* **44**(24), 2863 (2010).
- M. M. J. Treacy, T. W. Ebbesen, and J. M. Gibson, Exceptionally high Young's modulus observed for individual carbon nanotubes. *Nature* **381**(6584), 678 (1996).
- M. Pumera, The electrochemistry of carbon nanotubes: fundamentals and applications. *Chemistry-A European Journal* **15**(20), 4970 (2009).
- M. Pacios, M. Del Valle, J. Bartroli, and M. Esplandiú, Electrochemical behavior of rigid carbon nanotube composite electrodes. *Journal of Electroanalytical Chemistry*, **619**, 117 (2008).
- A. G. Crevillén, M. Ávila, M. Pumera, M. C. González, and A. Escarpa, Food analysis on microfluidic devices using ultrasensitive carbon nanotubes detectors. *Analytical chemistry* **79**(19), 7408 (2007).
- Q. Zhao, Z. Gan, and Q. Zhuang, Electrochemical sensors based on carbon nanotubes. *Electroanalysis* **14**(23), 1609–1613 (2002).
- A. A. Ganash, Electrochemical synthesis and corrosion behavior of polypyrrole and polypyrrole/carbon nanotube nanocomposite films. *Journal of Composite Materials* **48**(18), 2215 (2014).

18. J. Shi, Z. Wang, and H.-I. Li, Electrochemical fabrication of polyaniline/multi-walled carbon nanotube composite films for electrooxidation of methanol. *J Mater Sci* **42**(2), 539 (2007).
19. S. K. Vashist, D. Zheng, K. Al-Rubeaan, J. H. T. Luong, and F.-S. Sheu, Advances in carbon nanotube based electrochemical sensors for bioanalytical applications. *Biotechnology Advances* **29**(2), 169 (2011).
20. Y. Liu, Z. Su, Y. Zhang, L. Chen, T. Gu, S. Huang, Y. Liu, L. Sun, Q. Xie, and S. Yao, Amperometric determination of ascorbic acid using multiwalled carbon nanotube-thiolated polyaniline composite modified glassy carbon electrode. *Journal of Electroanalytical Chemistry*, **709**, 19 (2013).
21. M. Noonan, Glucose biosensor based on carbon nanotube epoxy composites. *Nanoscience and Nanotechnology*, **5**, 1694 (2005).
22. J. Muñoz, J. Bastos-Arrieta, M. Muñoz, D. Muraviev, F. Céspedes, and M. Baeza, Simple green routes for the customized preparation of sensitive carbon nanotubes/epoxy nanocomposite electrodes with functional metal nanoparticles. *RSC Advances* **4**(84), 44517 (2014).
23. M. Liang, F. Jin, R. Liu, R. Su, W. Qi, Y. Yu, L. Wang, and Z. He, Enhanced electrochemical detection performance of multiwall carbon nanotubes functionalized by aspartame. *J Mater Sci* **48**(16), 5624 (2013).
24. D. Ragupathy, A. I. Gopalan, and K.-P. Lee, Electrocatalytic oxidation and determination of ascorbic acid in the presence of dopamine at multiwalled carbon nanotube-silica network-gold nanoparticles based nanohybrid modified electrode. *Sensors and Actuators B: Chemical* **143**(2), 696 (2010).
25. R. Olivé-Monllau, A. Pereira, J. Bartrolí, M. Baeza, and F. Céspedes, Highly sensitive CNT composite amperometric sensors integrated in an automated flow system for the determination of free chlorine in waters. *Talanta*, **81**(4-5), 1593 (2010).
26. R. L. McCreery, Advanced Carbon Electrode Materials for Molecular Electrochemistry. *Chemical Reviews* **108**(7), 2646 (2008).
27. B. Krause, T. Villmow, R. Boldt, M. Mende, G. Petzold, and P. Pötschke, Influence of dry grinding in a ball mill on the length of multiwalled carbon nanotubes and their dispersion and percolation behavior in melt mixed polycarbonate composites. *Composites Science and Technology* **71**(8), 1145 (2011).
28. M. Morcom, K. Atkinson, and G. P. Simon, The effect of carbon nanotube properties on the degree of dispersion and reinforcement of high density polyethylene. *Polymer* **51**(15), 3540 (2010).
29. W. Bauhofer and J. Z. Kovacs, A review and analysis of electrical percolation in carbon nanotube polymer composites. *Composites Science and Technology* **69**(10), 1486 (2009).
30. P. Pyotishkumar, E. Logakis, S. M. George, J. Pionteck, L. Häussler, R. Haßler, P. Pissis, and S. Thomas, Preparation and properties of multiwalled carbon nanotube/epoxy-amine composites. *Journal of Applied Polymer Science* **127**(4), 3063 (2013).
31. S. Carabineiro, M. Pereira, J. Nunes-Pereira, J. Silva, C. Caparros, V. Sencadas, and S. Lanceros-Méndez, The effect of nanotube surface oxidation on the electrical properties of multiwall carbon nanotube/poly (vinylidene fluoride) composites. *J Mater Sci* **47**(23), 8103 (2012).
32. J. Muñoz, J. Bartrolí, F. Céspedes, and M. Baeza, Influence of raw carbon nanotubes diameter for the optimization of the load composition ratio in epoxy amperometric composite sensors. *Journal of Materials Science*, **1** (2014).
33. R. Olivé-Monllau, M. Baeza, J. Bartrolí, and F. Céspedes, Novel Amperometric Sensor Based on Rigid Near-Percolation Composite. *Electroanalysis* **21**(8), 931 (2009).
34. M. Pumera and H. Iwai, Metallic impurities within residual catalyst metallic nanoparticles are in some cases responsible for "electrocatalytic" effect of carbon nanotubes. *Chemistry-An Asian Journal* **4**(4), 554 (2009).
35. D. Vilela, A. Ansón-Casaos, M. T. Martínez, M. C. González, and A. Escarpa, High NIR-purity index single-walled carbon nanotubes for electrochemical sensing in microfluidic chips. *Lab on a Chip* **12**(11), 2006-2014 (2012).
36. A. Eatemadi, H. Daraee, H. Karimkhanloo, M. Kouhi, N. Zarghami, A. Akbarzadeh, M. Abasi, Y. Hanifehpour, and S. W. Joo, Carbon nanotubes: properties, synthesis, purification, and medical applications. *Nanoscale research letters* **9**(1), 1 (2014).
37. M. Penza, M. Tagliente, P. Aversa, M. Re, and G. Cassano, The effect of purification of single-walled carbon nanotube bundles on the alcohol sensitivity of nanocomposite Langmuir-Blodgett films for SAW sensing applications. *Nanotechnology*, **18**(18), 185502 (2007).
38. R. Pearce, M. Andersson, J. Belmonte, I. Gracia, M. Stevens, K. Buchholt, J. Shaw, M. Shaffer, and A. L. Spetz, A Comparison of the Gas Sensing Properties of Purified and Platinum Decorated Chemical Vapor Deposition Grown Multi Walled Carbon Nanotubes. In *Smart Sensors and Sensing Technology*, Springer: 2008; pp 85.
39. Y. Li, X. Zhang, J. Luo, W. Huang, J. Cheng, Z. Luo, T. Li, F. Liu, G. Xu, X. Ke, L. Li, and H. J. Geise, Purification of CVD synthesized single-wall carbon nanotubes by different acid oxidation treatments. *Nanotechnology*, **15**(11), 1645 (2004).
40. E. Mansfield, A. Kar, and S. A. Hooker, Applications of TGA in quality control of SWCNTs. *Analytical and bioanalytical chemistry* **396**(3), 1071 (2010).
41. S. Alegret, F. Céspedes, E. Martínez-Fàbregas, D. Martorell, A. Morales, E. Centelles, and J. Muñoz, Carbon-polymer biocomposites for amperometric sensing. *Biosensors and Bioelectronics* **11**(1), 35 (1996).
42. M. Alvaro, C. Aprile, B. Ferrer, and H. Garcia, Functional molecules from single wall carbon nanotubes. Photoinduced solubility of short single wall carbon nanotube residues by covalent anchoring of 2, 4, 6-Triarylpyrylium units. *Journal of the American Chemical Society* **129**(17), 5647 (2007).
43. K. J. Ziegler, Z. Gu, H. Peng, E. L. Flor, R. H. Hauge, and R. E. Smalley, Controlled oxidative cutting of single-walled carbon nanotubes. *Journal of the American Chemical Society* **127**(5), 1541 (2005).
44. L. S. Pang, J. D. Saxby, and S. P. Chatfield, Thermogravimetric analysis of carbon nanotubes and nanoparticles. *The Journal of Physical Chemistry* **97**(27), 6941(1993).
45. A. J. Bard and L. R. Faulkner, *Electrochemical methods: fundamentals and applications*. Wiley New York: 1980; Vol. 2.
46. G. Palasantzas and G. M. E. A. Backx, Roughness effects on the double-layer charge capacitance: the case of Helmholtz layer induced roughness attenuation. *Surface Science* **540**(2-3), 401 (2003).
47. J. Wang, *Analytical electrochemistry*. John Wiley & Sons: 2006.
48. C. E. Banks, T. J. Davies, G. G. Wildgoose, and R. G. Compton, Electrocatalysis at graphite and carbon nanotube modified electrodes: edge-plane sites and tube ends are the reactive sites. *Chemical Communications* **7**, 829 (2005).
49. R. Olivé-Monllau, C. S. Martínez-Cisneros, J. Bartrolí, M. Baeza, and F. Céspedes, Integration of a sensitive carbon nanotube composite electrode in a ceramic micro-analyzer for the amperometric determination of free chlorine. *Sensors and Actuators B: Chemical* **151**(2), 416 (2011).
50. R. Montes, J. Bartrolí, F. Céspedes, and M. Baeza, Towards to the improvement of the analytical response in voltammetric sensors based on rigid composites. *Journal of Electroanalytical Chemistry*, **733**, 69 (2014).



CrossMark
 click for updates

Cite this: *RSC Adv.*, 2014, 4, 44517

Simple green routes for the customized preparation of sensitive carbon nanotubes/epoxy nanocomposite electrodes with functional metal nanoparticles

Jose Muñoz, Julio Bastos-Arrieta, Maria Muñoz, Dmitri Muraviev, Francisco Céspedes and Mireia Baeza*

In this communication, we report novel, simple and effective methodologies for the incorporation of functional metal nanoparticles in carbon nanotubes/epoxy nanocomposite electrodes. The incorporation of nanoparticles was obtained by three different routes: (a) *in situ* functionalization of carbon nanotube surfaces, (b) incorporation and dispersion into a composite matrix and (c) composite surface modification by drop-attachment. These techniques offer a customized route for the preparation of sensitive amperometric sensors. Independent of the route of noble metal nanoparticle incorporation, the final result is a significant enhancement of the electroanalytical response.

Received 18th July 2014
 Accepted 27th August 2014

DOI: 10.1039/c4ra07294d

www.rsc.org/advances

Introduction

Carbon nanotubes (CNTs) represent an important group of nanomaterials, which are used in different applications since their discovery because of their remarkable electrical, chemical, mechanical, thermal and structural properties.^{1–3} Currently, significant interest is focused on nanocomposites based on CNTs, especially in multiwalled carbon nanotubes (MWCNTs), because of their electrocatalytic activity. The unique qualities of MWCNTs make them highly attractive for the development of CNTs-based chemical (bio)sensors, in general, and electrochemical detection, in particular.^{4–8} Furthermore, CNTs can be considered as feasible supports for heterogeneous catalysts such as functional metal nanoparticles (FMNPs).^{9–11}

Recently, FMNPs have been used extensively in the fields of physical, chemical and material sciences because of their surface-volume ratio that provides them unique properties different from the analogous bulk material.^{12–14}

Modified-CNT electrodes combined with these nanoparticles have shown excellent electrocatalytic activity because of the fast electron transfer ability of CNTs,^{15,16} as can be seen in the electrochemical detection of hydrogen peroxide and glucose.^{17,18} Accordingly, FMNPs have received considerable attention for their catalytic and electrochemical features for the preparation of amperometric sensors and biosensors,^{19–21} leading to an enhancement of the electron transfer between redox centers in

the analyte and electrode, decreasing the overpotentials of several analytically important electrochemical reactions.^{22,23}

Despite these advantages, the surface modification of CNTs with nanocrystals as FMNPs usually involves thermal evaporation,²⁴ electroless deposition by galvanic replacement,²⁵ MNPs hydrosol absorption²⁶ or electrochemical deposition.²⁷ Greener synthesis routes have also been used for the preparation of FMNPs on CNTs, such as seed-mediated growth,^{28,29} in which metal salt solutions can be reduced by a strong reducing agent (*e.g.* NaBH₄) at room temperature and in an aqueous solution. The possible aggregation of the FMNPs limits their application in electrochemical systems. Because of this fact, the preparation of FMNPs must provide an extra level of stability and a favourable distribution in the final nanocomposite material.²⁰ Regarding this, the intermatrix synthesis (IMS) technique becomes a valid FMNPs preparation methodology. IMS takes advantage of the ion-exchange properties of the support matrix (*e.g.* sulfonic resins, CNTs) for consecutive loading and reduction processes during the synthesis of FMNPs with a favourable distribution in the final composite material.^{30,31} IMS is based on the following two sequential steps:

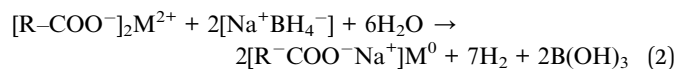
i. Introduction of the FMNPs precursors into the polymer by loading their functional groups with the desired metal ions or metal complex precursors of the nanoparticles.

ii. Their reduction to zero-valent state inside the support matrix is carried out by using an appropriate reducing agent such as NaBH₄ or ascorbic acid.

Eqn (1) and (2) present the classical IMS on cationic exchangers (*e.g.* carboxylic functionality):



Departament de Química, Facultat de Ciències, Universitat Autònoma de Barcelona, Edifici C-Nord, Cerdanyola del Vallès (Bellaterra), Barcelona, 08193, Spain. E-mail: mariadelmar.baeza@uab.cat; Tel: +34 93581 4927



During stage 2 of IMS, the ion-exchange functionality of the support matrix is regenerated, which allows repeating sequential loading and reduction stages to increase the amount of FMNPs content and their thickness.

As a result, MWCNTs have been used for the construction of sensitive amperometric sensors based on modified-MWCNTs/epoxy nanocomposites for hydrogen peroxide detection. An IMS technique is proposed as a route for the modification of MWCNTs with FMNPs. Finally, this communication is focused on three different routes of functionalization of the transducer material with Au- and Pd-FMNPs, using the IMS(-modified) technique.

Experimental

Chemicals and reagents

Raw MWCNTs used in this research was provided by SES Research (Houston, TX, USA), the physical properties of which are >95% of carbon purity, 10–30 nm is the outer diameter and about 5–15 μm in length. It was produced using a chemical vapour deposition (CVD) method. Epotek H77A and its corresponding hardener Epotek H77B were obtained from Epoxy Technology (Billerica, MA, USA) and were used as a polymeric matrix. Metal nanoparticles were synthesized using inorganic salts. All the metal salts were supplied by Sigma-Aldrich (St. Louis, MO, USA) and did not require any further treatment. All the dissolutions were prepared using deionised water from a Milli-Q system (Millipore, Billerica, MA, USA). Potassium ferricyanide/ferrocyanide (99.8%), potassium chloride (99.5%), potassium phosphate dibasic anhydrous (>99.0%) and potassium phosphate monobasic (>99.0%) were purchased from Sigma-Aldrich (St. Louis, MO, USA). Finally, sodium borohydride (96%) was provided by Panreac (Castellar del Vallès, Barcelona, Spain), and ion-exchange resins were kindly supplied by Purolite® (Purolite Iberica S.L., Barcelona, Spain). All reagents were of the highest grade available and used without further purification.

Electrochemical experiments

Cyclic voltammetry (CV) measurements, linear sweep voltammetry (LSV) and electrochemical impedance spectroscopy (EIS) were performed using a computer-controlled Autolab PGSTAT30 potentiostat/galvanostat (EcoChemie, Utrecht, The Netherlands) using a GPES (v.4.9) software package provided by the manufacturer. A three-electrode configuration cell was used for voltammetric and impedimetric measurements. A double-junction reference electrode Ag/AgCl Orion 900200 (Thermo Electron Corporation, Beverly, MA, USA) and a platinum-based electrode 52-671 (Crison Instruments, Alella, Barcelona, Spain) were used as the reference and auxiliary, respectively. The different MWCNTs composite electrodes with/without metal nanoparticles were used as working electrodes. EIS and CV measurements were made in a 10.0 mL of 0.1 M potassium

chloride (KCl) solution containing 0.01 M potassium ferricyanide/ferrocyanide, $[\text{Fe}(\text{CN})_6]^{3-/4-}$, under quiescent conditions. It is known that the kinetic processes of such electroactive species are strongly dependent on the state of the electrode surface. The experiments were performed at room temperature (25 °C). The impedance spectra were recorded in the frequency range of 0.1 Hz to 100 kHz at the redox equilibrium potential. The signal amplitude to perturb the system was 10 mV. Cyclic and linear sweep voltammograms were recorded at the same experimental condition (10 mV s^{-1} of scan rate) for each composite electrode. For LSV measurements, different hydrogen peroxide concentrations were added in 10.0 mL of phosphate buffer solution in 0.1 M KCl (PBS) at pH 7.0. PBS solution was used as a background electrolyte.

Amperometric measurements were performed using an amperimeter LC-4C (Bio Analytical Systems INC., West Lafayette, IN, USA). Amperometric detection was made under force convection by stirring the solution with a magnetic stirrer. A freshly prepared 0.01 M hydrogen peroxide solution (H_2O_2) was used as a stock solution. Standard solutions were prepared by the dilution of the stock solution. Solution of PBS at pH 7.0 was used as a background electrolyte in amperometric detection of hydrogen peroxide.

Microscopy characterization

Scanning electron microscopy (SEM) images were taken using Zeiss® MERLIN FE-SEM. High resolution transmission electron microscopy (HR-TEM) images and energy dispersive X-ray spectroscopy analysis (EDS) were obtained by JEM-1400 unit with an acceleration voltage of 120 kV. Approximately 1 mg of MWCNTs sample was dispersed in 5 mL of acetone as organic solvent and then placed in ultrasound bath for 1 h for HR-TEM. Finally, a drop of the suspension was placed on a grid and allowed to dry before HR-TEM and EDS analysis. The FMNPs distribution was evaluated with the study of at least 200 nanoparticles from different TEM images.

Metal content in MWCNTs by thermogravimetric analysis

Thermogravimetric analysis (TGA) were performed on a Netzsch instrument, model STA 449 F1 Jupiter® (Selb, Bavaria, Germany), with a flow of air. A ~ 20 mg sample was heated to 1000 °C at 10 °C min^{-1} , using a flow of air. The mass of the sample was continuously measured as a function of temperature, and the rate of weight loss (d.t.g.) was automatically recorded.

Nanocomposite preparation methodology: synthesis and incorporation of FMNPs

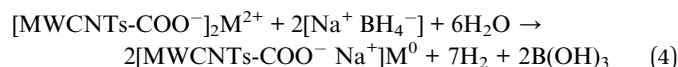
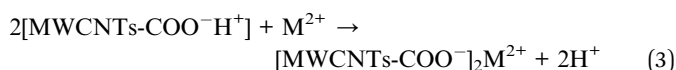
Working nanocomposite electrodes were prepared following the fundamental methodology, which was previously established in our research group.³² A resin Epotek H77 and its corresponding hardener compound were mixed in the ratio 20 : 3 (w/w). The composites were homogenized for 1 h. The composite paste electrodes were allowed to harden for 24 h at 80 °C.⁸ Later, electrode surfaces were polished with various sandpapers of decreasing grain size. The final electrode

dimensions were 28 mm² and 3 mm for its physical area and thickness, respectively.

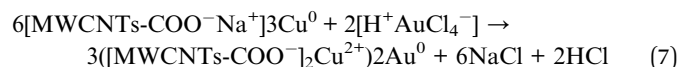
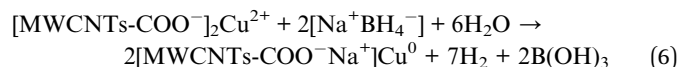
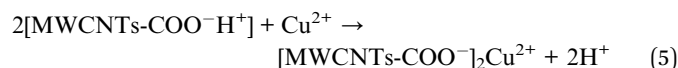
Three different methodologies were carried out for the modification of the transducer material with FMNPs: (a) *in situ* functionalization of carbon nanotube surface, (b) incorporation and dispersion into composite matrix and (c) composite surface modification by drop-attachment. These methodologies are shown in Fig. 1 and are described as follows:

(a) Route A (RA). The FMNPs are synthesized *in situ* on the CNTs surface. The composite was prepared by loading a 10% (w/w) of functionalized-MWCNTs with FMNPs (FMNPs@MWCNTs) into the epoxy resin before hardening. Previously, it was necessary to make the mixture of Au-FMNPs@MWCNTs and Pd-FMNPs@MWCNTs obtained separately, for which 3 : 2 ratio was used.

Concerning this, the general IMS procedure for FMNPs was carried out as shown in eqn (3) and (4). The functional groups of the carbon nanotubes were previously activated with 2.5 M HNO₃. The pH was then adjusted to 6.0. Thus, the next step consists of the metal loading of the MWCNTs by using 0.01 M cationic metal (M²⁺) aqueous solution (20 mL) followed by reduction with 0.1 M NaBH₄ under magnetic stirring at ambient conditions.



As the precursor for Au-FMNPs is HAuCl₄, a previous IMS of Cu-FMNPs was needed as sacrifice nanotemplates. As a result, the nanocomposite materials containing the Cu-FMNPs were immersed in a 0.01 M HAuCl₄ solution for a stoichiometry galvanic replacement reaction between Au³⁺ and Cu⁰ as presented in eqn (5)–(7).



The FMNPs prepared by this procedure were Ag-, Au-, Cu-, Pd- and Pt-FMNPs.

(b) Route B (RB). The raw FMNPs are dispersed into the composite matrix. The composite was prepared by loading a 10% amount of raw MWCNTs adding FMNPs powder into the epoxy resin before hardening.

For RB, the only difference for the preparation of the FMNPs from that of RA is the supporting matrix. Therefore, the IMS of

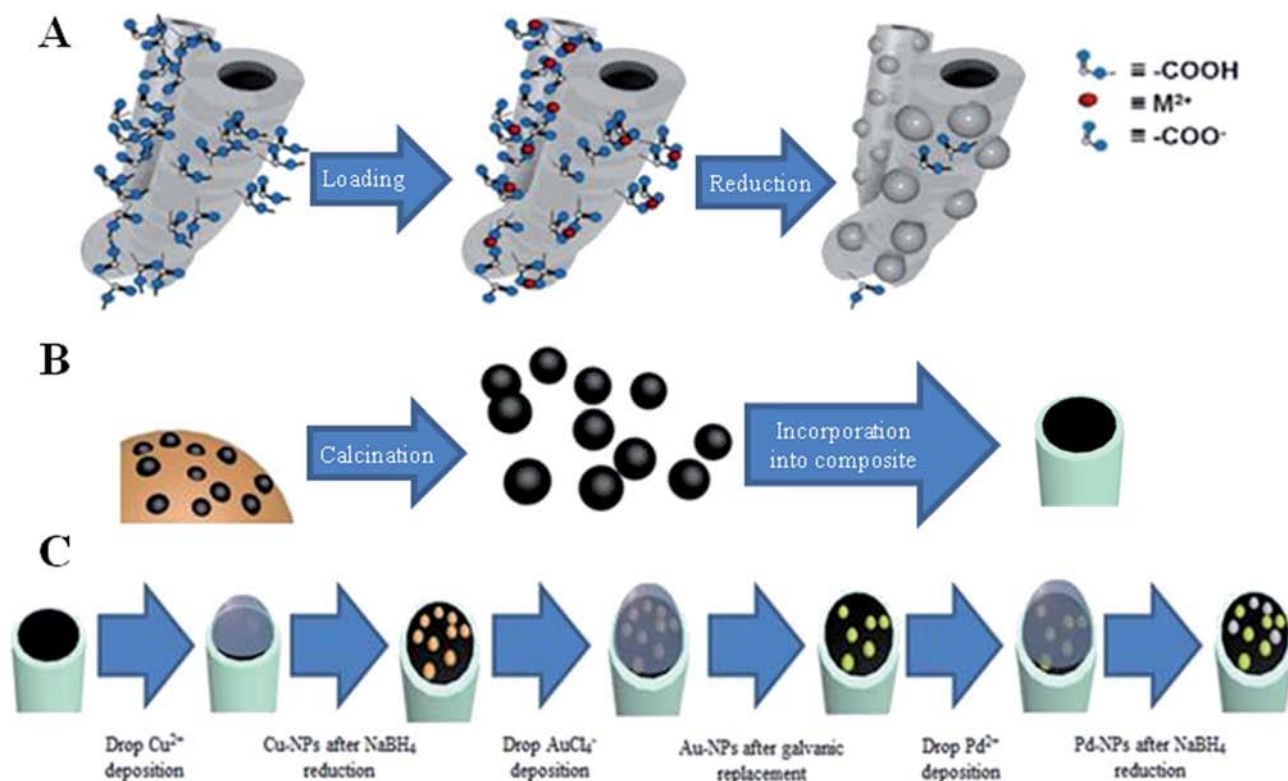
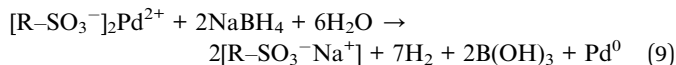


Fig. 1 Routes of modification scheme: (A) example of *in situ* functionalization of carbon nanotube surface for a M²⁺ by IMS technique, RA; (B) after the calcination of the polymeric support, the remaining FMNPs are incorporated into the composite matrix, RB; and (C) Au- and Pd-FMNPs are incorporated on the composite surface by drop-attachment, RC.

FMNPs was carried out on a gel-type ion-exchange resin instead of the MWCNTs. The IMS stages are described in eqn (8) and (9) for the IMS of Pd-FMNPs on a sulfonic gel-type exchange resin.



Then, the resulting nanocomposite material is calcinated at 600 °C for 4 h to obtain the FMNPs powder, which keeps their crystallographic properties. Au- and Pd-FMNPs were used for this route in a ratio of 3 : 2.

(c) Route C (RC). The FMNPs are synthesized by drop-attachment modifying the electrode surface. The composite was prepared by loading 10% amount of raw MWCNTs into the epoxy resin before hardening. Finally, when the composite is polished, its surface functional groups were activated by 2.5 M nitric acid treatment for 2 h. The FMNPs were directly synthesized on the electrode surface.

Regarding the surface incorporation of the FMNPs, the metal loading was achieved by dropping 0.01 M of cationic metal (M^{n+}) aqueous solution (1.5 mL), followed by rinsing with Milli-Q water and immersion under 0.1 M NaBH_4 at ambient conditions. Finally, the electrode was rinsed once again with Milli-Q water. This procedure was used for the incorporation of Au- and Pd-FMNPs on the electrode surface in a 3 : 2 ratio. Therefore, the incorporation of Au-FMNPs was achieved by the galvanic replacement of previously prepared Cu-FMNPs as sacrificial nanotemplates. With the subsequent incorporation of the Au-FMNPs, the Pd-FMNPs were introduced.

It is important to highlight that in each case, after the redox stage and the consequent appearance of the FMNPs, a rinse procedure was carried out with Milli-Q water.

Results and discussion

Functional metal nanoparticles characterization

The IMS technique provides a favorable distribution of the FMNPs on the MWCNTs surface as shown in the HR-TEM

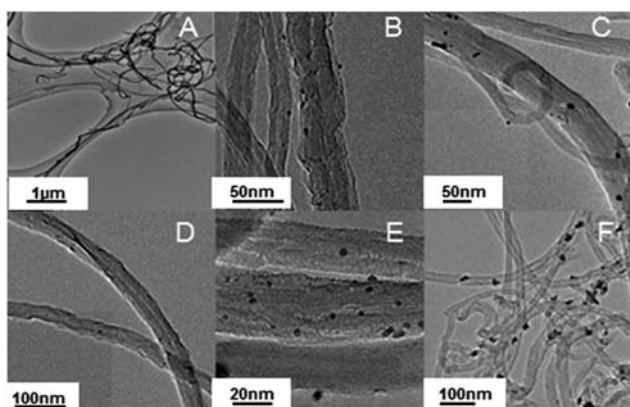


Fig. 2 HR-TEM images of: (A) raw MWCNTs; (B) Ag-; (C) Au-; (D) Cu-; (E) Pd-; and (F) Pt-FMNPs@MWCNTs are showed.

images (Fig. 2). Furthermore, the support provides their stability and simplifies their access for reagents in the catalytic or electrocatalytic applications of the final nanocomposite electrode material.

In addition to the distribution of the FMNPs, a homogenous size distribution is observed over the surface of the MWCNTs. No agglomeration of FMNPs is detected by the HR-TEM images. The identification of the metal content in each case was accomplished by EDS spectra (Fig. 3) and TGA analysis, differentiating the FMNPs from the catalyst remaining from the industrial synthesis of the raw MWCNTs (see Table 1). TGA analysis showed that the weight loss for MWCNTs took place in a single step with a maximum of weight loss at around 600 °C. The residue at the end of the analysis corresponds to the total metal content. The amount of the metal impurities of raw MWCNTs after acidic treatment was 2% in the catalyst. When the different FMNPs@MWCNTs were analyzed, the remaining 2% of the catalyst was subtracted in order to quantify the FMNPs content. It is important to emphasize that TGA provides only quantitative information on the presence of total metal content in CNT material. EDS analysis is needed for the qualitative determination of the metal composition.

With these results, the fact that the FMNPs are well distributed over the surface of the MWCNTs leads to the idea of increasing the electrochemical conductivity and an overall enhancement of the electrochemical features, as proven in the corresponding electroanalytical characterization.

Electrochemical characterization of FMNPs@MWCNTs/epoxy nanocomposite electrodes

The effect of FMNPs on the MWCNTs surface was also observed. Different functionalized-MWCNTs/epoxy composite electrodes were electrochemically characterized by CV and EIS and compared with non-modified electrodes. On the basis of the

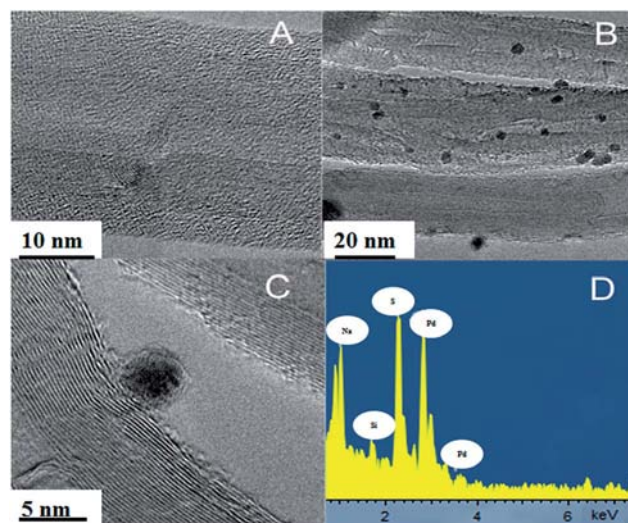


Fig. 3 HR-TEM images of: (A) raw MWCNTs; (B) Pd-FMNPs@MWCNTs; (C) Pd-FMNPs@MWCNTs amplification; and (D) EDS spectra from (C).

Table 1 Electrochemical characterization of various FMNPs@MWCNTs/epoxy composites was taken by EIS and TGA analyses. EIS data were carried out in a 0.01 M $[\text{Fe}(\text{CN})_6]^{3-/4-}$ and a 0.1 M KCl solution

FMNPs@MWCNTs	R_{Ω} (Ω)	R_{ct} (Ω)	C_{dl} (μF)	TGA (% in FMNPs)
Raw MWCNTs	138.0	530.0	9.02	98% in C
Pd-FMNPs@MWCNTs	111.3	501.0	7.11	1.7
Ag-FMNPs@MWCNTs	113.5	464.0	6.34	5.6
Au-FMNPs@MWCNTs	131.2	173.3	7.95	6.6
Cu-FMNPs@MWCNTs	136.5	599.0	5.22	7.0
Pt-FMNPs@MWCNTs	221.2	173.7	8.63	8.5

previous results, all composite electrodes used contain 10% of MWCNTs as a conducting component (either modified or non-modified).³³

Ohmic resistance (R_{Ω}), charge-transfer resistance (R_{ct}) and double-layer capacitance (C_{dl}) were evaluated for MWCNTs/epoxy composite electrodes, which could contain different FMNPs on the carbon surface by the EIS technique, depending on the final application. These parameters were obtained by fitting the impedance spectra to a simple equivalent circuit; $R_{\Omega}(R_{ct}C_{dl})$.³³ This circuit was sufficiently suitable to interpret the R_{Ω} , R_{ct} and C_{dl} values in terms of the interfacial phenomena that occur at the electrochemical cell.

Various MWCNTs/epoxy electrodes were studied changing the FMNPs nature on the MWCNTs surface. For each FMNPs@MWCNTs/epoxy composition, the electrodes were fabricated and evaluated. Impedance values showed an optimum kinetically controlled response for these electrodes based on FMNPs@MWCNTs/epoxy nanocomposites.

The R_{Ω} parameter consists of the solution resistance in series with the contact or the ohmic composite resistance. A slight decrease of R_{Ω} for FMNPs@MWCNTs/epoxy nanocomposite electrodes was observed with respect to the non-modified MWCNTs (see Table 1). This is because the ohmic resistance is more controlled by the solution resistance for composites containing a higher load of conductor material.³⁴ However, the Pt-FMNPs@MWCNTs/epoxy electrode showed an increase of R_{Ω} , which can be attributed to the morphology of the Pt nanoparticles (see Fig. 2).

R_{ct} is a parameter inversely proportional to the heterogeneous charge-transfer rate and also affects the sensitivity and response time of the electrode (see Table 1). A decrease of R_{ct} with the incorporation of FMNPs on the MWCNTs surface was observed. As the conductor material load increases, the probability of having both more electroactive sites and the electrode kinetics increases. Thus, the active area becomes different from the same percentage of MWCNTs, depending on the percentage of FMNPs in the composite. Table 1 also shows a decrease of R_{ct} for these functionalized-MWCNTs/epoxy nanocomposite electrodes resulting in a higher load of FMNPs by TGA. Accordingly, Pt-FMNPs@MWCNTs/epoxy and Au-FMNPs@MWCNTs/epoxy electrodes, which contain 8.5% and 6.6% in FMNPs, respectively, showed the highest decrease, whereas a Pd-FMNPs@MWCNTs/epoxy electrode, which contains 1.7% in

nanoparticles, showed the lowest decrease. Furthermore, it was also observed that nanocomposites with low charge-transfer resistances were the most appropriate to be used in the electrochemical measurements, suggesting that the use of composites with FMNPs confirms rapid electron exchange. On the other hand, for the Cu-FMNPs@MWCNTs/epoxy electrode, the increase of R_{ct} could be attributed to the higher trend to oxidation of these nanoparticles. Despite the enhanced kinetics, a high load of conducting material can increase the background current and smear the Faradaic signal response, especially when the electroactive species are present in low concentration. As a result, it is important to consider the remaining impedance parameter represented by the double-layer capacitance, which is directly related to the charge or background current.

The C_{dl} parameter should exhibit increased values for the electrodes with high surface areas of conducting material. Thus, when the load of the MWCNTs increases into the composite, the C_{dl} value also increases because of the electrode capacitance, which can be determined almost exclusively by the exposed carbon.³³ However, when FMNPs are incorporated on the MWCNTs surface, the catalytic effect causes a significant decrease of the C_{dl} value (see Table 1), reducing the background current.

According to the impedance results, an improvement in the R_{Ω} , R_{ct} and C_{dl} parameters was observed when the MWCNTs/epoxy composite electrodes were functionalized with FMNPs. This functionalization improves the properties that an electrode must have, such as rapid response time, low limit of detection and high sensitivity.

Electroanalytical responses of Au/Pd-FMNPs@MWCNTs/epoxy nanocomposite electrodes

Au-FMNPs@MWCNTs and Pd-FMNPs@MWCNTs have been used for the construction of electrochemical sensors in order to study the analytical response of the functionalized-MWCNTs/epoxy nanocomposite electrodes. Concretely, Au/Pd-FMNPs@MWCNTs/epoxy electrodes, which contain Au-FMNPs@MWCNTs and Pd-FMNPs@MWCNTs in 3 : 2 ratio, respectively, were the focus of the study. The catalytic effect of these noble metals in the oxidation of hydrogen peroxide has already been studied.^{3,35-36} The electroanalytical response of these sensors has been compared with that of the sensors based on non-modified MWCNTs with FMNPs. A limit of detection (LOD)

Table 2 Electroanalytical characterization of the Au/Pd-FMNPs@MWCNTs/epoxy composite sensor and the raw MWCNTs/epoxy composite sensor. The redox probe $[\text{Fe}(\text{CN})_6]^{3-/4-}$ was used by EIS data. PBS buffer pH 7.0 was used by hydrodynamic amperometric measurements, which exhibit their respective 95% confidence interval ($n = 3$)

Composite containing	R_{Ω} (Ω)	R_{ct} (Ω)	C_{dl} (μF)	LOD ^a (μM)
Raw MWCNTs	138.0	530.0	9.02	2.80 ± 0.06
Au/PdFMNPs@MWCNTs	137.9	246.6	6.50	0.80 ± 0.03

was estimated three times ($n = 3$) by the $S/N = 3$ criterion.³⁷ A limit of quantification (LOQ) was determined three times ($n = 3$) as the lowest concentration of the lineal response range (log intensity vs. log concentration). Both LOD and LOQ were obtained by hydrodynamic amperometry using hydrogen peroxide as the analyte in PBS solution at pH 7.0 (see Table 2). Electrochemical and analytical responses were enhanced for sensors containing MWCNTs modified with Au- and Pd-FMNPs on their surfaces.

The sensors containing raw MWCNTs demonstrated electrochemical responses for the oxidation of hydrogen peroxide, which was substantially enhanced after the incorporation of Au- and Pd-FMNPs into the composite material as it can be seen in Table 2. The presence of noble FMNPs, such as Pd or Au, leads to a remarkable decrease in the R_{ct} value and to 3.5 times decrease in LOD in comparison with sensors made of FMNP-free material. Although the presence of Au- and Pd-FMNPs does not present a notable decrease of the R_{Ω} value, a significant enhancement of the C_{dl} value is observed due to the decrease from 9.02 to 6.50 μF , corresponding to a decrease of around 30%.

Electroanalytical sensor response was evaluated by hydrodynamic amperometry for hydrogen peroxide detection. The LOD obtained with Au/Pd-FMNPs@MWCNTs/epoxy nanocomposite electrode is 0.8 μM , a decade of concentration less in comparison to the composite with raw MWCNTs, see Table 2.

Linear sweep voltammetry was used to determine the hydrogen peroxide oxidation potential based on the working electrodes used. Various concentrations of hydrogen peroxide ranging from 0–2 ppm were added in 10.0 mL of PBS at pH 7.0.

This electrochemical characterization also demonstrated a significant decrease to 700 mV of the oxidation potential of the system for the Au/Pd-FMNPs@MWCNTs/epoxy nanocomposite electrodes, compared to 900 mV value obtained for the electrodes containing raw MWCNTs, which shows the electrocatalytic effect of these FMNPs for the hydrogen peroxide oxidation. Therefore, further research needs to be conducted in order to optimize the transducer composition by changing the Au- to Pd-FMNPs ratio as it has been previously performed for raw-MWCNTs/epoxy materials.³³ An optimum load of FMNPs in the composite electrode could further improve its electrocatalytic effect.

Electroanalytical response of (MWCNTs/epoxy)-modified nanocomposite electrodes with Au- and Pd-FMNPs

The methodology to integrate these FMNPs as part of the transducer material has been the focus of study. Accordingly,

three different forms for incorporating Au- and Pd-FMNPs were tested in order to optimize the electrochemical response of the (MWCNTs/epoxy)-modified sensors for the amperometric response of hydrogen peroxide as the analyte.

In Table 3, it is observed that the RA electrode presented a significant increase in the electroanalytical values obtained by EIS and hydrodynamic amperometry in comparison with the non-modified electrodes. For RB, the FMNPs were incorporated in the form of powder into the polymeric matrix in the same proportion that TGA analysis determined for RA (Table 1). EIS parameters are similar for both the routes, providing the same LOD. Furthermore, the RB electrode also showed an LOQ lower than the RA electrode. Whereas in RA, the FMNPs incorporated on the transducer material are limited for the carboxylic groups on the MWCNT surface, the advantage of RB is the tunability of functionalization. Finally, both the routes were compared with RC. The main disadvantage of this route is that the sensor surface is non-renewable. Thus, the FMNPs have to be re-incorporated when the electrode is polished; accordingly, these electrodes had a non-homogeneous and reproducible modified surface (see Fig. 4). Despite these limitations, the best LOD and LOQ were obtained for RC electrode (see Table 3).

Fig. 5 shows the typical cyclic voltammograms of the four different electrodes studied in this work (raw MWCNTs containing electrode, RA, RB and RC electrodes) in 0.1 M $[\text{Fe}(\text{CN})_6]^{3-/4-}$ and 1.0 M KCl solution at a scan rate of 10 mV s^{-1} .

Different parameters such as peak separation potential (ΔE) and peak height (I_p) have been extracted from the cyclic voltammograms. According to these results, electrodes modified with Au- and Pd-FMNPs show that an enhancement in the I_p is independent of the route of FMNP incorporation. The maximum increase in I_p , which was around 75%, was observed for the electrode modified by RA; RB electrode showed a similar behaviour because both the electrodes contain the same amount of FMNPs. Nevertheless, electrode prepared by RC presented a minimum increase in I_p because of the lower amount of FMNPs (only on the electrode surface). Accordingly, I_p increases with FMNP load, which leads to an increase of the electroactive area.

Simultaneously, a comparison of the ΔE was evaluated for all the electrodes. As it can be observed in Fig. 5, RA electrode showed a insignificant increase of ΔE (from 0.48 V to 0.51 V), which can be explained by the fact that total amount of conductor material present in the epoxy matrix is the same (10% of Au/Pd-FMNPs@MWCNTs regarding to 10% raw

Table 3 Electrochemical impedance spectroscopy data of 0.01 M $[\text{Fe}(\text{CN})_6]^{3-/4-}$ in 0.1 M KCl are showed. Three different routes for functionalizing the MWCNTs/epoxy composite electrodes with Au- and Pd-FMNPs were electroanalytically compared by EIS and hydrodynamic amperometry. PBS buffer pH 7.0 was used by hydrodynamic amperometric measurements, which exhibit their respective 95% confident interval ($n = 3$)

Sensor resulting	R_{Ω} (Ω)	R_{ct} (Ω)	C_{dl} (μF)	LOD ^a (ppm)	LOQ ^a (ppm)	Sensitivity ^a (ppm^{-1})
Raw MWCNTs	138.0	530.0	9.02	0.095 ± 0.002	0.190 ± 0.002	0.0151 ± 0.0003
Route A	137.9	246.6	6.50	0.027 ± 0.001	0.068 ± 0.001	0.066 ± 0.001
Route B	116.4	462.3	6.32	0.027 ± 0.002	0.041 ± 0.001	0.037 ± 0.002
Route C	269.1	1303.0	3.28	0.014 ± 0.001	0.027 ± 0.002	0.031 ± 0.002

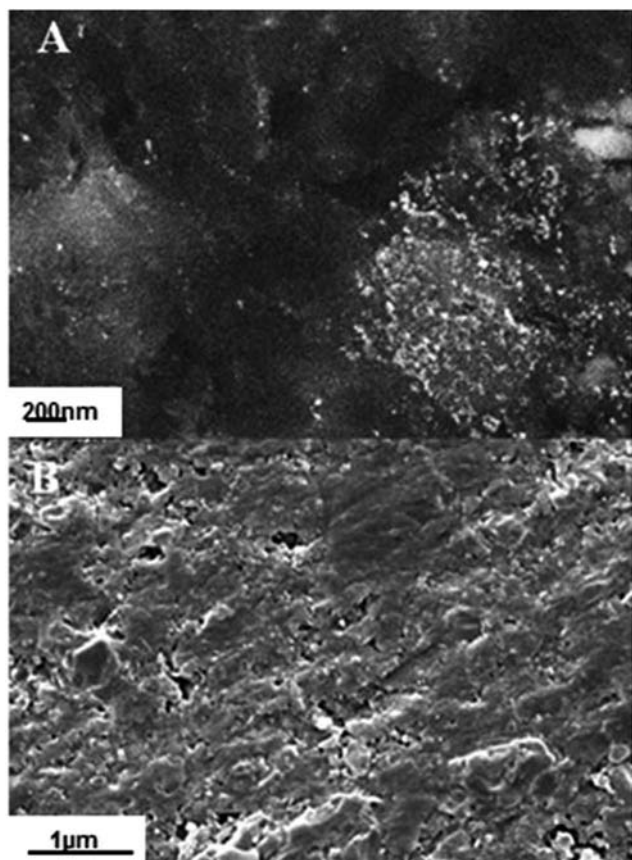


Fig. 4 SEM images obtained for: (A) sensor with Au- and Pd-FMNPs on its surface; and (B) without FMNPs on its surface.

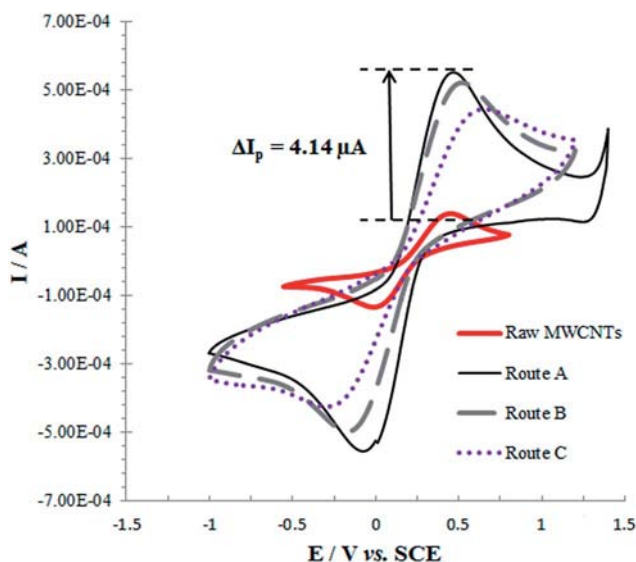


Fig. 5 Cyclic voltammograms recorded in 0.01 M $[\text{Fe}(\text{CN})_6]^{3-/4-}$ for electrodes containing raw MWCNTs and electrodes resulting from RA, RB and RC. Scan rate: 10 mV s^{-1} .

MWCNTs). Conversely, the RB electrode showed a higher increase of ΔE , increasing from 0.48 V to 0.63 V. In this case, because the FMNPs are integrated into the matrix as powder, they are not in direct contact with the main conductor material (MWCNTs), and the electron-transfer rate becomes more difficult. Finally, the RC electrode provided the highest ΔE increase, until 0.94 V, because of the electrode-surface modification with carboxylic groups under acidic conditions for incorporating the FMNPs, which considerably changed its surface. This increment of ΔE turns into partial decrease in the system reversibility.³⁸

Conclusions

Three different routes to functionalize MWCNTs/epoxy nanocomposite electrodes with FMNPs by the IMS technique have been developed in order to obtain sensitive amperometric sensors. First, MWCNTs functionalized with FMNPs represent novel electrocatalytically active nanocomposite materials, with an enhanced electrochemical response for the detection of hydrogen peroxide and a substantial decrease of both LOD and C_{dl} values. According to these results, functionalized-composite electrodes prepared by three different routes with FMNPs were compared with raw MWCNT composite electrodes.

All the modified electrodes showed high electroanalytical response for hydrogen peroxide as the analyte, obtaining the lowest LOD and LOQ for sensors containing FMNPs on the electrode surfaces. The incorporation of FMNPs by IMS opens a new simple route to customize sensitive modified-electrodes based on MWCNT/epoxy nanocomposites. A characterization of the new transducer material and the new nanocomposite is necessary to obtain the optimum transducer/polymer ratio. Finally, the IMS technique appears to be a valuable, efficient and environmentally friendly methodology for the synthesis and introduction of FMNPs in carbon nanotubes/epoxy composites.

Acknowledgements

We are sincerely grateful to all our associates cited throughout the text for making this publication possible. Part of this work was supported by Research Grant MAT2006-03745, 2006–2009 from the Ministry of Science and Technology of Spain, which is also acknowledged for the financial support of Dmitri Muraviev. Jose Muñoz and Julio Bastos-Arrieta also thank the Universitat Autònoma de Barcelona for the personal grant.

References

- 1 D. Wang, Z.-C. Li and L. Chen, *J. Am. Chem. Soc.*, 2006, **128**, 15078–15079.
- 2 C. Gao, W. Li, H. Morimoto, Y. Nagaoka and T. Maekawa, *J. Phys. Chem. B*, 2006, **110**, 7213–7220.
- 3 K. Balasubramanian and M. Burghard, *Small*, 2005, **1**, 180–192.
- 4 R. Olivé-Monllau, A. Pereira, J. Bartrolí, M. Baeza and F. Céspedes, *Talanta*, 2010, **81**, 1593–1598.

- 5 Q. Zhao, Z. Gan and Q. Zhuang, *Electroanalysis*, 2002, **14**, 1609–1613.
- 6 S. K. Vashist, D. Zheng, K. Al-Rubeaan, J. H. T. Luong and F.-S. Sheu, *Biotechnol. Adv.*, 2011, **29**, 169–188.
- 7 J. Wang and M. Musameh, *Anal. Chem.*, 2003, **75**, 2075–2079.
- 8 M. Pumera, A. Merkoçi and S. Alegret, *Sens. Actuators, B*, 2006, **113**, 617–622.
- 9 Y. Wang and C. Bi, *RSC Adv.*, 2014, **4**, 31573–31580.
- 10 Y. Lee, H. J. Song, H. S. Shin, H. J. Shin and H. C. Choi, *Small*, 2005, **1**, 975–979.
- 11 Y. Shi, R. Yang and P. K. Yuet, *Carbon*, 2009, **47**, 1146–1151.
- 12 L. Bao, S. Mahurin, R. Haire and S. Dai, *Anal. Chem.*, 2003, **75**, 6614–6620.
- 13 R. Ma, T. Sasaki and Y. Bando, *J. Am. Chem. Soc.*, 2004, **126**, 10382–10388.
- 14 R. K. Shervedani and A. Amini, *Electrochim. Acta*, 2014, **121**, 376–385.
- 15 K. R. Ward, M. Gara, N. S. Lawrence, R. S. Hartshorne and R. G. Compton, *J. Electroanal. Chem.*, 2013, **695**, 1–9.
- 16 B. Habibi and M. Jahanbakhshi, *Electrochim. Acta*, 2014, **118**, 10–17.
- 17 T. You, O. Niwa, M. Tomita and S. Hirono, *Anal. Chem.*, 2003, **75**, 2080–2085.
- 18 S. Li, Y. Zheng, G. W. Qin, Y. Ren, W. Pei and L. Zuo, *Talanta*, 2011, **85**, 1260–1264.
- 19 Y. Liu, Z. Su, Y. Zhang, L. Chen, T. Gu, S. Huang, Y. Liu, L. Sun, Q. Xie and S. Yao, *J. Electroanal. Chem.*, 2013, **709**, 19–25.
- 20 M. Yang, Y. Yang, Y. Liu, G. Shen and R. Yu, *Biosens. Bioelectron.*, 2006, **21**, 1125–1131.
- 21 J. Wang, *Analyst*, 2005, **130**, 421–426.
- 22 J. Wang, A.-N. Kawde and M. Musameh, *Analyst*, 2003, **128**, 912–916.
- 23 Y.-G. Zhou, F. W. Campbell, S. R. Belding and R. G. Compton, *Chem. Phys. Lett.*, 2010, **497**, 200–204.
- 24 C. Bittencourt, A. Felten, J. Ghijsen, J.-J. Pireaux, W. Drube, R. Erni and G. Van Tendeloo, *Chem. Phys. Lett.*, 2007, **436**, 368–372.
- 25 H. C. Choi, M. Shim, S. Bangsaruntip and H. Dai, *J. Am. Chem. Soc.*, 2002, **124**, 9058–9059.
- 26 K. Y. Lee, M. Kim, J. Hahn, J. S. Suh, I. Lee, K. Kim and S. W. Han, *Langmuir*, 2006, **22**, 1817–1821.
- 27 L. Qu, L. Dai and E. Osawa, *J. Am. Chem. Soc.*, 2006, **128**, 5523–5532.
- 28 B. Nikoobakht and M. A. El-Sayed, *Chem. Mater.*, 2003, **15**, 1957–1962.
- 29 C. J. Murphy and N. R. Jana, *Adv. Mater.*, 2002, **14**, 80.
- 30 D. N. Muraviev, *Contrib. Sci.*, 2005, **3**, 19.
- 31 P. Ruiz, M. Muñoz, J. Macanás and D. N. Muraviev, *Chem. Mater.*, 2010, **22**, 6616–6623.
- 32 S. Alegret, F. Céspedes, E. Martínez-Fàbregas, D. Martorell, A. Morales, E. Centelles and J. Muñoz, *Biosens. Bioelectron.*, 1996, **11**, 35–44.
- 33 R. Olivé-Monllau, M. J. Esplandiu, J. Bartrolí, M. Baeza and F. Céspedes, *Sens. Actuators, B*, 2010, **146**, 353–360.
- 34 L. Rassaei, F. Marken, M. Sillanpää, M. Amiri, C. M. Cirtiu and M. Sillanpää, *TrAC, Trends Anal. Chem.*, 2011, **30**, 1704–1715.
- 35 F. Céspedes, F. Valero, E. Martínez-Fàbregas, J. Bartrolí and S. Alegret, *Analyst*, 1995, **120**, 2255–2258.
- 36 C. M. Welch and R. G. Compton, *Anal. Bioanal. Chem.*, 2006, **384**, 601–619.
- 37 R. Olivé-Monllau, C. S. Martínez-Cisneros, J. Bartrolí, M. Baeza and F. Céspedes, *Sens. Actuators, B*, 2011, **151**, 416–422.
- 38 J. Wang, *Analytical electrochemistry*, John Wiley & Sons, 2006.



Modified multiwalled carbon nanotube/epoxy amperometric nanocomposite sensors with CuO nanoparticles for electrocatalytic detection of free chlorine



Jose Muñoz, Francisco Céspedes, Mireia Baeza *

Departament de Química, Facultat de Ciències, Edifici C-Nord, Universitat Autònoma de Barcelona, 08193 Cerdanyola del Vallès (Bellaterra), Barcelona, Spain

ARTICLE INFO

Article history:

Received 22 December 2014
Received in revised form 9 April 2015
Accepted 1 May 2015
Available online 7 May 2015

Keywords:

Amperometric sensor
Nanocomposite
Carbon nanotubes
CuO nanoparticles
Free chlorine

ABSTRACT

The benefit of using copper (II) oxide nanoparticles (CuO-NPs), which have catalytic activity for the decomposition of hypochlorite solutions, for the amperometric detection of free chlorine is reported. Cyclic voltammetry and electrochemical impedance spectroscopy have been applied for the electrochemical characterization of nanocomposite materials. If the amperometric detection of free chlorine was determined previously using multiwall carbon nanotube (MWCNT) based epoxy nanocomposite sensors, the electrocatalytic reduction of hypochlorite using modified MWCNT/epoxy nanocomposite sensors with CuO-NPs to obtain sensitive devices capable to amperometrically determine traces of free chlorine in water is demonstrated here. The CuO-NPs were incorporated in the nanocomposite electrode in two different ways i) on the MWCNT surface, Route A and ii) in the nanocomposite matrix in powder form, Route B. Both modified-nanocomposite sensors have shown a fast electron transfer exchange, high electroactive area and an enhancement on the electroanalytical signal. Accordingly, a greater sensitivity compared to raw MWCNT/epoxy nanocomposite sensors has been observed, obtaining the lowest limit of detection for the CuO-NPs modified nanocomposite sensors obtained by Route B.

© 2015 Elsevier B.V. All rights reserved.

1. Introduction

Carbon nanotubes (CNTs) represent an important group of nanomaterials, which are used in a variety of applications since their discovery in 1991 [1,2,3] mainly due to their unique mechanical [4], chemical [5], electrical [6], thermal [7] and structural properties [8]. Currently, significant interest is focused on nanocomposites based on CNTs, especially in multiwalled carbon nanotubes (MWCNTs), because of their electrocatalytic activity.

The unique qualities of MWCNTs make them highly attractive for the development of MWCNT-based chemical (bio)sensors, in general, and electrochemical detection, in particular. In this way, these sensors have shown extensive use for the detection of compounds such as glucose, hydrogen peroxide, ascorbic acid and free chlorine, among others [9,10,11,12]. MWCNTs dispersed in an inert matrix provide attractive electrochemical properties since the polymeric matrix, together with the MWCNTs, confers mechanical robustness and high electric conductivity to the final nanocomposite electrode. Furthermore, its high malleability before being hardened permits an easy incorporation of a variety of nanoparticles (NPs), [13,14] enzymes [15] and chemical recognition agents [16]. Compared to other carbon allotropic forms,

CNTs offer to the composite a higher area to volume ratio, lower resistivity and higher mechanical and chemical stability.

Some parameters, such as the composite resistivity, the heterogeneous electron transfer rate, the material stability and the background capacitance current are strongly influenced by the raw MWCNT nature (such as purity, diameter and length), which in turn also affects the ratio of MWCNT/polymer nanocomposite materials [17,18]. Then, the optimization of the raw MWCNT load is mandatory to obtain nanocomposite electrodes which have a similar behavior to a microelectrodes array. In this context, an exhaustive study regarding the characterization and optimization of the MWCNT loading in a polymeric matrix (epoxy resin, Epotech H77) was previously performed to improve its electrochemical properties [17,19]. The optimal nanocomposite composition, which was 10% (w/w) in carbon loads for the MWCNTs used in this work, combined easy manipulation during the fabrication procedure, low background current and an improved response compared to the conventional conducting composite electrodes used in the vast majority of works reported using a higher carbon load (20%, w/w in carbon loads) [20,21]. Afterwards, the feasibility of these optimum MWCNT-based nanocomposite sensors was evaluated for the amperometric reduction of hypochlorite (ClO^-) for the determination of free chlorine in aqueous solution [22].

NaClO is a compound registered in the Toxic Substances Control Act (TSCA) Chemical Substance Inventory that is frequently used for water

* Corresponding author.

E-mail address: mariadelmar.baeza@uab.cat (M. Baeza).

disinfection and purification, including drinking water, swimming pool water, treated wastewater for non-potable reuse and others. Normally it is handled as concentrated aqueous solutions and needs periodical control of its concentration to adjust dosages due to the possibility of decomposition and the formation of undesirable byproducts [23].

Chlorine and hypochlorite are related by following chemical equation:



The sum of ClO^- , Cl_2 and HClO is known in hydrochemistry as free chlorine and its concentration can be expressed as mass of Cl_2 per liter. This criteria has also been followed in this paper.

NaClO slowly self-decomposes in solution [24] but can rapidly decompose in the presence of different metal ion catalysts, such as Ni, Co and Cu [25,26]. Recently, CuO -NPs, NiO -NPs and Co_3O_4 -NPs have demonstrate a higher catalytic activity to decompose the NaClO [23,27]. While CuO -NPs and NiO -NPs do not show any degradation in catalytic performance for the decomposition of hypochlorite during repeated uses, Co_3O_4 catalyst continuously decreased with repeated use [27]. In addition, it is known the catalytic activity of the CuO -NPs for the amplification signal of different analytes, such as glucose, hydrogen peroxide, rhodamine B (RhB) and different carbohydrates [28,29,30,31].

Accordingly, in this work the catalytic properties of CuO -NPs for their incorporation as a catalytic support in the optimum MWCNT/epoxy nanocomposite composition to develop sensitive amperometric nanocomposite sensors for the analysis of free chlorine have been exploited. CuO -NPs were synthesized by an environmentally friendly technique (Intermatrix Synthesis, IMS) and were incorporated in the nanocomposite electrode by two different routes: i) on the MWCNT surface (Route A) and ii) in the nanocomposite matrix in powder form (Route B). Then, the nanocomposite electrodes containing CuO -NPs were characterized by cyclic voltammetry and electrochemical impedance spectroscopy in order to study their electrochemical behavior. Finally, the obtained results have been compared with the ones obtained by the raw MWCNT/epoxy nanocomposite sensors.

2. Experimental

2.1. Chemicals and reagents

All solutions were prepared using deionized water from a Milli-Q system (Millipore, Billerica, MA, USA). Sodium hypochlorite (NaClO , 10–15%), potassium chloride (KCl , 99.5%), potassium ferricyanide/ferrocyanide ($\text{K}_3[\text{Fe}(\text{CN})_6]/\text{K}_4[\text{Fe}(\text{CN})_6]$, 99.8%), potassium phosphate dibasic anhydrous (K_2HPO_4 , >99.0%) and potassium phosphate monobasic (KH_2PO_4 , >99.0%) were obtained from Sigma-Aldrich (St. Louis, MO, USA). L-purified multiwalled carbon nanotube (MWCNT) growth using the chemical vapor deposition process (purity >95%, length 5–15 μm , outer diameter 10–30 nm) was purchased from SES Research (Houston, TX, USA). Resin Epotek H77A and its corresponding hardener Epotek H77B, supplied by Epoxy Technology (Billerica, MA, USA), were used as polymeric matrix. Copper (II) nitrate trihydrate ($\text{Cu}(\text{NH}_3)_2 \cdot 3\text{H}_2\text{O}$, 99%) and sodium hydroxide (NaOH >98%) and the different salts used for the interfering experiments were purchased from Sigma-Aldrich and were used as-received.

2.2. Apparatus and procedure

Cyclic voltammetry (CV) and electrochemical impedance spectroscopy (EIS) studies were carried out using a computer controlled AUTOLAB PGSTAT 30 and FRA boards (Eco Chemie, Utrecht, The Netherlands). EIS and CV measurements were made in a 10.0 mL of 0.1 M KCl solution containing 0.01 M $\text{K}_3[\text{Fe}(\text{CN})_6]/\text{K}_4[\text{Fe}(\text{CN})_6]$, using a three-electrode configuration. Moreover, CV studies in the presence of

free chlorine were carried out in 10.0 mL of 0.1 M KCl containing phosphate buffer solution (PBS) at pH 5.5. A single junction reference electrode Ag/AgCl Orion 900100 (Thermo Electron Corporation, Beverly, MA, USA) and a platinum-based electrode 52-671 (Crison Instruments, Alella, Barcelona, Spain) and the constructed MWCNT/epoxy nanocomposite electrodes (modified or none with metal oxide nanoparticles) were used as reference, auxiliary and working electrodes, respectively. The voltammograms scan rate was $50 \text{ mV} \cdot \text{s}^{-1}$ and the impedance spectra were recorded in the frequency range of 0.1 Hz–100 kHz at the redox equilibrium potential previously obtained by CV. The resistance parameters were obtained by fitting the impedance spectra to a simple equivalent circuit: $R_{\Omega} \cdot (R_{ct} \cdot C_{dl})$.

Electroanalytical experiments were carried out in a 10.0 mL PBS solution at pH 5.5. This solution was used as a background electrolyte and the experiments were made using a three-electrode configuration. Amperometric measurements were performed using an amperimeter LC-4C (Bioanalytical Systems, Inc., West Lafayette, IN, USA). Amperometric detection was performed under stirring conditions with a Teflon-coated magnetic stirring bar (working potential: $E_{app} = -0.35 \text{ V vs. Ag}/\text{AgCl}$) and constant agitation. A freshly prepared 1000 ppm NaClO solution was used as a stock solution. Standard solutions were prepared by the dilution of the stock solution. All the experiments were made at room temperature (25 °C). The NaClO solutions were previously analyzed using the standard N,N-diethyl-p-phenylenediamine (DPD) colorimetric method [32,33] which consists in a Kit-commercial colorimeter (HACH, Düsseldorf, Germany) that provides measurements directly in $\text{mg} \cdot \text{L}^{-1}$ of free chlorine.

The metal oxide contained on MWCNT surface was evaluated by thermogravimetric analysis (TGA), using a Netzsch instrument; model STA 449 F1 Jupiter®. Approximately 20 mg of sample was heated to 1000 °C at 10 °C/min, using flow of air. The mass of the sample was continuously measured as a function of temperature and the rate of weight loss (d.t.g.) was automatically recorded.

The presence of CuO -NPs on the MWCNT surface (CuO -NPs@MWCNT) was observed by high resolution transmission electron microscopy (HR-TEM) images and energy dispersive X-Ray spectroscopy (EDS), using a JEM-1400 unit with an acceleration voltage of 120 kV. Approximately 1 mg of sample was dispersed in 5 mL of acetone as organic solvent and then placed in an ultrasound bath for 1 h. Finally, a drop of this solution was placed on a gold grid and let it dry before HR-TEM and EDS analysis.

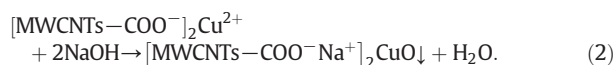
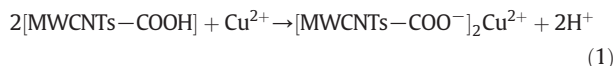
2.3. Nanocomposite preparation methodology: synthesis and incorporation of CuO -NPs

Handmade working nanocomposite electrodes were prepared following the conventional methodology described in our previous works [13,17]. The working electrodes based on nanocomposites were prepared by mixing polymer Epotek H77A and its corresponding H77B hardener in a 20:3 (w/w) ratio and adding a 10% load of MWCNTs (either modified or none). The (modified-)MWCNTs were dispersed in the resin and hardener agents by manually homogenization for 1 h. For the electrode construction, the mixture was placed into a cylindrical PVC tube (6 mm of internal diameter and 20 mm of length) containing a copper disk soldered to an electrical connector end. The mixture was incorporated in the hollow end of a PVC tube to form the body of the electrode. The final paste-filled cavity was 3 mm long inside the PVC tube. Then, the nanocomposite paste electrodes were allowed to harden during 24 h at 80 °C. Afterwards, in order to obtain a reproducible electrochemical surface, electrode surfaces were polished with different sandpapers of decreasing grain size (800 and 1200 grits) and finally with alumina paper (polishing strips 948201, Orion). The resultant geometric area for the final electrodes was 28 mm^2 .

Two different methodologies were carried out for the modification of the transducer material with CuO -NPs: (i) *in situ* functionalization of MWCNT surface previously to their mixture incorporation and

(ii) incorporation and dispersion of the powder nanoparticles in bulk as a third component. Both methodologies are summarized in Fig. 1 and described as follows:

- (i) Route A. The CuO-NPs were synthesized *in situ* on the MWCNT surface, resulting CuO-NPs@MWCNTs. For this aim, the functional groups of the MWCNTs (e.g. -OH, -COOH or -C=O) were previously generated (activation process) with 2.5 M HNO₃. The pH was adjusted to 6. Then, the synthesis of CuO-NPs on the activated-MWCNT surface (MWCNTs-COOH) was carried out adapting the synthesis procedure to the IMS technique [13]. The resultant procedure is based on Eqs. (1) and (2), as is detailed as follows:



The first step which is shown in Eq. (1) consisted of the metal loading of 260 mg of MWCNTs by using 0.02 M Cu²⁺ aqueous solution in 300 mL of Milli-Q water and then added 1 mL of glacial acetic acid to avoid hydrolyzation of Cu²⁺ ions. The solution was rinsed during 20 min. Afterwards, 0.01 g of PVP as stabilizer and 1.0 M NaOH as precipitating agent were added into the above mixture (Eq. 2) and stirred with a Teflon-coated magnetic stirring bar (rotation speed: 800 rpm) for 10 min at 80 °C in a water bath [34]. The pH of the initial solution was adjusted to 12. The resultant dark blue suspension was followed by high-intensity ultrasonication horn at 20 kHz in ambient air for 2 h. On completion of sonication, the suspension turned black. The modified-MWCNTs were centrifuged at 4000 rpm for 8 min and washed with Milli-Q water and ethanol for several times. The resultant product was dried at 80 °C for 24 h. Finally, nanocomposite electrodes were prepared by loading a 10% (w/w) of CuO-NPs@MWCNTs into the epoxy resin before hardening, CuO-NPs@MWCNTs/epoxy nanocomposite electrodes. TGA analysis determined 9.1% in CuO-NPs upon the MWCNT walls.

- (ii) Route B. The CuO-NPs were synthesized in the same way of Route A but without the presence of MWCNTs. In order to keep constant the proportion of conductor material in bulk (10% w/w), nanocomposite electrodes were prepared by loading 9.09% of raw MWCNTs adding 0.91% of CuO-NPs (in powder form) into epoxy resin before hardening, resulting the CuO-NPs/MWCNT/epoxy nanocomposite electrodes. Thus, the total content of CuO-NPs in the nanocomposite was the same that the one obtained by TGA in Route A.

3. Results and discussion

3.1. Physical characterization of the CuO-NPs

Two different routes were used to modify the MWCNTs/epoxy nanocomposite electrodes with CuO-NPs (see Fig. 1). In both cases, the structural morphology of the CuO-NPs prepared *via* hydrolysis of copper (II) nitrate trihydrate in the presence of sodium hydroxide with high ultrasonication in ambient air for 2 h is presented in Fig. 2, showing an ellipsoidal particle shape.

Concerning CuO-NPs@MWCNTs obtained by Route A, HR-TEM images from Fig. 2B–C provided that the CuO-NPs were coated homogeneously on the walls of the MWCNTs and no agglomeration of CuO-NPs was detected. Due to their metallic properties, CuO-NPs provide stability and supply the access of reagents in the catalytic or electrocatalytic applications of the final nanocomposite electrode material. The identification of the copper (II) oxide was accomplished by EDS spectra (Fig. 2D) and TGA analysis, differentiating the CuO-NPs from the catalyst remaining from the industrial synthesis of the raw MWCNTs. TGA analysis showed the maximum of weight loss around 600 °C. The residue at the end of analysis corresponds to the total metal content. The amount of metal impurities of raw MWCNTs after acidic treatment was 2.0%. When the CuO-NPs@MWCNTs were analyzed, this 2.0% of metal impurities was subtracted in order to quantify the CuO-NPs content. The CuO-NPs content on the MWCNTs surface resulted 9.1%. It is important to highlight that TGA provides only quantitative information on the presence of total metal content in carbon material. Then, EDS analysis is needed for the qualitative determination of the CuO-NPs (see Fig. 2D and F).

On the other hand, Fig. 2E shows the local view of CuO-NPs product formed by Route B, which indicated that the product consists of small particles. The low magnification HR-TEM image shown in Fig. 2E (inset) further indicated the formation of nanoparticles with an ellipsoidal shape. Its EDS spectra also determined the presence of CuO (Fig. 2F).

According to TGA and EDS results and taking into account the dispersion of CuO-NPs on the MWCNTs surface observed in HR-TEM images, 9.1% of CuO-NPs (regarding MWCNTs) were incorporated as a catalyst component in the MWCNT/epoxy nanocomposite electrodes by two different routes. The electrocatalytic effect of the CuO-NPs on reduction of free chlorine was studied by CV and verified for analytical application by hydrodynamic amperometry. Furthermore, the electrochemical and electrocatalytic behaviors of the CuO-NPs in the nanocomposite electrodes were compared with the non-modified nanocomposite electrodes (raw MWCNT/epoxy nanocomposite electrodes).

3.2. Cyclic voltammetry analysis

The electrocatalytic performance of three different nanocomposite electrodes toward the reduction of NaClO in acidic medium (pH 5.5) was demonstrated by CV. The voltammograms were carried out in a

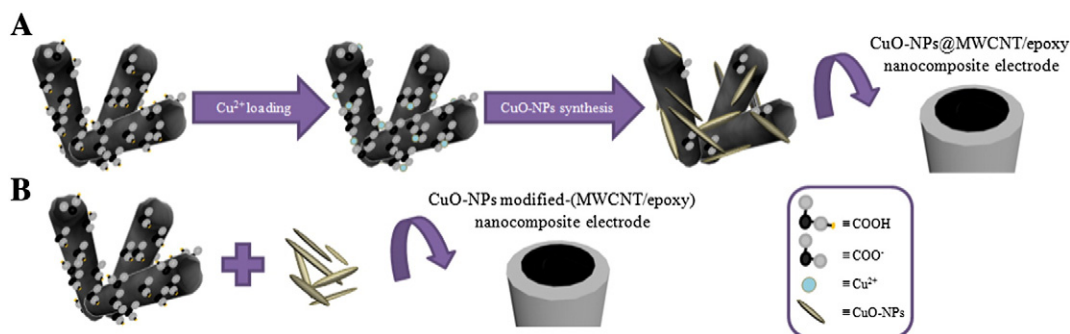


Fig. 1. Scheme of the two different routes for the incorporation of CuO-NPs in the MWCNT/epoxy nanocomposite electrodes: A) *in situ* synthesis of CuO-NPs on the MWCNTs surface, Route A; and B) synthesis of CuO-NPs and their incorporation as powder form in bulk, Route B.

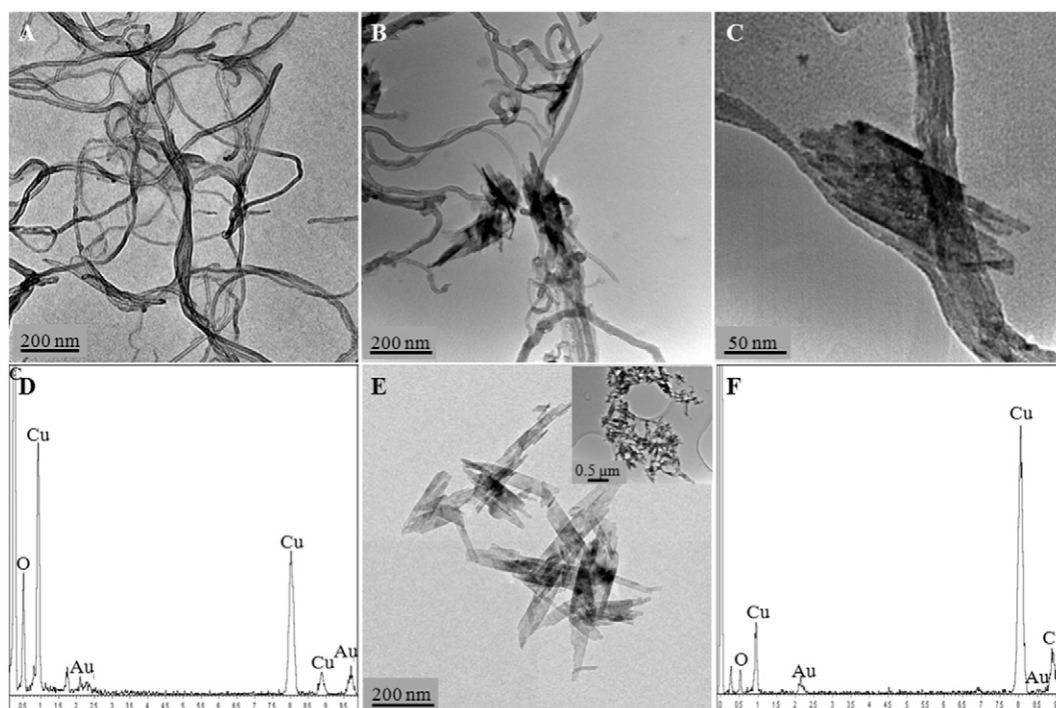


Fig. 2. HR-TEM images of A) raw MWCNTs; B) CuO-NPs@MWCNTs; C) amplification of a single CuO-NPs@MWCNTs; D) EDS spectra of CuO-NPs@MWCNTs; E) CuO-NPs and low magnification image (inset) and F) its EDS spectra.

PBS solution (pH 5.5) in the scan direction from +1.2 V to -0.8 V. The composition of conductor material in each type of nanocomposite electrode was 10%, which was estimated previously as the optimum MWCNT composition for this sample [17]. Fig. 3 displays the voltammetric behavior of the raw MWCNT/epoxy, CuO-NPs@MWCNT/epoxy and CuO-NPs/MWCNTs/epoxy nanocomposite electrodes in the presence of $0.6 \text{ mg} \cdot \text{L}^{-1}$ free chlorine (Fig. 3B). One control experiment was also performed by studying the CV behavior of each electrode in the absence of free chlorine (Fig. 3A).

Experimental controls presented in Fig. 3A (curves b and c) show two pairs of well-defined anodic and cathodic peaks at both MWCNT/epoxy nanocomposite electrodes containing CuO-NPs, which is believed to be due to the redox reactions of CuO-NPs. The first pair of well-defined peaks (E_{a1}/E_{c1}) was found between +0.56 V vs. Ag/AgCl (E_{c1}) and +0.66 V vs. Ag/AgCl (E_{a1}) for CuO-NPs@MWCNT/epoxy nanocomposite electrodes and +0.60 V vs. Ag/AgCl (E_{c1}) and +0.65 V vs. Ag/AgCl (E_{a1}) for CuO-NPs/MWCNT/epoxy nanocomposite electrodes. Both

waves might correspond to a Cu(II)/Cu(III) redox couple similar to the previous reports [36]. Another pair of well-defined redox peaks (E_{a2}/E_{c2}) could be observed: oxidation peak about +0.07 V and +0.13 V vs. Ag/AgCl and reduction peak about -0.08 V and -0.09 V vs. Ag/AgCl for CuO-NPs@MWCNT/epoxy and CuO-NPs/MWCNT/epoxy nanocomposite electrodes, respectively, which might correspond to a Cu(I)/Cu(II) redox couple. These peaks evidence the presence of CuO-NPs on the nanocomposite electrode surface.

On the other hand, as is shown in Fig. 3B, the two modified-electrodes with CuO-NPs presented a remarkable catalytic current cathodic peak (I_{pc}) at -0.35 V vs. Ag/AgCl, more emphasized for the CuO-NPs/MWCNT/epoxy nanocomposite electrodes. This fact is mainly caused by the higher content of CuO-NPs on the electrode surface when they are incorporated by Route B. The I_{pc} increase demonstrated the electrocatalytic behavior of the CuO-NPs in the presence of ClO^- . Compared to the raw MWCNT/epoxy nanocomposite electrodes, nanocomposite electrodes containing CuO-NPs displayed a substantial negative

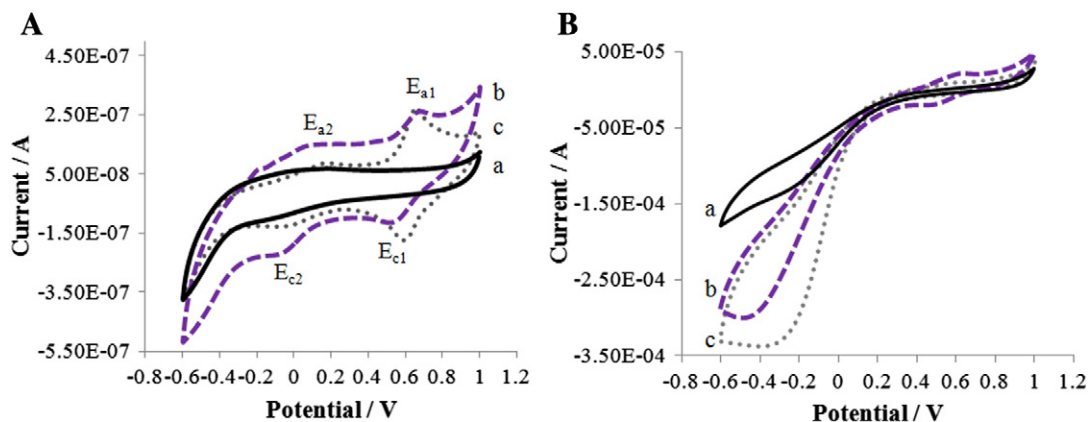


Fig. 3. Cyclic voltammograms of nanocomposite electrodes containing a) raw MWCNTs; b) CuO-NPs@MWCNTs and c) CuO-NPs in bulk, in the absence A) and in the presence B) of $0.6 \text{ mg} \cdot \text{L}^{-1}$ free chlorine. CV measurement were recorded in a 10.0 mL solution of 0.1 M KCl containing PBS at pH 5.5. Scan rate: $0.05 \text{ V} \cdot \text{s}^{-1}$.

Table 1

Electrochemical parameters obtained by CV in 0.1 M KCl containing 0.01 M $[\text{Fe}(\text{CN})_6]^{3-/4-}$ solution at $0.05 \text{ V} \cdot \text{s}^{-1}$ for the raw MWCNT/epoxy, CuO-NPs@MWCNT/epoxy and CuO-NPs/MWCNT/epoxy nanocomposite electrodes. A, I_p and ΔE parameters correspond to electroactive area, peak cathodic height and separation potential, respectively.

Nanocomposite electrode	A (cm ²)	I_p (mA)	ΔE (V)
Raw MWCNT/epoxy	0.25	0.132	0.48
CuO-NPs@MWCNT/epoxy	1.27	0.680	0.12
CuO-NPs/MWCNT/epoxy	2.84	1.52	0.24

shift of the cathodic peak potential (from -0.1 V to -0.35 V vs. Ag/AgCl), which suggests a high electrocatalytic activity of the nanocomposite electrodes containing CuO-NPs in the direct reduction of ClO^- . The overpotential shifted negatively, which can be attributed to a kinetic effect by an increase in the electroactive area and the rate of electron transfer from ClO^- to the nanocomposite electrodes containing CuO-NPs [35].

In addition, CV technique was also used to determine the electroactive area (A) of the nanocomposite electrodes, as well as the separation potential (ΔE) and the peak height (I_p), see Table 1. For this aim, the measurements were made in a 10.0 mL 0.1 M KCl solution containing 0.01 M $[\text{Fe}(\text{CN})_6]^{3-/4-}$. The kinetic processes of those species are strongly dependent on the state of the electrode surface. The electroactive area can be calculated in terms of peak current: I_p (A), and scan rate: ν ($\text{V} \cdot \text{s}^{-1}$), according to the modified Randles–Sevcik equation [37]:

$$I_p = 3.01 \times 10^5 \cdot n^{3/2} \cdot (\alpha D_{\text{red}} \nu)^{1/2} A \cdot C_{\text{red}}^*$$

This equation is adequate for electron transfer-controlled processes [21], where n is the number of electrons ($n = 1$), C_{red}^* is the bulk concentration of the electroactive species ($C_{\text{red}}^* = 0.01 \text{ M}$), D_{ox} corresponds to the diffusion coefficient of the reduced species ($D_{\text{red}} = 6.32 \times 10^{-6} \text{ cm}^2 \cdot \text{s}^{-1}$), α represents the symmetry factor which was taken approximately as 0.5 and ν represents the scan rate ($\nu = 0.05 \text{ V} \cdot \text{s}^{-1}$). The calculated values of A based on the redox peaks of $[\text{Fe}(\text{CN})_6]^{3-/4-}$ were 0.25 cm^2 , 1.27 cm^2 and 2.84 cm^2 for raw MWCNT/epoxy, CuO-NPs@MWCNT/epoxy and CuO-NPs/MWCNT/epoxy nanocomposite electrodes, respectively (see Table 1). These results confirmed the improvement of the electroactive area with the incorporation of CuO-NPs in the nanocomposite material, independently of the route of CuO-NPs incorporation. The highest value of A was obtained for the CuO-NPs/MWCNT/epoxy nanocomposite electrodes, which improved around 90% vs. the raw MWCNT/epoxy nanocomposite electrodes and 55% vs. the CuO-NPs@MWCNTs nanocomposite electrodes. These results revealed that the CuO-NPs are more exposed on the electrode surface when they were incorporated in bulk by Route B. This fact is also in concordance with the significant increase of current

observed in Fig. 3B. Simultaneously, a comparison of the ΔE was also evaluated for all electrodes. As can be seen in Table 1, the incorporation of CuO-NPs in both routes presented a slight decrease of ΔE (from 0.48 V to 0.12 V and 0.24 V). This enhancement of ΔE turns into a partial increase in the system reversibility [38], mainly contributed by the electrocatalytic activity of the CuO-NPs. The electrochemical values shown in Table 1 verified once again the electrocatalytic activity of these CuO-NPs in the nanocomposite electrodes.

3.3. Impedimetric analysis

Before probing the electrocatalytic properties of the modified-nanocomposite electrodes with CuO-NPs toward hypochlorite reduction, the electrodes were characterized to know their resistance/impedance by EIS technique. Ohmic resistance (R_Ω) and charge transfer resistance (R_{ct}) were evaluated for the three different nanocomposite electrodes: raw MWCNT/epoxy, CuO-NPs@MWCNT/epoxy and CuO-NPs/MWCNT/epoxy nanocomposite electrodes. These parameters were obtained by fitting the impedance spectra to a simple equivalent circuit: $R_\Omega \cdot (R_{\text{ct}} \cdot \text{Cdl})$, which is shown in the inset from Fig. 4A, using the equilibrium potential previously obtained by CV.

The Nyquist plots of the EIS presented in Fig. 4A were recorded in the frequency range: 0.1 Hz to 100 kHz, in a 0.1 M KCl solution containing 0.01 M $[\text{Fe}(\text{CN})_6]^{3-/4-}$. The Nyquist plots consist of a semicircular portion and a linear portion, which corresponds to the electron transfer limited process and the diffusion limited process, respectively. EIS experiments exhibited a well defined semicircle for raw MWCNT/epoxy and CuO-NPs@MWCNT/epoxy nanocomposite electrodes. However, the CuO-NPs/MWCNT/epoxy nanocomposite electrode spectrum included two segments. First segment at higher frequency range, seen as circular portion, is due to an electron transfer limited process. The second segment, at lower frequency range linear portion, is due to the diffusion controlled process (Fig. 4B).

R_Ω parameter, which is dependent on the ionic concentration, the type of ions and also the electrode area, consists of the solution resistance in series with the contact or the ohmic nanocomposite resistance. Nanocomposite electrodes containing CuO-NPs showed a R_Ω decreased at the same time that their electroactive areas increased. Thus, while raw MWCNT/epoxy nanocomposite electrode presented an ohmic resistance value of 126.7Ω , CuO-NPs@MWCNT/epoxy and CuO-NPs/MWCNT/epoxy nanocomposite electrodes presented lower ohmic resistance values (92.6Ω and 13.7Ω , respectively). Accordingly, the lower R_Ω values exhibited for both modified nanocomposite materials containing CuO-NPs verified that these metal oxide nanoparticles act as an electron mediator [39].

Concerning R_{ct} , this parameter is well known as a useful parameter reflecting the facility of electrode reaction, which may be measured by EIS from the semicircle diameter in the Nyquist plot [19]. Moreover, the charge transfer resistance is inversely proportional to the

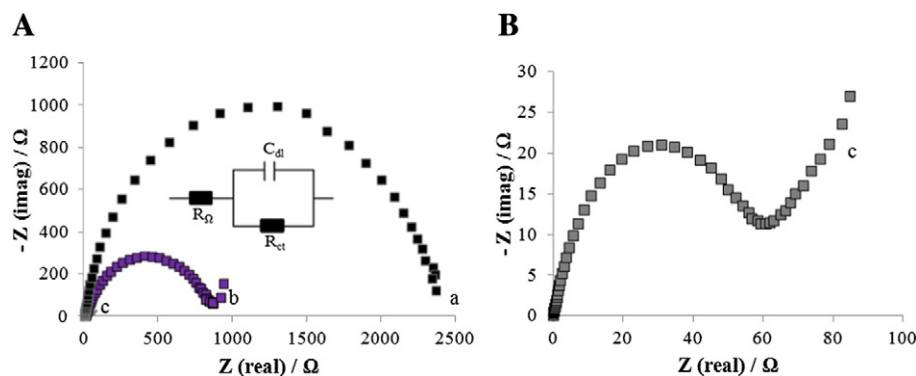


Fig. 4. A) Electrochemical impedance spectra of nanocomposite electrodes containing a) raw MWCNTs; b) CuO-NPs@MWCNTs and c) CuO-NPs in bulk examined in a 0.1 M KCl solution containing 0.01 M $[\text{Fe}(\text{CN})_6]^{3-/4-}$. Inset shows the equivalent circuit used for the impedance spectra fitting. B) Magnification of the c) spectra.

Table 2

Electroanalytical parameters obtained for the both modified-nanocomposite electrodes with CuO-NPs. The results are also compared with the obtained for the raw MWCNT/epoxy nanocomposite sensor. LOD and LOQ which their respectively 95% confidence interval ($n = 3$) were obtained by hydrodynamic amperometry in 0.1 M KCl containing PBS at pH 5.5 solution.

Nanocomposite sensor	LOD ($\mu\text{g}\cdot\text{L}^{-1}$)	LOQ ($\mu\text{g}\cdot\text{L}^{-1}$)	Sensitivity ($\text{nA}\cdot\text{L}\cdot\text{mg}^{-1}$)
Raw MWCNT/epoxy [22]	20 ± 10	–	–150
CuO-NPs@MWCNT/epoxy	4.4 ± 0.1	8.8 ± 0.2	–432.5
CuO-NPs/MWCNT/epoxy	0.6 ± 0.1	1.1 ± 0.1	–446.2

heterogeneous charge transfer rate and also affects the sensitivity and response time of the electrode. In general, MWCNT-based nanocomposite electrodes with low R_{ct} are preferable for electrochemical measurements in order to guarantee fast electron transfer. As shown in Fig. 4A, CuO-NPs@MWCNT/epoxy and CuO-NPs/MWCNT/epoxy nanocomposite electrodes exhibited a smaller semicircle compared to the raw MWCNT/epoxy nanocomposite electrode, indicating a lower resistance of electron transfer, mainly caused for the electrocatalytic effect provided by CuO-NPs. Thereby, the R_{ct} values obtained for each nanocomposite electrodes were 2360.3Ω for raw MWCNT/epoxy, 976.4Ω for CuO-NPs@MWCNT/epoxy and 84.9Ω for CuO-NPs/MWCNT/epoxy.

In agreement with the EIS results, the significant decrease of R_{Ω} and R_{ct} for the CuO-NPs/MWCNT/epoxy nanocomposite electrode suggests that when the nanoparticles are incorporated in bulk (Route B), they are more accessible on the electrode surface, emphasizing their electrocatalytic activity. These results indicate the role of CuO-NPs in the enhancement of the electron transfer process. According to impedimetric results, the significant R_{ct} and R_{Ω} decrease in the presence of CuO-NPs resulted in an effective charge transfer, leading to an enhanced electrocatalytic activity for degradation of NaClO and hence, to detect low concentrations of free chlorine.

3.4. Hydrodynamic amperometry analysis

The feasibility of both nanocomposite sensors containing CuO-NPs in terms of analytical response has been amperometrically evaluated for the reduction of hypochlorite for the determination of free chlorine under stirring conditions ($E_{app} = -0.35 \text{ V}$ vs. Ag/AgCl; constant stirring). Three different sensors for each kind of modified-nanocomposite materials were used for this aim. Limit of detection (LOD) was estimated three times by the $S/N = 3$ criterion [40]. Limit of quantification (LOQ) was determined also three times as the lowest concentration of the lineal response range.

If the raw MWCNT/epoxy nanocomposite sensors demonstrated a great electroanalytical response for the detection of free chlorine in water [22], the nanocomposite sensors containing CuO-NPs exhibited

Table 3

Comparison of sensing abilities for free chlorine determination with different electrodes.

Electrodes	Analytes	E_{app} (V)	Reaction	LOD ($\mu\text{g}\cdot\text{L}^{-1}$)	Ref.
Pt, Au, GCE	Cl	+1.1	Oxidation	1988	[40]
Nano Au-PEDOT/GCE	HClO	0.0	Reduction	71	[41]
Gold thin-film	Cl	+0.35	Oxidation	398	[42]
MWCNT/epoxy	Cl	–0.1	Reduction	398	[22]
Boron doped diamond	Cl	+1.4	Oxidation	16	[43]
CuO-NPs@MWCNT/epoxy	Cl	–0.35	Reduction	4.4	This work
CuO-NPs/MWCNT/epoxy	Cl	–0.35	Reduction	0.6	This work

a substantially enhanced of its response, also accompanied by an electrocatalytic effect, as shown in Table 2.

For CuO-NPs@MWCNT/epoxy nanocomposite sensors, the calibration curve for the free chlorine sensor is shown in Fig. 5A. The regression equation, $I_{pa} \text{ (nA)} = 0.007-432.5 [\text{free chlorine}] \text{ (mg}\cdot\text{L}^{-1})$, with $r^2 = 0.9998$ ($n = 10$), was obtained. The sensors displayed a LOD of $4.4 \mu\text{g}\cdot\text{L}^{-1}$ and a LOQ of $8.8 \mu\text{g}\cdot\text{L}^{-1}$. The LOD obtained for these sensors exhibited an enhancement in the LOD of 0.7 decades of concentration less than the ones non-modified.

Fig. 5B shows the calibration curve for the free chlorine detection obtained by the CuO-NPs/MWCNT/epoxy nanocomposite sensors. As in the previous case, the electroanalytical parameters obtained for these modified-sensors also improved respected to the raw MWCNT/epoxy nanocomposite sensors. The regression equation obtained was $I_{pa} \text{ (nA)} = 0.056-446.2 [\text{free chlorine}] \text{ (mg}\cdot\text{L}^{-1})$, $r^2 = 0.999$ ($n = 12$). The LOD was $0.6 \mu\text{g}\cdot\text{L}^{-1}$ and the LOQ was $1.1 \mu\text{g}\cdot\text{L}^{-1}$. Consequently, this parameter is 1.5 decades of concentration better than the raw MWCNT/epoxy nanocomposite sensors.

The LOD of both MWCNT/epoxy nanocomposite sensors containing CuO-NPs is obviously improved regarding to those using MWCNTs, glassy carbon and other modified-sensors which contain different nanoparticles as working electrodes, which are summarized in Table 3. This may be attributed to the CuO-NPs loading on MWCNTs arrays, which significantly increase the electrocatalytic active areas and promote electron transfer in the reduction of hypochlorite. These experimental results show that the amperometric sensors based on CuO-NPs exhibit the characteristics that an electrode must have, such as high sensitivity, low LOD and fast response time. Furthermore, as can be seen in Fig. 5, reproducibility (three different nanocomposite sensors) and repetitively (three measures per sensor) are better for the CuO-NPs/MWCNT/epoxy nanocomposite sensors, which have shown minor experimental error.

Accordingly, the best electroanalytical and electrocatalytic responses were obtained for the sensors in which the CuO-NPs were incorporated in bulk by Route B. These results can be explained since the CuO-NPs are more exposed on the sensor surface, increasing their electrocatalytic activity for the detection of free chlorine.

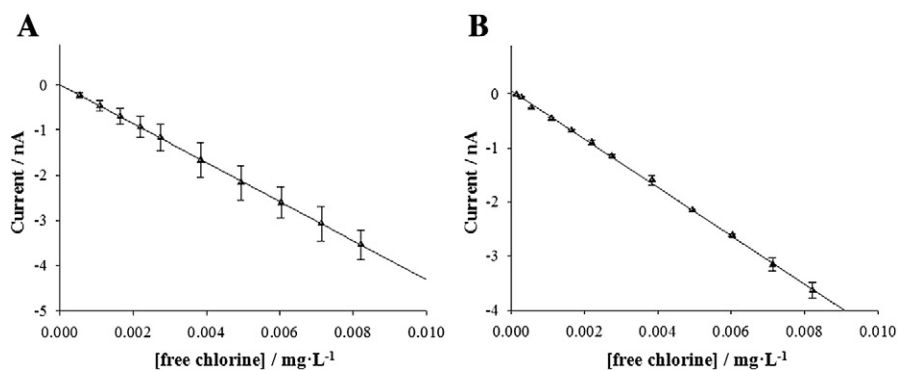


Fig. 5. Calibration curve of current vs. concentration of free chlorine at the A) CuO-NPs@MWCNT/epoxy nanocomposite sensor and B) CuO-NPs/MWCNT/epoxy nanocomposite sensor. The calibration curves, which are represented with their corresponding error bars ($n = 3$), were recorded in a PBS solution at pH 5.5; E_{app} : -0.35 V vs. Ag/AgCl; rotation speed: 1100 rpm.

Table 4

Variation of the CuO-NPs/MWCNT/epoxy nanocomposite sensor sensitivity upon carrying out successive free chlorine calibration experiments for a 7-day period time. Sensitivity values expressed with its respectively 95% confidence interval ($n = 3$) was obtained by hydrodynamic amperometry in 0.1 M KCl containing PBS (pH 5.5) solution ($E_{app} = -0.35$ V vs. Ag/AgCl).

Day	Sensitivity ($\text{nA} \cdot \text{L} \cdot \text{mg}^{-1}$)	r^2 ($n = 12$)
1	-446 ± 12	0.999
2	-436 ± 16	0.998
5	-440 ± 17	0.997
7	-433 ± 12	0.999

3.5. Stability and reproducibility

The stability and reproducibility of the sensors which presented the best electroanalytical response, the CuO-NPs/MWCNT/epoxy nanocomposite sensors, were evaluated. The hydrodynamic amperometric measurements were carried out in a PBS solution (pH 5.5) at -0.35 V vs. Ag/AgCl. To investigate the stability of the sensors, five successive measurements of free chlorine were carried out using one sensor. The relative standard deviation (RSD) was 1.9%, indicating that the sensor was stable. On the other hand, three different CuO-NPs/MWCNT/epoxy nanocomposite sensors were prepared and evaluated in order to compare their amperometric current responses. The measurements, which were carried out in triplicate ($n = 3$), yielded an RSD of 1.1%, confirming that the preparation method was highly reproducible. Afterwards, multiple calibration experiments were performed with these three CuO-NPs/MWCNT/epoxy nanocomposite sensors within a 7-day period in order to make an estimation of the loss of sensitivity to both short and long time.

The mean value of the calibration plots carried out the first working day was used as the control sensitivity value. As is shown in Table 4, successive calibration plots were performed during 7 consecutive days. During this period, the sensors were exposed to air without renewing their surface. Regarding these results, it is important to highlight that a simple approach was implemented with the aim of keeping the electrode surface active for longer without needing to renew its surface. This pretreatment consisted of applying, before each calibration, a $+1.23$ V vs. Ag/AgCl fix potential during 30 s. After 7 days, the current response of the CuO-NPs/MWCNT/epoxy nanocomposite sensor was approximately 96.5% of its original counterpart (see Table 4). This fact can be mainly attributed to the chemical stability of CuO-NPs. The results demonstrated that the simple procedure explained above enables the sensor to be used for at least 7 days without having significant differences in sensitivity (RSD of 1.3%), keeping its original properties. Furthermore and according to previous reports, these results also

demonstrate that the CuO-NPs do not show any degradation under the presence of NaClO during repeated uses and thus, keep their catalytic activity for the electrocatalytic detection of free chlorine in water [27].

3.6. Interference study

Finally, the selectivity of this sensing method for free chlorine was evaluated. Anti-interference property is also an important factor for sensors. Because of the high content of different ions such as Na^+ , K^+ , Ca^{2+} , NO_3^- , Cl^- , and SO_4^{2-} which usually co-exist with free chlorine in water, the electrochemical response of the interfering species was also examined at the CuO-NPs/MWCNT/epoxy nanocomposite sensor, as shown in Fig. 6. Hydrodynamic amperometric response of CuO-NPs/MWCNT/epoxy nanocomposite sensor was monitored in a PBS solution at pH 5.5. The interference experiments were carried out by successive injection of 0.1 mM NaClO and 1.0 mM interfering species ($E_{app} = -0.35$ V vs. Ag/AgCl). Fig. 6 shows the current response for (a) blank, (b) a + 0.1 mM NaClO, (c) b + 0.1 mM NaClO, (d) c + 1.0 mM NaCl, (e) d + 1.0 mM KCl, (f) e + 1.0 mM KNO_3 , (g) f + 1.0 mM K_2SO_4 , (h) g + 1.0 mM CaSO_4 and (i) h + 0.1 mM NaClO, respectively. Well-defined NaClO responses were observed (see Fig. 6 b–c), while insignificant responses were observed for interfering species (Fig. 6 d–h). Thus, the current response increased only for NaClO, even in the presence of 1.0 mM Na^+ , 4.0 mM K^+ , 1.0 mM Ca^{2+} , 1.0 mM NO_3^- , 2.0 mM Cl^- and 2.0 mM SO_4^{2-} . It is important to highlight that these concentrations are similar to those commonly found in tap and recreational water. Furthermore, the similar phenomenon for the addition (i) was also found. According to the results, it can be concluded that small amounts of different usually ions presented in water samples, such as Na^+ , K^+ , Ca^{2+} , NO_3^- , Cl^- , and SO_4^{2-} can be neglected. In other words, the present sensing system based on MWCNT/epoxy nanocomposite containing CuO-NPs in bulk apparently exhibits excellent selectivity for the detection of free chlorine in water.

4. Conclusions

CuO-NPs have successfully been synthesized by an environmentally friendly technique and incorporated either on the MWCNT surface or in the matrix nanocomposite, for the development of sensitive amperometric nanocomposite sensors based on MWCNT/epoxy. Novelty, CuO-NPs have been introduced as a catalytic component in this nanocomposite material for the electrocatalytic detection of free chlorine.

The incorporation of CuO-NPs in the nanocomposite electrode by two different routes has been electrochemically studied by CV and EIS techniques and the results were compared with the obtained by raw MWCNT/epoxy nanocomposite electrode. CuO-NPs containing

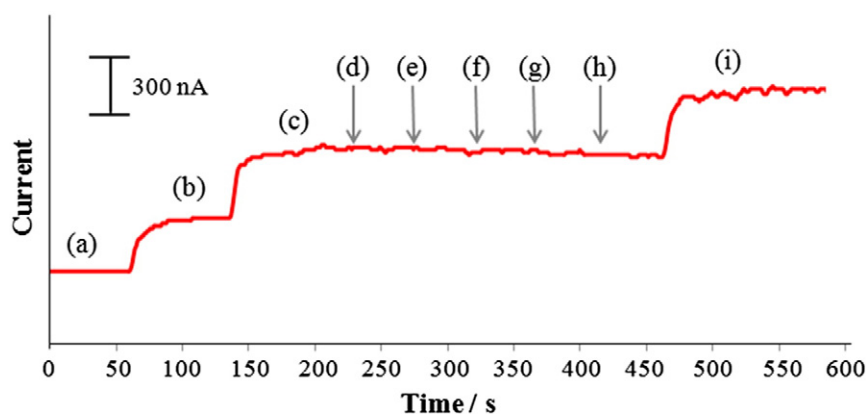


Fig. 6. Amperometric response of CuO-NPs/MWCNT/epoxy nanocomposite sensors examined in a PBS solution (pH 5.5) under stirring conditions ($E_{app} = -0.35$ V vs. Ag/AgCl; rotation speed: 1100 rpm). The interference experiment shows the current response for (a) blank, (b) a + 0.1 mM NaClO, (c) b + 0.1 mM NaClO, (d) c + 1.0 mM NaCl, (e) d + 1.0 mM KCl, (f) e + 1.0 mM KNO_3 , (g) f + 1.0 mM K_2SO_4 , (h) g + 1.0 mM CaSO_4 and (i) h + 0.1 mM NaClO, respectively.

nanocomposite electrodes presented many attractive electrochemical features such as good electrocatalytic activity, high electroactive area and fast electron transfer.

Electroanalytical results verified the electrocatalytic effect of CuO-NPs for the detection of free chlorine, independent of the route of introducing the CuO-NPs in the nanocomposite sensor. The analytical parameters of both modified-nanocomposite sensors were better than the obtained by the raw MWCNT/epoxy nanocomposite sensor.

The catalytic activity of the CuO-NPs in the modified-nanocomposite sensors for the decomposition of hypochlorite and thus for the free chlorine determination, was suitable to determine traces in the order of parts per billion ($\mu\text{g}\cdot\text{L}^{-1}$), around a decade of concentration less than the obtained by the raw MWCNT/epoxy nanocomposite sensor. The obtained results demonstrate the capability of these modified-nanocomposite sensors with CuO-NPs for the sensitive sensing of free chlorine.

The most advantageous route to enhance the electrocatalytic activity of the modified-sensors is when the CuO-NPs are incorporated in powder form in the nanocomposite matrix (Route B), obtaining the best analytical parameters, such as sensitivity, LOD and LOQ.

Finally, the CuO-NPs/MWCNT/epoxy nanocomposite sensors present many attractive analytical characteristics such as valuable electrocatalytic activity, high sensitivity, strong stability, good reproducibility and selectivity, as well as quick response, which is mainly attributed to the improvement of electroactive surface area and the synergistic electrocatalytic activity resulting from the combination of MWCNTs and CuO-NPs.

Acknowledgment

This work was supported by the project CTQ2012-36165. Jose Muñoz thanks the Universitat Autònoma de Barcelona (UAB) for the award of PIF studentship.

References

- [1] S. Iijima, Helical microtubules of graphitic carbon, *Nature* 354 (1991) 56–58.
- [2] E.T. Thostenson, Z. Ren, T.-W. Chou, Advances in the science and technology of carbon nanotubes and their composites: a review, *Compos. Sci. Technol.* 61 (2001) 1899–1912.
- [3] M. Trojanowicz, Analytical applications of carbon nanotubes: a review, *TrAC Trends Anal. Chem.* 25 (2006) 480–489.
- [4] M. Cadek, J. Coleman, V. Barron, K. Hedicke, W. Blau, Morphological and mechanical properties of carbon-nanotube-reinforced semicrystalline and amorphous polymer composites, *Appl. Phys. Lett.* 81 (2002) 5123–5125.
- [5] Z. Spitalsky, D. Tasis, K. Papagelis, C. Galiotis, Carbon nanotube–polymer composites: chemistry, processing, mechanical and electrical properties, *Prog. Polym. Sci.* 35 (2010) 357–401.
- [6] I. Dumitrescu, N.R. Wilson, J.V. Macpherson, Functionalizing single-walled carbon nanotube networks: effect on electrical and electrochemical properties, *J. Phys. Chem. C* 111 (2007) 12944–12953.
- [7] S. Berber, Y.-K. Kwon, D. Tomanek, Unusually high thermal conductivity of carbon nanotubes, *Phys. Rev. Lett.* 84 (2000) 4613.
- [8] T.W. Odom, J.-L. Huang, P. Kim, C.M. Lieber, Structure and electronic properties of carbon nanotubes, *J. Phys. Chem. B* 104 (2000) 2794–2809.
- [9] J. Wang, M. Musameh, Carbon nanotube/teflon composite electrochemical sensors and biosensors, *Anal. Chem.* 75 (2003) 2075–2079.
- [10] J. Shi, Z. Wang, H.-I. Li, Electrochemical fabrication of polyaniline/multi-walled carbon nanotube composite films for electrooxidation of methanol, *J. Mater. Sci.* 42 (2007) 539–544.
- [11] S.K. Vashist, D. Zheng, K. Al-Rubeaan, J.H. Luong, F.-S. Sheu, Advances in carbon nanotube based electrochemical sensors for bioanalytical applications, *Biotechnol. Adv.* 29 (2011) 169–188.
- [12] T.-W. Lin, C.-J. Liu, C.-S. Dai, Ni₃S₂/carbon nanotube nanocomposite as electrode material for hydrogen evolution reaction in alkaline electrolyte and enzyme-free glucose detection, *Appl. Catal. B Environ.* 154–155 (2014) 213–220.
- [13] J. Muñoz, J. Bastos-Arrieta, M. Muñoz, D. Muraviev, F. Céspedes, M. Baeza, Simple green routes for the customized preparation of sensitive carbon nanotubes/epoxy nanocomposite electrodes with functional metal nanoparticles, *RSC Adv.* 4 (2014) 44517–44524.
- [14] X. Yang, J. Zheng, M. Zhen, X. Meng, F. Jiang, T. Wang, C. Shu, L. Jiang, C. Wang, A linear molecule functionalized multi-walled carbon nanotubes with well dispersed PtRu nanoparticles for ethanol electro-oxidation, *Appl. Catal. B Environ.* 121 (2012) 57–64.
- [15] D. Ivnitski, K. Artyushkova, R.A. Rincon, P. Atanassov, H.R. Luckarift, G.R. Johnson, Entrapment of enzymes and carbon nanotubes in biologically synthesized silica: glucose oxidase-catalyzed direct electron transfer, *Small* 4 (2008) 357–364.
- [16] X. Kan, Y. Zhao, Z. Geng, Z. Wang, J.-J. Zhu, Composites of multiwalled carbon nanotubes and molecularly imprinted polymers for dopamine recognition, *J. Phys. Chem. C* 112 (2008) 4849–4854.
- [17] J. Muñoz, J. Bartroli, F. Céspedes, M. Baeza, Influence of raw carbon nanotubes diameter for the optimization of the load composition ratio in epoxy amperometric composite sensors, *J. Mater. Sci.* (2014) 1–10.
- [18] R.L. McCreery, Advanced carbon electrode materials for molecular electrochemistry, *Chem. Rev.* 108 (2008) 2646–2687.
- [19] R. Olivé-Monllau, M.J. Esplandiu, J. Bartroli, M. Baeza, F. Céspedes, Strategies for the optimization of carbon nanotube/polymer ratio in composite materials: applications as voltammetric sensors, *Sensors Actuators B Chem.* 146 (2010) 353–360.
- [20] M. Pumera, A. Merkoçi, S. Alegret, Carbon nanotube-epoxy composites for electrochemical sensing, *Sensors Actuators B Chem.* 113 (2006) 617–622.
- [21] M. Pacios, M. Del Valle, J. Bartroli, M. Esplandiu, Electrochemical behavior of rigid carbon nanotube composite electrodes, *J. Electroanal. Chem.* 619 (2008) 117–124.
- [22] R. Olivé-Monllau, A. Pereira, J. Bartroli, M. Baeza, F. Céspedes, Highly sensitive CNT composite amperometric sensors integrated in an automated flow system for the determination of free chlorine in waters, *Talanta* 81 (2010) 1593–1598.
- [23] J. March, B. Simonet, A green method for the determination of hypochlorite in bleaching products based on its native absorbance, *Talanta* 73 (2007) 232–236.
- [24] Y.S. Su, D. Morrison III, R.A. Ogle, Chemical kinetics of calcium hypochlorite decomposition in aqueous solutions, *J. Chem. Health Saf.* 16 (2009) 21–25.
- [25] I. Sizeneva, N. Kondrashova, V. Val'tsifer, Spontaneous decomposition of industrially manufactured sodium hypochlorite solutions, *Russ. J. Appl. Chem.* 78 (2005) 541–545.
- [26] V. Londhe, P. Kamath, A note on the catalytic decomposition of waste sodium hypochlorite solution, *Water Res.* 9 (1975) 1009–1010.
- [27] K.-W. Kim, E.-H. Lee, D.-Y. Chung, J.-K. Moon, H.-S. Shin, J.-S. Kim, D.-W. Shin, Manufacture characteristics of metal oxide–hydroxides for the catalytic decomposition of a sodium hypochlorite solution, *Chem. Eng. J.* 200 (2012) 52–58.
- [28] S. Liu, J. Tian, L. Wang, X. Qin, Y. Zhang, Y. Luo, A.M. Asiri, A.O. Al-Youbi, X. Sun, A simple route for preparation of highly stable CuO nanoparticles for nonenzymatic glucose detection, *Catal. Sci. Technol.* 2 (2012) 813–817.
- [29] X.-M. Miao, R. Yuan, Y.-Q. Chai, Y.-T. Shi, Y.-Y. Yuan, Direct electrocatalytic reduction of hydrogen peroxide based on Nafion and copper oxide nanoparticles modified Pt electrode, *J. Electroanal. Chem.* 612 (2008) 157–163.
- [30] S. Liu, J. Tian, L. Wang, Y. Luo, X. Sun, One-pot synthesis of CuO nanoflower-decorated reduced graphene oxide and its application to photocatalytic degradation of dyes, *Catal. Sci. Technol.* 2 (2012) 339–344.
- [31] C. Batchelor-McAuley, Y. Du, G.G. Wildgoose, R.G. Compton, The use of copper (II) oxide nanorod bundles for the non-enzymatic voltammetric sensing of carbohydrates and hydrogen peroxide, *Sensors Actuators B Chem.* 135 (2008) 230–235.
- [32] A. Apha, Wef, Standard Methods for the Examination of Water and Wastewater, 21st ed. American Public Health Association, Washington, DC, 2005. 94–100 (Part, 8000).
- [33] L. Moberg, B. Karlberg, S. Blomqvist, U. Larsson, Comparison between a new application of multivariate regression and current spectroscopy methods for the determination of chlorophylls and their corresponding pheopigments, *Anal. Chim. Acta* 411 (2000) 137–143.
- [34] S. Anandan, G.-J. Lee, J.J. Wu, Sonochemical synthesis of CuO nanostructures with different morphology, *Ultrason. Sonochem.* 19 (2012) 682–686.
- [35] Z. Zhuang, X. Su, H. Yuan, Q. Sun, D. Xiao, M.M. Choi, An improved sensitivity non-enzymatic glucose sensor based on CuO nanowire modified Cu electrode, *Analyst* 133 (2008) 126–132.
- [36] M. Pourbaix, Atlas d'équilibres électrochimiques à 25°C Gauthier-Villars, Editeur, Paris, 1963.
- [37] C.O. Laoire, S. Mukerjee, K. Abraham, E.J. Plichta, M.A. Hendrickson, Elucidating the mechanism of oxygen reduction for lithium-air battery applications, *J. Phys. Chem. C* 113 (2009) 20127–20134.
- [38] J. Wang, Analytical Electrochemistry, John Wiley & Sons, 2006.
- [39] J.S. Ye, H.F. Cui, X. Liu, T.M. Lim, W.D. Zhang, F.S. Sheu, Preparation and characterization of aligned carbon nanotube–ruthenium oxide nanocomposites for supercapacitors, *Small* 1 (2005) 560–565.
- [40] F. Kodera, M. Umeda, A. Yamada, Determination of free chlorine based on anodic voltammetry using platinum, gold, and glassy carbon electrodes, *Anal. Chim. Acta* 537 (2005) 293–298.
- [41] T.-H. Tsai, K.-C. Lin, S.-M. Chen, Electrochemical synthesis of poly (3, 4-ethylenedioxythiophene) and gold nanocomposite and its application for hypochlorite sensor, *Int. J. Electrochem. Sci.* 6 (2011) 2672–2687.
- [42] R. Olivé-Monllau, J. Orozco, C. Fernández-Sánchez, M. Baeza, J. Bartroli, C. Jimenez-Jorquera, F. Céspedes, Flow injection analysis system based on amperometric thin-film transducers for free chlorine detection in swimming pool waters, *Talanta* 77 (2009) 1739–1744.
- [43] M. Murata, T.A. Ivandini, M. Shibata, S. Nomura, A. Fujishima, Y. Einaga, Electrochemical detection of free chlorine at highly boron-doped diamond electrodes, *J. Electroanal. Chem.* 612 (2008) 29–36.

ANNEX B

Submitted Publications

Journal of Materials Science

CdS quantum dots as a scattering nanomaterial of carbon nanotubes in polymeric nanocomposite sensors for microelectrode array behavior

--Manuscript Draft--

Manuscript Number:	JMISC-D-15-02776	
Full Title:	CdS quantum dots as a scattering nanomaterial of carbon nanotubes in polymeric nanocomposite sensors for microelectrode array behavior	
Article Type:	Manuscript (Regular Article)	
Keywords:	Nanocomposite * Amperometric sensor * CdS Quantum Dots * Multiwalled carbon nanotubes * Microelectrode array behavior * Electrochemical characterization	
Corresponding Author:	Mireia Baeza UAB Bellaterra, Cerdanyola del Vallès SPAIN	
Corresponding Author Secondary Information:		
Corresponding Author's Institution:	UAB	
Corresponding Author's Secondary Institution:		
First Author:	Jose Muñoz	
First Author Secondary Information:		
Order of Authors:	Jose Muñoz	
	Julio Bastos-Arrieta	
	María Muñoz	
	Dmitri Muraviev	
	Francisco Céspedes	
	Mireia Baeza	
Order of Authors Secondary Information:		
Abstract:	<p>This work is focused on evaluating the direct electrochemical effect of semi-conducting nanocrystals when they are integrated in bulky nanocomposite sensors based on multiwalled carbon nanotubes (MWCNTs). For this aim, MWCNTs have successfully been functionalized with CdS quantum dots (CdS-QDs@MWCNTs) and then dispersed within an insulating polymeric matrix, as epoxy resin, for electroanalytical sensing purposes. After an accurate voltammetric and impedimetric characterization, some electrochemical parameters were surprisingly enhanced regarding the non-modified sensors, such as peak current height, electroactive area and emphasizing the double-layer capacitance. These results can be explained since CdS-QDs confer to the nanocomposite sensor a microelectrode array behavior, dispersing the conductive microzones through the polymeric matrix, as revealed morphological experiments. The feasibility of this approach was amperometrically evaluated for ascorbic acid and hydrogen peroxide, both used as reference analytes. Electroanalytical results demonstrated that this approach provides to the CdS-QDs modified-nanocomposite sensors the capability to determine low concentrations of analytes and improved sensitivities.</p>	
Funding Information:	Universitat Autònoma de Barcelona (PIF) MINECO (CTQ2012-36165)	Jose Muñoz Dr. Mireia Baeza

Manuscript Number: CSTE-D-15-00705

Title: Characterization protocol to improve the electroanalytical response of graphene-polymer nanocomposite sensors

Article Type: Full Length Article

Section/Category: Materials science, chemistry and bio-composites

Keywords: A. Nano composites,
A. Polymer-matrix composites (PMCs),
B. Electrical properties,
B. Impact behaviour,
B. Transport properties,

Corresponding Author: Dr. Mireia Baeza,

Corresponding Author's Institution: Universitat Autònoma de Barcelona

First Author: Jose Muñoz

Order of Authors: Jose Muñoz; Lorcan J Brennan; Francisco Céspedes; Yurii K Gun'ko; Mireia Baeza

Abstract: This work is focused on the application of advanced characterization techniques in the development of optimized electrochemical sensors based on graphene-polymer nanocomposites. Reduced graphene oxide (rGO) was synthesized in order to be used as conducting nanofiller material in nanocomposite electrodes based on epoxy resin. A series of rGO/epoxy nanocomposite electrodes were fabricated containing 8% to 20% of nanofiller material. Composition ratios have been studied using percolation theory and characterized by different electrochemical techniques. After an accurate electrical and electrochemical characterizations, it has been demonstrated that an optimization of the rGO/epoxy composition ratio is necessary in order to enhance electrochemical performance. The optimal nanocomposite electrode composition, which was found between 12% and 14% in rGO loading, takes into account the high electrode sensitivity, low limit of detection, fast response and electroanalytical reproducibility. The potential of this approach in terms of electroanalytical response has been demonstrated by means of the amperometric detection of ascorbic acid, which was used as a model analyte. Furthermore, different morphological experiments were carried out in order to confirm the electrochemical and electroanalytical enhancement obtained for the optimized-nanocomposite sensors. Accordingly, the presented characterization protocol makes it possible to obtain more efficient electrochemical sensors by optimizing different physical parameters, such as resistance of the solution, electron transfer rate and double-layer capacitance, which are directly related to the sensitivity, response time and signal-to-noise ratio, respectively.

Suggested Reviewers: Gleb B Sukhorukov

School of Engineering and Materials Science, University of London

G.Sukhorukov@qmul.ac.uk

He has a high background regarding to composite materials fabrication and characterization.



Near-percolation nanocomposite sensor based on modified-graphene for the sensitive electrochemical biorecognition of Thyroxine

Journal:	<i>ChemComm</i>
Manuscript ID:	CC-COM-07-2015-005825
Article Type:	Communication
Date Submitted by the Author:	14-Jul-2015
Complete List of Authors:	Muñoz, Jose; Universitat Autònoma de Barcelona, Chemistry Riba-Moliner, Marta; Institut de Ciència de Materials de Barcelona (ICMAB-CSIC), Molecular Nanoscience and Organic Materials Brennan, Lorcan; Trinity College Dublin, Chemistry Gunko, Y; Trinity College Dublin, School of Chemistry Céspedes, Francisco; Universitat Autònoma de Barcelona, Dept. of Chemistry Gonzalez-Campo, Arantzas; Institut de Ciència de Materials de Barcelona (ICMAB-CSIC), Molecular Nanoscience and Organic Materials Baeza, Mireia; Universitat Autònoma de Barcelona, Chemistry

SCHOLARONE™
Manuscripts

ANNEX C

Curriculum Vitae

Jose María Muñoz Martín

PERSONAL DATA

Date of birth: 17th January 1988
Place of birth: Sabadell (Spain)
Nationality: Spanish
Address: Collserola Street 41
08207, Sabadell - Spain
Telf: (0034) 635099588
E-mail: Josemaria.munoz88@gmail.com
Linkedin: es.linkedin.com/in/jmunoz88

EDUCATION

Oct. 2011 – Present **PhD Studies in Chemistry and Research Professor in training**
Autonomous University of Barcelona (UAB)
Title: “Advanced amperometric nanocomposite sensors based on carbon nanotubes and graphene: Characterization, Optimization, Functionalization and Applications”.
Teaching: Teach in different subjects in the field of Analytical Chemistry. More than 250 credited hours.
Grant: PIF scholarship from 2011 to 2015.

Sept. 2010 – Sept. 2011 **Master Degree: Chemistry Science and Technology (MSc)**
Institute of Science of Materials of Barcelona (ICMAB–CSIC)
Title: “Development of a synthetic method for coupling aromatic rings on metallocarboranes by B–C bond.
Qualification: A⁺
Grant: MEC scholarship 2011.

Sept. 2006 – Jun. 2010 **University Degree: Chemistry (BSc)**
Autonomous University of Barcelona (UAB)
Qualification: B⁺
Grant: MEC scholarship from 2006 to 2010.

TRAINING ABROAD / FURTHER EDUCATION

Dec. 2014 – Mar. 2015

School of Chemistry and CRAAN InstituteTrinity College of Dublin, Ireland. *3 months***Grant:** PIF mobility 2015.

- Development of a novel strategie for the characterization of graphene/polymer composition ratio for the optimization of electrochemical nanocomposite sensors.
- Synthesis of Graphene Oxide and Reduced Graphene Oxide: characterization and functionalization with Gold Nanoparticles.
- Development of an amperometric nanocomposite sensor based on modified-graphene for the sensitive biorecognition of Thyroxine, using supramolecular chemistry.
- Training of some spectroscopic techniques, such as FTIR, Raman and UV-vis.

Sept. – Nov. 2014

Entrepreneurship Course in Enviromental SciencesBellaterra, Barcelona. *120 h*

- Presentation of an uranium micronalyzer device and composition of business plan.

Jun. 2014 – Jul. 2014

Summer SchoolBellaterra, Barcelona. *36 h*

- Magnetic particles based platforms and bioassays.

LENGUAGE SKILLS

Spanish

Mother tongue

Catalan

Mother tongue

English

Fluent

(Advanced B2.2 Level)

ACCEPTED PUBLICATIONS

- **J. Muñoz**, J. Bastos-Arrieta, M. Muñoz, D. Muraviev, F. Céspedes and M. Baeza. "Simple green routes for the customized preparation of sensitive carbon nanotubes/epoxy nanocomposite electrodes with Functional Metal Nanoparticles". *RSC Advances*, **(2014)** 4(84), 44517–44524. DOI: 10.1039/c4ra07294d

- **J. Muñoz**, J. Bartrolí, F. Céspedes and M. Baeza. "Influence of raw carbon nanotubes diameter for the optimization of the load composition ratio in epoxy amperometric composite sensors". *Journal of Materials Science*, (2014) 50(2), 652–661. DOI: 10.1007/s1085-014-8624-2
- **J. Muñoz**, F. Céspedes and M. Baeza. "Modified multiwalled carbon nanotube/epoxy amperometric nanocomposite sensors with CuO nanoparticles for electrocatalytic detection of free chlorine". *Microchemical Journal*, (2015) 122, 189–196. DOI: 10.1016/j.microc.2015.05.001
- **J. Muñoz**, F. Céspedes and M. Baeza. "Effect of carbon nanotube purification on electroanalytical response of near-percolation amperometric nanocomposite sensors". *Journal of the Electrochemical Society*, (2015) 162(8), B217–B224. DOI: 10.1149/2.0531508jes

CONFERENCES

- **ICREA Workshop on Graphene Nanobiosensors** (Barcelona, Spain), May 2015. Poster: "Characterization protocol to improve the electroanalytical response of graphene-polymer nanocomposite (bio)sensors". **J. Muñoz**, L.J. Brennan, Y.K. Gun'ko, F. Céspedes and M. Baeza.
- **XVIX Transfronterera of Sensors and Biosensors** (Bellaterra, Spain), September 2014. Poster: "Simple green routes for the customized preparation of sensitive carbon nanotubes/epoxy nanocomposite electrodes with Functional Metal Nanoparticles". **J. Muñoz**, J. Bastos-Arrieta, M. Muñoz, D. Muraviev, F. Céspedes and M. Baeza.
- **Trends in Nanotechnology 2013 Congress (TNT2013)** (Sevilla, Spain), September 2013. Poster: "Carbon Nanotubes doped with different noble metal nanoparticles by near – percolation amperometric sensors". **J. Muñoz**, J. Bartrolí, F. Céspedes and M. Baeza.
- **XVIII Transfronterera of Sensors and Biosensors** (Ale, France), September 2013. Poster: "Highly sensitive CNTs composite amperometric sensors doped with different noble metal nanoparticles". **J. Muñoz**, J. Bastos-Arrieta, M. Muñoz, D. Muraviev, F. Céspedes and M. Baeza.
- **NT13: The Fourteenth International Conference on the Science and Application of Nanotubes** (Espoo, Finland), June 2013. Poster: "Effect of MWCNTs purity in electrochemical response of near-percolation amperometric composites". **J. Muñoz**, J. Bartrolí, M. Baeza and F. Céspedes.
- **3rd International Conference on Bio-Sensing Technology** (Sitges, Spain), May 2013. Poster: "The way for the customized construction of MWCNT composite electrodes is opened". **J. Muñoz**, J. Bartrolí, M. Baeza and F. Céspedes.

- **XI Workshop sobre Mètodes ràpids i automatització en microbiologia alimentària** (Bellaterra, Spain), November 2012. Assistant.
- **Rethinking Nano Workshop: From Discovery to design** (Barcelona, Spain), November 2012. Assistant.
- **XVII Transfronterera of Sensors and Biosensors** (Tarragona, Spain), September 2012. Poster 1: “Physical properties effects of MWCNT on electrochemical response of (bio)sensors”. **J. Muñoz**, R. Montes, J. Bartrolí, M. Baeza and F. Céspedes. Poster 2: “Determination of low concentrations using amperometric enzymatic biosensors. Characterization and optimization of biocomposites using new alternative techniques”. R. Montes, **J. Muñoz**, J. Bartrolí, M. Baeza and F. Céspedes.
- **XVI Transfronterera of Sensors and Biosensors** (Toulouse, France), September 2011. Assistant.

